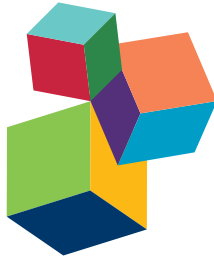


CNS RECOVERY AFTER STRUCTURAL AND/OR PHYSIOLOGICAL/PSYCHOLOGICAL DAMAGE

EDITED BY: Marie Mofteh and Emmanuel Moyses
PUBLISHED IN: *Frontiers in Cellular Neuroscience*





frontiers

Frontiers Copyright Statement

© Copyright 2007-2016 Frontiers Media SA. All rights reserved.

All content included on this site, such as text, graphics, logos, button icons, images, video/audio clips, downloads, data compilations and software, is the property of or is licensed to Frontiers Media SA ("Frontiers") or its licensees and/or subcontractors. The copyright in the text of individual articles is the property of their respective authors, subject to a license granted to Frontiers.

The compilation of articles constituting this e-book, wherever published, as well as the compilation of all other content on this site, is the exclusive property of Frontiers. For the conditions for downloading and copying of e-books from Frontiers' website, please see the Terms for Website Use. If purchasing Frontiers e-books from other websites or sources, the conditions of the website concerned apply.

Images and graphics not forming part of user-contributed materials may not be downloaded or copied without permission.

Individual articles may be downloaded and reproduced in accordance with the principles of the CC-BY licence subject to any copyright or other notices. They may not be re-sold as an e-book.

As author or other contributor you grant a CC-BY licence to others to reproduce your articles, including any graphics and third-party materials supplied by you, in accordance with the Conditions for Website Use and subject to any copyright notices which you include in connection with your articles and materials.

All copyright, and all rights therein, are protected by national and international copyright laws.

The above represents a summary only. For the full conditions see the Conditions for Authors and the Conditions for Website Use.

ISSN 1664-8714

ISBN 978-2-88945-040-4

DOI 10.3389/978-2-88945-040-4

About Frontiers

Frontiers is more than just an open-access publisher of scholarly articles: it is a pioneering approach to the world of academia, radically improving the way scholarly research is managed. The grand vision of Frontiers is a world where all people have an equal opportunity to seek, share and generate knowledge. Frontiers provides immediate and permanent online open access to all its publications, but this alone is not enough to realize our grand goals.

Frontiers Journal Series

The Frontiers Journal Series is a multi-tier and interdisciplinary set of open-access, online journals, promising a paradigm shift from the current review, selection and dissemination processes in academic publishing. All Frontiers journals are driven by researchers for researchers; therefore, they constitute a service to the scholarly community. At the same time, the Frontiers Journal Series operates on a revolutionary invention, the tiered publishing system, initially addressing specific communities of scholars, and gradually climbing up to broader public understanding, thus serving the interests of the lay society, too.

Dedication to Quality

Each Frontiers article is a landmark of the highest quality, thanks to genuinely collaborative interactions between authors and review editors, who include some of the world's best academicians. Research must be certified by peers before entering a stream of knowledge that may eventually reach the public - and shape society; therefore, Frontiers only applies the most rigorous and unbiased reviews.

Frontiers revolutionizes research publishing by freely delivering the most outstanding research, evaluated with no bias from both the academic and social point of view.

By applying the most advanced information technologies, Frontiers is catapulting scholarly publishing into a new generation.

What are Frontiers Research Topics?

Frontiers Research Topics are very popular trademarks of the Frontiers Journals Series: they are collections of at least ten articles, all centered on a particular subject. With their unique mix of varied contributions from Original Research to Review Articles, Frontiers Research Topics unify the most influential researchers, the latest key findings and historical advances in a hot research area! Find out more on how to host your own Frontiers Research Topic or contribute to one as an author by contacting the Frontiers Editorial Office: researchtopics@frontiersin.org

CNS RECOVERY AFTER STRUCTURAL AND/OR PHYSIOLOGICAL/PSYCHOLOGICAL DAMAGE

Topic Editors:

Marie Mofteh, Alexandria University, Egypt

Emmanuel Moyses, Université François Rabelais de Tours, France

There is an assumption that environmental threats could cause important damages in central nervous system. As a consequence, several forms of brain structural plasticity could be affected. The environmentally mediated risks include generally physical (such as brain and spinal cord injury) and psychological / psychosocial influences (e.g. stress). In general, the response of the organism to these environmental challenges passes via adaptive responses to maintain homeostasis or functional recovery. These processes engage the immune system, the autonomic nervous system (ANS) besides the hypothalamo-hypophyseo-adrenal (HPA) axis via specific hormones, neurotransmitters, neuropeptides and other factors which participate, in several cases, in structural remodeling in particular brain areas. To what extent a brain and / or spinal cord recovery after structural and / or physiological / psychological damage could occur and by which mechanisms, this is the goal of this Research Topic. It concerns neurogenesis, growth factors and their receptors, and morphological plasticity. On the other hand, it is well known that stress experienced an obvious impact on many behavioral and physiological aspects. Thus, environmental stress affects neuroendocrine structure and function and hence such aspects may influence brain development. Knowing normal organization of neurotensin receptors' system during postnatal development in human infant will help understanding the dysfunction of this neuropeptidergic system in "sudden infant syndrome" victims. Stress could affect also other non-neuroendocrine regions and systems. GABA is one of the classical neurotransmitter sensitive to stress either when applied acutely or repetitively as well as its receptor GABAA. Furthermore, the modulation of this receptor complex notably by neurosteroids is also affected by acute stress. These steroids seem to play a role in the resilience retained by the stressed brain. Their modulatory role will be studied in the context of chronic stress in rats. Finally, one of the major impacts of stress besides changes in psychological behavior is the alteration of food intake control causing in final eating disorders. This alteration is the result of changes occurring in activity of brain regions involved in stress responses (principally HPA and ANS) and which are also involved in food intake control. The series of studies presented here, will try to explain how different stress paradigms affect this function and the eventual interactions of glucocorticoids with orexigenic (neuropeptide Y: NPY/Agouti Related Peptide: AgRP) and anorexigenic peptides (Pre-opiomelanocortin peptide: POMC/Cocaine Amphetamine regulatory Transcript peptide: CART).

Citation: Mofteh, M., Moyses, E., eds. (2016). CNS Recovery after Structural and/or Physiological/ Psychological Damage. Lausanne: Frontiers Media. doi: 10.3389/978-2-88945-040-4

Table of Contents

- 04 Editorial: CNS Recovery after Structural and/or Physiological/Psychological Damage**
Marie Z. Moftah and Emmanuel Moyses
- 06 Leptin is required for hypothalamic regulation of miRNAs targeting POMC 3'UTR**
Adel Derghal, Mehdi Djelloul, Coraline Airault, Clément Pierre, Michel Dallaporta, Jean-Denis Troadec, Vanessa Tillement, Catherine Tardivel, Bruno Bariohay, Jérôme Trouslard and Lourdes Mounien
- 16 Leptin-dependent neurotoxicity via induction of apoptosis in adult rat neurogenic cells**
Stéphanie Segura, Laurie Efthimiadi, Christophe Porcher, Sandrine Courtes, Valérie Coronas, Slavica Krantic and Emmanuel Moyses
- 30 Neurogenesis and growth factors expression after complete spinal cord transection in *Pleurodeles waltlii***
Amira Z. Zaky and Marie Z. Moftah
- 41 HMG-CoA reductase inhibition promotes neurological recovery, peri-lesional tissue remodeling, and contralesional pyramidal tract plasticity after focal cerebral ischemia**
Ertugrul Kilic, Raluca Reitmeir, Ülkan Kilic, Ahmet Burak Caglayan, Mustafa Caglar Beker, Taha Kelestemur, Muhsine Sinem Ethemoglu, Gurkan Ozturk and Dirk M. Hermann
- 51 Valproic acid potentiates curcumin-mediated neuroprotection in lipopolysaccharide induced rats**
Amira Zaky, Mariam Mahmoud, Doaa Awad, Bassma M. El Sabaa, Kamal M. Kandeel and Ahmad R. Bassiouny
- 63 Acquired equivalence associative learning in GTC epileptic patients: experimental and computational study**
Radwa Khalil, Noha Abo Elfetoh, Marie Z. Moftah and Eman M. Khedr
- 74 Developmental dynamics of neurotensin binding sites in the human hypothalamus during the first postnatal year**
Mohamed Najimi, Alain Sarrieau, Nicolas Kopp and Fatiha Chigr
- 83 Modulation of orexigenic and anorexigenic peptides gene expression in the rat DVC and hypothalamus by acute immobilization stress**
Fatiha Chigr, Fatima Rachidi, Catherine Tardivel, Mohamed Najimi and Emmanuel Moyses
- 91 Effects of cold exposure on behavioral and electrophysiological parameters related with hippocampal function in rats**
Hajar Elmarzouki, Youssef Aboussaleh, Soner Bitiktas, Cem Suer, A. Seda Artis, Nazan Dolu and Ahmed Ahami
- 101 Distribution of nitric oxide-producing cells along spinal cord in urodeles**
Mayada A. Mahmoud, Gehan H. Fahmy, Marie Z. Moftah and Ismail Sabry



Editorial: CNS Recovery after Structural and / or Physiological / Psychological Damage

Marie Z. Mofteh^{1*} and Emmanuel Moysé²

¹ Neuroplasticity and Pain Laboratory, Zoology Department, Alexandria University, Alexandria, Egypt, ² Unité PRC, INRA de Tours, François Rabelais University, Tours, France

Keywords: CNS recovery, structural damage, physiological damage, psychological damage, CNS

The Editorial on the Research Topic

CNS Recovery after Structural and / or Physiological / Psychological Damage

The central nervous system (CNS) is critically vulnerable to damage in post-natal and adult life, for two reasons. First, its major constitutive cell type, neuron, is more fragile than most other differentiated cell types, due to its exclusive dependency on glucose for energetic metabolism, to its high chronic demand of oxygen supply, to lower levels of antioxidant defenses and to extreme structural vulnerability of its long and thin axonal expansions. Second, any neuron damage or loss has dysfunctional outcome because of the specific dependency of nervous functions on the topography of neuronal interconnections. CNS damage can occur from environmental threats including both physical (injuries) and psychosocial (stress) risks. Consequently, several forms of brain plasticity can be affected and trigger adaptive responses to maintain homeostasis or functional recovery. These processes engage the immune system, the autonomic nervous system (ANS) besides the hypothalamo-hypophyseo-adrenal (HPA) axis via specific CNS-borne neurotransmitters, hormones, neuropeptides and growth factors. The goal of this Research Topic is to review the cellular and molecular mechanisms of damage-induced CNS plasticity through a selection of original research articles in this field. Derghal et al. use the neuroendocrine regulation of food intake to document the adaptive role of a recently emerged mechanism of neuroplasticity: neuronal synthesis of microRNAs (miRNAs) i.e., short non-coding RNA molecules that repress gene expression at the post-transcriptional level by binding to target mRNAs. They screened *in silico* the brain gene target of the major anorexigenic hormone leptin, POMC, for miRNA binding sites. It revealed 3 candidate miRNAs, which were indeed found upregulated in the hypothalamus of congenitally obese, leptin-deficient ob/ob mouse. This result provides a new mechanism of hormone-dependent neuronal plasticity with relevance to a physio-pathological adaptation. Segura et al. also use leptin hormonal signaling in the cerebral regulation of food intake, to document another effector mechanism of neuroplasticity: modulation of neurogenesis from adult neural stem cells. They report that leptin *in vitro* depresses adult neurogenesis from the canonical neural stem cells of the rodent subventricular zone (SVZ) through Ob-receptor-induction of apoptosis in immunocytochemically identified neuronal progenitors. This hormone-induced neurotoxicity is shown to be mediated through the signaling pathway of extracellular signal-regulated kinases ERK-1/2 and cyclin D1, i.e., the molecular switch between cell division and apoptosis. Zaky and Mofteh address post-lesional induction of neurogenesis-stimulating molecules in the spinal cord of the Amphibian *Pleurodeles*. This animal model displays extensive neural regeneration including both structural and locomotor restorations. They report post-lesional *in vivo* inductions of FGF2, i.e., the major intercellular mitogen for adult neural stem cells, and of the stem cell marker nestin. These data provide cues for post-lesional sequelae curing in adult mammals, especially via

OPEN ACCESS

Edited and reviewed by:

Egidio D'Angelo,
University of Pavia, Italy

*Correspondence:

Marie Z. Mofteh
marie.mofteh@alexu.edu.eg

Received: 22 August 2016

Accepted: 20 September 2016

Published: 06 October 2016

Citation:

Mofteh MZ and Moysé E (2016)
Editorial: CNS Recovery after
Structural and / or Physiological /
Psychological Damage.
Front. Cell. Neurosci. 10:225.
doi: 10.3389/fncel.2016.00225

cellular therapy. Kilic et al. characterize motor function and histological markers of brain plasticity following stroke induction by middle cerebral artery occlusion in adult mouse, treated or not with the secondary stroke-preventing clinical drug HMG-CoA reductase inhibitor rosuvastatin. They show rosuvastatin treatment increases functional motor recovery, neuronal survival and capillary density and decreases forebrain atrophy as compared to untreated lesioned mice. A single molecule-targeted drug can thus help neurological recovery via lesion-induced neuroplasticity potentiation. Zaky et al. use bacterial lipopolysaccharide (LPS)-induced neuroinflammation in adult rats as an *in vivo* model to investigate the mechanisms of neuroprotection by the drugs valproic acid (inhibitor of the epigenetically acting histone deacetylase-1) and curcumin. Strong synergy of the two drugs were shown by *in vivo* combination-induced additivity of their respective effects on histological and molecular markers of neuroinflammation, on biochemical markers of LPS-induced oxidative stress, and on LPS-induced repression of the five members of Let-7 miRNA family. The combined drugs suppressed LPS-induced neuroinflammation and restored oxidation marker, antioxidant defense and Let-7 miRNA to their control levels. Khalil et al. designed a computational assay to investigate the potential use of a recent cognitive psychological test of associative learning capacity (Acquired Equivalence Associative Learning Task, AEALT) to assess cognitive impairment of the Generalized Tonic Clonic (GTC) epilepsy in human clinics. Test application on a small cohort of GTC epileptic and control age- matched subjects confirmed the previously reported functional connectivity between hippocampus and basal ganglia, which validates the computational approach of this pathological brain plasticity. Najimi et al. provide a detailed mapping of the neuropeptide neurotensin high affinity receptors in the neonatal human hypothalamus and its evolution during the first year of age. They thus document developmental plasticity of the brain, reporting in particular strikingly higher densities of neurotensin receptors in the infant posterior hypothalamus than in adult, and a

density decrease in the preoptic area during the first neonatal year. Chigr et al. report a differential effect of acute stress on neurotransmitter expression in the two brain centers of food intake regulation in adult rat. In either center, anorexigenic neuropeptide expression is up-regulated first and followed by delayed upregulation of orexigenic neuropeptides, which accounts for stress-induced anorexia. This phenotypical plasticity occurs earlier in the brainstem satiety center than in the long-term modulatory hypothalamus. El Marzouki et al. investigate the effects of repeated cold stress on spatial learning and memory in adult rat. Daily behavioral evaluation of learning and memory was combined in all experimental rats with electrophysiological assay of hippocampal LTP at the end of the 5-day-period of repeated stress. Gender-differential impacts of stress on brain plasticity were thus characterized. Mahmoud et al. provide the first mapping of nitric oxide (NO)-producing neurons in Urodeles' spinal cord, indicating their involvement in the dually terrestrial-aquatic locomotion of Salamanders. NO is a short-lived gaseous neurotransmitter, which is involved in mammalian plasticity and in brain development. Salamander with its bimodal locomotion is a precious model for the mechanisms underlying the developmental plasticity of vertebrate locomotion.

AUTHOR CONTRIBUTIONS

All authors listed, have made substantial, direct and intellectual contribution to the work, and approved it for publication.

Conflict of Interest Statement: The authors declare that the research was conducted in the absence of any commercial or financial relationships that could be construed as a potential conflict of interest.

Copyright © 2016 Moftah and Moyses. This is an open-access article distributed under the terms of the Creative Commons Attribution License (CC BY). The use, distribution or reproduction in other forums is permitted, provided the original author(s) or licensor are credited and that the original publication in this journal is cited, in accordance with accepted academic practice. No use, distribution or reproduction is permitted which does not comply with these terms.

Leptin is required for hypothalamic regulation of miRNAs targeting POMC 3'UTR

Adel Derghal¹, Mehdi Djelloul^{1,2}, Coraline Airault¹, Clément Pierre³, Michel Dallaporta¹, Jean-Denis Troadec¹, Vanessa Tillement¹, Catherine Tardivel¹, Bruno Bariohay³, Jérôme Trouslard¹ and Lourdes Mounien^{1*}

¹ Faculté des Sciences, Aix Marseille Université, PPSN EA 4674, Marseille, France, ² Stem Cell Laboratory for CNS Disease Modeling, Department of Experimental Medical Science, Wallenberg Neuroscience Centre, Lund Stem Cell Center, Lund University, Lund, Sweden, ³ Biomeostasis, Nutritional Behavior and Metabolic Disorders, Marseille, France

OPEN ACCESS

Edited by:

Marie Z. Mofah,
Alexandria University, Egypt

Reviewed by:

Alexander K. Murashov,
East Carolina University, USA
Sherine Abdel Salam,
Alexandria University, Egypt

*Correspondence:

Lourdes Mounien,
Unité de Recherche Physiologie et
Physio-pathologie du Système
Nerveux Somato-moteur et
Neurovégétatif, Faculté des Sciences,
Université d'Aix-Marseille, Campus St.
Jérôme, BP 351-352, 13397
Marseille, France
lourdes.mounien@univ-amu.fr

Received: 14 November 2014

Accepted: 18 April 2015

Published: 06 May 2015

Citation:

Derghal A, Djelloul M, Airault C, Pierre C, Dallaporta M, Troadec J-D, Tillement V, Tardivel C, Bariohay B, Trouslard J and Mounien L (2015) Leptin is required for hypothalamic regulation of miRNAs targeting POMC 3'UTR. *Front. Cell. Neurosci.* 9:172. doi: 10.3389/fncel.2015.00172

The central nervous system (CNS) monitors modifications in metabolic parameters or hormone levels and elicits adaptive responses such as food intake regulation. Particularly, within the hypothalamus, leptin modulates the activity of pro-opiomelanocortin (POMC) neurons which are critical regulators of energy balance. Consistent with a pivotal role of the melanocortin system in the control of energy homeostasis, disruption of the *POMC* gene causes hyperphagia and obesity. MicroRNAs (miRNAs) are short noncoding RNA molecules that post-transcriptionally repress the expression of genes by binding to 3'-untranslated regions (3'UTR) of the target mRNAs. However, little is known regarding the role of miRNAs that target POMC 3'UTR in the central control energy homeostasis. Particularly, their interaction with the leptin signaling pathway remain unclear. First, we used common prediction programs to search for potential miRNAs target sites on 3'UTR of POMC mRNA. This screening identified a set of conserved miRNAs seed sequences for *mir-383*, *mir-384-3p*, and *mir-488*. We observed that *mir-383*, *mir-384-3p*, and *mir-488* are up-regulated in the hypothalamus of leptin deficient ob/ob mice. In accordance with these observations, we also showed that *mir-383*, *mir-384-3p*, and *mir-488* were increased in db/db mice that exhibit a non-functional leptin receptor. The intraperitoneal injection of leptin down-regulated the expression of these miRNAs of interest in the hypothalamus of ob/ob mice showing the involvement of leptin in the expression of *mir-383*, *mir-384-3p*, and *mir-488*. Finally, the evaluation of responsiveness to intracerebroventricular administration of leptin exhibited that a chronic treatment with leptin decreased *mir-488* expression in hypothalamus of C57BL/6 mice. In summary, these results suggest that leptin modulates the expression of miRNAs that target POMC mRNA in hypothalamus.

Keywords: microRNA, melanocortin, hypothalamus, leptin, food intake

Introduction

The control of energy homeostasis is finely tuned by endocrine and neural mechanisms that cooperate to maintain the balance between caloric intake and energy expenditure. In this respect, the central nervous system (CNS) continuously monitors modifications in metabolic

parameters (blood glucose) and/or hormones (insulin or leptin) and elicits adaptive responses such as food intake regulation and autonomic nervous system modulation (Cowley et al., 2001; Ibrahim et al., 2003; Plum et al., 2006; Mounien et al., 2010). It is now clearly established that specific neuronal networks of the hypothalamus play a pivotal role in energy homeostasis regulation (Morton et al., 2006). For instance, within the arcuate nucleus of the hypothalamus, pro-opiomelanocortin (POMC) neurons are critical regulators of energy balance and glucose homeostasis (Porte et al., 2002; Mounien et al., 2005, 2009, 2010; Parton et al., 2007; Hill et al., 2010). In accordance with this aspect, it has been shown that the disruption of the POMC and melanocortin receptor 4 (MC4R) genes in mice models causes obesity (Huszar et al., 1997; Yaswen et al., 1999), while MC3R gene-deficient mice have normal food consumption but accumulate fat (Chen et al., 2000). In humans, obesity can result from genetic deficiencies which produce a lack in the leptin receptor, POMC, or MC3/4R (Lee, 2009).

One important goal of current research is to identify the molecular mechanisms involved in the control of the expression of genes that are important to maintain energy homeostasis. It has long been acknowledged that the leptin acts as a key regulator of hypothalamic genes expression via different signaling cascades (Morton et al., 2006). For instance, when the leptin binds to the extracellular domain of its receptor (LepR), it recruits and activates the Janus kinase (JAK). JAK binds to and phosphorylates LepR at the same time. This mechanism activates signal transducer and activator of transcription 3 (STAT3). Once phosphorylated, STAT3 binds to POMC promoters, stimulating POMC expression (Morton et al., 2006). Interestingly, mice with genetic inactivation of STAT3 gain body weight (Gao et al., 2004). Altogether, the above collected data strongly suggest that the stability of energy homeostasis during environmental variation requires metabolic adjustments that are achieved through a fine regulation of genes's expression.

Because microRNAs (miRNAs) have been depicted to be another layer of gene regulation, it is not surprising that they are also involved in leptin-regulated gene expression. The miRNAs are endogenous, single-stranded, small, ~22-nucleotides noncoding RNAs, and are generally regarded as negative regulators of gene expression because they inhibit translation and/or promote mRNA degradation by base pairing to complementary sequences within the 3'untranslated region (3'UTR) of protein-coding mRNA transcripts (Bagga et al., 2005). Several studies identified miRNAs that are differentially expressed in the liver, pancreas, and adipose tissue of leptin-deficient (ob/ob) or leptin receptor-deficient (db/db) mice compared to the control animals (Lovis et al., 2008; Li et al., 2009; Nakanishi et al., 2009; Xie et al., 2009). Among these miRNAs, it has been shown that the pancreatic expression levels of *mir-375* are aberrant in ob/ob mice, indicating that they contribute to insulin resistance in this model (Poy et al., 2009). Additional studies provide evidence for the involvement of *mir-335* in lipid metabolism of the liver and the adipose tissue of ob/ob and db/db mice (Nakanishi et al., 2009). In the context of CNS, it has been shown that *mir-200a*, *mir-200b*, and *mir-429* are up-regulated in the hypothalamus of ob/ob and db/db mice (Crépin et al., 2014).

Recently, it has been shown that conditional deletion of the RNase III ribonuclease Dicer (involved in miRNAs maturation) from POMC-expressing cells results in obesity and diabetes which is associated with a neurodegeneration of POMC neurons in the hypothalamus (Schneeberger et al., 2012; Greenman et al., 2013). These observations strongly suggest that miRNAs are important regulators of POMC neuron activity. In this context, the characterization of the miRNAs that target directly POMC mRNA and their interaction with the leptin signaling pathway remain unclear.

In the present study, we focused our attention on the specific miRNAs targeting POMC 3'UTR. Based on bioinformatic predictions of their involvement in POMC-signaling pathway and their conservation among vertebrates, the expression of *mir-383*, *mir-384-3p*, and *mir-488* were investigated in models of obesity characterized by a decrease of POMC mRNA expression and leptin insufficiency (ob/ob) or leptin insensitivity (db/db) (Mizuno et al., 1998). Then, we further analyzed the role of leptin on the expression level of these miRNAs using different models of leptin-treated mice.

Methods

Animals

Experiments were carried out on different types of mice: C57BL/6, ob/ob, and db/db mice were purchased from Charles River (France). Fluorescence *in situ* hybridization (FISH) experiments were performed using male POMC-Tau-Topaz GFP transgenic mice developed by Pinto et al. (2004). To assess GFP expression in POMC-Tau-Topaz GFP mice, we carried out PCR on tail genomic DNA. GFP transgene was detected using the forward primer 5'-GCCACAAGTTCAGCGTGTCC-3' and the reverse primer 5'-GCTTCTCGTTGGGGTCTTTGC-3', with the following PCR conditions: 5 min at 95°C, 36 cycles at 95°C for 30 s, 64°C for 30 s, and 72°C for 40 s, followed by a final step at 72°C for 7 min. The amplicon size was 573 bp.

All animals were individually housed in a pathogen-free facility at controlled temperature on a 12/12 h light/dark cycle (lights from 0700 to 1900 h) with standard pellet diet (AO4) and water available *ad libitum*. All experiments were conducted in conformity with the rules set by the EC Council Directive (2010/63/UE) and the French "Direction Départementale de la Protection des Populations des Bouches-du-Rhône" (License no. 13.435 and no. 13.430). Protocols used are in agreement with the rules set by the Comité d'Éthique de Marseille, our local Committee for Animal Care and Research. Every precaution was taken to minimize animal stress and the number of animals used.

miRNA Prediction

To search for miRNAs that might regulate mouse POMC expression, we used the following public prediction algorithms and database: Targetscan (<http://www.targetscan.org/>) and miRanda (<http://www.microrna.org/microrna/home.do>). Using these different algorithms, we selected the miRNAs that are conserved among the vertebrates (Targetscan) and that have a good miRSVR scores (miRanda).

Surgery and Injections

For the intraperitoneal injection (i.p.), ob/ob, and C57BL/6 mice were injected between 1100 and 1200 h with recombinant murine leptin (Peprotech, France) ($n = 5$, 5 mg/kg) or saline. Mice were sacrificed 4 h after i.p. injection.

Intracerebroventricular (i.c.v.) cannula placement and injections were performed as described previously (Girardet et al., 2011). Animals were anesthetized by an i.p. injection of ketamine (100 mg/kg; Imalgen 1000, Merial, France) and xylazine (6 mg/kg; Rompun, Bayer, France), and placed in a digital stereotaxic apparatus (Model 502600, WPI) coupled to the neurostar software (Neurostar GmbH, Germany). A 26-gauge stainless steel cannula was implanted into the lateral ventricle at the following coordinates: 0.3 mm posterior to bregma, 1.1 mm lateral to the midline, and 2.6 mm ventral to the skull surface. The cannula was secured to the skull with dental cement and sealed with removable obturators. The animals were sutured, placed in individual cages and allowed to recover for 7 days. During this recovery period, animals were injected with physiological saline every day for habituation. One week post-surgery, mice were administered either 10 μ l (2 μ l/min) of physiological saline or leptin (0.5 μ g/ μ l) solution at the beginning of the dark phase. The correct cannula positioning was checked for each animal at the end of the experiment by cresyl violet staining of brain sections (Supplementary Figure 1).

The exogenous leptin was detected in the hypothalamus of ob/ob and C57BL/6 mice after i.p. and i.c.v. injection by western blotting (Supplementary Figure 2 and Supplementary Material).

Quantitative RT-PCR (qRT-PCR) Analysis

Mice were killed by decapitation and the different brain regions were collected and frozen in liquid nitrogen and stored at -80°C until protein or RNA extraction. Total RNA was extracted with TRI Reagent (Sigma-Aldrich, France). For RNA quantification, cDNA was synthesized by 2 μ g total RNA with M-MLV Reverse Transcriptase (Promega Corporation, WI, USA). For miRNAs quantification, cDNA was synthesized by 1 μ g total RNA by the qScript microRNA Quantification System (Quanta Biosciences, MD, USA). For real-time PCR, we used LightCycler 480 (Roche, Germany). We used *Pomc* forward primer 5'-TGAACATCTTTGTCCCC AGAGA-3' and reverse 5'-TGCAGAGGCAAACAAGATTGG-3'; β Actin forward primer 5'-GATCTGGCACCACACCTT CTACA-3' and reverse 5'-TGGCGTGAGGGAGAGCATAG-3'; *Gapdh* forward primer 5'-TTCTCAAGCTCATTTCCT GGTATG-3' and reverse primer 5'-GGATAGGGCCTCTCTTG CTCA-3'. PCR was initiated by one cycle of 95°C for 10 min, followed by 40 cycles of 10 s at 95°C , 30 s at 60°C , and 2 s at 72°C , followed by a holding at 40°C . For miRNAs, *U6* and *Sno202* were used as normalizers for miRNA quantification. For *U6* we used forward primer 5'-ATTGGAACGATACAGAGAAGATT-3' and reverse primer 5'-GGAACGCTTCACGAATTTG-3'; *Sno202* forward primer 5'-CTTTTGAACCCTTTTCCATCTG-3' *mir-383* forward primer 5'-CAGATCAGAAGGTGACTGTG-3'; *mir-384-3p* forward primer 5'-TGTAACAATTCCTAGG CAATGA-3'; *mir-471-3p* forward primer 5'-TGAAAGGTGCCA TACTATGTAT-3'; *mir-488* forward primer 5'-CCCAGATAATA

GCACTCTCAA-3'; for the reverse primers we used the Universal Primer (Quanta Biosciences). We performed quantitative PCR according to the manufacturer's instructions (Quanta Biosciences).

miRNA Fluorescent *In Situ* Hybridization (FISH) and GFP Immunohistochemistry

For the detection of miRNAs in POMC neurons, POMC-Tau-Topaz GFP transgenic mice were perfused intracardially with heparin 10% in PBS-Diethylpyrocarbonate (DEPC)-treated (0.1% PBS, 0.1 M, pH 7.4) followed by 4% PFA in PBS-DEPC maintained at 4°C under ketamine/xylazine anesthesia (100 and 15 mg/kg, respectively). The brains were removed and postfixed for 2 h in 4% PFA/DEPC, cryoprotected for 48 h in 30% sucrose in PBS/DEPC at 4°C and frozen in O.C.T. (Tissue-Tek; Sakura Finetek, USA). Subsequently the brains were sliced at 12 μ m thickness from -1.34 to -2.70 mm relative to bregma and transferred serially on poly-L-lysine and gelatin-coated Super Frost slides (Fisher, PA, USA). Slides were stored at -20°C until FISH. The miRNA FISH was based on Thompson et al. (2007) protocol. Slides were removed from storage at -20°C and air dried at 37°C for 30 min then placed in 4% PFA in PBS-DEPC for 20 min and washed in PBS-DEPC 2 times for 10 min. Sections were treated with 10 mg/ml proteinase K for 6 min at room temperature and washed in PBS-DEPC for 10 min. Fixation with 4% PFA in PBS-DEPC was performed for 15 min and rinse in DEPC-treated water. Slides were treated with acetic anhydride (Triethanolamine, 0.1 M, pH 8.0; Acetic anhydride 1:400) 2 times for 5 min and washed with PBS-DEPC for 10 min. Sections were incubated in pre-hybridization buffer (50% Formamide; $5\times$ SSC; 0.3 mg/ml RNA Yeast; 100 μ g/ml heparin; $1\times$ Denhardt's solution (2% bovine serum albumin, 2% polyvinylpyrrolidone; 2% Ficoll 400); 0.1% Tween 20; 0.1% CHAPS; 5 mM EDTA; 0.3 nmole/ml DNA Random Primer 12-mer) for 2.5 h. Hybridization was performed overnight at 37°C in the same buffer with 3' end 6 Fluorescein amidite (6FAM)-labeled DNA oligonucleotide probes at 5 μ g/ml. We used the antisense probes 5'-AGCCACAGTCACCTTCTGATCTTT-3'-6FAM for *mir-383*; 5'-TTACATTGCCTAGGAATTGTTTACATA-3'-6FAM for *mir-384-3p*; 5'-AAAACCTCTCAGATAATAGAC CCTT-3'-6FAM for *mir-488*. Scrambled probes were used for negative control for each experiment. The scramble sequences were 5'-TTCCGACAACCTGCACTCTATGTTTC-3'-6FAM for scramble (sc) *mir-383*, 5'-CATGAATATTCCGTGGTTAAT CATTTA-3'-6FAM for *scmir-384-3p* and 5'-AGATTCTCAACCT GCTTTACAAAGC-3'-6FAM for *scmir-488*. Slides were washed with $2\times$ SSC for 15 min at 37°C . High-stringency tetramethyl ammonium chloride (TMAC, Acros Organics, NJ, USA) washes were performed 2 times for 5 min at 54°C and 1 time for 10 min at 54°C then rinsed in PBS-DEPC with 0.1% Triton X-100 (PBT) for 10 min. Slides were incubated in PBT with 20% horse serum for 1 h for blocking. Rabbit polyclonal antibody anti-fluorescein (1:500, Gen Tex, TX, USA) and mouse monoclonal anti-GFP (1:500, Abcam, MA, USA) antibodies in PBT with 20% horse serum were added to sections and incubated for overnight at 4°C . Slides were washed three times in PBT for 10 min. Alexa 488 fluor-conjugated goat anti-mouse and Alexa 594

fluor-conjugated donkey anti-rabbit (1:500, Life Technologies, France) with PBS 3% horse serum and 0.3% Triton X-100 were added sequentially to slides for 1.5 h at room temperature and sections were washed three times with PBS.

Sections were finally coverslipped with mounting medium for fluorescence microscope preparation. Sections were observed using a Zeiss LSM 700 confocal microscope (Zeiss, France) associated to ZEN 2012 software and a DXM 1200 Camera (Nikon, France) coupled to ACT-1 software. For quantitative analysis, cells were counted manually using the Image J analysis system (National Institutes of Health, USA). For sections stained for both eGFP and miRNA probes, the double labeled cells were examined at multiple focal levels and at appropriate magnifications to ensure that single cells were indeed immunoreactive for both eGFP and miRNA probes. Because POMC neurons constitute a heterogeneous population in relation to their sensitivity to regulatory factors (Mounien et al., 2006a,b; Williams et al., 2010), the average number of cells counted bilaterally in 8 sections at the anterior and posterior levels of the arcuate nucleus in each animal ($n = 4$) was used for statistical comparisons.

Statistical Analysis

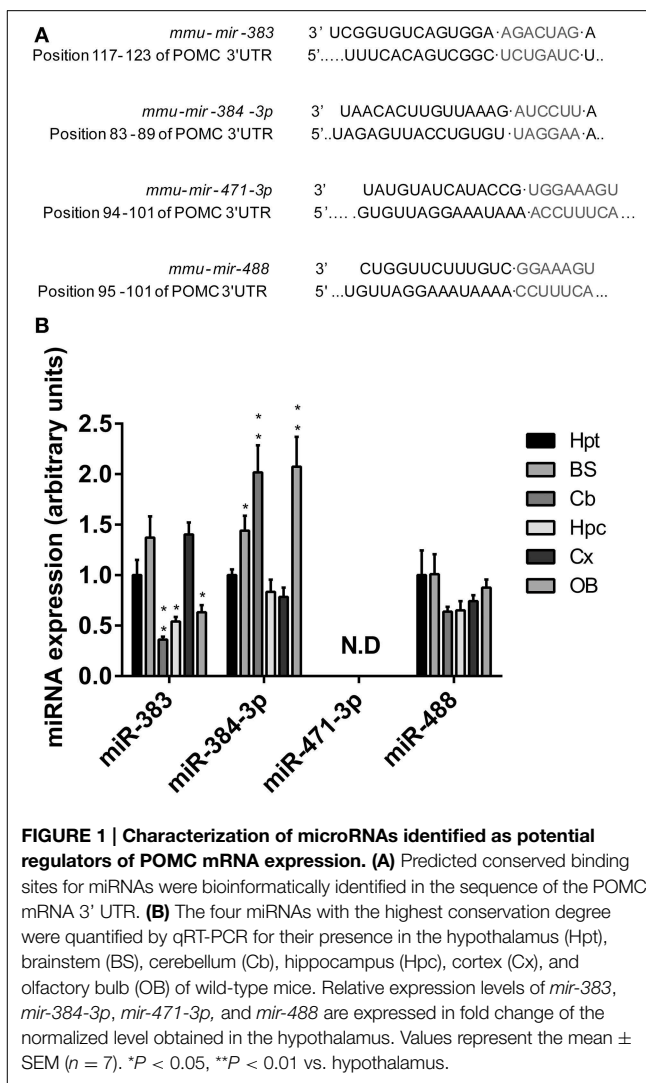
All data are expressed as mean \pm SEM. Statistical analysis was performed by an unpaired 2-tailed Mann-Whitney test. $P < 0.05$ was considered significant.

Results

Identification and Localization of miRNAs of Interest in the Hypothalamus

We used common prediction programs (<http://www.targetscan.org> and <http://www.microrna.org>) to search for potential miRNAs target sites on the 3'UTR of *Pomc* mRNA. In one hand, we identified three conserved miRNAs (*mir-383*, *mir-384-3p*, and *mir-488*) with targetscan.org. In the other hand, the conserved miRNAs with a good miRSVR scores identified with microrna.org are *mir-384-3p*, *mir-371-3p*, and *mir-488* (Figure 1A). The distributions of these miRNAs of interest in the mouse CNS were investigated by means of quantitative PCR.

The expression profiles of *mir-383*, *mir-384-3p*, and *mir-488* miRNAs presented many similarities, but also major differences. Thus, in the CNS, the hypothalamus, brainstem, and cortex were the three regions that contained the highest densities of *mir-383* miRNAs (Figure 1B). In other CNS structures such as the cerebellum, hippocampus, and olfactory bulb, much lower concentrations of *mir-383* miRNA were recorded (Figure 1B). The highest amounts of *mir-384-3p* miRNAs were found in the brainstem, cerebellum, and olfactory bulb (Figure 1B). Lower levels of *mir-384-3p* miRNAs were detected in the hypothalamus, hippocampus, and cortex (Figure 1B). The *mir-488* miRNAs were widely expressed throughout the CNS with the same intensity (Figure 1B). It should be noted that *mir-471-3p* miRNA expression was undetectable whatever the brain region studied (Figure 1B). Considering these expression patterns, we focused our work on *mir-383*, *mir-384-3p* as *mir-488* which are expressed in the hypothalamus.



The miRNAs of Interest are Expressed in the POMC Neurons of the Arcuate Nucleus

In POMC-Tau-Topaz GFP mice model, double-staining of brain sections with the fluorescein-labeled *mir-383* probe and the antibody against GFP showed that a large proportion of neurons in the arcuate nucleus contained simultaneously GFP and *mir-383* miRNAs (Figure 2A). Several GFP neurons did not contain *mir-383* miRNAs and, reciprocally, several *mir-383* miRNAs-expressing neurons did not contain GFP protein (Figure 2A). Similarly, double staining of brain sections with the GFP antibody and *mir-384-3p* or *mir-488* probes showed that a large proportion of GFP neurons expressed *mir-384-3p* or *mir-488* miRNAs (Figures 2B,C). Quantitative analysis of double-labeled neurons showed that, in the whole arcuate nucleus, $80.7 \pm 3.4\%$ of the GFP-positive neurons expressed *mir-383* miRNAs, $39.8 \pm 2.5\%$ of the GFP-positive cells expressed *mir-384-3p* miRNAs and $64.9 \pm 3.2\%$ of the GFP-immunoreactive cells contained *mir-488* miRNAs (Figures 2D-F). The proportion of GFP neurons that exhibited *mir-383*, *mir-384-3p*, or *mir-488* miRNAs were not

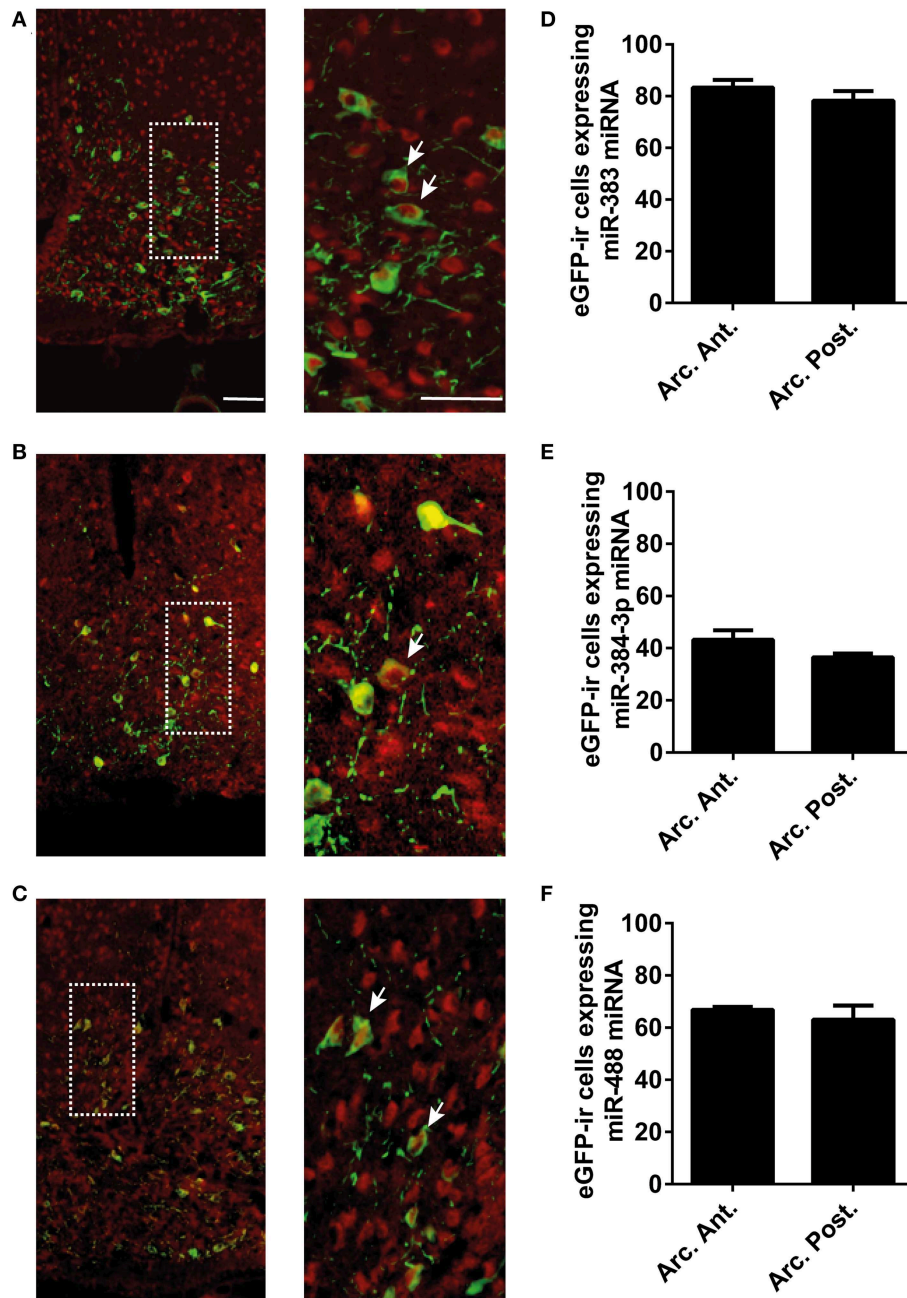


FIGURE 2 | Expression of miR-383, miR-384-3p, and miR-488 in POMC neurons of the arcuate nucleus. (A–C) *In situ* hybridization and immunofluorescence microscopy detection of miRNAs expression in GFP positive neurons at the arcuate nucleus level of POMC-Tau-Topaz GFP mice

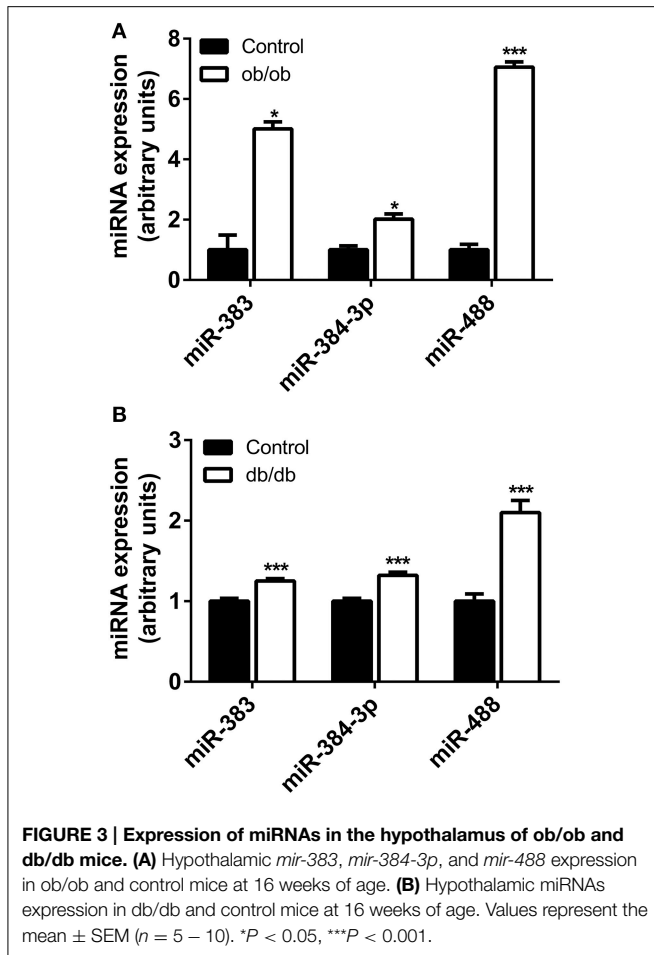
model. **(D–F)** Quantitative analysis of GFP-positive neurons that were labeled with miRNA oligonucleotide probes at anterior (arc. ant.) and posterior (arc. post.) level of the arcuate nucleus. Scale bar = 50 μ m. White arrowheads point to POMC neurons expressing miR-383, miR-384-3p or miR-488 miRNA.

different in the anterior and posterior subdivisions of the arcuate nucleus (**Figures 2D,F**). The control scrambled probes did not produce any labeling (Supplementary Figure 3).

The miRNA of Interest are Up-regulated in the Hypothalamus of *ob/ob* and *db/db* Mice Models

To evaluate whether leptin signaling in hypothalamus is essential for the expression of *mir-383*, *mir-384-3p*, or *mir-488* miRNAs,

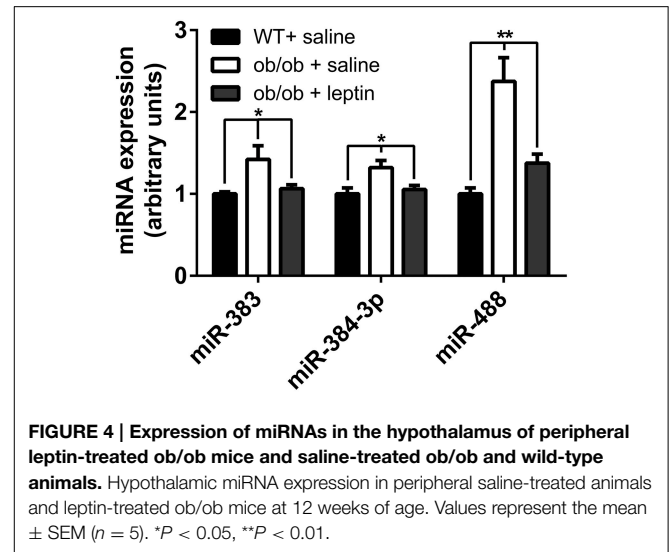
we analyzed the expression of these miRNAs among groups of leptin-deficient (*ob/ob*) mice and C57BL/6 controls. The levels of *mir-383*, *mir-384-3p*, and *mir-488* miRNAs in the hypothalamus of 16-week-old *ob/ob* and C57BL/6 mice were determined by qRT-PCR. Absence of leptin resulted in a significant increase in *mir-383*, *mir-384-3p*, and *mir-488* miRNAs (+400%, +101%; $P < 0.05$ and +605%; $P < 0.001$, respectively) (**Figure 3A**).



Because the lack of circulating leptin was associated with a significant increase in the miRNAs of interest, we measured the expression of *mir-383*, *mir-384-3p*, and *mir-488* miRNAs in the hypothalamus of db/db mice, a model that exhibits a non-functional leptin receptor leading to impaired leptin signaling. As shown in **Figure 3B**, the *mir-383*, *mir-384-3p*, and *mir-488* miRNAs levels were over-expressed in 16-week-old db/db mice compared to C57BL/6 animals (+25, +32 and +110%, respectively; $P < 0.001$).

The Expression of Selected miRNAs are Restored in the Hypothalamus of ob/ob Mice after Peripheral Leptin Administration

The above data suggest that leptin may be involved in the regulation of the expression of *mir-383*, *mir-384-3p*, and *mir-488* miRNAs in the hypothalamus. To directly test this hypothesis, ob/ob mice were i.p. injected with leptin at dose of 5 mg/kg and the hypothalamic expression of *mir-383*, *mir-384-3p*, and *mir-488* miRNAs was evaluated by qRT-PCR 4h later. We observed an up-regulation of *mir-383*, *mir-384-3p*, and *mir-488* miRNAs in 12-week-old ob/ob animals treated with vehicle compared to C57BL/6 control mice (+42, +32%; $P < 0.05$ and +137%; $P < 0.01$, respectively) (**Figure 4**). As expected, leptin treatment



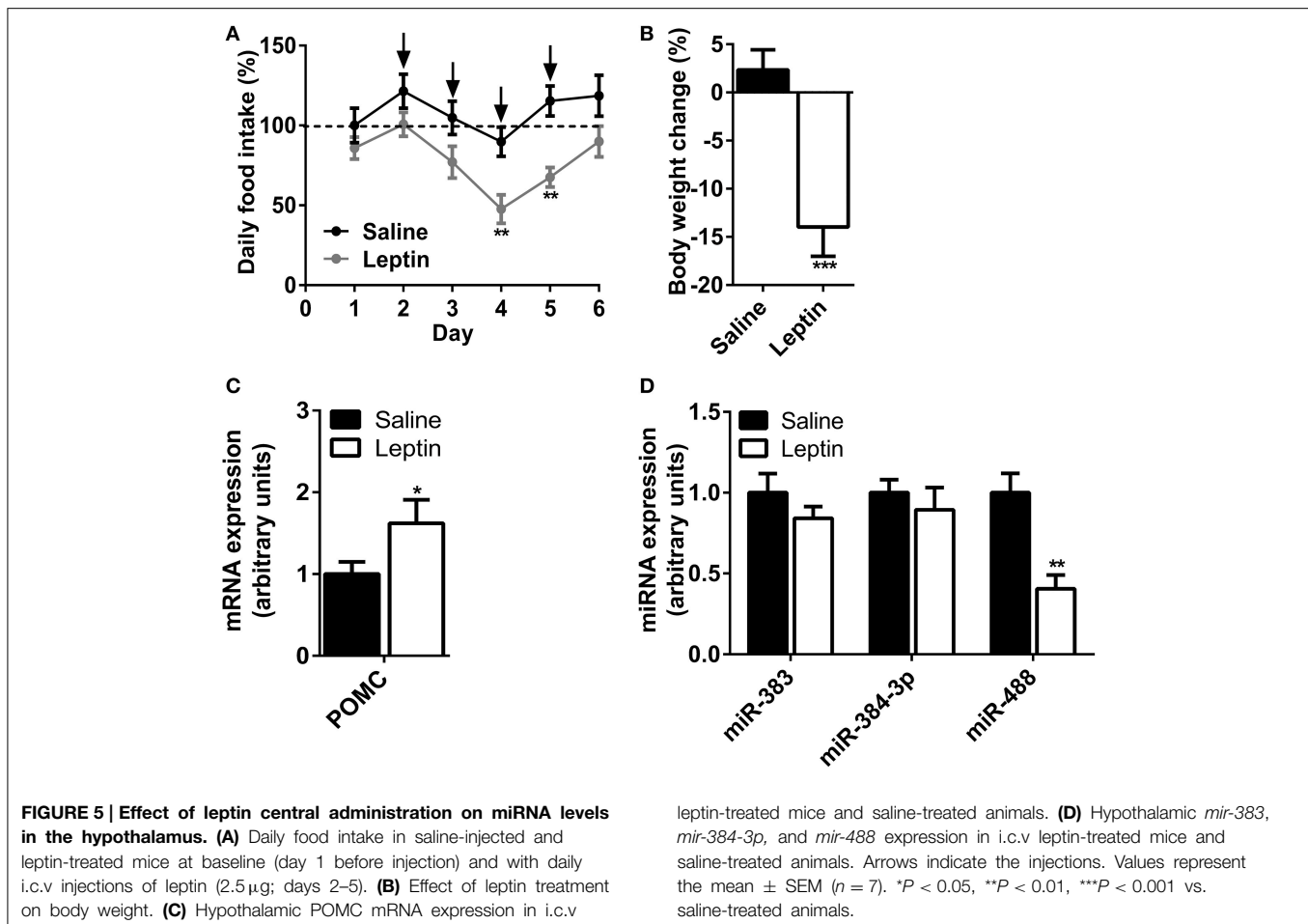
significantly reduced hypothalamic expression of *mir-383*, *mir-384-3p*, and *mir-488* miRNAs in 12-week-old ob/ob animals treated with leptin compared to vehicle-treated ob/ob mice (−25, −21%; $P < 0.05$ and −58%; $P < 0.01$, respectively) (**Figure 4**).

The Expression of *mir-488* is Decreased in the Hypothalamus of C57BL/6 Mice after Central Leptin Administration

Because leptin exhibits a large range of effect at peripheral level (Margetic et al., 2002), we next investigated the effect of a daily i.c.v leptin administration (5 μ g/mice) during 4 days on hypothalamic expression of *mir-383*, *mir-384-3p*, and *mir-488* miRNAs. The sub-chronic i.c.v leptin administration significantly reduced food consumption and body weight gain in C57BL/6 mice when compared with the control animals (**Figures 5A,B**). The i.c.v administration of leptin significantly increased POMC mRNA level in the hypothalamus of leptin-treated group compared with the vehicle-treated animals (+62%; $P < 0.05$) (**Figure 5C**). Concurrently, the effects of leptin on miRNAs levels were evaluated. Chronic i.c.v administration of leptin had no effect on *mir-383* and *mir-384-3p* miRNAs levels (**Figure 5D**). In contrast, leptin significantly decreased *mir-488* miRNA contents in the hypothalamus after treatment (−60%; $P < 0.01$) (**Figure 5D**).

Discussion

The relevance of miRNAs in the function of melanocortin pathways has been recently highlighted by the deletion of *Dicer* in POMC-expressing cells which led to a postnatal ablation of POMC neurons resulting in obesity (Schneeberger et al., 2012; Greenman et al., 2013). In this models, the absence of *Dicer* in POMC-positive neurons led to hyperphagia (Schneeberger et al., 2012) and a decrease of energy expenditure without any increase in food intake (Greenman et al., 2013). Taken together, the data



suggests that miRNAs are essential for the integrity of POMC neuron activity.

Firstly, we studied the pattern of expression of miRNAs, i.e., *mir-383*, *mir-384-3p*, and *mir-488*, in the CNS. It is already established that these miRNAs are highly expressed in the brain (Chiang et al., 2010). In agreement with this data, we have found by using qRT-PCR that the highest concentrations of *mir-383* occurred in the hypothalamus, brainstem, and cortex. The highest amounts of *mir-384-3p* miRNAs were found in the brainstem, cerebellum, and olfactory bulb while *mir-488* miRNAs were widely expressed throughout the structures studied. In many brain regions, *mir-383*, *mir-384-3p*, and *mir-488* miRNAs distribution patterns did not match each other suggesting that the three miRNAs also exert specific roles. For the first time, we found that the miRNAs encoding the *mir-383*, *mir-384-3p*, and *mir-488* miRNAs are abundant in the arcuate nucleus. This indicates that a large proportion of the different cell types present in the nucleus are equipped with these miRNAs of interest. The double-staining of POMC-Tau-Topaz GFP mice brain sections with the fluorescein-labeled probes and an antibody against GFP revealed that a high proportion of POMC neurons express *mir-383*, *mir-384-3p*, and *mir-488*, suggesting that these miRNAs target the expression of protein-coding genes that are distributed in this

neuronal population. Although *mir-383*, *mir-384-3p*, and *mir-488* miRNAs were evenly distributed along the rostro-caudal axis of the arcuate nucleus, the proportion of double labeled GFP/*mir-383*, GFP/*mir-384-3p*, and GFP/*mir-488* neurons did not reflect each other in terms of the proportion of their distribution. These observations are consistent with previous reports demonstrating that POMC neurons constitute a heterogeneous population in relation to their sensitivity to regulatory factors (Mounien et al., 2006a,b; Williams et al., 2010).

In the present context, of special interest is the fact that the POMC neurons are essential for the integration of peripheral signals such as hormones (leptin and insulin) and/or nutrients (glucose) (Morton et al., 2006). For instance, it has been shown recently that leptin directly acts through POMC neurons to stimulate energy expenditure (Berglund et al., 2012). One important goal of current research is to clarify the molecular mechanism involved in the integration of these multiple peripheral metabolic signals such as leptin. One path to reach this goal is to identify the intracellular mediators that allow these POMC neurons to respond to energy status modifications. Interestingly, we observed that the miRNAs targeting POMC mRNAs are up-regulated in *ob/ob* and *db/db* mice models. This data provides the first evidence that the expressions of *mir-383*,

mir-384-3p, and *mir-488* are associated with an impaired leptin signaling pathway. However, the miRNAs that target POMC 3'UTR may modulate the melanocortin system at other levels notably by regulating the expression and/or activity of the prohormone convertases PC1 and PC2 which are required for the processing of POMC and the formation of α -melanocyte-stimulating hormone (Smith and Funder, 1988). In accordance with this hypothesis, we observed in the databases that *mir-488* can also target PC1 3'UTR. In accordance with this hypothesis, PC1 gene expression is different in the arcuate nucleus of leptin-treated obese ob/ob mice (Nilaweera et al., 2003). It is also conceivable that miRNAs may control the biosynthesis of agouti-related protein; the endogenous antagonist of melanocortin receptors MC3R and MC4R (Ollmann et al., 1997).

Several miRNAs have been reported to be differentially expressed in the hypothalamus of ob/ob and db/db mice, but their precise role in the regulation of the hypothalamus function remains to be determined. Recently, it has been shown that *mir-200a*, *mir-200b*, and *mir-429* are up-regulated in the hypothalamus of ob/ob and db/db mice (Crépin et al., 2014). The same group showed that daily injection of a pegylated leptin antagonist predisposed rats to obesity, promoted leptin resistance and modified the hypothalamic miRNA expression profile (Benoit et al., 2013). In our study, we identified the presence of new miRNAs that are expressed differently in the hypothalamus of ob/ob and db/db animals compared to control mice. Additional studies will be necessary to understand the regulation of these different miRNAs in the hypothalamus during the progressive onset of the obese phenotype and to determine their complex role in the regulation of feeding behavior.

We observed that the fold change modification of the selected miRNAs in the ob/ob mice increased in an age dependent way. These results suggest that age positively regulates miRNAs expression in ob/ob mice. In accordance with this hypothesis, it has been also shown that *mir-184* is differentially expressed in the pancreatic islets of ob/ob mice from age 4–16 weeks (Tattikota et al., 2014). The present study shows that leptin peripheral treatment rescues the expression of *mir-383*, *mir-384-3p*, and *mir-488* in ob/ob mice. Thus, together with the altered expression of these miRNAs in ob/ob and db/db mice, these results support the idea that leptin plays an important role in the expression of the miRNAs that target POMC mRNA in the hypothalamus. However, leptin exhibits a wide range of effects at peripheral level (Margetic et al., 2002) and its effect on miRNAs expression in the hypothalamus could thus be indirect. In order to test the effect at central level, we then performed chronic i.c.v infusion of leptin. Surprisingly, i.c.v administration of leptin in mice only decreased the expression of *mir-488* in the hypothalamus suggesting that the expression of *mir-488* is under the control of leptin. The absence of effect by central infusion of leptin on the hypothalamic expression of *mir-383* and *mir-384-3p* can be explained by the peripheral effect of leptin. For instance, it has been shown that leptin increases insulin secretion which in turn modulates the POMC neurons activity and may modulate miRNA expression (Ceddia et al., 1999; Hill et al., 2010).

Interestingly, bioinformatics prediction analysis indicates that the miRNAs targeting POMC can also target genes involved

in the leptin signaling pathways such as STAT3 as well as the leptin receptor. For instance, *mir-488* could modulate the expression of STAT3. These observations suggest that, *mir-383*, *mir-384-3p*, and *mir-488* in the arcuate nucleus are involved in a complex network controlling the sensitivity of POMC neurons to peripheral signals. Additional *in vitro* experiments could clarify this last point. Recently, numerous studies identified several miRNAs as important for the hypothalamic regulation of energy homeostasis. Herzer et al. identified *mir-7a* as a hypothalamic-enriched miRNA with a high expression in Neuropeptide Y/Agouti-related orexigenic peptide neurons (Herzer et al., 2012). Interestingly, two extreme conditions of nutritional stress, i.e., caloric restriction and high fat diet-induced obesity, modified the hypothalamic pattern of expression of a set of miRNAs including *let7a*, *mir-9**, *mir-30e*, *mir-132*, *mir-145*, *mir-200a*, and *mir-218* (Sangiao-Alvarellos et al., 2014). Taken altogether, these different studies point to the importance of miRNAs as regulators and sensors of central energy homeostasis.

In conclusion, we observed that the impairment of leptin synthesis or signaling, induced a defect in the hypothalamic expression of a subset of miRNAs that target POMC 3'UTR. It was observed that *mir-383*, *mir-384-3p*, and *mir-488* were up-regulated in ob/ob and db/db mice and *mir-488* was down-regulated in leptin-treated mice. This indicates that the miRNAs that target POMC important mediators of leptin action in the hypothalamus. New miRNAs modulated by leptin could open important therapeutic perspectives for controlling metabolic disorders.

Author Contributions

LM planned the project. AD, MD, CA, CP, MD, VT, and CT performed experiments. LM wrote the manuscript. JT, BB, and JT helped with data evaluation, interpretation, and manuscript preparation.

Acknowledgments

This research was supported by funding obtained from Aix-Marseille University, the “Région Provence-Alpes-Côte d’Azur,” the “Conseil Général des Bouches-du-Rhône” (PACA, CG13) and Benjamin Delessert foundation. We also thank the Aix-Marseille University Microscopy Center CP2M for the access to confocal Microscopy and the AVB platform (Analyse et Valorisation de la Biodiversité, iSm2, UMR 7313, Marseille). AD is the recipient of a doctoral fellowship from the Ministry of Education. The authors are grateful to O. Knowles and S. Mounien for critical reading of the manuscript. We thank D. Chabbert for expert help with intracerebroventricular injection and Dr. M. Maresca for the gift of antibodies.

Supplementary Material

The Supplementary Material for this article can be found online at: <http://journal.frontiersin.org/article/10.3389/fncel.2015.00172/abstract>

References

- Bagga, S., Bracht, J., Hunter, S., Massirer, K., Holtz, J., Eachus, R., et al. (2005). Regulation by let-7 and lin-4 miRNAs results in target mRNA degradation. *Cell* 122, 553–563. doi: 10.1016/j.cell.2005.07.031
- Benoit, C., Ould-Hamouda, H., Crepin, D., Gertler, A., Amar, L., and Taouis, M. (2013). Early leptin blockade predisposes fat-fed rats to overweight and modifies hypothalamic microRNAs. *J. Endocrinol.* 218, 35–47. doi: 10.1530/JOE-12-0561
- Berglund, E. D., Vianna, C. R., Donato, J. Jr., Kim, M. H., Chuang, J.-C., Lee, C. E., et al. (2012). Direct leptin action on POMC neurons regulates glucose homeostasis and hepatic insulin sensitivity in mice. *J. Clin. Invest.* 122, 1000–1009. doi: 10.1172/JCI59816
- Ceddia, R. B., William, W. N. Jr., Carpinelli, A. R., and Curi, R. (1999). Modulation of insulin secretion by leptin. *Gen. Pharmacol.* 32, 233–237. doi: 10.1016/S0306-3623(98)00185-2
- Chen, A. S., Marsh, D. J., Trumbauer, M. E., Frazier, E. G., Guan, X. M., Yu, H., et al. (2000). Inactivation of the mouse melanocortin-3 receptor results in increased fat mass and reduced lean body mass. *Nat. Genet.* 26, 97–102. doi: 10.1038/79254
- Chiang, H. R., Schoenfeld, L. W., Ruby, J. G., Auyeung, V. C., Spies, N., Baek, D., et al. (2010). Mammalian microRNAs: experimental evaluation of novel and previously annotated genes. *Genes Dev.* 24, 992–1009. doi: 10.1101/gad.1884710
- Cowley, M. A., Smart, J. L., Rubinstein, M., Cerdán, M. G., Diano, S., Horvath, T. L., et al. (2001). Leptin activates anorexigenic POMC neurons through a neural network in the arcuate nucleus. *Nature* 411, 480–484. doi: 10.1038/35078085
- Crépin, D., Benomar, Y., Riffault, L., Amine, H., Gertler, A., and Taouis, M. (2014). The over-expression of miR-200a in the hypothalamus of ob/ob mice is linked to leptin and insulin signaling impairment. *Mol. Cell. Endocrinol.* 384, 1–11. doi: 10.1016/j.mce.2013.12.016
- Gao, Q., Wolfgang, M. J., Neschen, S., Morino, K., Horvath, T. L., Shulman, G. I., et al. (2004). Disruption of neural signal transducer and activator of transcription 3 causes obesity, diabetes, infertility, and thermal dysregulation. *Proc. Natl. Acad. Sci. U.S.A.* 101, 4661–4666. doi: 10.1073/pnas.0303992101
- Girardet, C., Bonnet, M. S., Jdir, R., Sadoud, M., Thirion, S., Tardivel, C., et al. (2011). Central inflammation and sickness-like behavior induced by the food contaminant deoxynivalenol: a PGE2-independent mechanism. *Toxicol. Sci.* 124, 179–191. doi: 10.1093/toxsci/kfr219
- Greenman, Y., Kuperman, Y., Drori, Y., Asa, S. L., Navon, I., Forkosh, O., et al. (2013). Postnatal ablation of POMC neurons induces an obese phenotype characterized by decreased food intake and enhanced anxiety-like behavior. *Mol. Endocrinol. (Baltimore Md)* 27, 1091–1102. doi: 10.1210/me.2012-1344
- Herzer, S., Silahatoglu, A., and Meister, B. (2012). Locked nucleic acid-based *in situ* hybridisation reveals miR-7a as a hypothalamus-enriched microRNA with a distinct expression pattern. *J. Neuroendocrinol.* 24, 1492–1504. doi: 10.1111/j.1365-2826.2012.02358.x
- Hill, J. W., Elias, C. F., Fukuda, M., Williams, K. W., Berglund, E. D., Holland, W. L., et al. (2010). Direct insulin and leptin action on pro-opiomelanocortin neurons is required for normal glucose homeostasis and fertility. *Cell Metab.* 11, 286–297. doi: 10.1016/j.cmet.2010.03.002
- Huszar, D., Lynch, C. A., Fairchild-Huntress, V., Dunmore, J. H., Fang, Q., Berkemeier, L. R., et al. (1997). Targeted disruption of the melanocortin-4 receptor results in obesity in mice. *Cell* 88, 131–141. doi: 10.1016/S0092-8674(00)81865-6
- Ibrahim, N., Bosch, M. A., Smart, J. L., Qiu, J., Rubinstein, M., Ronnekleiv, O. K., et al. (2003). Hypothalamic proopiomelanocortin neurons are glucose responsive and express K(ATP) channels. *Endocrinology* 144, 1331–1340. doi: 10.1210/en.2002-221033
- Lee, Y. S. (2009). The role of leptin-melanocortin system and human weight regulation: lessons from experiments of nature. *Ann. Acad. Med. Singapore* 38, 34–41.
- Li, S., Chen, X., Zhang, H., Liang, X., Xiang, Y., Yu, C., et al. (2009). Differential expression of microRNAs in mouse liver under aberrant energy metabolic status. *J. Lipid Res.* 50, 1756–1765. doi: 10.1194/jlr.M800509-JLR200
- Lovis, P., Roggli, E., Laybutt, D. R., Gattesco, S., Yang, J.-Y., Widmann, C., et al. (2008). Alterations in microRNA expression contribute to fatty acid-induced pancreatic beta-cell dysfunction. *Diabetes* 57, 2728–2736. doi: 10.2337/db07-1252
- Margetic, S., Gazzola, C., Pegg, G. G., and Hill, R. A. (2002). Leptin: a review of its peripheral actions and interactions. *Int. J. Obes. Relat. Metab. Disord.* 26, 1407–1433. doi: 10.1038/sj.ijo.0802142
- Mizuno, T. M., Kleopoulos, S. P., Bergen, H. T., Roberts, J. L., Priest, C. A., and Mobbs, C. V. (1998). Hypothalamic Pro-opiomelanocortin mRNA is reduced by fasting in ob/ob and db/db mice, but is stimulated by Leptin. *Diabetes* 47, 294–297. doi: 10.2337/diab.47.2.294
- Morton, G. J., Cummings, D. E., Baskin, D. G., Barsh, G. S., and Schwartz, M. W. (2006). Central nervous system control of food intake and body weight. *Nature* 443, 289–295. doi: 10.1038/nature05026
- Mounien, L., Bizet, P., Boutelet, I., Gourcerol, G., Basille, M., Gonzalez, B., et al. (2006a). Expression of PACAP receptor mRNAs by neuropeptide Y neurons in the rat arcuate nucleus. *Ann. N.Y. Acad. Sci.* 1070, 457–461. doi: 10.1196/annals.1317.061
- Mounien, L., Bizet, P., Boutelet, I., Gourcerol, G., Fournier, A., Vaudry, H., et al. (2006b). Pituitary adenylate cyclase-activating polypeptide directly modulates the activity of proopiomelanocortin neurons in the rat arcuate nucleus. *Neuroscience* 143, 155–163. doi: 10.1016/j.neuroscience.2006.07.022
- Mounien, L., Bizet, P., Boutelet, I., Vaudry, H., and Jégou, S. (2005). Expression of melanocortin MC3 and MC4 receptor mRNAs by neuropeptide Y neurons in the rat arcuate nucleus. *Neuroendocrinology* 82, 164–170. doi: 10.1159/000091737
- Mounien, L., Do Rego, J.-C., Bizet, P., Boutelet, I., Gourcerol, G., Fournier, A., et al. (2009). Pituitary adenylate cyclase-activating polypeptide inhibits food intake in mice through activation of the hypothalamic melanocortin system. *Neuropsychopharmacology* 34, 424–435. doi: 10.1038/npp.2008.73
- Mounien, L., Marty, N., Tarussio, D., Metref, S., Genoux, D., Preitner, F., et al. (2010). Glut2-dependent glucose-sensing controls thermoregulation by enhancing the leptin sensitivity of NPY and POMC neurons. *FASEB J.* 24, 1747–1758. doi: 10.1096/fj.09-144923
- Nakanishi, N., Nakagawa, Y., Tokushige, N., Aoki, N., Matsuzaka, T., Ishii, K., et al. (2009). The up-regulation of microRNA-335 is associated with lipid metabolism in liver and white adipose tissue of genetically obese mice. *Biochem. Biophys. Res. Commun.* 385, 492–496. doi: 10.1016/j.bbrc.2009.05.058
- Nilaweera, K. N., Barrett, P., Mercer, J. G., and Morgan, P. J. (2003). Precursor-protein convertase 1 gene expression in the mouse hypothalamus: differential regulation by ob gene mutation, energy deficit and administration of leptin, and coexpression with prepro-orexin. *Neuroscience* 119, 713–720. doi: 10.1016/S0306-4522(02)00869-2
- Ollmann, M. M., Wilson, B. D., Yang, Y. K., Kerns, J. A., Chen, Y., Gantz, I., et al. (1997). Antagonism of central melanocortin receptors *in vitro* and *in vivo* by agouti-related protein. *Science* 278, 135–138. doi: 10.1126/science.278.5335.135
- Parton, L. E., Ye, C. P., Coppari, R., Enriori, P. J., Choi, B., Zhang, C.-Y., et al. (2007). Glucose sensing by POMC neurons regulates glucose homeostasis and is impaired in obesity. *Nature* 449, 228–232. doi: 10.1038/nature06098
- Pinto, S., Roseberry, A. G., Liu, H., Diano, S., Shanabrough, M., Cai, X., et al. (2004). Rapid rewiring of arcuate nucleus feeding circuits by Leptin. *Science* 304, 110–115. doi: 10.1126/science.1089459
- Plum, L., Belgardt, B. F., and Brüning, J. C. (2006). Central insulin action in energy and glucose homeostasis. *J. Clin. Invest.* 116, 1761–1766. doi: 10.1172/JCI29063
- Porte, D. Jr., Baskin, D. G., and Schwartz, M. W. (2002). Leptin and insulin action in the central nervous system. *Nutr. Rev.* 60, S20–S29. discussion: S68–S84, 85–87. doi: 10.1301/002966402320634797
- Poy, M. N., Hausser, J., Trajkovski, M., Braun, M., Collins, S., Rorsman, P., et al. (2009). miR-375 maintains normal pancreatic alpha- and beta-cell mass. *Proc. Natl. Acad. Sci. U.S.A.* 106, 5813–5818. doi: 10.1073/pnas.0810550106
- Sangiao-Alvarellos, S., Pena-Bello, L., Manfredi-Lozano, M., Tena-Sempere, M., and Cordido, F. (2014). Perturbation of hypothalamic microRNA expression patterns in male rats after metabolic distress: impact of obesity and conditions of negative energy balance. *Endocrinology* 155, 1838–1850. doi: 10.1210/en.2013-1770
- Schneeberger, M., Altirriba, J., García, A., Esteban, Y., Castaño, C., García-Lavandera, M., et al. (2012). Deletion of miRNA processing enzyme Dicer in POMC-expressing cells leads to pituitary dysfunction, neurodegeneration and development of obesity. *Mol. Metab.* 2, 74–85. doi: 10.1016/j.molmet.2012.10.001

- Smith, A. I., and Funder, J. W. (1988). Proopiomelanocortin processing in the pituitary, central nervous system, and peripheral tissues. *Endocr. Rev.* 9, 159–179. doi: 10.1210/edrv-9-1-159
- Tattikota, S. G., Rathjen, T., McAnulty, S. J., Wessels, H.-H., Akerman, I., van de Bunt, M., et al. (2014). Argonaute2 mediates compensatory expansion of the pancreatic β cell. *Cell Metab.* 19, 122–134. doi: 10.1016/j.cmet.2013.11.015
- Thompson, R. C., Deo, M., and Turner, D. L. (2007). Analysis of microRNA expression by *in situ* hybridization with RNA oligonucleotide probes. *Methods (San Diego Calif.)* 43, 153–161. doi: 10.1016/j.ymeth.2007.04.008
- Williams, K. W., Margatho, L. O., Lee, C. E., Choi, M., Lee, S., Scott, M. M., et al. (2010). Segregation of acute leptin and insulin effects in distinct populations of arcuate proopiomelanocortin neurons. *J. Neurosci.* 30, 2472–2479. doi: 10.1523/JNEUROSCI.3118-09.2010
- Xie, H., Lim, B., and Lodish, H. F. (2009). MicroRNAs induced during adipogenesis that accelerate fat cell development are downregulated in obesity. *Diabetes* 58, 1050–1057. doi: 10.2337/db08-1299
- Yaswen, L., Diehl, N., Brennan, M. B., and Hochgeschwender, U. (1999). Obesity in the mouse model of pro-opiomelanocortin deficiency responds to peripheral melanocortin. *Nat. Med.* 5, 1066–1070. doi: 10.1038/12506

Conflict of Interest Statement: The authors declare that the research was conducted in the absence of any commercial or financial relationships that could be construed as a potential conflict of interest.

Copyright © 2015 Derghal, Djelloul, Airault, Pierre, Dallaporta, Troadec, Tillement, Tardivel, Bariohay, Trouslard and Mounien. This is an open-access article distributed under the terms of the Creative Commons Attribution License (CC BY). The use, distribution or reproduction in other forums is permitted, provided the original author(s) or licensor are credited and that the original publication in this journal is cited, in accordance with accepted academic practice. No use, distribution or reproduction is permitted which does not comply with these terms.



Leptin-dependent neurotoxicity via induction of apoptosis in adult rat neurogenic cells

Stéphanie Segura^{1†}, Laurie Efthimiadi^{2†}, Christophe Porcher², Sandrine Courtes², Valérie Coronas³, Slavica Krantic^{2,4‡} and Emmanuel Moyses^{1*‡}

¹ Physiologie de la Reproduction et des Comportements, UMR 85 Institut National de la Recherche Agronomique, Centre INRA de Tours, Université François Rabelais de Tours, Nouzilly, France, ² Institut National de la Santé et de la Recherche Médicale Unité 901, Institut de Neurobiologie de la Méditerranée, Parc Scientifique de Luminy, Aix-Marseille Université, Marseille, France, ³ Signalisation et Transports Ioniques Membranaires, ERL 7368 Centre National de la Recherche Scientifique, Université de Poitiers, Poitiers, France, ⁴ Centre de Recherche des Cordeliers, UMR_S 1138 INSERM, Paris Descartes University, Sorbonne Paris Cité, Pierre and Marie Curie University, Paris, France

OPEN ACCESS

Edited by:

Gerald W. Zamponi,
University of Calgary, Canada

Reviewed by:

Oliver von Bohlen und Halbach,
Universitätsmedizin Greifswald,
Germany

João O. Malva,
University of Coimbra, Portugal

*Correspondence:

Emmanuel Moyses,
UMR 85 Institut National de la
Recherche Agronomique, Centre
INRA de Tours, Université François
Rabelais de Tours, 37380 Nouzilly,
France
emmanuel.moyse@univ-tours.fr

[†] These authors have contributed
equally to this work as first co-authors.

[‡] These authors have contributed
equally to this work as co-directors.

Received: 03 September 2014

Accepted: 21 August 2015

Published: 07 September 2015

Citation:

Segura S, Efthimiadi L, Porcher C,
Courtes S, Coronas V, Krantic S and
Moyse E (2015) Leptin-dependent
neurotoxicity via induction of
apoptosis in adult rat neurogenic cells.
Front. Cell. Neurosci. 9:350.
doi: 10.3389/fncel.2015.00350

Adipocyte-derived hormone leptin has been recently implicated in the control of neuronal plasticity. To explore whether modulation of adult neurogenesis may contribute to leptin control of neuronal plasticity, we used the neurosphere assay of neural stem cells derived from the adult rat subventricular zone (SVZ). Endogenous expression of specific leptin receptor (ObRb) transcripts, as revealed by RT-PCR, is associated with activation of both ERK and STAT-3 pathways via phosphorylation of the critical ERK/STAT-3 amino acid residues upon addition of leptin to neurospheres. Furthermore, leptin triggered withdrawal of neural stem cells from the cell cycle as monitored by Ki67 labeling. This effect was blocked by pharmacological inhibition of ERK activation thus demonstrating that ERK mediates leptin effects on neural stem cell expansion. Leptin-dependent withdrawal of neural stem cells from the cell cycle was associated with increased apoptosis, as detected by TUNEL, which was preceded by cyclin D1 induction. Cyclin D1 was indeed extensively colocalized with TUNEL-positive, apoptotic nuclei. Cyclin-D1 silencing by specific shRNA prevented leptin-induced decrease of the cell number per neurosphere thus pointing to the causal relationship between leptin actions on apoptosis and cyclin D1 induction. Leptin target cells in SVZ neurospheres were identified by double TUNEL/phenotypic marker immunocytofluorescence as differentiating neurons mostly. The inhibition of neural stem cell expansion via ERK/cyclin D1-triggered apoptosis defines novel biological action of leptin which may be involved in adiposity-dependent neurotoxicity.

Keywords: leptin, neurospheres, adult neural stem cells, proliferation, neuronal death, STAT3, ERK, rat

Abbreviations: aCSF, artificial cerebrospinal fluid; AKT, protein kinase B; AMPK, 5'-adenosine monophosphate-activated protein kinase; bFGF, basic fibroblast growth factor; CNTF, ciliary neurotrophic factor; DAPI, diamidino-2-phenylindole; DIV, days *in vitro*; DMEM, Dulbecco's modified Eagle's medium; EGF, epidermal growth factor; ERK, extracellular signal-regulated kinase; MAPK, mitogen-activated protein kinase; ObRb, leptin receptor; PCR, polymerase chain reaction; RNA, ribonucleic acid; shRNA, short hairpin ribonucleic acid; siRNA, silencing RNA; STAT, signal transducer and activator of transcription; SVZ, subventricular zone.

Introduction

Leptin has been identified as a fat storage-reducing hormone in adipose tissue (Zhang et al., 1994). In adult mammals, it is secreted by adipocytes proportionally to their lipidic charge and negatively regulates energy homeostasis (Oswal and Yeo, 2010). Leptin also exerts direct long-term inhibition of feeding behavior at the central level by regulating the key centres of food intake, including hypothalamus (Grill and Hayes, 2012; Morton et al., 2014). These leptin actions are mediated by specific membrane receptors (OBRb; Villanueva and Myers, 2008) that are widely distributed in the adult brain (Elmqvist et al., 1998; Myers et al., 2009). Activation of OBRb by leptin binding triggers multiple signaling pathways: (i) Signal Transducer and Activator of Transcription 3 (STAT3), (ii) mitogen-activated protein kinase (MAPK)/extracellular signal-regulated kinase (ERK), (iii) phosphatidylinositol 3-kinase (PI3K)-AKT cascades, (iv) STAT5, (v) 5' adenosine monophosphate-activated protein kinase (AMPK; Villanueva and Myers, 2008; Coppari and Bjørnbæk, 2012).

At the cellular level, leptin regulates structural plasticity of the neuronal networks in rodent hypothalamus, both during development (Bouret et al., 2004; Bouret, 2013) and in adult (Pinto et al., 2004). Among the mechanisms regulating neuronal network plasticity inherent to physiological adaptations, neurogenesis has been established to play an important role (Braun and Jessberger, 2014). Notably, the adult neurogenesis located to the neurogenic niche of rodent hypothalamus (Cheng, 2013; Hann et al., 2013), has been recently involved in food intake regulation (Kokoeva et al., 2005; Pierce and Xu, 2010; Lee et al., 2012; McNay et al., 2012). In addition, leptin has been shown to stimulate adult neurogenesis in murine hypothalamus *in vivo* via expansion of hypothalamic neural stem cells in the context of energy homeostasis and feeding (McNay et al., 2012; Bless et al., 2014).

Food intake regulation is also determined by olfactory perception and memory which is shaped by adult neurogenesis in olfactory bulb (Gheusi and Lledo, 2014) and is modulated by leptin (Palouzier-Paulignan et al., 2012). The exclusive source of olfactory bulb adult neurogenesis is the neural stem cell niche of the subventricular zone of the telencephalon (SVZ) (Braun and Jessberger, 2014). However, SVZ has not been investigated so far in terms of possible regulation of adult neurogenesis by leptin. In the present study, we therefore asked whether leptin regulates adult neurogenesis in the SVZ. To address this question, we used the *in vitro* culture system known as the neurosphere assay (Louis et al., 2013) and analyzed leptin effects on neurospheres derived from adult rat SVZ.

Materials and Methods

Animals

Forty adult male Wistar rats (ICO: OFA-S.D. [IOPS.Caw]; Charles River, Les Oncins, France), weighing 150–200 g, were used in this study. These animals were bred and handled in accordance with the Guide for the Care and Use of Laboratory Animals (National Research Council, 1996) and the

European Communities Council Directive of 24 November 1986 (86/609/EEC). The experimental protocols were carried out in compliance with institutional Ethical Committee guidelines for animal research. All efforts were made to minimize the number of animals used and their suffering.

Primary Culture of Neural Stem Cells

The “neurosphere assay” was performed as previously described (Charrier et al., 2006; Louis et al., 2013). Brains were obtained from adult rats anesthetized and euthanized by decapitation. 500 μm -thick coronal forebrain slices were rapidly cut with a tissue-chopper at the level of anterior striatum, and transferred into ice-cold low-calcium artificial cerebrospinal fluid (aCSF: 124 mM NaCl, 5 mM KCl, 3.2 mM MgCl₂, 0.1 mM CaCl₂, 26 mM NaHCO₃, 100 mM glucose, pH 7.38) for microdissection of the SVZ under binoculars. The tissue samples were digested in 10 U activated papain (Sigma, L'Isle d'Abeau, France) and then by 1X TrypLe™ Express (Invitrogen, Cergy-Pontoise, France), each for 8 min at 37°C, while being triturated gently with a pipet cone. The resulting cell suspension was diluted with 800 μL of culture medium (DMEM [Sigma], 20 μM HEPES [Invitrogen], 200 U/mL penicilline and 200 $\mu\text{g}/\text{mL}$ streptomycine [Invitrogen], 1X B27 [Invitrogen, Cergy Pontoise, France], 20 ng/mL basic Fibroblast Growth Factor (bFGF) [Invitrogen], 8 or 20 ng/mL Epidermal Growth Factor (EGF) [Invitrogen]). The cell suspension was then centrifuged at 400 \times g for 8 min, the pellet was resuspended in 500 μL of culture medium and triturated with a 1 mL 26G syringe. The cells were seeded at 10,000 cells per 1 mL culture medium per well (24-well plates for non-adherent cells [Corning, Avon, France]) with or without murine recombinant leptin [Amgen, Thousand Oaks, CA, USA]). For passaging, the neurospheres were pooled in a tube and incubated for 30 min at 37°C in 1 mL TrypLe™ Express (Invitrogen). The cell suspension was then diluted with 800 μL of culture medium and centrifuged. The resulting pellet was dissociated, the cell density was counted and adjusted as above. Cell culture medium was changed every 2 days and, when relevant, leptin was added daily.

Cytochemical Assays

For cytochemical assays, primary cultures of adult rat SVZ EGF were grown in the presence of 8 nM during 5 DIV on poly-D-lysine (Sigma)-coated glass coverslips (inserted at the bottom of the 24-well plates) in the absence (control) or in the presence of leptin at the physiologically relevant dose 6.2 nM (Bariohay et al., 2005), rinsed in PBS, fixed 30 min at 4°C with a 4% paraformaldehyde solution in 0.05 M sodium phosphate buffer (pH 7.4), rinsed three times in PBS, and permeabilized in PBS containing 0.1% Triton X-100 and 1% BSA. For immunocytochemistry, primary antibodies (list in **Table 1**) were incubated in PBS containing 0.1% Triton X-100, 1% BSA, 1% normal serum overnight at 4°C, revealed with relevant Alexa-fluorescent secondary antibodies, counterstained with diamidino-2-phenylindole (DAPI) and mounted on glass slides with Vectashield (Vector labs). *In situ* labeling of apoptotic nuclear DNA fragmentation (TUNEL assay) was performed as previously described (Bauer et al., 2003) for initial quantification

TABLE 1 | List of primary antibodies and details of immunohistochemical procedures used.

Antigen	Source	Cell-type specificity	Dilution
Nestin	Mouse monoclonal, Millipore	Neural stem cells	1:300
Sox-2	Goat polyclonal, Santa-Cruz	Neural stem cells	1:100
Doublecortin (DCX)	Goat polyclonal, Santa-Cruz	Immature/migrating neurons	1:200
Ki-67	Mouse monoclonal, BD Biosciences	Proliferating cells in cell cycle	1:1,000
Cyclin D1	Rabbit monoclonal, Neomarker	Cycling cells in G1/S phases	1:500
Glial fibrillary acidic protein (GFAP)	Rabbit polyclonal, Dako	Astrocytes, neural stem cells, radial glia	1:500
S-100- β	Rabbit polyclonal, Dako, Z0311	Astrocytes	1:400
Oligodendrocytic protein O4	Rabbit polyclonal, Chemicon	Oligodendrocytes	1:75
Microtubule-associated protein-2 (MAP2)	Mouse monoclonal, Sigma-Aldrich	Mature neurons	1:300–1:500
Axonal β III-tubulin	Mouse monoclonal, Sigma-Aldrich	Mature neurons	1:150

of leptin effects. Briefly, the coverslips were incubated 15 min at room temperature with proteinase K at 20 μ g/mL in PBS, then 10 min with 2% H₂O₂ in PBS, 5 min in Tris-cacodylate-CoCl₂ (300:140:1 mM) buffer (pH 7.5) and 2 h at 37°C in the same buffer with 150 U/mL terminal-transferase (TdT, Roche-Diagnostics, Meylan, France) and 6 nM biotinylated d-UTP (Roche), rinsed 15 min at room temperature in SSC 1X, and revealed with Alexa-fluorescent avidin (Molecular Probes). For the phenotypic identification of apoptotic cells, a proteinase-K-free fluorescent detection kit was used (Roche Diagnostic, Meylan, France) following the manufacturer's instructions, prior to subsequent immunocytofluorescent labeling of neurogenesis stage markers (Table 1).

mRNA Extraction and RT-PCRs

Neurospheres (obtained from two rats) were collected after 5–10 DIV and centrifuged 8 min at 400 g. The resulting pellet was subjected to TRIzol (Invitrogen) RNA extraction according to the manufacturer's instructions. RNA was then reverse-transcribed using the Transcriptor First Strand cDNA Synthesis Kit (Roche Applied Science, Mannheim, Germany) with 2.5 μ M anchored-oligo(dT)18 primer and 60 μ M random hexamer primer in a 20 μ l final volume, according to the manufacturer's instructions. PCR amplification was performed using Taq polymerase (Sigma, 1 unit per μ l cDNA template) with forward primer 5'-AGTTGTGGTGAAATCACATTGG-3' and reverse primer 5'-GATATTTGGTCCTCTTCTTCTGG-3', i.e., the Blast-derived rat homolog of the primer pair that we had used previously for rat ObRb (Fombonne et al., 2007) generating a ObR-specific 438-bp DNA fragment; after 3 min denaturation at 96°C, 33 cycles of 45 s denaturation at 96°C, 30 s annealing at 58°C, 90 s extension at 72°C, and a final 10 min extension at 72°C, amplicons were subjected to electrophoresis on 1% agarose gel pre-stained with ethidium bromide. For quantitative real-time RT-PCR (qPCR), the primers used were Ccnd1 (QT00185241) generating a cyclin D1-specific 109-bp DNA fragment (GenBank NM_022267) and QT00199640 generating an HPRT-specific 125-bp DNA fragment (GenBank NM_012583). qPCR was carried out with the LightCycler 480 SYBR Green I Master (Roche Applied Science) with 1 μ l cDNA per 20 μ l, 4 mM MgCl₂, 0.4 μ M each primer, in a LightCycler 480 (Roche Applied Science) for

40 cycles: 10 s at 95°C, 5 s at 60°C, 10 s at 72°C. The threshold cycle (Ct) value, corresponding to the PCR cycle number at which fluorescence was detected above threshold, was calculated from Lightcycler 480 software version 1.3 (Roche Applied Science) by using the second derivative maximum method. Relative mRNA values were calculated with RealQuant Software (Roche Applied Science) by using HPRT as the reference gene.

Immunocytochemical Quantification of STAT3 and Phospho-STAT3 on Neurospheres

One day before stimulation with leptin (i.e., at 13 DIV), one-half of the culture medium was changed to MEM with 2% B27 supplement. To reduce the basal level of STAT3 phosphorylation, cultures were incubated for 30 min in TTX (1 μ M). The cultures were then stimulated with leptin (6.2 nM) for 5, 10, or 20 min. After stimulation, all culture wells were fixed with buffered 4% formaldehyde at 4°C and rinsed several times. Coverslips were then pre-incubated in PBS-Triton X-100 (0.1%)-goat serum (5%) for 1 h at room temperature and incubated overnight with rabbit antiphospho-STAT3 (pSTAT3) or rabbit anti-STAT3 (Cell Signalling Technology Inc. Danvers, MA, USA) and with mouse anti-MAP2 (Sigma) primary antibodies. Alexa 488-conjugated goat anti-rabbit IgG (FluoProbes, France) and Cy3-conjugated goat anti-mouse IgG (Jackson ImmunoResearch Laboratories, Inc., PA, USA) were used as secondary antibodies. All procedures were performed in phosphate-free solution containing 140 mM NaCl, 5 mM KCl, and 10 mM HEPES-Na, pH 7.4.

Images were acquired with a LSM 510 laser-scanning confocal microscope (Zeiss, Germany). The acquisition of A488 (pSTAT3 or STAT3) and then Cy3 (MAP2) was sequential to avoid overlap of excitation and emission of fluorescence. The optical sections were digitized (1024 \times 1024 pixels) and processed using Image J software. Ten randomly chosen optical fields were analyzed from each experiment (3–15 neurons per field). For analysis of the intensity of pSTAT3 or STAT3 staining in neuronal cells, we first created a binary mask from MAP2-positive cells and then analyzed pSTAT3/STAT3 intensity in regions overlapping with the binary mask. This procedure allowed avoiding detection of pSTAT3 in non-neuronal cells. All acquisitions and analysis were done blind. Acquisition parameters were same for every set of experiments. STAT3 immunostaining was performed in

parallel cultures treated in the same condition as for pSTAT3 experiments. The pSTAT3 to STAT3 intensity ratio was expressed as means value ratio of the pSTAT3 staining intensity vs. the STAT3 staining intensity in cultures run in parallel.

Western Blotting

Protein extraction from 2 to 10 rats and Western blotting were performed as described previously (Fombonne et al., 2007). In brief, soluble neurosphere extracts were adjusted at 30 µg protein/sample after protein quantification with the BCA Protein Assay Kit (Pierce, Rockford), resolved through 4–20% Tris-Glycine gels (Invitrogen) and transferred to nitrocellulose membranes. Membranes were incubated overnight at 4°C with a relevant primary antibody: rabbit monoclonal anti-cyclin D1 (NeoMarker, 1:500), rabbit polyclonal anti-phospho(Thr202/Tyr204)p42/p44 ERK, anti-phospho(Thr308)AKT, or anti-phospho(Tyr705)-STAT3 (Cell Signaling Technology, 1: 1000), then 2 h at room temperature with horseradish peroxidase (HRP)-conjugated goat anti-rabbit IgG (1:3000) (Santa Cruz Biotechnology, Paso Robles, CA, USA). After rinsing in PBST-tween and incubation for 1–5 min in ECL-Plus reagent (Perkin-Elmer, Waltham, MA, USA), nitrocellulose membranes were exposed to Hyper Performance Chemiluminescence film. Subsequent to cyclin D1 detection, the membranes were re-incubated with rabbit polyclonal anti-β-actin antibody (Sigma, 1:10,000) according to the same experimental procedure to serve as a loading control. After detection of each phosphorylated protein, the bound antibodies were stripped off and the membranes were reblotted with either rabbit anti-p42/p44 ERK, anti-AKT, or anti-STAT3 polyclonal antibodies (Cell Signaling Technology, 1:1000). Immunolabeled bands were quantified using the public domain NIH Image program (National Institutes of Health, Bethesda, MD, USA). The relative amount of cyclin D1 protein was measured and expressed as the ratio over β-actin expression whereas the amounts of phosphorylated proteins were determined as a ratio over relevant total protein expression.

Cyclin D1-specific shRNA Design and Transfections

The sequence of cyclin-specific shRNA of the cyclin D1 (CCND1) gene was designed by using siRNA Target Designer (www.promega.com/siRNA Designer/program/default.asp) software. Among designed sequences, the one corresponding to the coding region (233–255) was chosen for single-strand cDNA synthesis. The chosen forward sequence was: 5' TTTGACCTGC GCGCCCTCCGTTTCTTTCAAGAGAAGAAACGGAGGGCG CGCAGGTCTTTTT3' and the chosen reverse sequence was 5' CTAGAAAAAGACCTGCGCGCCCTCCGTTTCTTCTCTTG AAAGAAACGGAGGGCGCGCAGGT 3'. After annealing of synthesized single strand cDNAs, the resulting shRNA was ligated into mU6pro vector (Promega) and resulting plasmid was amplified as previously described (Efthimiadi et al., 2012). The primers used to identify mU6pro vector containing the chosen shRNA sequence were: F1F (CATTCAAGGCTGCGCAACTGTTG) and M13R2 (CACAGGAAACAGCTATGACCAT) giving rise to an amplified

fragment of 810 bp. After the PCR verification, plasmidic DNA was purified by using plasmid mini-prep kit (Invitrogen), the presence of cDNA sequence corresponding to the chosen shRNA was checked by sequencing (GATC Biotech, Marseille) and the relevant cDNA was amplified by using plasmid maxi-prep (Invitrogen).

Transfection experiments were performed by using tertiary neurosphere cultures with plasmidic cDNAs corresponding to pEGFP (BD Biosciences) and generated mU6pro-cyclinD1 shRNA and NeuroMag[®] magnetofection kit (OZ Biosciences) according to the manufacturer's instructions. Briefly, 0.3 µg of cDNAs corresponding to pEGFP were transfected alone to serve as a transfection control or in combination with 0.7 µg of cDNAs corresponding to mU6pro-cyclinD1 shRNA. After 24 h-period of transfection, the cell cultures were treated or not with leptin (6.2 nM). At the end of the treatments, the neurospheres were fixed with 4% paraformaldehyde for immunocytochemistry.

Statistical Analysis

Immunoblotting intensities and enumeration data obtained from cytochemical studies were compared between experimental groups with One-Way ANOVA followed by Newman-Keuls (for cellular assays) or Fisher's PLSD (for Western blots) post-tests for multiple comparisons. Unpaired Student's *t*-test (Prism software, Graph-Pad, San Diego, CA, USA) was used in experiments where only two sets of values were compared.

Results

SVZ-derived Neurospheres Respond to Exogenous Leptin by Decreased Expansion and Express Endogenous ObRb Receptor Transcripts

Microdissected SVZ tissues yielded 90,000 dissociated cells per rat. The majority of initially seeded cells died in agreement with their well-known low survival rate in the standard neurosphere culture conditions (Louis et al., 2013). Surviving cells proliferated, giving rise to growing spherical masses of undifferentiated cells. Plating at 10,000 cells per ml, when cultured 10 days *in vitro* (DIV) in the presence of 20 ng/ml of mitogens (EGF and bFGF), yielded 1700–1900 neurospheres per rat SVZ pair. The primary cultures of SVZ neurospheres were passaged at 10–11 DIV, i.e., before sphere diameter exceeded 100–120 µm in size. Passaging cells after dissociation of these neurospheres gave rise to morphologically similar neurospheres up to five successive generations. Upon differentiation by retrieval of growth factors after 10 DIV, the three neural lineages (neurons, astrocytes, oligodendrocytes) could be identified by immunocytochemistry of phenotypic markers (βIII-tubulin, GFAP, O4 respectively, data not shown) as already reported in our previous study (Charrier et al., 2006). This indicated that the cells comprised in the neurospheres fulfill the criteria for *bone fida* adult neural stem cells (Louis et al., 2013). Besides, during these preliminary experiments and the set-up of optimal culture conditions, we observed that reducing EGF concentration in the culture medium to 8 ng/ml still allowed neurosphere yield of 70–75% the values obtained with 20 ng/mL EGF at 10 DIV from adult SVZ tissues.

In all further experiments leptin effects on neurosphere expansion were therefore systematically assessed in the presence of 8 ng/mL EGF. Treatment with 6.2 nM leptin (Bariohay et al., 2005) strongly inhibited neurosphere growth in adult SVZ cultures as compared to controls carried in the presence of EGF but in the absence of leptin (Figure 1A). At 10 DIV, the number of neurospheres in leptin-treated SVZ cultures fell by 35% (Figure 1A).

The first step in addressing the molecular mechanisms behind leptin actions on SVZ neurospheres was to ascertain that in our experimental conditions the neurospheres express the specific leptin receptor (Obrb). As in hypothalamus, which served as a positive control, RT-PCR performed on the whole RNAs extracts obtained from SVZ-derived neurospheres yielded a specific transcript of the expected 438-bp size corresponding to Obrb leptin receptor (Figure 1B).

Leptin Recruits Two Obrb Post-receptor Pathways in SVZ Neurospheres

To explore whether detected Obrb mRNA expression corresponds to the presence of functional leptin receptors, we first studied if leptin could alter STAT3 expression and phosphorylation in SVZ neurospheres by double immunocytochemistry and confocal microscopy. In both control and leptin-treated neurospheres, unphosphorylated (inactive) STAT3 was expressed only in MAP2-immunoreactive, i.e., neuronal cells; reciprocally all neuronal cells displayed STAT3 immunoreactivity (Figures 2 C,D,G,H,K,L,O,P). In the absence of leptin, the phosphorylated form of STAT3 (pSTAT3) was almost undetectable in neurosphere cultures

(Figures 2A,B). However, leptin triggered rapid and transient STAT3 phosphorylation which peaked 10 min after its addition (Figures 2 E,I,M,Q) and was restricted to MAP2-labeled neuronal cells (Figures 2 E,F,I,J,M,N).

We also assessed the putative activation of the AKT-phosphoinositide-3 (PI3) pathway by leptin in SVZ neurospheres, since this pathway is generally activated in leptin targets relevant to energy metabolism regulation (Coppari and Björbaek, 2012). No activation-specific phosphorylation of amino-acid residues (Thr³⁰⁸) in AKT was detectable (data not shown), thus indicating that this pathway is not involved in signaling leptin actions on SVZ neurospheres.

We next investigated whether leptin actions also involve the ERK pathway. We found that addition of leptin to SVZ cultures triggers an increased phosphorylation of critical threonine/tyrosine residues (Thr²⁰²/Tyr²⁰⁴) in both ERK1 and ERK2 (p44 and p42, respectively; Figure 3A). This increase in P-ERK pointing to ERK activation could be detected 5 min after leptin addition and was maintained over control levels up to 5 DIV (Figure 3B). Interestingly, leptin-mediated activation of ERK was the most pronounced after 5-days treatment (Figure 3). The specificity of leptin-mediated ERK activation was assessed by using U0126, an inhibitor of the upstream kinase (MEK1) that selectively activates ERK1/2. At the concentration used (10 μ M), U0126 markedly inhibited leptin-induced ERK activation at all time points studied, from 5 min to 5 days (Figure 3).

The results from this set of experiments therefore indicated that endogenously expressed Obrb receptor transcripts correspond to the leptin receptors that are functionally coupled to STAT3 and ERK signaling pathways. Leptin receptor coupling

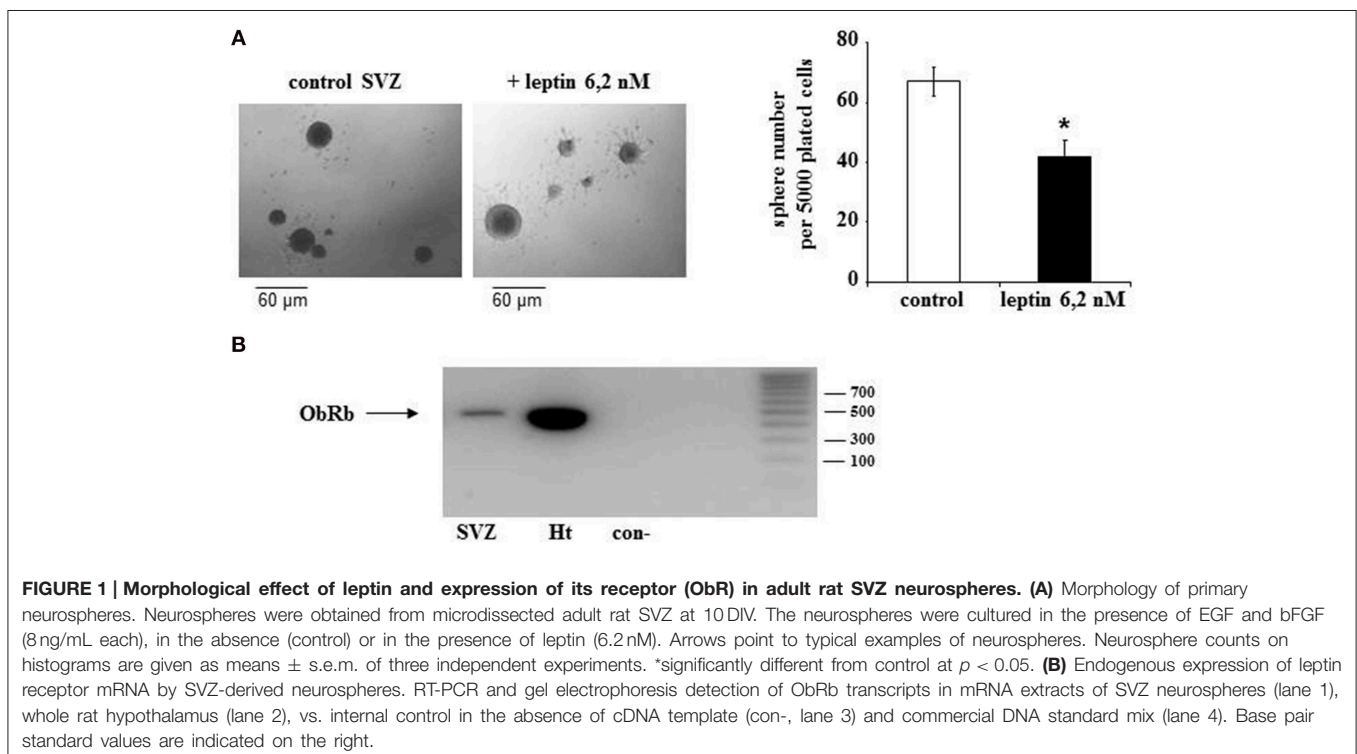
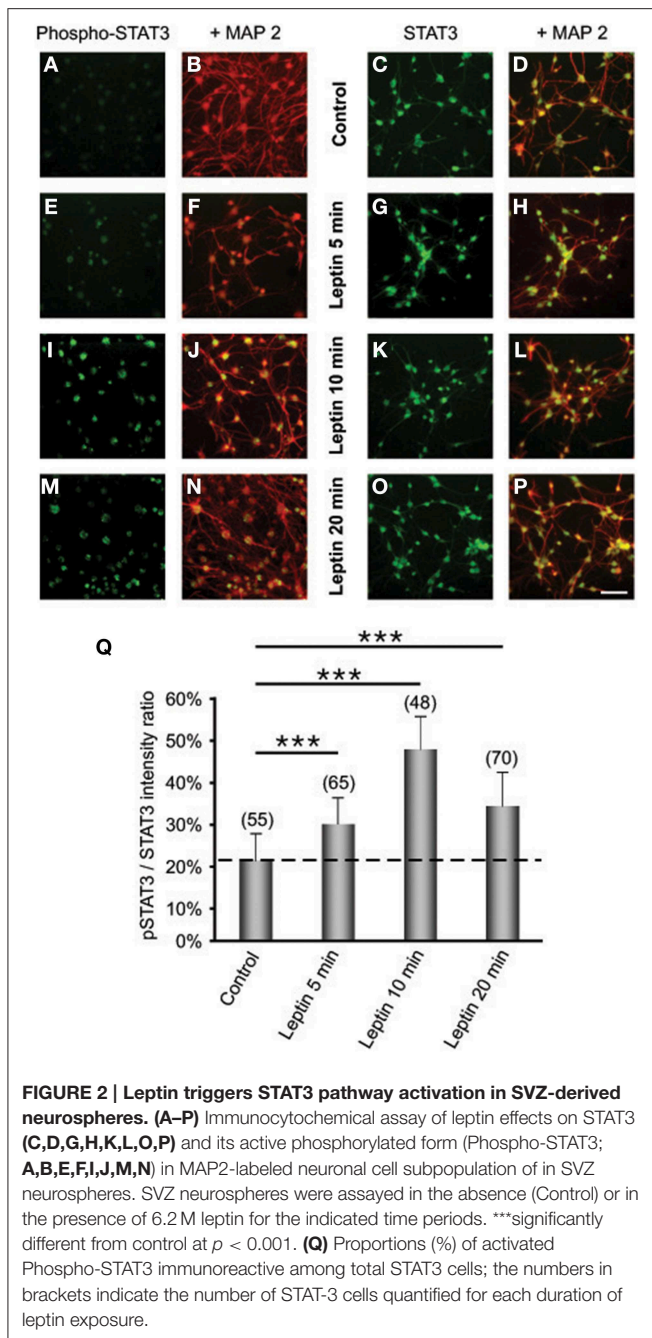


FIGURE 1 | Morphological effect of leptin and expression of its receptor (Obrb) in adult rat SVZ neurospheres. (A) Morphology of primary neurospheres. Neurospheres were obtained from microdissected adult rat SVZ at 10 DIV. The neurospheres were cultured in the presence of EGF and bFGF (8 ng/mL each), in the absence (control) or in the presence of leptin (6.2 nM). Arrows point to typical examples of neurospheres. Neurosphere counts on histograms are given as means \pm s.e.m. of three independent experiments. *significantly different from control at $p < 0.05$. **(B)** Endogenous expression of leptin receptor mRNA by SVZ-derived neurospheres. RT-PCR and gel electrophoresis detection of Obrb transcripts in mRNA extracts of SVZ neurospheres (lane 1), whole rat hypothalamus (lane 2), vs. internal control in the absence of cDNA template (con-, lane 3) and commercial DNA standard mix (lane 4). Base pair standard values are indicated on the right.



to STAT3 and ERK transduction pathways appears selective since another major leptin-activated signaling pathway, AKT-PI3, is not involved in the leptin actions on adult rat neurospheres.

Leptin Increases Cyclin D1 Expression via ERK1/2 in Cultured SVZ Neurospheres

Given that cyclin D1 is one of the major regulators of cell division and growth (Sherr and Roberts, 2004) and the reported involvement of ERK pathway in the control of cyclin D1 expression (Lefloch et al., 2009), we sought to determine whether leptin might alter cyclin D1 expression in SVZ neurospheres.

Indeed, since leptin inhibited the growth of neurospheres in our *in vitro* assay, we hypothesized that leptin may also inhibit cyclin D1 expression via ERK activation. Unexpectedly, as indicated by cyclin D1 western blot (Figure 4A), leptin clearly did not trigger a decrease in cyclin D1 expression. Moreover, after 5 DIV, the cyclin D1 expression was increased almost two-fold over basal expression (Figure 4A). The ERK1/2 inhibitor U0126 could reduce leptin-triggered induction of cyclin D1 protein to at least one-half of that seen in the absence of the inhibitor (Figure 4A) thus pointing to a specific involvement of ERK1/2 in leptin's action on cyclin D1 expression. Leptin-dependent induction of cyclin D1 was confirmed at the transcriptomal level by qRT-PCR at the time point (i.e., 5 DIV) where the maximal cyclin D1 protein expression was observed (Figure 4B). Indeed, after 5 DIV, leptin consistently increased the expression of cyclin D1 transcripts by itself (Figure 4B: no EGF condition). This effect was comparable to the cyclin D1 mRNA induction by the mitogen EGF (in the absence of leptin), used here as a positive control.

The above combined biochemical and pharmacological approaches therefore show that leptin increases cyclin D1 expression. This leptin effect is synergistic with the EGF-mediated cyclin D1 induction thus suggesting that leptin and EGF mediate the increase in cyclin D1 via different mechanisms.

Leptin Triggers Withdrawal from the Cell Cycle and Cell Death in SVZ Neurospheres

The observed leptin-mediated increase of cyclin D1 (Figure 4) appeared paradoxical in the light of our findings concerning the inhibition of neurosphere neural cell proliferation by leptin (Figure 1). To understand the mechanism behind such paradoxical effect of leptin, we checked directly leptin effects on the cell cycle by immunocytochemical analysis of Ki-67 labeling. This marker is expressed by cycling cells in any phase of the cell cycle but not by quiescent cells (Scholzen and Gerdes, 2000). In the absence of leptin, the majority of cells (about 60% of the total cell population as identified by DAPI-staining of their nuclei) were in the cell division cycle (Figure 5A). Addition of leptin resulted in a significant decrease in the proportion of the Ki-67-positive cells as compared to control cultures (Figure 5A).

The inhibitory actions of leptin on neurosphere growth are therefore associated with the inhibition of cell division in the presence of leptin but not with an expected decrease in cyclin D1 expression. Because in some paradigms of neuronal death, induction of cyclin D1 precedes the cell death (Di Giovanni et al., 2005; Krantic et al., 2005), we asked whether leptin could trigger cell death in our neurosphere assays. Assessment of apoptosis by TUNEL staining indicated that, indeed, leptin treatment yielded a two-fold increase of the number of TUNEL-positive cells (Figure 5B).

Cyclin D1 Expression in TUNEL-positive Neurosphere Cells after Leptin Treatment

To address whether cyclin D1 induction could be involved in leptin-stimulated apoptosis, TUNEL staining was combined with cyclin D1 immunocytochemistry on proliferating SVZ neurosphere cultures. Cyclin D1 immunoreactivity was

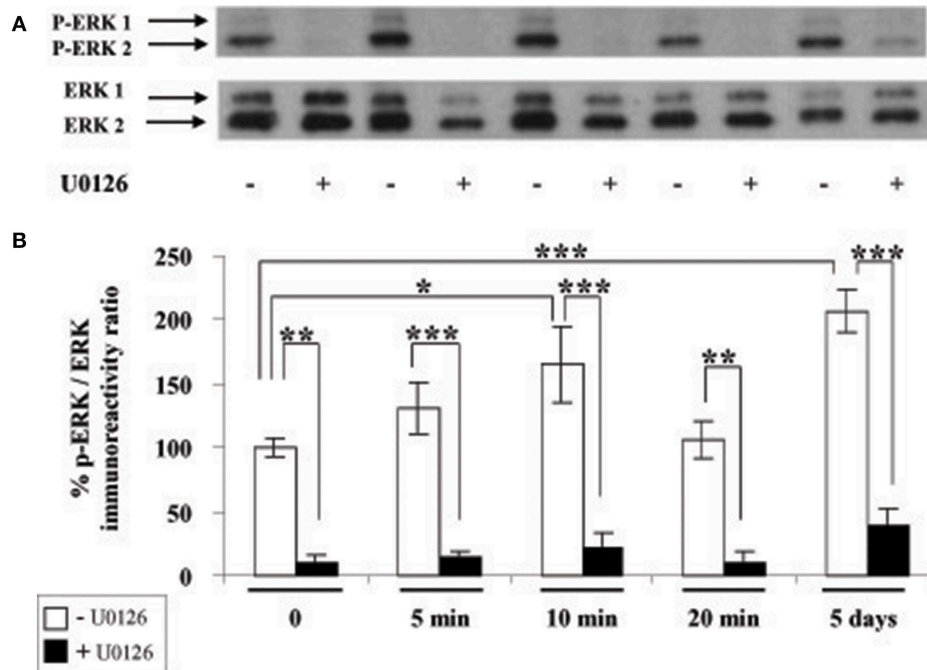


FIGURE 3 | Leptin triggers ERK pathway activation in SVZ-derived neurospheres. (A) Western-blot of phosphorylated ERK 1, 2 (P-ERK1, P-ERK2) and of total ERK1 and ERK2 performed on soluble protein extracts obtained from SVZ neurospheres that were plated and cultured in the presence of 6.2 nM leptin without (–) or with (+) 10 μ M U0126 for the indicated time periods. **(B)** Densitometric quantification of chemiluminescence-revealed immunoreactivities is depicted on the histogram as the ratio of phospho-ERK vs. total ERK labeling. *, **, ***significantly different from control at $p < 0.05$, $p < 0.01$, and $p < 0.001$, respectively.

much more abundant in leptin-treated neurospheres than in control cultures. In leptin-treated neurospheres, cyclin D1-immunoreactive cells splitted into two strikingly different subpopulations: small cells with cyclin D1 restriction in the cell nucleus, and large neuron-like cells expressing cyclin D1 throughout cytoplasm but not in nuclei (Figure 6). TUNEL staining was extensively and exclusively colocalized with nuclear cyclin D1, and never associated with cytoplasmic cyclin D1-containing cells (Figure 6).

Silencing Cyclin D1 Expression by Specific shRNA Prevents Leptin-induced Decrease of the Neural Stem Cell Number

To assess a causal relationship between leptin-mediated cyclin D1 expression and cell death, we performed RNA silencing experiments with a cyclin D1-specific shRNA. Knock-down of cyclin D1 by specific shRNA resulted in a decrease of the number of cyclin D1-positive cells per neurosphere (Figures 7A,B), thus confirming the functionally efficient knock-down of cyclin D1 expression.

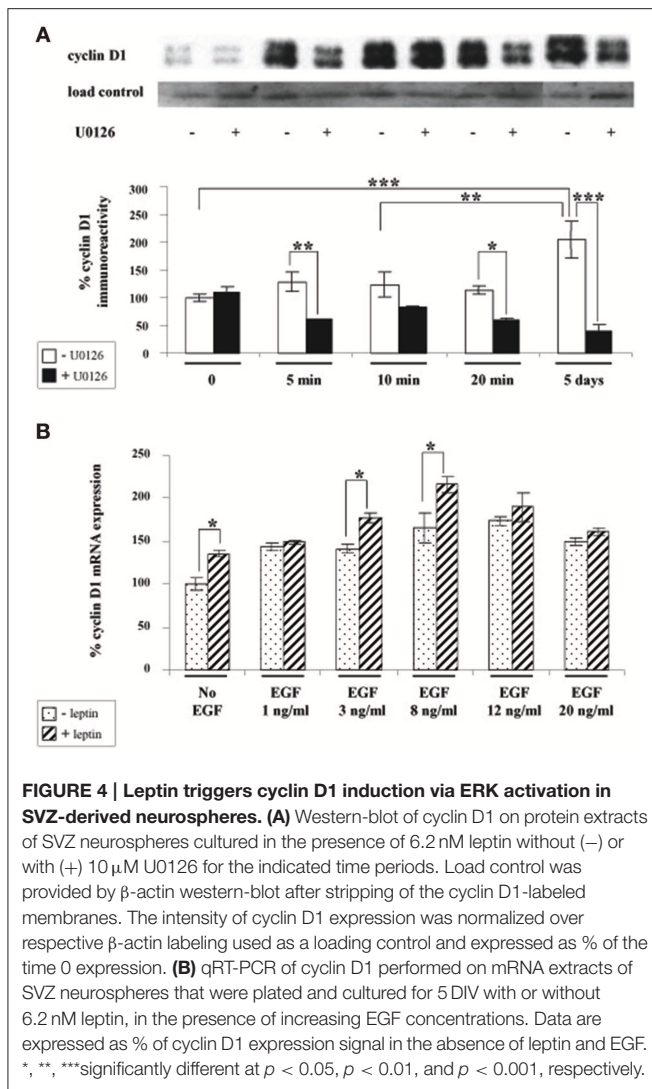
Moreover, when cyclin D1-specific shRNA-transfected neurospheres were treated with leptin (6.2 nM), a decrease in the number of cyclin D1-labeled cells due to the transfection could not be over-come by leptin-mediated increase in cyclin D1 expression (Figure 7A: cyclin D1 row, and Figure 7B for quantification) seen in previous experiments (Figure 4). Interestingly, such decrease in the number of cyclin D1-labeled

cells precluded the leptin triggered-decrease in the number of cells per neurosphere (Figure 7A: GFP row, and Figure 7C for quantification).

Taken together, these data show that functional knock-down of cyclin D1 expression is sufficient to rescue leptin-mediated decrease in the cell number per neurosphere.

Phenotypic Identification of Apoptotic Cells in Leptin-treated Neurospheres

In order to identify the cell types that are committed to apoptosis in response to leptin among the neuroipoietic lineage, TUNEL was combined with immunocytochemistry of each among eight phenotypic markers on neurosphere cultures from adult rat SVZ (Figure 8). Proportions of marker-immunoreactivity among TUNEL-positive cells and of TUNEL positivity among each phenotypic subpopulation of SVZ neurosphere cells were quantified on large numbers of cells in three distinct cultures at least (above 100 in each case) and respectively plotted in histograms of Figure 8. The neural stem cell marker Sox-2 rarely co-localized with TUNEL, although numerous TUNEL-positive and Sox-2 immunoreactive cells were detected (Figure 8, two first rows). No TUNEL colocalization was detected with the other neural stem cell marker, nestin (Figure 8). A small proportion of TUNEL colocalization was detected with the marker of immature migrating neurons doublecortin (DCX) (Figure 8). By contrast, TUNEL staining extensively colocalized with three markers of differentiated neurons: the microtubule-associated protein-2

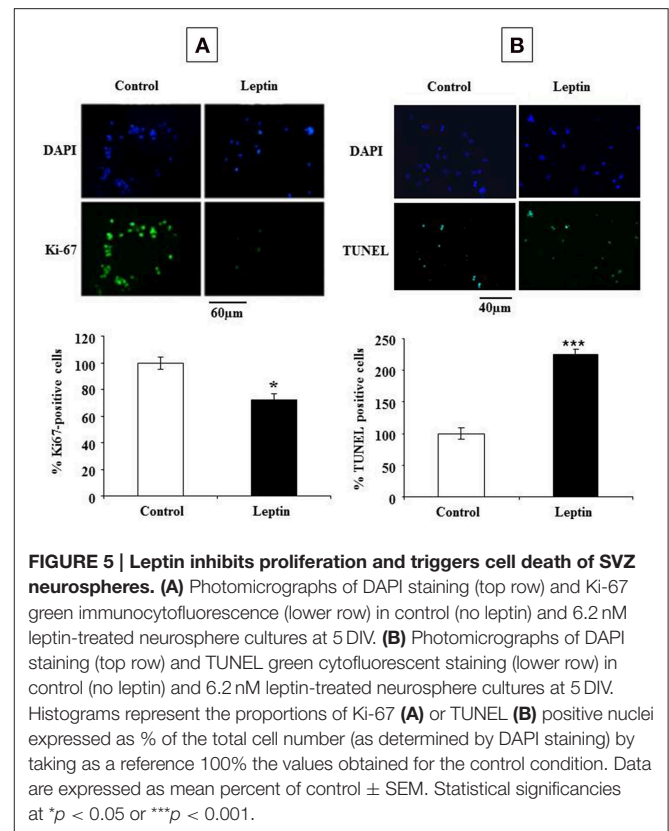


(MAP2), the neuronal nuclear antigen NeuN and the axonal protein β -III-tubulin (Figure 8). No TUNEL colocalization was detected with the astrocyte marker S100 β (Figure 8).

Discussion

The present study provides the first report on leptin-mediated inhibition of neural stem cell expansion in neurospheres derived from the adult rat neurogenic niche, SVZ. These leptin actions are mediated, at least in part, by apoptosis involving cyclin D1 induction as a prelude to cell death. The characterized novel actions of leptin on adult brain neural stem cells involve receptors and overlapping post-receptor mechanisms also relevant for its classical effects on energy metabolism.

Our neural stem cell culture conditions were validated by the fact that in control conditions, the primary cultures from adult rat SVZ yielded similar growth kinetics as those previously reported by our group and others (Charrier et al., 2006; Louis et al., 2013). *In vitro* inhibition of neurosphere expansion is due to a decrease in the number of stem cells (Louis et al., 2013), which in turn



results from either neural stem cell death or entry into quiescence (Daynac et al., 2013). In our experiments, the inhibitory effect of leptin on neural stem cell expansion could be revealed *in vitro* by lowering the EGF concentration from standard 20 ng/mL (Louis et al., 2013; Charrier et al., 2006) to 8 ng/mL, in agreement with previous studies (Palma et al., 2004; Louis et al., 2013).

The novel actions of leptin characterized in the present study involve the receptor molecule, Obrb, shared by all known leptin target cells. Indeed, Obrb transcripts were amplified from SVZ neurosphere RNAs by using primers designated for amplification of the conserved cDNA sequences. Although the performed RT-PCR assay does not allow for the accurate quantification, Obrb expression level in SVZ neurospheres appears lower than in hypothalamus, which is one of the major leptin targets in adult mammals organism (Elmqvist et al., 1998; Villanueva and Myers, 2008; Myers et al., 2009; Gautron and Elmqvist, 2011; Coppari and Bjørnbæk, 2012; Park and Ahima, 2014). The functionality of Obrb in SVZ neurospheres is attested by leptin activation of the specific transduction pathways: STAT3 and ERK1/2. In particular, phospho-STAT3 immunoreactivity is established as a universal index of functional recruitment of leptin receptor in target cells. Indeed, among the five intracellular pathways that can be recruited by leptin reception in its numerous target cell types, the Jak2/STAT3 is the only one that is systematically activated by leptin (Villanueva and Myers, 2008; Coppari and Bjørnbæk, 2012; Rasmussen et al., 2014). Interestingly, STAT3 phosphorylation-dependent activation was exclusively detected in MAP2-immunoreactive cells. As a corollary, the STAT3

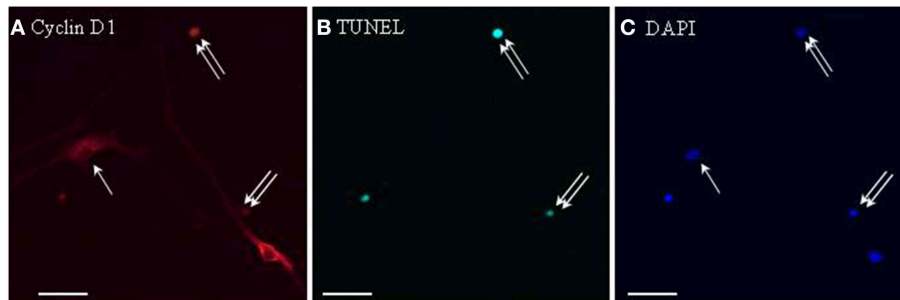
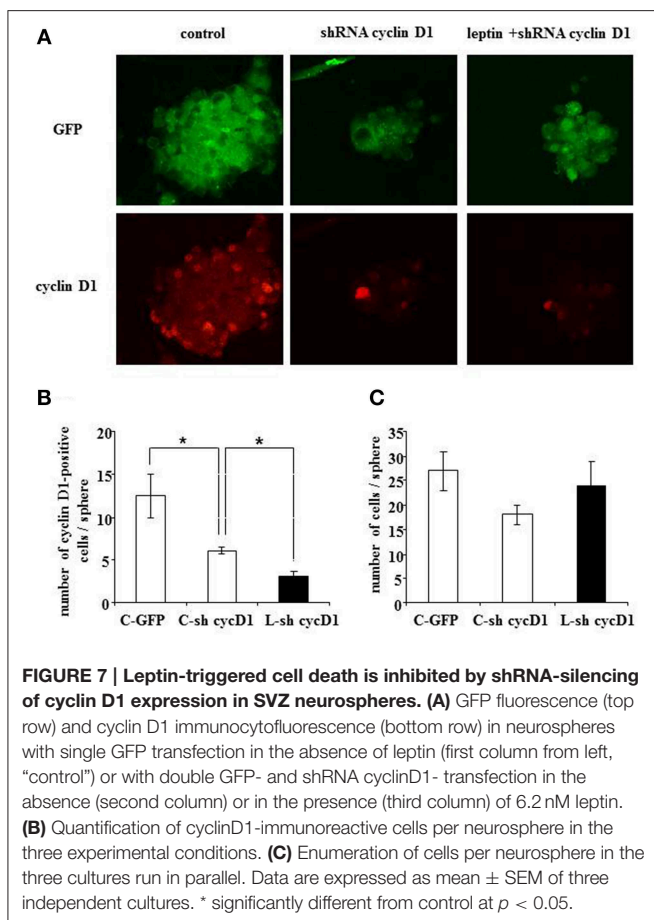


FIGURE 6 | Cyclin D1 immunoreactivity colocalizes with TUNEL-positive cells in leptin-treated neurospheres. A series of identical culture wells of leptin-treated secondary neurospheres from adult rat SVZ were processed in parallel for either (A) cyclin D1 immunocytochemistry (revealed in red), (B) TUNEL (revealed in green), (C) DAPI staining (revealed in blue). Single and double arrows point respectively, to TUNEL⁻/cyclinD1⁺ and TUNEL⁺/cyclinD1⁺ representative cells. Note the occurrence of TUNEL-negative cyclin-D1-immunoreactive cells, and the differential morphologies of the two subpopulations of labeled cells (see Results text for details).



transduction pathway may be involved in leptin-mediated induction of differentiation via commitment of the neural stem cells to neural progenitors. Differentiation-related actions of leptin were out of the scope of this study. It is nevertheless likely that commitment of neural stem cells to differentiation toward a neural lineage may be preceded by the observed withdrawal of neural stem cells from the cell cycle, as shown

by our Ki67 labeling experiments. Ki67 is a nuclear protein which is exclusively expressed by dividing cells (Scholzen and Gerdes, 2000). The observed decrease in Ki67 labeling in the presence of leptin therefore points to the inhibitory role of leptin in the control of SVZ neural stem cell expansion. This novel action of leptin on neurospheres adds to the well-known complexity of leptin-mediated control of cell division pointing to both inhibitory and stimulatory effects of leptin (reviewed in Garofalo and Surmacz, 2006; King et al., 2013). For instance, anti-proliferative actions of leptin combined with leptin-mediated induction of cell death, have been documented in immune, epithelial, endothelial, adipose cells, and some tumors (Garofalo and Surmacz, 2006; Tang, 2008). In line with these findings, the inhibitory effect of leptin on adult SVZ neural stem cell expansion shown here was also associated to apoptosis induction. Moreover, apoptosis was preceded by ERK-mediated cyclin D1 induction. In agreement, ERK has been previously shown to be involved in the control of cyclin D1 expression (Meloche and Pouyssegur, 2007). The specificity of ERK mediation was further attested by the capacity of the ERK kinase MEK1 inhibitor (U0126) to prevent cyclin D1 induction and cell death upon leptin addition to SVZ neurospheres. At the cellular level, cyclin D1 expression by the apoptotic cells was directly demonstrated by colocalization of cyclin D1 immunoreactivity and TUNEL staining in numerous nuclei of leptin-treated neurosphere cultures from adult rat SVZ. Furthermore, this experiment revealed that a subpopulation of differentiated, TUNEL-negative, neuron-like cells displayed strong cytoplasmic accumulation of cyclin D1 protein. It suggests that leptin-dependent induction of cyclin D1 might trigger either apoptosis or differentiation of neurosphere cells.

The specificity of cyclin D1 involvement in cell death induction was demonstrated by our RNA silencing experiments. Interestingly, cyclin D1 silencing in the absence of leptin resulted in withdrawal from the cell cycle as shown by decreased Ki67 expression. In these control conditions, the basal cyclin D1 expression by neurosphere cells is likely due to the presence of a low level of EGF concentration in culture medium. Indeed EGF, like other mitogens, has the capacity to trigger cyclin D1 expression and subsequent entry into the cell division cycle

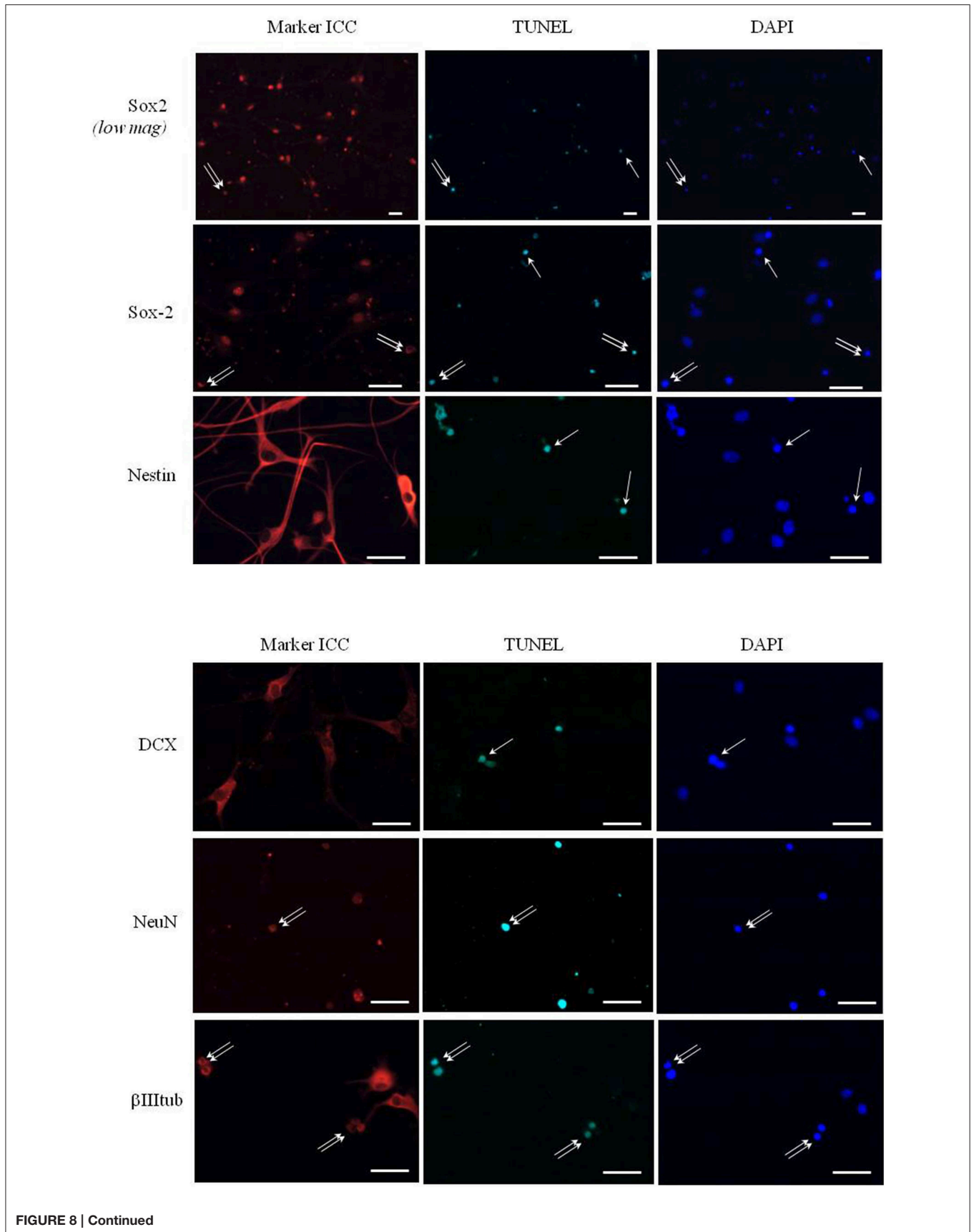


FIGURE 8 | Continued

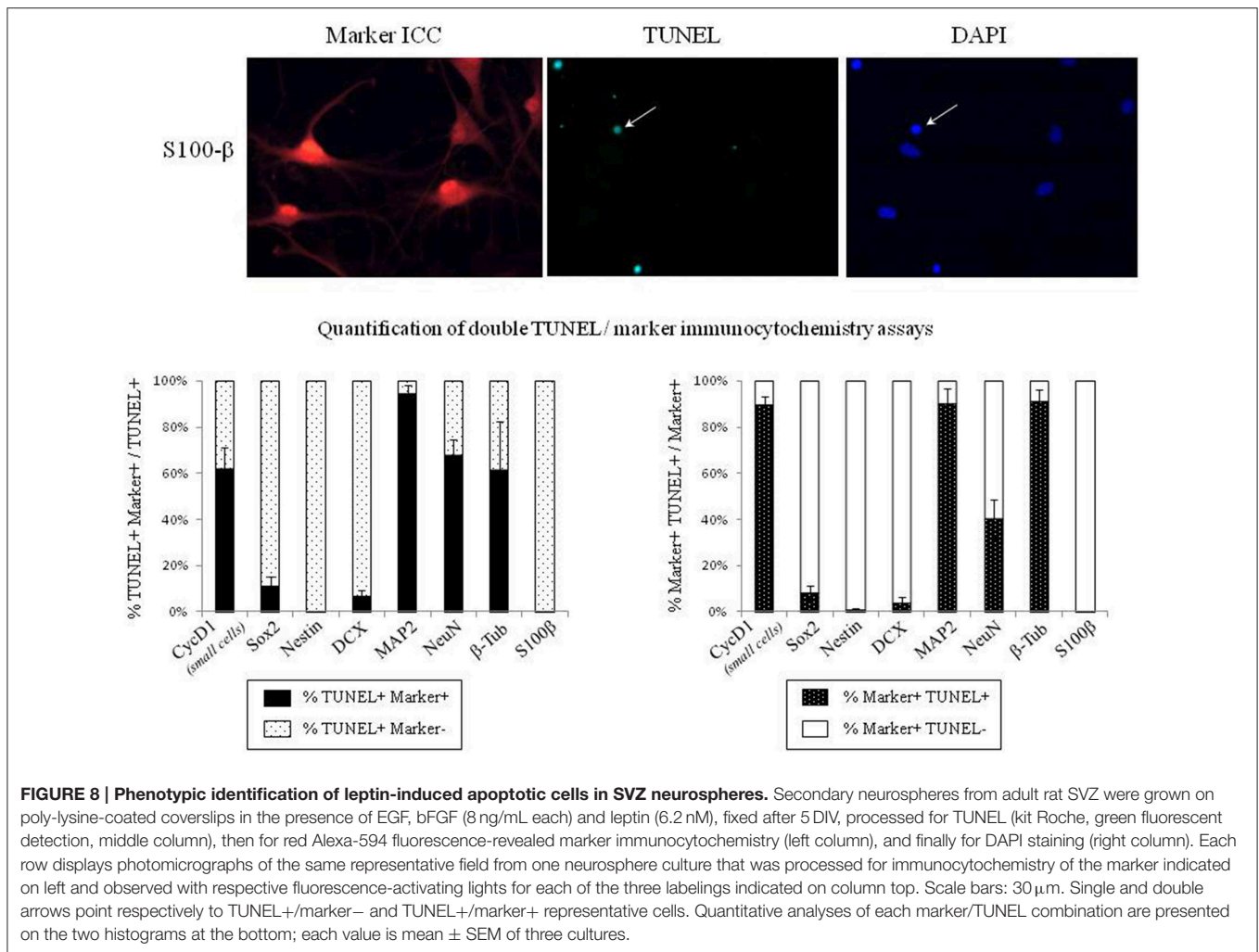


FIGURE 8 | Phenotypic identification of leptin-induced apoptotic cells in SVZ neurospheres. Secondary neurospheres from adult rat SVZ were grown on poly-lysine-coated coverslips in the presence of EGF, bFGF (8 ng/mL each) and leptin (6.2 nM), fixed after 5 DIV, processed for TUNEL (kit Roche, green fluorescent detection, middle column), then for red Alexa-594 fluorescence-revealed marker immunocytochemistry (left column), and finally for DAPI staining (right column). Each row displays photomicrographs of the same representative field from one neurosphere culture that was processed for immunocytochemistry of the marker indicated on left and observed with respective fluorescence-activating lights for each of the three labelings indicated on column top. Scale bars: 30 μ m. Single and double arrows point respectively to TUNEL+/marker- and TUNEL+/marker+ representative cells. Quantitative analyses of each marker/TUNEL combination are presented on the two histograms at the bottom; each value is mean \pm SEM of three cultures.

(Sherr and Roberts, 2004; Meloche and Pouyssegur, 2007). Therefore, in the absence of leptin, cyclin D1 likely acts in its normal capacity as a positive regulator of the cell division cycle (Sherr and Roberts, 2004). However, because it has been demonstrated that the over-expression of cyclin D1 leads to increased proliferation in immature, i.e., cycling, neurons (Oliver et al., 2003) whereas it triggers cell death in mature, i.e., differentiated, neurons (Kranenburg et al., 1996; Timsit et al., 1999), our data suggest that the present pro-apoptotic action of leptin might be associated with its concomitant pro-differentiative effects on SVZ cells. This hypothesis is supported by the following experimental evidence: (i) morphological signs of differentiation (neurite growth, cell migration), similar to those seen in pro-differentiative culture conditions such as mitogen retrieval, were consistently observed in the presence of leptin; (ii) this leptin-dependent differentiation is associated with cyclin D1 in the cytoplasm of neurosphere cells; (iii) leptin triggers neural stem cell withdrawal from the cell cycle, as monitored by decreased Ki67 labeling, which is generally required for induction of cell differentiation (Gao and Zelenka, 1997). Relevantly, it has been demonstrated already that failure

in differentiation leads to cell death in other paradigms such as in EGF-induced differentiation of somato-lactotrope precursors into PRL-secreting lactotrope cells (Fombonne et al., 2004) or in erythropoietin-induced differentiation of hematopoietic lineage (Lesault et al., 2002).

Leptin targets for commitment to apoptosis in SVZ neurospheres, i.e., in the “neuropoietic lineage,” were identified by a double TUNEL/immunocytochemical approach, as differentiated neurons predominantly. Less than 10% of TUNEL-positive cells indeed expressed Sox2 or DCX in the present culture conditions. These data are in keeping with the result of our previous time-course assay of leptin-dependent transduction effector, STAT-3 phosphorylation, which occurred exclusively in neurosphere neurons (see above). It indicates that leptin impacts late stages of neuropoiesis, even though its present action is detected in proliferating neurospheres and primarily targets the early cell division factor cyclin D1. Consistently, it is established that neuron differentiation markers are already expressed during the proliferative state of neural stem/progenitor cells in the presence of mitogens (Liard et al., 2009; Rosa et al., 2010). Cyclin D1 was recently shown in neural

stem cells of fetal rodent brain, to block astroglial differentiation and to stimulate neuronal differentiation *via* STAT-3 activation (Bizen et al., 2014). This latter finding is similar to the presently characterized actions of leptin on adult rat SVZ cells, although it was characterized on neural progenitors from late fetus. Further, our cytochemical assays clearly showed that leptin-induced cyclin D1 colocalizes with TUNEL-stained apoptosis in the nuclei of small SVZ cells, whereas cyclin D1 is also extensively expressed in much larger, neuron-like, non-apoptotic cells. This dual subcellular distribution of cyclin D1 is suggestive of its alternative roles that have recently emerged and are independent of cell cycle onset (Pestell, 2013).

From a more integrated point of view, the presently characterized leptin actions on adult SVZ neural stem cells provide a putative mechanism for *in vivo* leptin-dependent physiological adaptations. Functional deficiency of leptin actions in genetic (db/db mice) (Ramos-Rodriguez et al., 2014) or physiological (long-term intermittent fasting, Manzanero et al., 2014) models leads to increased neural stem cell proliferation in adult rat SVZ. Likewise, daily exercise in adult rats has been reported to increase neurogenesis in the adult hippocampus while decreasing leptinemia (Speisman et al., 2013). In contrast, increased levels of leptin, resulting from a high-fat diet, inhibit neurogenesis in the adult mouse hippocampus without neuronal loss (Park et al., 2010). Consistently, obesity decreases the number of neurosphere-producing cells in hypothalamus-derived primary neurosphere cultures (Bless et al., 2014). The putative leptin-dependent decrease of neurogenic rate in adult olfactory bulb, as suggested by the present *in vitro* study, should alter olfactory perception since odor discrimination and memory were recently demonstrated to depend on adult SVZ-fed neurogenesis in olfactory bulb (Gheusi and Lledo, 2014). The relevance of leptin impact on SVZ neural stem cells for food intake regulation though appears complex since olfactory perception could be optimized both by net increase (Sultan et al., 2010) and decrease (Mouret et al., 2009) of olfactory bulb neurogenesis in adult rat.

In conclusion, the present data further extend the known role of leptin in the control of neural plasticity in adult mammals. More precisely, since our data show that *in vitro* leptin inhibition of adult neural stem cell expansion is associated with specific receptor-mediated induction of apoptosis, and since *in vivo* the leptin hormone is secreted in direct proportion to adiposity, the present study suggests that adiposity/obesity may be considered

as a neurotoxicity paradigm. This view is further supported by the recent *in vivo* report that a high-fat leptin-inducing diet during 2 months in adult mouse and rat triggers apoptosis in mature hypothalamic neurons (Moraes et al., 2009). These recent findings extend the physiological pleiotropy of leptin beyond hormonal action toward a multifaceted growth factor in adult mammals. In this light, it is interesting to stress that the major post-receptor intracellular relays of leptin (STAT3, ERK1/2, AMPK, AKT) play a role in the control of both the cell cycle in proliferating cells and metabolite/metabolic sensing in post-mitotic neurons of the brain feeding regulatory centers (Rahmouni et al., 2009; Haissaguerre et al., 2014; Rehman et al., 2014). Stem cell control by leptin may therefore provide an exciting paradigm for the study of the cross-talk between these two regulation registers (Mans and Haramis, 2014). Several questions are raised by the present results about the function and relevance of leptin and leptin receptors in the SVZ neurogenic niche, such as the type(s) of leptin-receptive cells, the impact of leptin on differentiation/migration and behavioral alteration of stem cell progenies. Answering these questions definitively requires future studies that will focus on these exciting issues.

Funding

This work was supported by CNRS, INRA, La Ligue Contre le Cancer Grand Ouest Comités de la Vienne et des Deux Sèvres, University of Poitiers, University François Rabelais of Tours. SS, SC were recipients of French Government Doctoral Fellowships (SS: Biology of Ageing; SC: Neurosciences). LE was recipient of PACA Region/INSERM Doctoral Fellowship.

Acknowledgments

We thank Amgen (USA) for gracious gift of murine recombinant leptin and Pr Anne-Marie Prêt (University of Versailles-St-Quentin, Center for Molecular Genetics CNRS, Gif-sur-Yvette, France) for English language revision. This study was supported by funds from Institut National de la Recherche Agronomique (INRA), Centre National de la Recherche Scientifique (CNRS), Universities of Tours and Poitiers (Action Collaborative de Recherche Poitiers-Tours), La Ligue Contre le Cancer Grand Ouest Comités de la Vienne et des Deux Sèvres and by PhD fellowships from French government, in Biology of Ageing (SS) and Neuroscience (LE, SC).

References

- Bariohah, B., Lebrun, B., Moysse, E., and Jean, A. (2005). Brain-Derived Neurotrophic Factor plays a role as an anorexigenic factor in the dorsal vagal complex. *Endocrinology* 146, 5612–5620. doi: 10.1210/en.2005-0419
- Bauer, S., Moysse, E., Jourdan, F., Colpaert, F., Martel, J. C., and Marien, M. (2003). Effects of the α 2-adrenoreceptor antagonist dexefaroxan on neurogenesis in the olfactory bulb of the adult rat *in vivo*: selective protection against neuronal death. *Neuroscience* 117, 281–291. doi: 10.1016/S0306-4522(02)00757-1
- Bizen, N., Inoue, T., Shimizu, T., Tabu, K., Kagawa, T., and Taga, T. (2014). A growth-promoting signaling component cyclin D1 in neural stem cells has antiastroglial function to execute self-renewal. *Stem Cells* 32, 1602–1615. doi: 10.1002/stem.1613
- Bless, E. P., Reddy, T., Acharva, K. D., Beltz B. S., and Tetl, M. J. (2014). Oestradiol and diet modulate energy homeostasis and hypothalamic neurogenesis in the adult female mouse. *J. Neuroendocrinol.* 26, 805–816. doi: 10.1111/jne.12206
- Bouret, S. G., Draper, S. J., and Simerly, R. B. (2004). Trophic action of leptin and diet modulate energy homeostasis and hypothalamic neurogenesis in the adult female mouse. *J. Neuroendocrinol.* 26, 805–816. doi: 10.1111/jne.12206
- Bouret, S. G. (2013). Organizational actions of metabolic hormones. *Front. Neuroendocrinol.* 34, 18–26. doi: 10.1016/j.yfrne.2013.01.001

- Braun, S. M. G., and Jessberger, S. (2014). Adult neurogenesis: mechanisms and functional significance. *Development* 141, 1983–1986. doi: 10.1242/dev.104596
- Charrier, C., Coronas, V., Fombonne, J., Roger, M., Jean, A., Krantic, S., et al. (2006). Characterization of neural stem cells in the dorsal vagal complex of adult rat brainstem by *in vivo* proliferation labelling and *in vitro* neurosphere assay. *Neuroscience* 138, 5–16. doi: 10.1016/j.neuroscience.2005.10.046
- Cheng, M. F. (2013). Hypothalamic neurogenesis in the adult brain. *Front. Neuroendocrinol.* 34, 167–78. doi: 10.1016/j.yfrne.2013.05.001
- Coppari, R., and Björbaek, C. (2012). Leptin revisited: its mechanism of action and potential for treating diabetes. *Nat. Rev. Drug Discov.* 11, 692–708. doi: 10.1038/nrd3757
- Daynac, M., Chicheportiche, A., Pineda, J. R., Gauthier, L. R., Boussin, F. D., and Mouthon, M. A. (2013). Quiescent neural stem cells exit dormancy upon alteration of GABAAR signalling following radiation damage. *Stem Cell Res.* 11, 516–528. doi: 10.1016/j.scr.2013.02.008
- Di Giovanni, S., Movsesyan, V., Ahmed, F., Cernak, I., Schinelli, S., Stoica, B., et al. (2005). Cell cycle inhibition provides neuroprotection and reduces glial proliferation and scar formation after traumatic brain injury. *Proc. Natl. Acad. Sci. U.S.A.* 102, 8333–8338. doi: 10.1073/pnas.0500989102
- Efthimiadi, L., Farso, M., Quirion, R., and Krantic, S. (2012). Cyclin D1 induction preceding neuronal death via the excitotoxic NMDA pathway involves selective stimulation of extrasynaptic NMDA receptors and JNK pathway. *Neurodegener. Dis.* 10, 80–91. doi: 10.1159/000335911
- Elmqvist, J. K., Björbaek, C., Ahima, R. S., Flier, J. S., and Saper, C. B. (1998). Distributions of leptin receptor mRNA isoforms in the rat brain. *J. Comp. Neurol.* 395, 535–547.
- Fombonne, J., Charrier, C., Goddard, I., Moysse, E., and Krantic, S. (2007). Leptin-mediated decrease of cyclin A2 and increase of cyclin D1 expression: relevance for the control of prepubertal rat Leydig cell division and differentiation. *Endocrinology* 148, 2126–2137. doi: 10.1210/en.2006-1218
- Fombonne, J., Reix, S., Rasolonjanahary, R., Danty, E., Thirion, S., Laforge-Anglade, G., et al. (2004). Epidermal growth factor triggers an original, caspase-independent pituitary cell death with heterogeneous phenotype. *Mol. Biol. Cell.* 15, 4938–4948. doi: 10.1091/mbc.E04-07-0601
- Gao, C. Y., and Zelenka, P. S. (1997). Cyclins, cyclin-dependent kinases and differentiation. *Bioessays* 19:307–315.
- Garofalo, C., and Surmacz, E. (2006). Leptin and cancer. *J. Cell. Physiol.* 207, 12–22. doi: 10.1002/jcp.20472
- Gautron, L., and Elmqvist, J. K. (2011). Sixteen years and counting: an update on leptin in energy balance. *J. Clin. Invest.* 121, 2087–2093. doi: 10.1172/JCI45888
- Gheusi, G., and Lledo, P. M. (2014). Adult neurogenesis in the olfactory system shapes odor memory and perception. *Prog. Brain Res.* 208, 157–175. doi: 10.1016/B978-0-444-63350-7.00006-1
- Grill, H. J., and Hayes, M. R. (2012). Hindbrain neurons as an essential hub in the neuroanatomically distributed control of energy balance. *Cell Metab.* 16, 296–309. doi: 10.1016/j.cmet.2012.06.015
- Haissaguerre, M., Saucisse, N., and Cota, D. (2014). Influence of mTOR in energy and metabolic homeostasis. *Mol. Cell. Endocrinol.* 397, 67–77. doi: 10.1016/j.mce.2014.07.015
- Hann, N., Goodman, T., Nadji-Samiei, A., Stratford, C. M., Rice, R., El Agha, E., et al. (2013). Fgf10-expressing tanycytes add new neurons to the appetite/energy balance regulating centres of the postnatal and adult hypothalamus. *J. Neurosci.* 33, 6170–6180. doi: 10.1523/JNEUROSCI.2437-12.2013
- King, B., Jiang, Y., Su, X., Xu, J., Xie, L., Standard, J., et al. (2013). Weight control, endocrine hormones and cancer prevention. *Exp. Biol Med.* 238, 502–508. doi: 10.1177/1535370213480695
- Kokoeva, M. V., Yin, H., and Flier, J. S. (2005). Neurogenesis in the hypothalamus of adult mice: potential role in energy balance. *Science* 310, 679–683. doi: 10.1126/science.1115360
- Kranenburg, O., van der Eb, A. J., and Zantema, A. (1996). Cyclin D1 is an essential mediator of apoptotic neuronal cell death. *EMBO J.* 15, 46–54.
- Krantic, S., Mechawar, N., Reix, S., and Quirion, R. (2005). Molecular basis of programmed cell death involved in neurodegeneration. *Trends Neurosci.* 28, 670–676. doi: 10.1016/j.tins.2005.09.011
- Lee, D. A., Bedont, J. L., Pak, T., Wang, H., Song, J., Miranda-Angulo, A., et al. (2012). Tanycytes of the hypothalamic median eminence form a diet-responsive neurogenic niche. *Nat. Neurosci.* 15, 700–702. doi: 10.1038/nn.3079
- Lefloch, R., Pouysegur, J., and Lenormand, P. (2009). Total ERK1/2 activity regulates cell proliferation. *Cell Cycle* 8, 705–711. doi: 10.4161/cc.8.5.7734
- Lesault, I., Quang, C. T., Frampton, J., and Ghysdael, J. (2002). Direct regulation of BCL-2 by FLI-1 is involved in the survival of FLI-1-transformed erythroblasts. *EMBO J.* 21, 694–703. doi: 10.1093/emboj/21.4.694
- Liard, O., Segura, S., Pascual, A., Gaudreau, P., Fusai, T., and Moysse, E. (2009). *In vitro* isolation of neural precursor cells from the adult pig subventricular zone. *J. Neurosci. Methods* 182, 172–179. doi: 10.1016/j.jneumeth.2009.06.008
- Louis, S. A., Mak, C. K. H., and Reynolds, B. A. (2013). Methods to culture, differentiate, and characterize neural stem cells from the adult and embryonic mouse central nervous system. *Meth. Mol. Biol.* 946, 479–506. doi: 10.1007/978-1-62703-128-8_30
- Mans, L. D., and Haramis, A. P. (2014). Burn to cycle: energetics of cell-cycle control and stem cell maintenance. *Front. Biosci.* 19, 1003–1014. doi: 10.2741/4263
- Manzanero, S., Erion, J. R., Santro, T., Steyn, F. J., Chen, C., Arumugam, T. V., et al. (2014). Intermittent fasting attenuates increases in neurogenesis after ischaemia and reperfusion and improves recovery. *J. Cereb. Blood Flow Metab.* 34, 897–905. doi: 10.1038/jcbfm.2014.36
- McNay, D. E. G., Briançon, N., Kokoeva, M. V., Maratos-Flier, E., and Flier, J. S. (2012). Remodeling of the arcuate nucleus energy-balance circuit is inhibited in obese mice. *J. Clin. Invest.* 122, 142–152. doi: 10.1172/JCI43134
- Meloche, S., and Pouyssegur, J. (2007). The ERK 1/2 mitogen-activated protein kinase pathway as a master regulator of the G1- to S-phase transition. *Oncogene* 26, 3227–3239. doi: 10.1038/sj.onc.1210414
- Moraes, J. C., Coope, A., Morari, J., Cintra, D. E., Roman, E. A., Pauli, J. R., et al. (2009). High-fat diet induces apoptosis of hypothalamic neurons. *PLoS ONE* 4:e5045. doi: 10.1371/journal.pone.0005045
- Morton, G. J., Meak, T. H., and Schwartz, M. W. (2014). Central nervous system control of food intake and body weight. *Nat. Rev. Neurosci.* 15, 367–378. doi: 10.1038/nrn3745
- Mouret, A., Lepousez, G., Gras, J., Gabellec, M. M., and Lledo, P. M. (2009). Turnover of newborn olfactory bulb neurons optimizes olfaction. *J. Neurosci.* 29, 12302–12314. doi: 10.1523/JNEUROSCI.3383-09.2009
- Myers, M. G. Jr., Münzberg, H., Lehninger, G. M., and Leshan, R. L. (2009). The geometry of leptin action in the brain: more complicated than a simple ARC. *Cell Metab.* 9, 117–123. doi: 10.1016/j.cmet.2008.12.001
- National Research Council, N. R. C. (1996). *Guide for Care and use of Laboratory Animals, 8th Edn.* Washington, DC: The National Academies Press.
- Oliver, T. G., Grasdeder, L. L., Carroll, A. L., Kaiser, C., Gillingham, C. L., Lin, S. M., et al. (2003). Transcriptional profile of the Sonic hedgehog response: a critical role for N-myc in proliferation of neuronal precursors. *Proc. Natl. Acad. Sci. U.S.A.* 100, 7331–7336. doi: 10.1073/pnas.0832317100
- Oswal, A., and Yeo, G. (2010). Leptin and the control of body weight: a review of its diverse central targets, signaling mechanisms, and role in the pathogenesis of obesity. *Obesity* 18, 221–229. doi: 10.1038/oby.2009.228
- Palma, V., Lim, D. A., Dahmane, N., Sánchez, P., Brionne, T. C., Herzberg, C. D., et al. (2004). Sonic hedgehog controls stem cell behavior in the postnatal and adult brain. *Development* 132, 335–344. doi: 10.1242/dev.01567
- Palouzier-Paulignan, B., Lacroix, M. C., Aimé, P., Baly, C., Caillol, M., Congar, P., et al. (2012). Olfaction under metabolic influences. *Chem. Senses* 37, 769–797. doi: 10.1093/chemse/bjs059
- Park, H. K., and Ahima, R. S. (2014). Leptin signaling. *F1000Prime Rep.* 6:73. doi: 10.12703/P6-73
- Park, H. R., Park, M., Choi, J., Park, K. Y., Chung, H. Y., and Lee, J. (2010). A high-fat diet impairs neurogenesis: involvement of lipid peroxidation and brain-derived neurotrophic factor. *Neurosci. Lett.* 482, 235–239. doi: 10.1016/j.neulet.2010.07.046
- Pestell, R. G. (2013). New roles of cyclin D1. *Am. J. Pathol.* 183, 3–9. doi: 10.1016/j.ajpath.2013.03.001
- Pierce, A. A., and Xu, A. W. (2010). De novo neurogenesis in adult hypothalamus as a compensatory mechanism to regulate energy balance. *J. Neurosci.* 30, 723–730. doi: 10.1523/JNEUROSCI.2479-09.2010
- Pinto, S., Roseberry, A. G., Liu, H., Diano, S., Shanabrough, M., Cai, X., et al. (2004). Rapid rewiring of arcuate nucleus feeding circuits by leptin. *Science* 304, 110–115. doi: 10.1126/science.1089459

- Rahmouni, K., Sigmund, C. D., Haynes, W. G., and Mark, A. L. (2009). Hypothalamic ERK mediates the anorectic and thermogenic sympathetic effects of leptin. *Diabetes* 58, 536–542. doi: 10.2337/db08-0822
- Ramos-Rodriguez, J. J., Molina-Gil, S., Ortiz-Barajas, O., Jimenez-Palomares, M., Perdomo, G., Cozar-Castellano, I., et al. (2014). Central proliferation and neurogenesis is impaired in type 2 diabetes and prediabetes animal models. *PLoS ONE* 9:e89229. doi: 10.1371/journal.pone.0089229
- Rasmussen, B. A., Breen, D. M., Duca, F. A., Côté, C. D., Filippi, B. M., and Lam, T. K. T. (2014). Jejunal leptin-PI3K signaling lowers glucose production. *Cell Metab.* 19, 155–161. doi: 10.1016/j.cmet.2013.11.014
- Rehman, G., Shehzad, A., Khan, A. L., and Hamayun, M. (2014). Role of AMP-activated protein kinase in cancer therapy. *Arch. Pharm.* 347, 457–468. doi: 10.1002/ardp.201300402
- Rosa, A. I., Gonçalves, J., Cortes, L., Bernardino, L., Malva, J. O., and Agasse, F. (2010). The angiogenic factor angiopoietin-1 is a proneurogenic peptide on subventricular zone stem/progenitor cells. *J. Neurosci.* 30, 4573–4584. doi: 10.1523/JNEUROSCI.5597-09.2010
- Scholzen, T., and Gerdes, J. (2000). The Ki-67 protein: from the known and the unknown. *J. Cell. Physiol.* 182, 311–322. doi: 10.1002/(SICI)1097-4652(200003)182:3<311::AID-JCP1>3.0.CO;2-9
- Sherr, C. J., and Roberts, J. M. (2004). Living with or without cyclins and cyclin-dependent kinases. *Genes Dev.* 18, 2699–2711. doi: 10.1101/gad.1256504
- Speisman, R. B., Kumar, A., Rani, A., and Foster, T. C. (2013). Daily exercise improves memory, stimulates hippocampal neurogenesis and modulates immune and neuroimmune cytokines in aging rats. *Brain Behav. Immun.* 28, 25–43. doi: 10.1016/j.bbi.2012.09.013
- Sultan, S., Mandairon, N., Kermen, F., Garcia, S., Sacquet, J., and Didier, A. (2010). Learning-dependent neurogenesis in the olfactory bulb determines long-term olfactory memory. *FASEB J.* 24, 2355–2363. doi: 10.1096/fj.09-151456
- Tang, B. L. (2008). Leptin as a neuroprotective agent. *Biochem. Biophys. Res. Commun.* 368, 181–185. doi: 10.1016/j.bbrc.2008.01.063
- Timsit, S., Rivera, S., Ouaghi, P., Guisard, F., Tremblay, E., Ben-Ari, Y., et al. (1999). Increased cyclin D1 in vulnerable neurons in the hippocampus after ischemia and epilepsy: a modulator of *in vivo* programmed cell death? *Eur. J. Neurosci.* 11, 263–278.
- Villanueva, E. C., and Myers, M. G. Jr. (2008). Leptin receptor signaling and the regulation of mammalian physiology. *Int. J. Obes.* 32(Suppl. 7), S8–S12. doi: 10.1038/ijo.2008.232
- Zhang, F., Proenca, R., Maffei, M., Barone, M., Leopold, L., and Friedman, J. M. (1994). Positional cloning of the mouse obese gene and its human homologue. *Nature* 372, 425–432. doi: 10.1038/372425a0

Conflict of Interest Statement: The authors declare that the research was conducted in the absence of any commercial or financial relationships that could be construed as a potential conflict of interest.

Copyright © 2015 Segura, Efthimiadi, Porcher, Courtes, Coronas, Krantic and Moysé. This is an open-access article distributed under the terms of the Creative Commons Attribution License (CC BY). The use, distribution or reproduction in other forums is permitted, provided the original author(s) or licensor are credited and that the original publication in this journal is cited, in accordance with accepted academic practice. No use, distribution or reproduction is permitted which does not comply with these terms.



Neurogenesis and growth factors expression after complete spinal cord transection in *Pleurodeles waltlii*

Amira Z. Zaky¹ and Marie Z. Mofteh^{2*}

¹ Biochemistry Department, Faculty of Science, Alexandria University, Alexandria, Egypt

² Zoology Department, Faculty of Science, Alexandria University, Alexandria, Egypt

Edited by:

Dirk M. Hermann, University Hospital Essen, Germany

Reviewed by:

Valerie Coronas, Université de Poitiers, France

Slavica Krantic, Centre National de la Recherche Scientifique, France

*Correspondence:

Marie Z. Mofteh, Zoology Department, Faculty of Science, Alexandria University, Baghdad Street, the Dean's Office Building, Alexandria E-21151, Egypt
e-mail: marie.mofteh@alexu.edu.eg

Following spinal lesion, connections between the supra-spinal centers and spinal neuronal networks can be disturbed, which causes the deterioration or even the complete absence of sublesional locomotor activity. In mammals, possibilities of locomotion restoration are much reduced since descending tracts either have very poor regenerative ability or do not regenerate at all. However, in lower vertebrates, there is spontaneous locomotion recuperation after complete spinal cord transection at the mid-trunk level. This phenomenon depends on a translesional descending axon re-growth originating from the brainstem. On the other hand, cellular and molecular mechanisms underlying spinal cord regeneration and in parallel, locomotion restoration of the animal, are not well known. Fibroblast growth factor 2 (FGF-2) plays an important role in different processes such as neural induction, neuronal progenitor proliferation and their differentiation. Studies had shown an over expression of this growth factor after tail amputation. Nestin, a protein specific for intermediate filaments, is considered an early marker for neuronal precursors. It has been recently shown that its expression increases after tail transection in urodeles. Using this marker and western blots, our results show that the number of FGF-2 and FGFR2 mRNAs increases and is correlated with an increase in neurogenesis especially in the central canal lining cells immediately after lesion. This study also confirms that spinal cord re-growth through the lesion site initially follows a rostrocaudal direction. In addition to its role known in neuronal differentiation, FGF-2 could be implicated in the differentiation of ependymal cells into neuronal progenitors.

Keywords: neurogenesis, spinal cord, growth factors, gap replacement, locomotion recovery

INTRODUCTION

It was in the late 1990s that scientists started to gather interesting information about urodeles. These animals were found to be best suited to study regeneration because they are easy and inexpensive to maintain and breed in the laboratory. Microsurgery is simple, wound healing is rapid and requires very few sutures, and thus a minimal post-operative care is required. Morbidity and mortality are low and results are obtained relatively fast. Their tissues are easy to harvest and process for histological or immuno-cytochemical staining or molecular analysis. On the other hand, known mammalian regenerative mechanisms *in situ* include compensatory hyperplasia (such as in the case of liver and pancreas), and activation of resident stem cells, but not dedifferentiation or trans-differentiation. Moreover, neurogenic ability in most regions of the central nervous system (CNS) is very limited (Goldman, 2004) and the production of new neurons is demonstrated to be almost arrested in adulthood (Hegedus et al., 2007).

The spinal salamander was chosen for this study because it is an ideal model to study not only regeneration but also neuronal and locomotor plasticity. Adult urodele amphibians regenerate their spinal cords following a cut or crush injury,

achieving functional recovery. This process is intrinsically appealing (Stocum, 1995, for review) although the time course of regeneration in urodeles depends on the nature of the lesion and on the age of the animal. However, a frequently arising question is whether understanding spinal cord regeneration in urodeles has relevance to spinal cord injury (SCI) in higher (amniote) vertebrates, such as humans (Chernoff, 1996).

Urodeles have two locomotor modes: swimming and over ground stepping, they switch from one mode to the other (functional plasticity) and spontaneously recover locomotion following a severe CNS injury (post lesional plasticity). Regeneration that occurs in embryonic or larval animals involves the formation of substantial numbers of new neurons and is qualitatively different from adult regeneration (Stensaas, 1983; Davis et al., 1989). Different aspects of spinal cord regeneration can be examined at different points in the life cycle, emphasizing neurogenesis or axonal regrowth (Chernoff et al., 2003). It is noteworthy that urodele amphibians are the only tetrapod vertebrates that can regenerate all regions of their spinal cord as adults (Chernoff, 1996).

Despite the fact that a new spinal cord is formed through cellular re-differentiation after tail amputation, body spinal cord

regeneration is often a fraction size of the normal spinal cord. It contains few or no neurons, has greatly reduced white matter and has little or no neuropil (Holder and Clarke, 1988). Recovery of locomotion has been demonstrated after transection of brachial, thoracic, lumbar, and tail spinal cord (Stensaas, 1983; Clarke et al., 1988; Davis et al., 1989; O'Hara et al., 1992; Benraiss et al., 1999; Chevallier et al., 2004). Most of these studies use axonal regrowth to measure regeneration as it reflects some degree of rearrangement of the intraspinal circuitry (Becker et al., 2005).

Regenerated axons contribute to the restoration of locomotor initiation below a healed spinal transection. Some of them are brainstem neurons (Chevallier et al., 2004). In some cases, however, recovery of behavior, which had been lost after injury, has been reported in conjunction with the reappearance of distinct types of new neurons (Scharff et al., 2000; Kuscha et al., 2012a,b). Spinal Cord also regenerates through gap replacement. Experimental analyses undertaken in the brain of several vertebrate classes suggested that the constitutive ventricular progenitors serve as a stem cell population that becomes activated to replace the lost tissue upon injury (Font et al., 2001; Zupanc and Clint, 2003; Endo et al., 2007; Parish et al., 2007; Kaslin et al., 2008; Tanaka and Ferretti, 2009; González-Granero and Gracia-Verdugo, 2011; Kroehne et al., 2011; Kizil et al., 2012a,b).

One of the main factors described to promote this phenomenon is basic fibroblast growth factor (bFGF), which is known to be an important growth factor that increases neurite extensions in cultured dissociated cells of the urodele spinal cord (Moftah, 2007), in PC12 cells (Rydel and Greene, 1987) and in embryonic stem cell (ESC)-derived neural cells (Lam et al., 2010). It also increases neurogenesis from human neural progenitor cells (NPCs; Nelson and Svendsen, 2006) and stimulates neural cell differentiation (Wilson and Stice, 2006; Moftah et al., 2008; Lam et al., 2010). bFGF is also used to maintain the neural stem cell pool in the mouse brain SVZ (Zheng et al., 2004) and the undifferentiated human ESCs (Xu et al., 2005). Some of the FGFs are probably released from cells when they are damaged (Chernoff, 1996). For example, following injury, ependymal cells upregulate bFGF production both in urodeles (Moftah et al., 2008) and in rodents (Del Bigio, 1995). It is produced by astrocytes in the CNS. It has been suggested that astrocytes orchestrate proliferation in the neurogenic niches by providing FGF-2 among other factors to the neural stem cells. However, for neurogenesis to be completed, progenitors have to stop proliferating, differentiate and survive (Hagg, 2005).

In considering applications to human disease, it has been reported that nestin is not only expressed in mice but also in human neuroepithelial cells suggesting the existence of neural precursors since it is an intermediate filament marker that characterizes embryonic neuroepithelial cells (Lendahl et al., 1990). It was also mentioned that it is expressed in undifferentiated cells during CNS development (Almqvist et al., 2002) and that it loses its expression early during the differentiation of a neural stem cell line (Mellodew et al., 2004). Such findings encourage the possibility that precursor cells from

the human CNS may be used in cell replacement or gene therapy strategies directed toward human neurodegenerative disorders.

In the present study, we show that the ependymal cells remained active, filled the gap between both spinal cord stumps and expressed nestin (intermediate filament marker), bFGF, one of its receptors (FGFR2) and neurofilament (NF, adult neurons marker). We therefore describe neurogenesis in adult vertebrate spinal cord after complete transection in the mid-trunk region.

MATERIAL AND METHODS

ANIMALS

Experiments were carried out as previously described (Moftah et al., 2008). In brief, 25 urodele amphibians (*Pleurodeles waltlii*) were obtained from Blades Biological Ltd (Kent, UK) and kept in aquaria at 19°C. Surgical procedures, handling and housing of the animals were in accordance with protocols approved by the INSERM Ethics Committee and conformed to NIH guidelines.

SPINALIZATION

Surgery was performed in aseptic conditions under general anesthesia as previously described (Moftah et al., 2008). In short, anesthetized animals were operated by completely cutting the spinal cord between segments 12 and 13. The wound was sutured and wound healing was complete 8–10 day post-operative. Sham-operated animals were exposed to laminectomy but not spinal cord transection.

IN SITU HYBRIDIZATION

All animal groups were anesthetized and treated for *in situ* hybridization as previously described (Moftah et al., 2008). In summary, spinal cords were exposed by laminectomy then divided into two segments (anterior and posterior) corresponding respectively to the pre- and post-lesional parts of the cord (in spinalized animals). Specimens were immediately but separately frozen by immersion in -50°C isopentane (Merck) without fixation. All samples were stored in embedding medium (Tissue Tek, Sakura) to be sectioned and processed later on.

Spinal cord sections (265 section/region/animal/experiment) were 14 μm thick and processed as described earlier (Landry et al., 2000). Briefly, sections were incubated at 42°C with 0.5 ng of each of the radioactively labeled probes. After hybridization, they were rinsed for four times at 55°C followed by 30 min at room temperature. Radioactivity was revealed by dipping sections into Ilford K5 nuclear emulsion (Ilford, Mobberly, Cheshire, UK), diluted with distilled water in a 1:1 ratio. They were then developed in the Kodak D19 developing solution and fixed in the Kodak 3000 fixative. Sections were then counterstained with 0.25% cresyl violet acetate (pH 4) (Sigma) and mounted in glycerol.

OLIGONUCLEOTIDE PROBES

For *in situ* detection of FGF-2 and FGFR2 mRNA, we used the following four fifty-mer oligonucleotide probes (Eurogentech, Seraing, Belgium) based on previously published gene sequences (Zhang et al., 2000; Moftah et al., 2002) respectively.

FGF-2:

- 5' GTTGATCCGCAGAAAGAAGCCCCGTTCTTGCAGTACAGCTCTTGGGTC3'
- 5' TTCAGCGCCATAAGCCTGCCGTCATCCTTCATAGCGA GATAGCGGTTTGC3'

FGFR2:

- 5' GGAAATGGACCAGGAAGCTTACTCTAAAAAGATGGTCA GCTGGGATTCGGG3'
- 5' CCTGGTGTCCAGGCTAGGTGAATACTGCTCCAG AGGTCGCTGAGGT3'

Probes were chosen from regions presenting few homologies with related mRNA sequences and were checked against the GenBank database.

As previously described (Landry et al., 2000), oligonucleotides were labeled in cobalt containing buffer with ³⁵S-dATP (Amersham) to a specific activity of $1-4 \times 10^9$ cpm/ μ g and purified by ethanol precipitation.

WESTERN BLOTS

The presence of FGF2 protein was determined by western blot analysis. All animal groups were anesthetized and treated as previously described (Moftah et al., 2012). In summary, spinal cords were exposed by laminectomy then divided into two segments (anterior and posterior) corresponding respectively to the pre- and post-lesional parts of the cord (in spinalized animals). Specimens were immediately frozen by immersion in -50°C isopentane (Merck) without fixation.

Previously removed and frozen spinal cord portions ($n = 5$) were treated as previously described (Moftah et al., 2012). In short, specimens were separately homogenized in ice cold buffer. Homogenates were centrifuged and 1% Triton X-100 (Sigma) was added. The supernatants were centrifuged for 1 h at 4°C . Protein content was determined using Bradford assay (Bio-Rad, Hercules, CA, USA). Western blots were performed with 40 μ g of proteins and repeated five times. Samples were resuspended in Laemmli Buffer (Laemmli, 1970), fractionated by SDS-PAGE using a 10% acrylamide gel and then transferred to PVDF membrane (Bio-Rad). Membranes were washed several times in blocking buffer and incubated overnight at 4°C with rabbit anti-FGF-2 (Chemicon, Temecula, CA, USA) primary antibody (1:200 in blocking buffer: BIORAD, Marnes-la-Coquette, France). Immunoreactivity was detected using anti-rabbit horseradish peroxidase (HRP)-conjugated secondary antibody (Dako) and visualized using enhanced chemiluminescence (ECL) detection system (Cell Signaling, Beverly, MA, USA). Anti-beta-actin was used as control.

IMMUNOHISTOCHEMISTRY

Anesthetized animals ($n = 5$ /experiment) were perfusion-fixed via the ascending aorta. Spinal cord was dissected out and treated as described earlier (Moftah et al., 2012). In summary, blocked sections were incubated (1:1000 in 2,4,6-trinitrotoluene, TNT/bovine serum albumin, BSA) with rabbit anti-nestin (Abcam, Paris, France) and mouse anti-pan neural NF (Sternberger Monoclonals Incorp., Lutherville, MD, USA) primary

antibodies. After rinsing in TNT, they were incubated with anti-rabbit Alexa fluor 488-conjugated and anti-mouse Alexa fluor 568-conjugated (Invitrogen, Cergy Pontoise, France) secondary antibodies (1:500 in 1,3,5-Trinitrobenzene, TNB). Slides were then rinsed and mounted.

IMAGING

Slides were examined; bright field light microscopy micrographs were taken using a Zeiss Axiophot 2 microscope (Zeiss, Jena, Germany). Immunostainings were analyzed with a Leica DMR PCS SP2 AOBs confocal microscope (Leica, Heidelberg, Germany) using a $20\times$, $40\times$ or $63\times$ oil-immersion lens. In all cases, scans were carried out sequentially with the 488 nm and 568 nm lines of the laser. Digital images were optimized for image resolution (300 dpi final resolution), brightness and contrast using Adobe Photoshop 6.0 (Adobe System, San Jose, CA, USA).

DATA ANALYSIS

Comparisons between groups (five animals each) were made on sections treated together on the same slides under identical conditions. The number of labeled cells and the labeling intensity were quantified as previously described (Landry et al., 2000). Cellular profiles containing three times more grains than mean background grain densities were considered labeled. Cell profiles were manually outlined as previously described (Moftah et al., 2008). Delineation was based exclusively on staining and not on shape, size or other measurable quantities. The number of silver grains per cresyl violet counterstained cell was counted semi automatically using MetaMorph Offline 6.1 software (Universal Imaging Corporation). Data were expressed as grain density per $\mu\text{m}^2 \pm \text{SEM}$ in calibrated photomicrographs. Transmitted light photomicrographs were taken for at least 500 fields ($700 \mu\text{m}^2$ each), in each experiment.

Data were imported into a spreadsheet program (Sigma Plot software, Jandel Scientific) that calculated and graphed the density of FGF-2 and FGFR2 mRNA expression. Data were compared using one way ANOVA tests and processed using standard statistical analysis techniques (Sigma Stat software, Jandel Scientific). Differences were considered to be significant when $p \leq 0.05$.

RESULTS**NESTIN EXPRESSION IN SPINALLY TRANSECTED ANIMALS THROUGHOUT SPINAL CORD REGENERATION**

Using nestin as a marker for intermediate filaments and thus neurogenesis, we investigated spinal cord regeneration after complete transection in the mid-trunk region. At 1 week after transection, spinal cord was separated into two stumps, a rostral (R) and a caudal (C) one (Figure 1A). Nestin was expressed mainly in the rostral stump around the central canal. This implies that regeneration started in the anterior portion of the spinal cord (Ant SC: the pre-lesional stump) right after transection thus preceding the posterior portion (Post SC), in which nestin is still faint at 1 week after the operation. Starting at 2 weeks post-operatively, a gap replacement is starting to appear, i.e., the gap between the two stumps started to be filled with neuronal progenitors as seen by the equally distributed nestin expression in both parts of the central canal and at the lesion site (Figure 1B). Fifteen

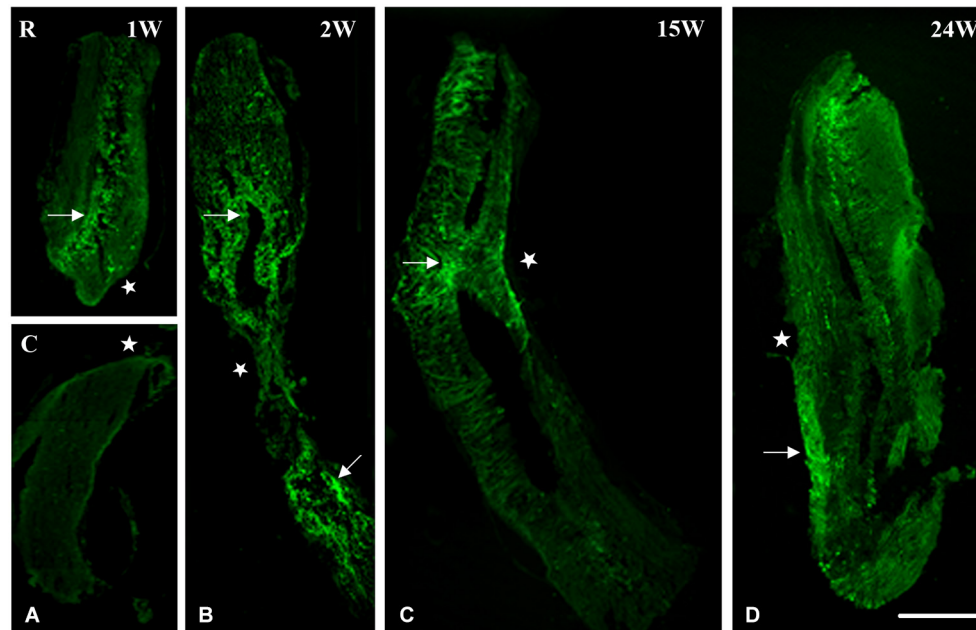


FIGURE 1 | Immunohistochemical analysis of nestin labeling during spinal cord regeneration. (A) Separated stumps at 1 week (1 W) post-operatively (R: Rostral; C: Caudal; lesion site denoted by a white star). **(B)** Nestin is seen in the central canal region (arrow), stumps connect and nestin is equally distributed in both parts of the central

canal at 2 weeks after transection (2 W: arrows). **(C)** Continuous cord and nestin is mainly expressed at the lesion site after 15 weeks of transection (15 W: arrow). **(D)** Normal spinal cord and few traces of nestin are still obvious 24 weeks post-operatively (24 W: arrow). Scale bar: 200 μ m.

weeks after transection; when animals recover their locomotor activity; spinal cord (as seen in **Figure 1C**) became continuous, completed gap replacement, due to the prominent expression of nestin at the lesion site. After 24 weeks of spinal cord transection, animals recovered both locomotor activities, i.e., stepping and swimming. On the cellular level, we noticed that spinal cord was normal in shape. Nevertheless, few traces of nestin are still obvious (**Figure 1D**).

NESTIN AND NEUROFILAMENT EXPRESSION IN SPINALLY TRANSECTED ANIMALS 1 WEEK AFTER SPINAL CORD LESION

In an attempt to get a closer look to the cellular level, we examined the distribution of nestin and NF during spinal cord regeneration. At 1 week after transection, when the animal is completely paralyzed and the spinal cord is separated into a rostral and a caudal stump, we found that nestin expression in the rostral part is prominent next to the lesion site (**Figure 2A**). The labeling orientation implies a possibility of neuronal progenitor migration from the upper part of the rostral stump to the lesion site in an attempt to replace the missing tissue. Meanwhile, adult neurons have been lost due to transection and the remaining cells disintegrated. We show here that NF, the neuronal marker, is almost absent 1 week post-operatively; a unique neurone is seen near the lesion site (**Figure 2B**). No colocalization is noticed between NF and nestin (**Figure 2D**), which implies that nestin is not expressed by neurons but instead is expressed by neuroglial cells as shown in our previous study (Fahmy and Moftah, 2010).

In the caudal stump, however, we found that nestin expression is prominent not only next to the lesion site but also in the

deep layers of the lesioned spinal cord (**Figure 2E**). The labeling orientation implies the same possibility of migration seen in the rostral stump although in a lesser organization. Meanwhile, adult neurons have not been completely lost from the caudal stump after transection. Using NF, we showed that, 1 week after injury, neurons are still abundant in the deep layers of the transected spinal cord (**Figure 2F**). Although their presence in masses, there still is no colocalization between NF and nestin (**Figure 2H**), implying the *de novo* formation of neural cells after differentiation of the neural progenitors expressing nestin. When nestin, the marker of neuronal progenitors is more abundant in the rostral stump, NF; the marker of adult neurons is more abundant in the caudal one. This could suggest that the regeneration process follows a rostro-caudal direction.

NESTIN AND NEUROFILAMENT EXPRESSION IN SPINALLY TRANSECTED ANIMALS 6 WEEKS AFTER SPINAL CORD LESION

Six weeks after spinal cord transection, when the animal started to recover some of its locomotor activity, the expression of nestin on the cellular level increased dramatically. Cells become more organized and both stumps of the lesioned spinal cord get connected at the transection site; replacing thus the gap created by the operation (**Figures 3A–D**). Meanwhile, new, very rare adult neurons start appearing next to the central canal as shown in **Figures 3E,F**.

A more obvious view of nestin expression in cells lining the central canal is seen in a transverse section of the neural axis at the lesion site, 6 weeks after transection (**Figure 3G**).

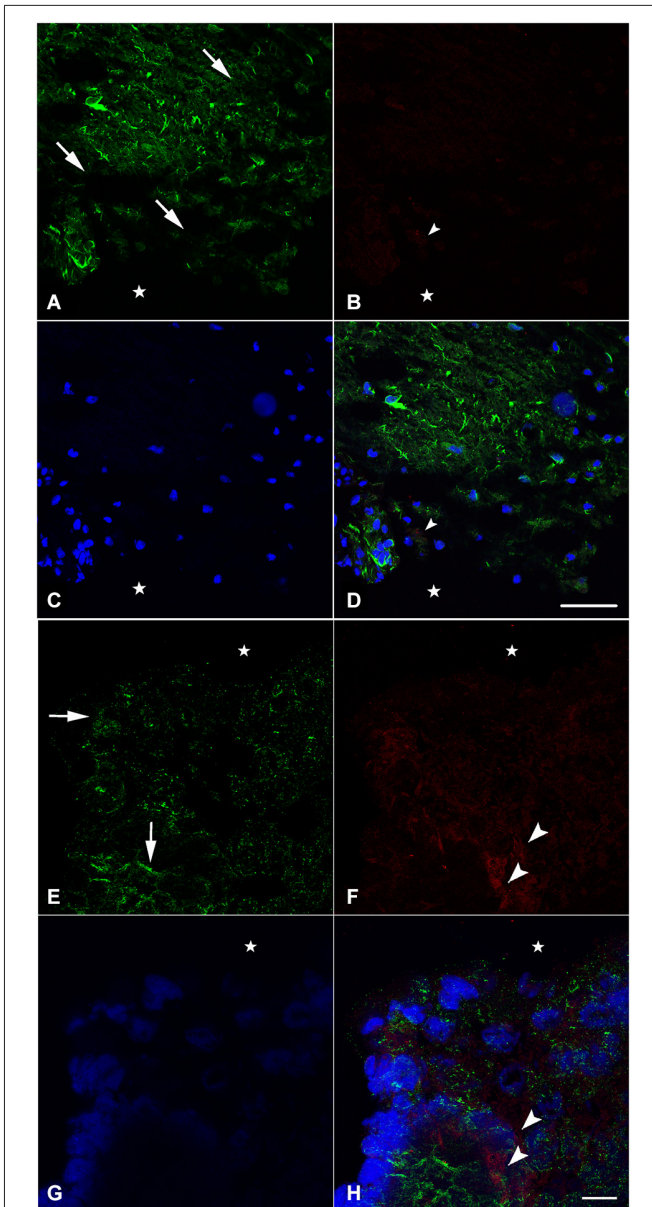


FIGURE 2 | Immunohistochemical analysis of nestin (green) and NF (red) labeling during spinal cord regeneration in the rostral (A–D) and caudal (E–H) stumps after 1 week of spinal cord transection (stars show the lesion site). In (A) and (E), nestin expression shows the orientation of neural progenitor cells towards the lesion site in the rostral and caudal stumps of the regenerating spinal cord respectively (arrows show the orientation direction). The neurofilament marker NF is very faint in (B) although abundant in (F) (arrowheads). (C) and (G) show the nuclei demarked by Bis-Benzimide while (D) is an overlay snapshot showing a single NF-labeled cell (arrowhead) and the abundant nestin labeling surrounding blue nuclei. (H) is an overlay snapshot showing NF-labeled cells far from the lesion site (arrowheads) and the abundant nestin labeling closer to the lesion site. Scale bar for (A–D) = 120 μm ; for (E–G) = 20 μm .

NESTIN AND NEUROFILAMENT EXPRESSION IN SPINALLY TRANSECTED ANIMALS 24 WEEKS AFTER SPINAL CORD LESION

At the end of the process of spinal cord regeneration, when the animal completely recovered its locomotor activity after 24 weeks

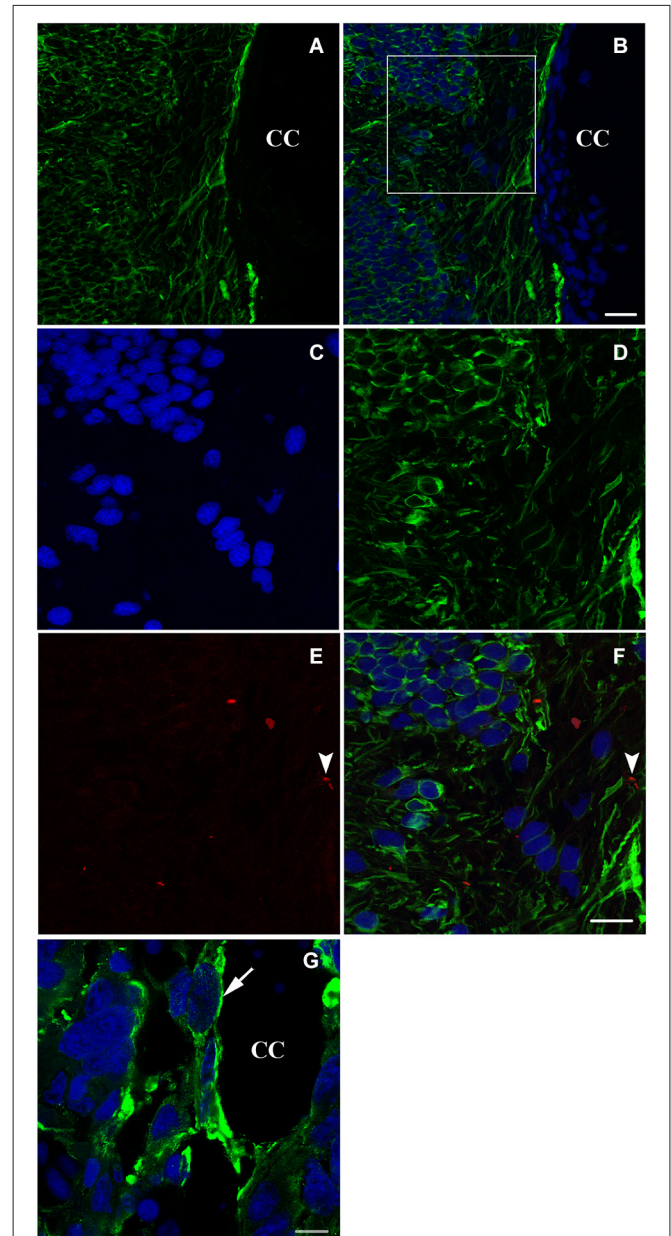


FIGURE 3 | Longitudinal sections (A–F) and a transverse section (G) showing immunohistochemical analysis of nestin (green) and NF (red in E,F) labeling during spinal cord regeneration after 6 weeks of spinal cord transection. In (A), nestin expression increases dramatically. (B) represents an overlay of nestin and bis-benzimide-labeled nuclei. The white square is magnified in (C–F). (C) shows the bis-benzimide-labeled nuclei. (D) shows nestin-labeled cells. The neurofilament marker NF is rare in (E: arrowhead). (F) is an overlay snapshot showing a single NF-labeled cell (arrowhead) and the abundant nestin labeling. In (G), nestin is localizing around the central canal (CC) during spinal cord regeneration, 6 weeks after transection. Scale bar in (B) stands for (A,B) = 70 μm , in (F) stands for (C–F) = 40 μm and in (G) = 20 μm .

of the operation, sections taken in the lesion site showed the disappearance of the big amount of nestin leaving behind instead a faint labeling (Figure 4A). In the same location, we saw a stronger labeling of NF (Figure 4B), which implies that the

newly formed neurons are finally differentiated expressing only NF. This is confirmed by the absence of colocalization between nestin remnants and the neurofilament marker NF as shown in (Figure 4D).

FGF-2 AND FGFR2 mRNA IN SHAM-OPERATED AND SPINALLY-TRANSECTED ANIMALS

In previous studies (Moftah et al., 2008, 2012), we correlated the recovery of locomotor activity with FGF-2 and FGFR2 mRNAs expression. To investigate the relation between the transcriptional activity of this growth factor and its receptor with neurogenesis, we studied the distribution of FGF-2 and FGFR2 mRNA in the same regions we used for nestin immunohistochemistry, by using *in situ* hybridization (Figure 5). Analysis of grain density showed that lesioned animals, 15 weeks after the operation, express high levels of FGF-2 (Figure 5B) and FGFR2 (Figure 5E) mRNA compared to sham-operated animals (Figures 5A,D). FGF-2 mRNA was mainly seen in a ventrolateral position as shown in Figures 5A,B. However, grains demarking FGFR2 mRNA were more prominent in the cells lining the central canal, namely the ependymal cells, as shown in Figures 5D,E. mRNAs grain density quantification showed that FGF-2 significantly increased in lesioned animals 15 weeks post-operatively ($p = 0.005$) compared to the shams (Figure 5C). This increase is consistent as to FGFR2 mRNA but has a smaller magnitude ($p = 0.03$) than its ligand (Figure 5F).

FGF-2 PROTEIN EXPRESSION IN INTACT, SHAM-OPERATED AND SPINALLY TRANSECTED ANIMALS

In intact animals, western blot assays showed significantly less FGF-2 protein in the anterior part of the spinal cord (Ant SC: corresponding to the pre-lesional portion in transected animals) than in the posterior portion of trunk spinal cord (Post SC; Figure 6A; upper left panel; $p = 0.01$). This was even more evident but inverted in the case of spinally-transected and sham-operated animals where the Ant SC showed more FGF-2 protein expression than Post SC (Figure 6A; upper middle and right panels). Although there was no spinal cord transection in shams, the fact that the skin, muscles and bones were lesioned caused the increase of FGF-2 in the anterior part of the neural axis. Figure 6B shows that the intensity of FGF-2 band of spinally-transected animals is significantly stronger than that of the sham-operated ones 15 weeks post-operatively ($p = 0.008$). This is probably due to spinal cord transection that is absent in shams. Compared to the beta-actin bands, the Ant SC of sham-operated animals was the closest, thus normalized to 100% of intensity. All other bands were compared to it. Figure 6C shows that the intensity of FGF-2 band of spinally-transected animals is slightly but not significantly stronger than that of the intact and the sham-operated ones 15 weeks post-operatively ($p = 0.01$). This implies that FGF-2 protein expression follows a rostrocaudal gradient after complete spinal transection.

DISCUSSION

Urodele amphibian spinal cord regeneration is a unique experimental system in that urodeles are the only tetrapod vertebrates

that are strong regenerators in adulthood (Nicolas et al., 1999). Retention of embryonic character is cited as a property that supports this regeneration process (Chernoff, 1996), but it is not clear to what extent embryonic processes involved in the CNS development is retained or re-expressed. Regenerating urodele spinal cord clearly does not recapitulate the early events of neurogenesis. However, the example of limb regeneration suggests that some embryonic patterning and differentiative processes would be required to structure and restore function completely (Stocum, 1996; Brockes, 1997; Christensen et al., 2002). In this study, we show some of these embryonic patterning phenomena and differentiative processes, namely, possible cell migration from the deep layers of the lesioned spinal cord towards the central canal (Figures 2A,E) and differentiation of neuronal progenitors expressing nestin into adult neurons expressing NF (Figures 4B,D).

Caudal regeneration studies have shown that multipotent cells are still present in the spinal cord of adult urodeles (Benraiss et al., 1996). The ependymogial cells of the adult urodele spinal cord are considered pluripotent stem cells that can be recruited for both CNS and peripheral nervous system (PNS) regeneration (Benraiss et al., 1996, 1997). They have been found to produce neuronal cells (Egar and Singer, 1972; Nordlander and Singer, 1978; Arsanto et al., 1992; Benraiss et al., 1996; Zhang et al., 2000). Ependymal cells line the central canal of the spinal cord in all vertebrates, but in regenerating spinal cord they either retain some of the developmental potential of the embryonic neuroepithelium, or they can be stimulated by injury to proliferate and remodel their tissue organization (Chernoff, 1996). We show in the present study, a strong expression of nestin in the cells lining the central canal throughout the regeneration process (Figure 3G), confirming that this neuroepithelium helped reorganize the spinal cord tissue after lesion.

Although proliferation and migration of neural stem cells in the central canal of spinal cord during injuries are well studied in mammals (Horner et al., 2000; Mothe and Tator, 2005), new-born neurons from neural stem cells post SCI are very limited and vulnerable (Dobkin and Havton, 2004; Otori et al., 2006). Moreover, recent data reveal that the ependymal stem cells eventually lose their proliferative capacity during their migration to the lesion site (Chi et al., 2006; Ke et al., 2006). In the present study, we showed that new-born neurons from both stumps of the injured spinal cord in urodele amphibians are oriented towards the lesion site giving the impression that they are migrating in order to fill the gap and form a new regenerated portion of the cord (Figure 1). We also illustrated that ependymal cells are most likely the major source of proliferative cells. Moreover, recent studies in zebra fish showed that new-born neurons were seen to be regenerated from proliferating ventricular radial glia precursors (Reimer et al., 2008, 2009; Kuscha et al., 2012a,b) and that they form synapses indicating functional integration of these cells into the nervous tissue (Adolf et al., 2006; Grandel et al., 2006; Kroehne et al., 2011; Rothenaigner et al., 2011).

In fact, an ependymal response occurs during spinal cord regeneration in all vertebrates that can regenerate injured spinal cord as adults: teleost fish, urodele amphibians and lizards in their

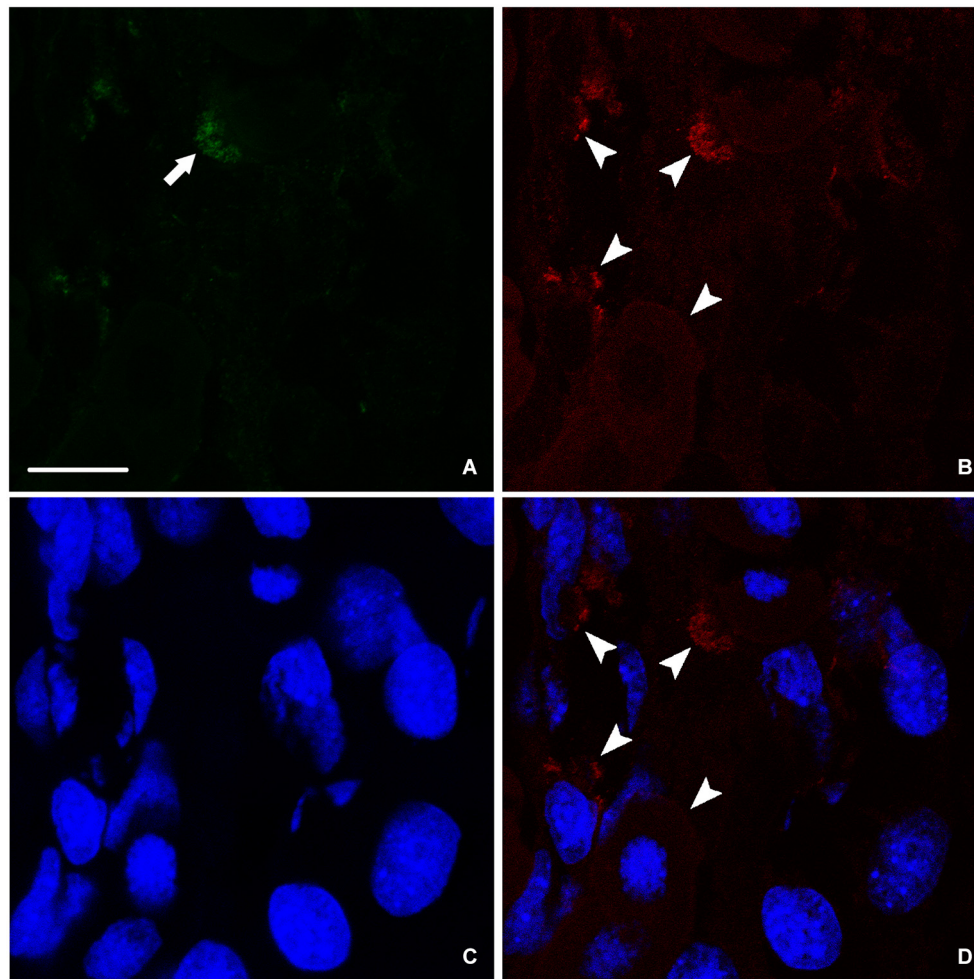


FIGURE 4 | Immunohistochemical analysis of nestin (green) and NF (red) labeling during spinal cord regeneration after 24 weeks of spinal cord transection. (A) Faint nestin expression (arrow) situated far from the central

canal. NF; arrowheads in (B), is prominent. (C) Nuclei demarked by Bis-Benzimide. (D) is an overlay snapshot showing neurofilament surrounding the blue nuclei (arrowheads). Scale bar = 25 μm .

tails (Simpson, 1968; Egar et al., 1970; Egar and Singer, 1972; Anderson et al., 1986, 1994; Alibardi and Meyer-Rochow, 1988; Duffy et al., 1992). It has been recently shown that quiescent ependymoglia cells can be activated to proliferate and regenerate the lost cells after a CNS lesion (Berg et al., 2010). As ependymal remodeling occurs, there are interactions between ependymal cells and neurons and, possibly, between ependymal cells and fibrous astrocytes and oligodendrocytes (Chernoff, 1996; Mofteh et al., 2008, 2012; Fahmy and Mofteh, 2010).

Glia cells have been recently demonstrated to be able to differentiate into neuronal lineages (Morrens et al., 2012), and participate in the neuronal replacement in CNS injuries (Buffo et al., 2005). During the regeneration process in urodele spinal cord, there are GFAP-positive cells (Zamora and Mutin, 1988; Fahmy and Mofteh, 2010). Bodega et al. (1994) surveyed 11 vertebrate species from fish to mammals examining GFAP expression in ependymal cells. They found that lower vertebrates had more GFAP in ependymal cells than higher

vertebrates. Previous studies argued that GFAP+ cells could differentiate into neurons (Garcia et al., 2004; Berninger et al., 2007; Namba et al., 2011), activate astrocytes (Fahmy and Mofteh, 2010) and that GFAP+ astroglia can resume proliferation after SCI.

The modulation of urodele ependymal cell proliferation and differentiation by bFGF demonstrates properties reminiscent of mammalian neural stem cells (O'Hara and Chernoff, 1994; Zhang et al., 2000; Temple, 2001). It is possible that, instead of retention of embryonic properties *per se*, regeneration capacity reflects expression of neural stem cell properties in specialized cell populations. As they respond to the early events following injury, ependymal cells may become a buffer between the neurons and the processes that trigger secondary cell death and axonal degeneration (Chernoff, 1996). In the present study we show that the up regulation of FGF-2 and its receptor FGFR2 is time-dependent. They increase right after lesion reaching a peak at 15 weeks post-transection, after which they decrease

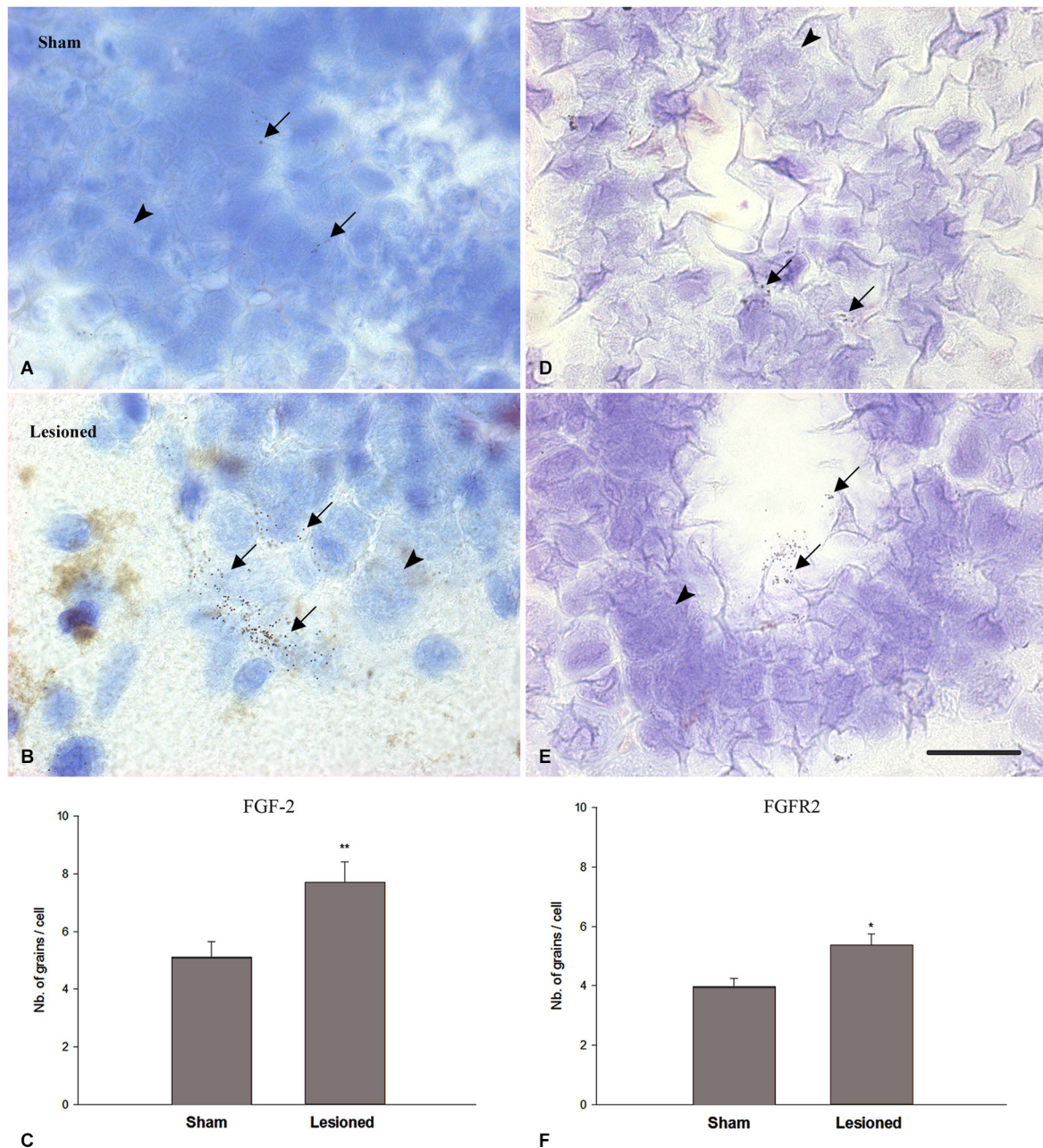
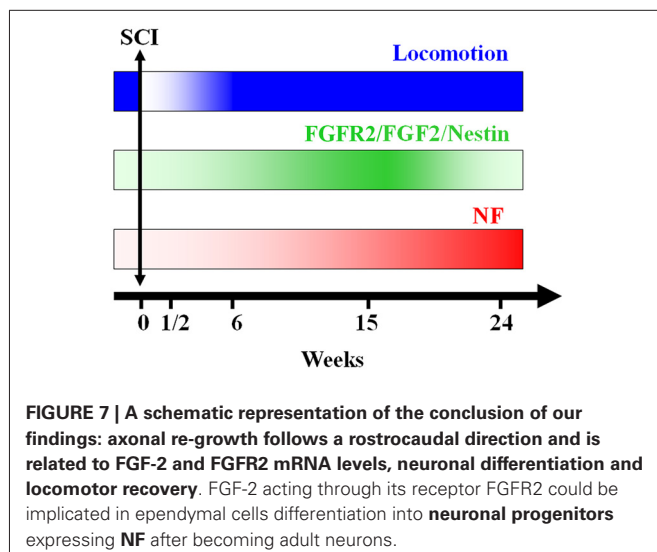
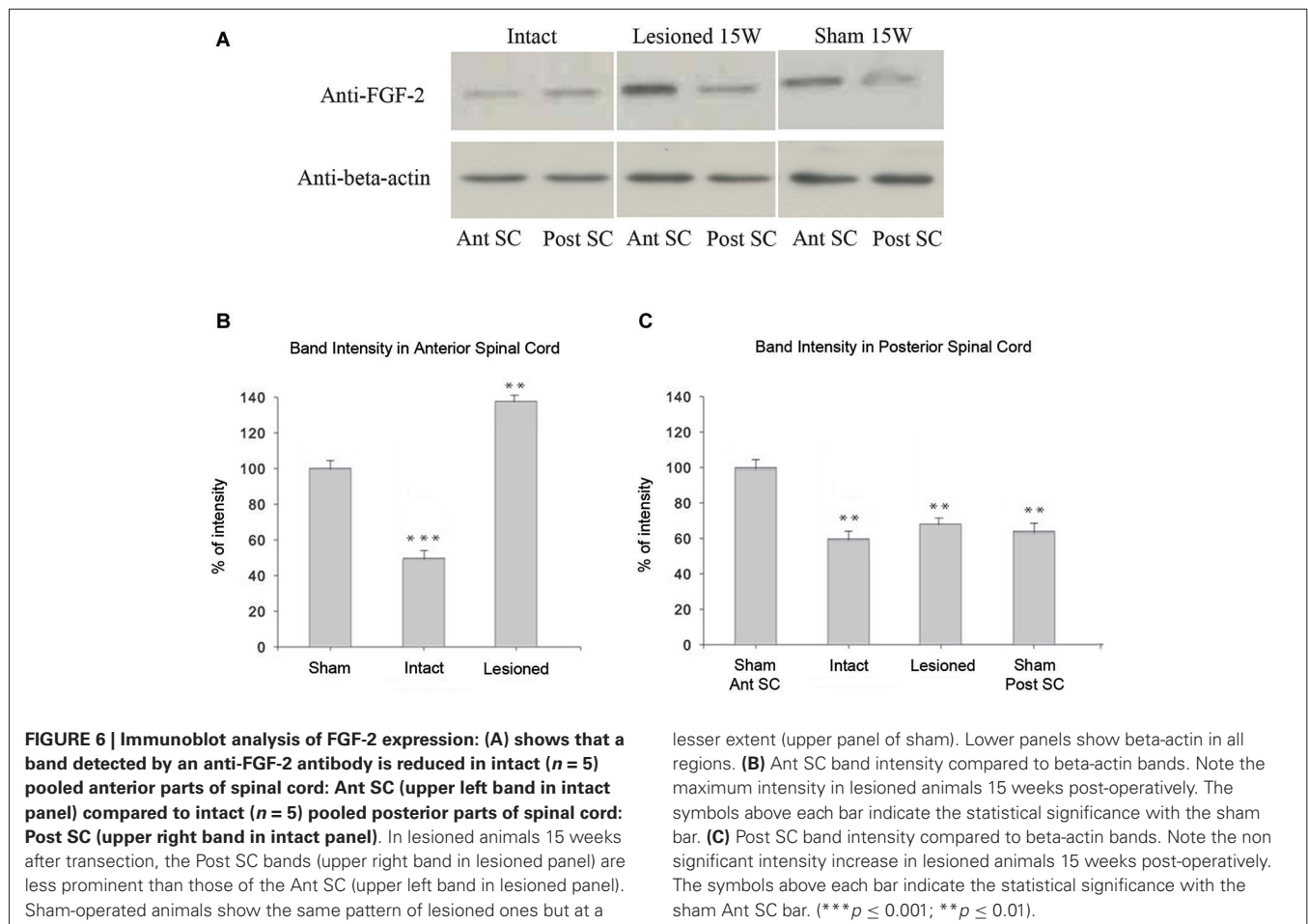


FIGURE 5 | FGF2 (A–C) and FGFR2 mRNA (D–F) expression (in pre-lesional spinal cord) in sham-operated (A,D) and spinal-transected (B,E) animals at 15 weeks post-operatively. (A) Localization of FGF-2 mRNA in cross sections of spinal cord showing *in situ* hybridization in the anterior region in sham-operated animals. (B) shows anterior spinal cord in lesioned animals. (D) Localization of FGFR2 mRNA in cross sections of spinal cord showing *in situ* hybridization in the anterior region in sham-operated animals. (E) shows anterior spinal cord in lesioned animals. All sections are dorsoventrally oriented. Arrows in (A,B,D,E) show the grains demarking hybridized FGF-2 (A,B) and FGFR2 (D,E) mRNAs, while arrowheads point at non

labeled cells. Grains demarking hybridized FGF-2 mRNAs are more pronounced in number ventrolaterally (arrows in B) while FGFR2 grain distribution is mainly seen in the ependymal cells, lining the central canal (arrows in E). Scale bar = 40 μ m. (C) Comparison between FGF-2 mRNA grain density in sham-operated and lesioned animals. In sham-operated animals, the level of grain density is significantly less compared to spinal-transected animals. (F) Comparison between FGFR2 mRNA grain density in sham-operated and lesioned animals. A slight increase was observed in lesioned animals compared to shams. Symbols above lesioned animals' bars indicate their statistical significance compared to sham-operated animals' bars. (** $p \leq 0.01$; * $p < 0.05$).

during locomotion recovery (Figure 7). It has been previously suggested that there is an autoregulatory mechanism by FGF-2

for producing appropriate numbers of neurons. As neurogenesis proceeds, the levels of FGF-2 increase to prevent further neuronal



production from progenitors. This may be through promotion of a specific glial progenitor at the expense of the neuronal progenitor (Nelson and Svendsen, 2006).

In conclusion, the present study shows that, after complete transection of the mid-trunk spinal cord, when the animal's

hind limbs are entirely paralyzed, Nestin, FGF-2 and FGFR2 are gradually expressed throughout the regeneration process reaching a peak at 15 weeks after lesion concomitant with recovery of the locomotor activity. Following this peak, the levels of these factors diminish dramatically while the neurofilament marker NF starts to increase showing the transformation of neural progenitors into adult neurons (Figure 7). This suggests that neurogenesis is a main player in the spontaneous regeneration observed in this species.

Finally, urodele spinal cord regeneration can make an important contribution by defining the requirements for successful CNS regeneration through experimental manipulation of a regenerating adult system that allows examination of the cell interactions that elicit regeneration. Nevertheless, it is clear that we are just starting to understand the integration of various molecular regulators of neurogenesis.

REFERENCES

- Adolf, B., Chapouton, P., Lam, C. S., Topp, S., Tannhauser, B., Strahle, U., et al. (2006). Conserved and acquired features of adult neurogenesis in the zebrafish telencephalon. *Dev. Biol.* 295, 278–293. doi: 10.1016/j.ydbio.2006.03.023
- Alibardi, L., and Meyer-Rochow, V. B. (1988). Ultrastructure of the neural component of the regenerating spinal cord in the tails of three species of New Zealand lizards. *N. Z. J. Zool.* 15, 535–550. doi: 10.1080/03014223.1988.10422633

- Almqvist, P. M., Mah, R., Lendahl, U., Jacobsson, B., and Hendson, G. (2002). Immunohistochemical detection of nestin in pediatric brain tumors. *J. Histochem. Cytochem.* 50, 147–158. doi: 10.1177/002215540205000203
- Anderson, M. J., Choy, C. Y., and Waxman, S. G. (1986). Self-organization of ependyma in regenerating teleost spinal cord: evidence from serial section reconstructions. *J. Embryol. Exp. Morphol.* 96, 1–18.
- Anderson, M. J., Rossetto, D. L., and Lorenz, L. A. (1994). Neuronal differentiation in vitro from precursor cells of regenerating spinal cord of the adult teleost *Apteronotus albifrons*. *Cell Tissue Res.* 278, 243–248. doi: 10.1007/s004410050213
- Arsanto, J. P., Komorowski, T. E., Dupin, F., Caubit, X., Diano, M., Geraudie, J., et al. (1992). Formation of the peripheral nervous system during tail regeneration in urodele amphibians: ultrastructural and immunohistochemical studies of the origin of the cells. *J. Exp. Zool.* 264, 273–292. doi: 10.1002/jez.1402640307
- Becker, T., Lieberoth, B. C., Becker, C. G., and Schachner, M. (2005). Differences in the regenerative response of neuronal cell populations and indications for plasticity in intraspinal neurons after spinal cord transection in adult zebrafish. *Mol. Cell. Neurosci.* 30, 265–278. doi: 10.1016/j.mcn.2005.07.008
- Benraiss, A., Arsanto, J. P., Coulon, J., and Thouveny, Y. (1997). Neural crest-like cells originate from the spinal cord during tail regeneration in adult amphibian urodeles. *Dev. Dyn.* 209, 15–28. doi: 10.1002/(sici)1097-0177(199705)209:1<15::aid-aja>3.3.co;2-c
- Benraiss, A., Arsanto, J. P., Coulon, J., and Thouveny, Y. (1999). Neurogenesis during caudal spinal cord regeneration in adult newts. *Dev. Genes Evol.* 209, 363–369. doi: 10.1007/s004270050265
- Benraiss, A., Caubit, X., Arsanto, J. P., Coulon, J., Nicolas, S., Le Parco, Y., et al. (1996). Clonal cell cultures from adult spinal cord of the amphibian urodele *Pleurodeles Waltlii* to study the identity and potentialities of cells during tail regeneration. *Dev. Dyn.* 205, 135–149. doi: 10.1002/(sici)1097-0177(199602)205:2<135::aid-aja>3.0.co;2-j
- Berg, D. A., Kirkham, M., Beljajeva, A., Knapp, D., Habermann, B., Ryge, J., et al. (2010). Efficient regeneration by activation of neurogenesis in homeostatically quiescent regions of the adult vertebrate brain. *Development* 137, 4127–4134. doi: 10.1242/dev.055541
- Berninger, B., Costa, M. R., Koch, U., Schroeder, T., Sutor, B., Grothe, B., et al. (2007). Functional properties of neurons derived from in vitro reprogrammed postnatal astroglia. *J. Neurosci.* 27, 8654–8664. doi: 10.1523/jneurosci.1615-07.2007
- Bodega, G., Suarez, I., Rubio, M., and Fernandez, B. (1994). Ependyma: phylogenetic evolution of glial fibrillary acidic protein (GFAP) and vimentin expression in vertebrate spinal cord. *Histochemistry* 102, 113–122. doi: 10.1007/bf00269015
- Brookes, J. P. (1997). Amphibian limb regeneration: rebuilding a complex structure. *Science* 276, 81–87. doi: 10.1126/science.276.5309.81
- Buffo, A., Vosko, M. R., Erturk, D., Hamann, G. F., Jucker, M., Rowitch, D., et al. (2005). Expression pattern of the transcription factor Olig2 in response to brain injuries: implications for neuronal repair. *Proc. Natl. Acad. Sci. U S A* 102, 18183–18188. doi: 10.1073/pnas.0506535102
- Chernoff, E. A. (1996). Spinal cord regeneration: a phenomenon unique to urodeles? *Int. J. Dev. Biol.* 40, 823–831.
- Chernoff, E. A., Stocum, D. L., Nye, H. L., and Cameron, J. A. (2003). Urodele spinal cord regeneration and related processes. *Dev. Dyn.* 226, 295–307. doi: 10.1002/dvdy.10240
- Chevallier, S., Landry, M., Nagy, F., and Cabelguen, J. M. (2004). Recovery of bimodal locomotion in the spinal-transected salamander, *Pleurodeles waltlii*. *Eur. J. Neurosci.* 20, 1995–2007. doi: 10.1111/j.1460-9568.2004.03671.x
- Chi, L., Ke, Y., Luo, C., Li, B., Gozal, D., Kalyanaraman, B., et al. (2006). Motor neuron degeneration promotes neural progenitor cell proliferation, migration and neurogenesis in the spinal cords of amyotrophic lateral sclerosis mice. *Stem Cells* 24, 34–43. doi: 10.1634/stemcells.2005-0076
- Christensen, R. N., Weinstein, M., and Tassava, R. A. (2002). Expression of fibroblast growth factors 4, 8 and 10 in limbs, flanks and blastemas of *Ambystoma*. *Dev. Dyn.* 223, 193–203. doi: 10.1002/dvdy.10049
- Clarke, J. D., Alexander, R., and Holder, N. (1988). Regeneration of descending axons in the spinal cord of the axolotl. *Neurosci. Lett.* 89, 1–6. doi: 10.1016/0304-3940(88)90471-5
- Davis, B. M., Duffy, M. T., Simpson, S. B. Jr. (1989). Bulbospinal and intraspinal connections in normal and regenerated salamander spinal cord. *Exp. Neurol.* 103, 41–51. doi: 10.1016/0014-4886(89)90183-0
- Del Bigio, M. (1995). The ependymal; a protective barrier between brain and cerebrospinal fluid. *Glia* 14, 1–13. doi: 10.1002/glia.440140102
- Dobkin, B. H., and Havton, L. A. (2004). Basic advances and new avenues in therapy of spinal cord injury. *Annu. Rev. Med.* 55, 255–282. doi: 10.1146/annurev.med.55.091902.104338
- Duffy, M. T., Lieblich, D. R., Garner, L. K., Hawrych, A., Simpson, S. B. Jr., and Davis, B. M. (1992). Axonal sprouting and frank regeneration in the lizard tail spinal cord: correlation between changes in synaptic circuitry and axonal growth. *J. Comp. Neurol.* 316, 363–374. doi: 10.1002/cne.903160307
- Egar, M., Simpson, S. B., and Singer, M. (1970). The growth and differentiation of the regenerating spinal cord of the lizard. *J. Morphol.* 131, 131–151. doi: 10.1002/jmor.1051310202
- Egar, M., and Singer, M. (1972). The role of ependyma in spinal cord regeneration in the urodele, *Triturus*. *Exp. Neurol.* 37, 422–430. doi: 10.1016/0014-4886(72)90085-4
- Endo, T., Yoshino, J., Kado, K., and Tochinai, S. (2007). Brain regeneration in anuran amphibians. *Dev. Growth Differ.* 49, 121–129. doi: 10.1111/j.1440-169x.2007.00914.x
- Fahmy, G. H., and Mofteh, M. Z. (2010). FGF-2 in Astroglial cells during Vertebrate spinal cord recovery. *Front. Cell. Neurosci.* 4:129. doi: 10.3389/fncel.2010.00129
- Font, E., Desfilis, E., Perez-Canellas, M. M., and Garcia-Verdugo, J. M. (2001). Neurogenesis and neuronal regeneration in the adult reptilian brain. *Brain Behav. Evol.* 58, 276–295. doi: 10.1159/000057570
- Garcia, A. D., Doan, N. B., Imura, T., Bush, T. G., and Sofroniew, M. V. (2004). GFAP-expressing progenitors are the principal source of constitutive neurogenesis in adult mouse forebrain. *Nat. Neurosci.* 7, 1233–1241. doi: 10.1038/nn1340
- Goldman, S. A. (2004). Directed mobilization of endogenous neural progenitor cells: the intersection of stem cell biology and gene therapy. *Curr. Opin. Mol. Ther.* 6, 466–472.
- González-Granero, S. L. M., and Gracia-Verdugo, J. M. (2011). “Adult neurogenesis in reptiles,” in *Neurogenesis in the Adult Brain* (Vol. 1), eds T. Seki, K. Sawamoto, J. M. Parent and A. Alvarez-Buylla (USA: Springer), 169–189.
- Grandel, H., Kaslin, J., Ganz, J., Wenzel, I., and Brand, M. (2006). Neural stem cells and neurogenesis in the adult zebrafish brain: origin, proliferation dynamics, migration and cell fate. *Dev. Biol.* 295, 263–277. doi: 10.1016/j.ydbio.2006.03.040
- Hagg, T. (2005). Molecular regulation of adult CNS neurogenesis: an integrated view. *Trends Neurosci.* 28, 589–595. doi: 10.1016/j.tins.2005.08.009
- Hegedus, B., Dasgupta, B., Shin, J. E., Emmett, R. J., Hart-Mahon, E. K., Elghazi, L., et al. (2007). Neurofibromatosis-1 regulates neuronal and glial cell differentiation from neuroglial progenitors in vivo by both cAMP- and Ras-dependent mechanisms. *Cell Stem Cell* 1, 443–457. doi: 10.1016/j.stem.2007.07.008
- Holder, N., and Clarke, J. D. (1988). Is there a correlation between continuous neurogenesis and directed axon regeneration in the vertebrate nervous system? *Trends Neurosci.* 11, 94–99. doi: 10.1016/0166-2236(88)90151-8
- Horner, P. J., Power, A. E., Kempermann, G., Kühn, H. G., Palmer, T. D., Winkler, J., et al. (2000). Proliferation and differentiation of progenitor cells throughout the intact adult rat spinal cord. *J. Neurosci.* 20, 2218–2228.
- Kaslin, J., Ganz, J., and Brand, M. (2008). Proliferation, neurogenesis and regeneration in the non-mammalian vertebrate brain. *Philos. Trans. R. Soc. Lond. B Biol. Sci.* 363, 101–122. doi: 10.1098/rstb.2006.2015
- Ke, Y., Chi, L., Xu, R., Luo, C., Gozal, D., and Liu, R. (2006). Early response of endogenous adult neural progenitor cells to acute spinal cord injury in mice. *Stem Cells* 24, 1011–1019. doi: 10.1634/stemcells.2005-0249
- Kizil, C., Dudczig, S., Kyritsis, N., Machate, A., Blaesche, J., Kroehne, V., et al. (2012a). The chemokine receptor cxcr5 regulates the regenerative neurogenesis response in the adult zebrafish brain. *Neural Dev.* 7:27. doi: 10.1186/1749-8104-7-27
- Kizil, C., Kaslin, J., Kroehne, V., and Brand, M. (2012b). Adult neurogenesis and brain regeneration in zebrafish. *Dev. Neurobiol.* 72, 429–461. doi: 10.1002/dneu.20918
- Kroehne, V., Freudenreich, D., Hans, S., Kaslin, J., and Brand, M. (2011). Regeneration of the adult zebrafish brain from neurogenic radial glia-type progenitors. *Development* 138, 4831–4841. doi: 10.1242/dev.072587
- Kuscha, V., Barreiro-Iglesias, A., Becker, C. G., and Becker, T. (2012a). Plasticity of tyrosine hydroxylase and serotonergic systems in the regenerating spinal cord of adult zebrafish. *J. Comp. Neurol.* 520, 933–951. doi: 10.1002/cne.22739
- Kuscha, V., Frazer, S. L., Dias, T. B., Hibi, M., Becker, T., and Becker, C. G. (2012b). Lesion-induced generation of interneuron cell types in specific dorsoventral

- domains in the spinal cord of adult zebrafish. *J. Comp. Neurol.* 520, 3604–3616. doi: 10.1002/cne.23115
- Laemmlí, U. K. (1970). Cleavage of structural proteins during the assembly of the head of bacteriophage T4. *Nature* 227, 680–685. doi: 10.1038/227680a0
- Lam, H. J., Patel, S., Wang, A., Chu, J., and Li, S. (2010). In vitro regulation of neural differentiation and axon growth by growth factors and bioactive nanofibers. *Tissue Eng. Part A* 16, 2641–2648. doi: 10.1089/ten.tea.2009.0414
- Landry, M., Holmberg, K., Zhang, X., and Hokfelt, T. (2000). Effect of axotomy on expression of NPY, galanin and NPY Y1 and Y2 receptors in dorsal root ganglia and the superior cervical ganglion studied with double-labeling in situ hybridization and immunohistochemistry. *Exp. Neurol.* 162, 361–384. doi: 10.1006/exnr.1999.7329
- Lendahl, U., Zimmermann, L. B., and McKay, R. D. (1990). CNS stem cells express a new class of intermediate filament protein. *Cell* 60, 585–595. doi: 10.1016/0092-8674(90)90662-x
- Melodew, K., Suhr, R., Uwanogho, D. A., Reuter, I., Lendahl, U., Hodges, H., et al. (2004). Nestin expression is lost in a neural stem cell line through a mechanism involving the proteasome and Notch signalling. *Brain Res. Dev. Brain Res.* 151, 13–23. doi: 10.1016/j.devbrainres.2004.03.018
- Mofteh, M. (2007). Differential effects of FGF-2 on cell cultures from juvenile brainstem and body spinal cord of the Urodele *Pleurodeles waltlii*. *Egypt Zool.* 48, 21–44.
- Mofteh, M., Downie, S. A., Bronstein, N. B., Mezentseva, N., Pu, J., Maher, P. A., et al. (2002). Ectodermal FGFs induce perinodular inhibition of limb chondrogenesis in vitro and in vivo via FGF receptor 2. *Dev. Biol.* 249, 270–282. doi: 10.1006/dbio.2002.0766
- Mofteh, M., Landry, M., Nagy, F., and Cabelguen, J. M. (2008). Fibroblast growth factor-2 mRNA expression in the brainstem and spinal cord of normal and chronic spinally transected urodeles. *J. Neurosci. Res.* 86, 3348–3358. doi: 10.1002/jnr.21776
- Mofteh, M., Landry, M., Nagy, F., and Cabelguen, J. M. (2012). Spatial distribution of fibroblast growth factor receptor 2 in normal and lesioned central nervous system of *Pleurodeles waltlii*. *Am. J. Neurosci.* 3, 41–53. doi: 10.3844/amjnsp.2012.41.53
- Morrens, J., Van Den Broeck, W., and Kempermann, G. (2012). Glial cells in adult neurogenesis. *Glia* 60, 159–174. doi: 10.1002/glia.21247
- Mothe, A. J., and Tator, C. H. (2005). Proliferation, migration and differentiation of endogenous ependymal region stem/progenitor cells following minimal spinal cord injury in the adult rat. *Neuroscience* 131, 177–187. doi: 10.1016/j.neuroscience.2004.10.011
- Namba, T., Mochizuki, H., Suzuki, R., Onodera, M., Yamaguchi, M., Namiki, H., et al. (2011). Time-lapse imaging reveals symmetric neurogenic cell division of GFAP-expressing progenitors for expansion of postnatal dentate granule neurons. *PLoS One* 6:e25303. doi: 10.1371/journal.pone.0025303
- Nelson, A. D., and Svendsen, C. N. (2006). Low concentrations of extracellular FGF-2 are sufficient but not essential for neurogenesis from human neural progenitor cells. *Mol. Cell. Neurosci.* 33, 29–35. doi: 10.1016/j.mcn.2006.06.003
- Nicolas, S., Caubit, X., Massacrier, A., Cau, P., and Le Parco, Y. (1999). Two Nkx-3-related genes are expressed in the adult and regenerating central nervous system of the urodele *Pleurodeles waltlii*. *Dev. Genet.* 24, 319–328. doi: 10.1002/(sici)1520-6408(1999)24:3/4<319::aid-dvg15>3.0.co;2-#
- Nordlander, R. H., and Singer, M. (1978). The role of ependyma in regeneration of the spinal cord in the urodele amphibian tail. *J. Comp. Neurol.* 180, 349–374. doi: 10.1002/cne.901800211
- O'Hara, C. M., and Chernoff, E. A. (1994). Growth factor modulation of injury-reactive ependymal cell proliferation and migration. *Tissue Cell* 26, 599–611. doi: 10.1016/0040-8166(94)90012-4
- O'Hara, C. M., Egar, M. W., and Chernoff, E. A. (1992). Reorganization of the ependyma during axolotl spinal cord regeneration: changes in intermediate filament and fibronectin expression. *Dev. Dyn.* 193, 103–115. doi: 10.1002/aja.1001930202
- Ohori, Y., Yamamoto, S., Nagao, M., Sugimori, M., Yamamoto, N., Nakamura, K., et al. (2006). Growth factor treatment and genetic manipulation stimulate neurogenesis and oligodendrogenesis by endogenous neural progenitors in the injured adult spinal cord. *J. Neurosci.* 26, 11948–11960. doi: 10.1523/jneurosci.3127-06.2006
- Parish, C. L., Beljajeva, A., Arenas, E., and Simon, A. (2007). Midbrain dopaminergic neurogenesis and behavioural recovery in a salamander lesion-induced regeneration model. *Development* 134, 2881–2887. doi: 10.1242/dev.002329
- Reimer, M. M., Kuscha, V., Wyatt, C., Sörensen, I., Frank, R. E., Knüwer, M., et al. (2009). Sonic hedgehog is a polarized signal for motor neuron regeneration in adult zebrafish. *J. Neurosci.* 29, 15073–15082. doi: 10.1523/JNEUROSCI.4748-09.2009
- Reimer, M. M., Sörensen, I., Kuscha, V., Frank, R. E., Liu, C., Becker, C. G., et al. (2008). Motor neuron regeneration in adult zebrafish. *J. Neurosci.* 28, 8510–8516. doi: 10.1523/JNEUROSCI.1189-08.2008
- Rothenaigner, I., Krecsmarik, M., Hayes, J. A., Bahn, B., Lepier, A., Fortin, G., et al. (2011). Clonal analysis by distinct viral vectors identifies bona fide neural stem cells in the adult zebrafish telencephalon and characterizes their division properties and fate. *Development* 138, 1459–1469. doi: 10.1242/dev.058156
- Rydell, R. E., and Greene, L. A. (1987). Acidic and basic fibroblast growth factors promote stable neurite outgrowth and neuronal differentiation in cultures of PC12 cells. *J. Neurosci.* 7, 3639–3653.
- Scharff, C., Kirn, J. R., Grossman, M., Macklis, J. D., and Nottebohm, F. (2000). Targeted neuronal death affects neuronal replacement and vocal behavior in adult songbirds. *Neuron* 25, 481–492. doi: 10.1016/s0896-6273(00)80910-1
- Simpson, S. B. Jr. (1968). Morphology of the regenerated spinal cord in the lizard, *Anolis carolinensis*. *J. Comp. Neurol.* 134, 193–210. doi: 10.1002/cne.901340207
- Stensaas, L. J. (1983). "Regeneration in the spinal cord of the newt *Notophthalmus (triturus) pyrrhogaster*," in *Spinal Cord Reconstruction*, eds C. C. Kao, R. P. Bunge and P. J. Reier (New York: Raven Press), 121–149.
- Stocum, D. L. (1995). "Tissue regeneration," in *Wound Repair, Regeneration and Artificial Tissues* (Austin, TX: R. G. Landes Publishing Company), 21–50.
- Stocum, D. L. (1996). A conceptual framework for analyzing axial patterning in regenerating urodele limbs. *Int. J. Dev. Biol.* 40, 773–783.
- Tanaka, E. M., and Ferretti, P. (2009). Considering the evolution of regeneration in the central nervous system. *Nat. Rev. Neurosci.* 10, 713–723. doi: 10.1038/nrn2707
- Temple, S. (2001). Stem cell plasticity—building the brain of our dreams. *Nat. Rev. Neurosci.* 2, 513–520. doi: 10.1038/35081577
- Wilson, P. G., and Stice, S. S. (2006). Development and differentiation of neural rosettes derived from human embryonic stem cells. *Stem Cell Rev.* 2, 67–77. doi: 10.1385/scr:2:1:67
- Xu, R. H., Peck, R. M., Li, D. S., Feng, X., Ludwig, T., and Thomson, J. A. (2005). Basic FGF and suppression of BMP signaling sustain undifferentiated proliferation of human ES cells. *Nat. Methods* 2, 185–190. doi: 10.1038/nmeth744
- Zamora, A. J., and Mutin, M. (1988). Vimentin and glial fibrillary acidic protein filaments in radial glia of the adult urodele spinal cord. *Neuroscience* 27, 279–288. doi: 10.1016/0306-4522(88)90237-0
- Zhang, F., Clarke, J. D., and Ferretti, P. (2000). FGF-2 Up-regulation and proliferation of neural progenitors in the regenerating amphibian spinal cord in vivo. *Dev. Biol.* 225, 381–391. doi: 10.1006/dbio.2000.9843
- Zheng, W., Nowakowski, R. S., and Vaccarino, F. M. (2004). Fibroblast growth factor 2 is required for maintaining the neural stem cell pool in the mouse brain subventricular zone. *Dev. Neurosci.* 26, 181–196. doi: 10.1159/000082136
- Zupanc, G. K., and Clint, S. C. (2003). Potential role of radial glia in adult neurogenesis of teleost fish. *Glia* 43, 77–86. doi: 10.1002/glia.10236

Conflict of Interest Statement: The authors declare that the research was conducted in the absence of any commercial or financial relationships that could be construed as a potential conflict of interest.

Received: 22 August 2014; accepted: 16 December 2014; published online: 13 January 2015.

Citation: Zaky AZ and Mofteh MZ (2015) Neurogenesis and growth factors expression after complete spinal cord transection in *Pleurodeles waltlii*. *Front. Cell. Neurosci.* 8:458. doi: 10.3389/fncel.2014.00458

This article was submitted to the journal *Frontiers in Cellular Neuroscience*.

Copyright © 2015 Zaky and Mofteh. This is an open-access article distributed under the terms of the Creative Commons Attribution License (CC BY). The use, distribution and reproduction in other forums is permitted, provided the original author(s) or licensor are credited and that the original publication in this journal is cited, in accordance with accepted academic practice. No use, distribution or reproduction is permitted which does not comply with these terms.



HMG-CoA reductase inhibition promotes neurological recovery, peri-lesional tissue remodeling, and contralesional pyramidal tract plasticity after focal cerebral ischemia

Ertugrul Kilic¹, Raluca Reitmeir², Ülkan Kilic³, Ahmet Burak Caglayan¹, Mustafa Caglar Beker¹, Taha Kelestemur¹, Muhsine Sinem Ethemoglu¹, Gurkan Ozturk¹ and Dirk M. Hermann^{2*}

¹ Department of Physiology, Istanbul Medipol University, Istanbul, Turkey

² Department of Neurology, University Hospital, Essen, Germany

³ Department of Medical Biology, Istanbul Medipol University, Istanbul, Turkey

Edited by:

Marie Z. Mofteh, Alexandria University, Egypt

Reviewed by:

Marco Bacigaluppi, Università

Vita-Salute San Raffaele, Italy

Yasemin Ozdemir, Hacettepe

University, Turkey

*Correspondence:

Dirk M. Hermann, Department of Neurology, University Hospital Essen, Hufelandstr. 55, Essen D-45122, Germany

e-mail: dirk.hermann@uk-essen.de

3-Hydroxy-3-methylglutaryl-coenzyme A (HMG-CoA) reductase inhibitors are widely used for secondary stroke prevention. Besides their lipid-lowering activity, pleiotropic effects on neuronal survival, angiogenesis, and neurogenesis have been described. In view of these observations, we were interested whether HMG-CoA reductase inhibition in the post-acute stroke phase promotes neurological recovery, peri-lesional, and contralesional neuronal plasticity. We examined effects of the HMG-CoA reductase inhibitor rosuvastatin (0.2 or 2.0 mg/kg/day i.c.v.), administered starting 3 days after 30 min of middle cerebral artery occlusion for 30 days. Here, we show that rosuvastatin treatment significantly increased the grip strength and motor coordination of animals, promoted exploration behavior, and reduced anxiety. It was associated with structural remodeling of peri-lesional brain tissue, reflected by increased neuronal survival, enhanced capillary density, and reduced striatal and corpus callosum atrophy. Increased sprouting of contralesional pyramidal tract fibers crossing the midline in order to innervate the ipsilesional red nucleus was noticed in rosuvastatin compared with vehicle-treated mice, as shown by anterograde tract tracing experiments. Western blot analysis revealed that the abundance of HMG-CoA reductase was increased in the contralesional hemisphere at 14 and 28 days post-ischemia. Our data support the idea that HMG-CoA reductase inhibition promotes brain remodeling and plasticity far beyond the acute stroke phase, resulting in neurological recovery.

Keywords: middle cerebral artery occlusion, neurological recovery, neuronal plasticity, restorative therapy, statin, tract tracing

INTRODUCTION

Major efforts have been made in recent years to promote stroke recovery by stimulation of axonal sprouting (Hermann and Chopp, 2012). A variety of strategies have been used for this purpose. Antibodies aiming at the neutralization of axonal growth inhibitors [e.g., Nogo-A (Papadopoulos et al., 2002; Wiessner et al., 2003)], pleiotropic growth factors [e.g., erythropoietin, vascular endothelial growth factor (Reitmeir et al., 2011, 2012)], and neural precursor/stem cells (Bacigaluppi et al., 2009; Andres et al., 2011) have been administered. These treatments are not easily transferrable to human patients due to the inexistence of systemic delivery strategies and/or potential side effects and complications that endanger therapeutic success [e.g., brain inflammation in case of antibodies targeting CNS epitopes (Orgogozo et al., 2003) or malignant transformation in case of cell-based therapies (Amariglio et al., 2009)]. Hence, the clinical translation of plasticity-promoting therapies is still on the way.

Following the stroke prevention by aggressive reduction in cholesterol levels trial (Amarenco et al., 2006), 3-hydroxy-3-methylglutaryl-coenzyme A (HMG-CoA) reductase inhibitors (also called statins) are widely used for secondary stroke prevention. Besides their cholesterol-lowering properties, HMG-CoA reductase inhibitors exert pleiotropic effects in the brain that are beneficial for stroke recovery, promoting post-ischemic neuronal survival (Sironi et al., 2003; Kilic et al., 2005), inhibiting inflammatory responses (Pahan et al., 1997; Kilic et al., 2005), restoring endothelial function (Endres et al., 1998; Amin-Hanjani et al., 2001), and promoting angiogenesis and neurogenesis (Chen et al., 2003).

Based on these multiple observations, we now examined if HMG-CoA reductase inhibition influences neurological recovery and brain plasticity in the post-acute stroke phase. Thus, we exposed mice to intraluminal middle cerebral artery occlusion (MCAO) and investigated effects of the HMG-CoA reductase inhibitor rosuvastatin, administered starting 3 days post-ischemia

(dpi), on functional neurological recovery, peri-lesional brain remodeling, and contralesional pyramidal tract plasticity.

MATERIALS AND METHODS

EXPERIMENTAL GROUPS AND INTERVENTIONS

Experiments were performed using male C57Bl6/j mice (23–25 g) in accordance to National Institutes of Health Guidelines for the Care and Use of Laboratory Animals with local government approval (Istanbul Medipol University, Turkey). A total of four sets of mice were examined:

The first set of mice was exposed to 30 min of left-sided MCAO. At 72 h post-ischemia, animals received implantations of cannula connected to miniosmotic pumps (Alzet 2004; Alzet, Cupertino, CA, USA) into the left lateral ventricle that were randomly filled with vehicle (0.9% NaCl) or rosuvastatin (0.2 or 2 mg/kg/day diluted in 0.9% NaCl) ($n = 10$ animals/group). These miniosmotic pumps were left in place during the subsequent 4 weeks and then removed. At 42 dpi, animals were sacrificed by transcardiac perfusion with 0.9% NaCl. These animals were used for functional neurological studies and conventional histochemistry (Figure S1A in Supplementary Material).

The second set of mice was subjected to 30 min MCAO, followed by implantation of miniosmotic pumps filled with vehicle or rosuvastatin (0.2 or 2 mg/kg/day) 72 h later using the same protocol ($n = 10$ animals/group). The miniosmotic pumps were again left in place for 4 weeks and then removed. At 42 dpi, animals were sacrificed by transcardiac perfusion with 4% paraformaldehyde. These animals were used for functional neurological studies, computer-based stereology, and volumetry (Figure S1B in Supplementary Material).

The third set of mice was submitted to 30 min of MCAO or sham-surgery, following by implantation of miniosmotic pumps filled with vehicle or rosuvastatin (2 mg/kg/day) 72 h later using the same protocol ($n = 10$ animals/group). The miniosmotic pumps were again left in place for 4 weeks and then removed. The animals were used for functional neurological studies and anterograde tract tracing. For this purpose, the anterograde tract tracers cascade-blue-labeled dextran amine [cascade blue (CB)] or biotinylated dextran amine (BDA) (both 10,000 MW; Molecular Probes, Eugene, OR, USA) were injected into the ipsilesional or contralesional motor cortices, respectively, at 42 dpi or 42 days post-sham surgery (Reitmeir et al., 2011, 2012). Ten days later (i.e., at 52 dpi), animals were sacrificed by transcardiac perfusion with 4% paraformaldehyde (Figure S1C in Supplementary Material).

The last set of mice was exposed to 30 min of MCAO followed by 3, 14, 28, or 42 days reperfusion or to sham-surgery followed by 3 days reperfusion ($n = 4$ animals/group) (Kilic et al., 2008). Animals were sacrificed by transcardiac perfusion with 0.9% NaCl. Brains were used for Western blot analysis of HMG-CoA reductase abundance (Figure S1D in Supplementary Material).

Animals were always randomly attributed to experimental groups in a blinded manner. Experimenters analyzing the data were blinded for experimental conditions.

INDUCTION OF FOCAL CEREBRAL ISCHEMIA

Animals were anesthetized with 1% isoflurane (30% O₂, remainder N₂O). Rectal temperature was maintained between 36.5 and

37.0°C using a feedback-controlled heating system. During the experiments, cerebral blood flow was measured by laser Doppler flow (LDF) recordings using a flexible 0.5 mm fiberoptic probe (Perimed, Stockholm, Sweden), which was attached to the intact skull overlying the middle cerebral artery territory (2 mm posterior/6 mm lateral from bregma). LDF changes were monitored up to 30 min after the onset of reperfusion. For intraluminal MCAO, a midline neck incision was made, and the left common and external carotid arteries were isolated and ligated. A microvascular clip (FE691; Aesculap, Tuttlingen, Germany) was temporarily placed on the internal carotid artery. A 8-0 nylon monofilament (Ethilon; Ethicon, Norderstedt, Germany) coated with silicon resin (Xantopren; Bayer Dental, Osaka, Japan; diameter of the coated filament: 180–190 μm) was introduced through a small incision into the common carotid artery and advanced 9 mm distal to the carotid bifurcation for MCAO. Thirty minutes later, reperfusion was initiated by filament removal. In sham-operated animals, a surgical intervention was performed, in which the neck was opened and the common carotid artery was exposed, but left intact, while LDF recordings were performed. After the surgery, wounds were carefully sutured, anesthesia was discontinued and animals were placed back into their cages.

Animals belonging to animal sets one to three (see Experimental Groups and Interventions) were reanesthetized with 1% isoflurane at 72 h post-ischemia. Cannula (Brain infusion kit 3; Alzet, Cupertino, CA, USA) were implanted into the left lateral ventricle (0.0 mm from bregma, 0.8 mm lateral to midline, 1.4 mm below brain surface), which were linked to miniosmotic pumps (Alzet 2004; Alzet), which were randomly filled with vehicle (0.9% NaCl) or rosuvastatin (sc-208316; Santa Cruz, Heidelberg, Germany; 0.2 or 2 mg/kg/day diluted in 0.9% NaCl) and which were placed on the animals backs. These pumps were left in place during the subsequent 4 weeks and then removed.

Animals belonging to animal set three (see Experimental Groups and Interventions) were reanesthetized with 1% isoflurane at 42 dpi or 42 days post-sham surgery. The anterograde tract tracers CB and BDA [both 10,000 MW; 10% dilutions in 0.01 M phosphate-buffered saline (PBS) at pH 7.2; Molecular Probes, Eugene, OR, USA] were injected into the ipsilesional or contralesional motor cortices, respectively, by means of microsyringe injections, as previously reported (Reitmeir et al., 2011, 2012). As such, a total volume of 2.1 μl tracer was administered to each animal, which was injected in three equal deposits located rostrally, medially, and caudally of the needle insertion site into the motor cortex. For this purpose, the needle was inclined 45°, 90°, and 135° against the midline and 45° against the brain surface (needle insertion for all three deposits: 0.5 mm rostral to bregma/2.5 mm lateral to midline; injection ~0.8 mm below brain surface) (Reitmeir et al., 2012, 2011).

FUNCTIONAL NEUROLOGICAL TESTS

Neurological recovery was assessed using grip strength, RotaRod, open field, elevated O maze, and light/dark tests at baseline and on days 7, 14, 28, and 42 after MCAO (Kilic et al., 2008, 2010; Reitmeir et al., 2011).

Grip strength test

The grip strength test consists of a spring balance coupled with a Newtonmeter (Medio-Line Spring Scale, metric, 300 g, Pesola, Switzerland) that is attached to a triangular steel wire, which the animal instinctively grasps. When pulled by the tail, the animal exerts force on the steel wire (Kilic et al., 2010). Grip strength was evaluated at the right paretic forepaw, the left non-paretic forepaw being wrapped with adhesive tape. Grip strength was evaluated five times on occasion of each test, for which mean values were calculated. From these data, percentage values (post-ischemic vs. pre-ischemic) were computed. Pre-ischemic results did not differ between groups.

RotaRod test

The RotaRod is a rotating drum with a speed accelerating from 6 to 40 rpm (model 47600; Ugo Basile, Comerio, Italy), which allows to assess motor coordination skills (Kilic et al., 2010). Maximum speed is reached after 245 s, and the time at which the animal drops off the drum is evaluated (maximum testing time: 300 s). Measurements were performed five times each on the same occasion when grip strength was evaluated. For all five measurements, mean values were computed, from which percentage values (post-ischemic vs. pre-ischemic) were calculated. Pre-ischemic data did not differ between groups.

Open field test

The open field is a round arena (diameter: 150 cm) covered by a white plastic floor, surrounded by a 35 cm high sidewall made of white polypropylene, which allows to measure spontaneous locomotor activity and exploration behavior (Kilic et al., 2008). The arena is divided into three sections, including an outer wall zone (17.7% of diameter, close to the wall), an intermediate transition zone (32.3% of diameter), and an inner zone (50% of diameter, the center of the arena). Each mouse was released near the wall and observed for 10 min. Animal paths were tracked with an electronic imaging system (Ethovision XT6; Noldus Information Technology, Wageningen, Netherlands), acquiring data at a frequency of 4.2 Hz with a spatial resolution of 576 × 768 pixels. Raw data were transferred to the wintrack 2.4 software for offline analysis. To determine measures of exploratory behavior and anxiety, the time resting and progressing, and the time spent in each of the three zones were assessed.

Elevated O maze

The elevated O maze consists of a round 5.5 cm wide polyvinylchloride runway with an outer diameter of 46 cm, which is placed 40 cm above the floor and measures correlates of fear and anxiety (Reitmeir et al., 2011). Two opposing 90° sectors are protected by 16 cm high inner and outer walls made of polyvinylchloride (closed sectors). The remaining two 90° sectors are not protected by walls (open sectors). Each mouse was released in one of the open sectors and observed for 10 min. Animal paths were again tracked with an electronic imaging system (Ethovision XT6). The time spent in the unprotected sector was measured whenever the animal entered this sector with all four paws.

Light/dark transition test

The light/dark transition test (40 cm × 20 cm × 20 cm) consists of two equal light and dark chambers, which are separated by a

divider with a 4 cm × 4 cm opening at the floor level. Each mouse was placed in the corner of the light chamber at distance from the dark chamber and monitored for 10 min. Animal paths were tracked with an electronic imaging system (Ethovision XT6). The time spent in the light chamber was evaluated and presented.

IMMUNOHISTOCHEMICAL ANALYSIS OF BRAIN REMODELING

Conventional immunohistochemistry

For conventional immunohistochemistry, 20 μm coronal sections were obtained at the level of the bregma (i.e., midstriatum) from animals that had been transcardially perfused with 0.9% NaCl at 42 dpi. After immersion fixation in 4% paraformaldehyde in 0.1 M PBS, sections were pre-treated for antigen retrieval with 0.01 M citrate buffer (pH 5.0), rinsed and immersed for 1 h in 0.1 M PBS containing 0.3% Triton X-100 (PBS-T) and 10% normal donkey serum. Sections were incubated overnight at 4°C with monoclonal mouse anti-NeuN (MAB377; Chemicon) and monoclonal rat anti-CD31 (#557355; BD Biosciences) antibodies (diluted 1:100 in 0.1 M PBS) that were detected with Cy3- or Cy2-conjugated secondary antibodies. Sections were finally incubated with 4'-6-diamidino-2-phenylindole (DAPI). In some experiments, primary antibodies were recognized by biotinylated secondary antibodies that were detected using an avidin-biotin kit (Vector Laboratories, Burlingame, CA, USA) by 3,3'-diaminobenzidine (DAB) staining. Sections were evaluated under a fluorescence microscope (Olympus BX41) connected to a CCD camera (CC12; Olympus). Surviving NeuN+ neurons and CD31+ microvessels were analyzed in a blinded way by counting numbers of cells or profiles in six defined regions of interests (ROI) in each striatum both ipsilateral and contralateral to the stroke (250 μm × 250 μm) (Kilic et al., 2006), for which mean values were calculated. With these measurements, neuronal survival and capillary density were determined. Stereometric analysis of post-ischemic striatum and corpus callosum atrophy was done using brain sections stained with modified Bielschowsky's silver solution, as previously described (Reitmeir et al., 2011).

Computer-based stereological analysis and brain volumetry

For stereological analysis of brain remodeling and brain volumetry, 20 μm coronal sections were obtained from six equidistant brain levels, 250 μm apart, of animals that had been transcardially perfused with 4% paraformaldehyde in 0.1 M PBS at 42 dpi. Sections were pre-treated for antigen retrieval with 0.01 M citrate buffer (pH 5.0), rinsed and immersed for 1 h in 0.1 M PBS-T and 10% normal donkey serum. Sections were incubated overnight at 4°C with Alexa Fluor 488-conjugated monoclonal mouse anti-NeuN (Mab377X; Chemicon), polyclonal rabbit anti-CD31 (ab28364; Abcam), and Alexa Fluor 555-conjugated monoclonal mouse anti-GFAP (#3656; Cell Signaling) antibodies (diluted 1:100 in 0.1 M PBS) that – in case of the non-conjugated antibody – was detected with Alexa Fluor 488-conjugated secondary antibody (A21206; Invitrogen). Sections were finally incubated with DAPI.

Sections were analyzed using a confocal Zeiss LSM 780 microscope. A software-controlled motorized stage provided accurate and fine movements for the x-, y-, and z-axes. In order not to miss any cell nuclei, the focus was adjusted from top to bottom for each slice. When the first nuclei were detected in the focus, the z-axis was

determined as top point and when last nuclei were lost in the focus, the *z*-axis was determined as bottom point. For each slice, the distance between the top and bottom was $\sim 16 \mu\text{m}$, which was divided into four focal planes and all images were further processed as a multiple intensity projection using Zen Black software to obtain sharp images. Using tile and *z*-stack functions of the motorized stage, all signals from NeuN+, CD31+, and GFAP+ cells in the striatum were detected using the GaAsP detector of the microscope. A single investigator analyzed all data in a blinded manner. Mean numbers of NeuN+ cells were analyzed in the ischemic and contralesional striatum. By dividing results obtained in both hemispheres, the percentage of surviving neurons in the ischemic striatum was determined. CD31+ microvessels were counted in the entire ipsilateral striatum. With the data obtained, the mean capillary number was calculated. In case of GFAP stainings, the area of scar tissue was outlined using the Zen Blue software (version 2012; Carl Zeiss). With all areas from various brain levels, the scar volume in cubic millimeter was calculated. For brain volumetry, sections collected throughout the forebrain at $250 \mu\text{m}$ intervals were stained with cresyl violet. On each section, the ipsilesional striatum and ipsilesional corpus callosum (that included the external capsule) were outlined using the Zen Blue software. By integrating areas measured across the brain, striatum, and corpus callosum volumes in cubic millimeter were determined.

IMMUNOHISTOCHEMISTRY FOR CB AND BDA

Brain sections of animals that had transcidentally been perfused with paraformaldehyde were rinsed three times for 10 min each in 50 mM Tris-buffered saline (pH 8.0) containing 0.5% Triton X-100 (TBS-T). For detection of CB, sections were immersed overnight at 4°C with polyclonal rabbit anti-cascade blue antibody (A-5760; Molecular Probes, 1:100), diluted 1:100 in 50 mM TBS-T, followed by incubation for 1 h at room temperature with a horseradish peroxidase-labeled secondary antibody (1:1000). For detection of BDA, sections were incubated overnight with avidin–biotin–peroxidase complex (ABC Elite; Vector Laboratories), followed by DAB staining.

ANALYSIS OF CORTICORUBRAL PROJECTIONS

To account for variabilities in tracer uptake in different mice, we first evaluated the number of tracer-stained fibers in the pyramidal tract at the level of the parvocellular red nucleus (bregma -3.0 to -3.5 mm). For this purpose, two consecutive sections were analyzed, counting the number of fibers crossing the sections in four regions of interest of $2865 \mu\text{m}^2$ each that had been selected in the dorsolateral, ventrolateral, dorsomedial, and ventromedial portion of the pyramidal tract. By measuring the total area of the pyramidal tract using the Cell Software image system (Olympus) connected to an Olympus BX42 microscope, we calculated the overall number of labeled pyramidal tract fibers (Z'Graggen et al., 1998; Reitmeir et al., 2011).

For evaluation of midline-crossing fibers, a $500 \mu\text{m}$ long-intersection line was superimposed on the brain midline. Along that line those fibers crossing into the contralateral hemisphere in direction of the red nucleus were quantified. For each animal and both tracers, the total number of fibers counted was normalized with the total number of labeled fibers in the pyramidal tract,

as determined for each tracer. This value was multiplied by 100, resulting in percent values of fibers crossing the midline. For both tracers always two consecutive sections were analyzed, of which mean values were determined.

WESTERN BLOTTING

Tissue samples were collected from both middle cerebral artery territories of animals sacrificed by transcardiac perfusion with 0.9% NaCl (Reitmeir et al., 2011). Following sodium dodecyl sulphate–polyacrylamide gel electrophoresis, polyvinylidene fluoride membranes were incubated with rabbit polyclonal HMG-CoA reductase antibody (Ab98018; Abcam, Cambridge, UK) that was detected by chemiluminescence labeling. Protein loading was controlled using a β -actin antibody. Protein abundance was evaluated by densitometry. Three independent blots were analyzed. For these blots, mean values were calculated, which were normalized with optical densities determined in corresponding samples of sham-operated mice.

STATISTICAL ANALYSIS

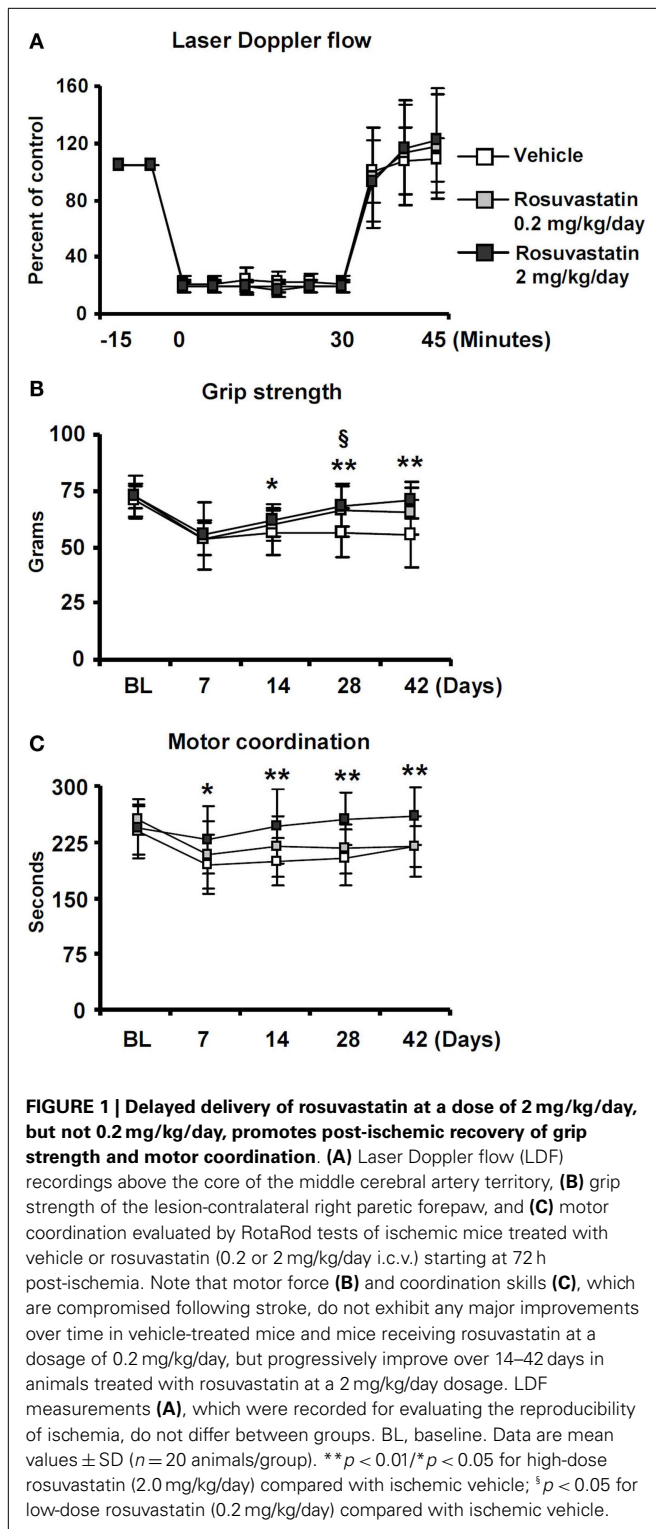
Neurological tests were evaluated by means of two-way repeated measurement analysis of variance (ANOVA) for all four time-points starting at 7 days post-stroke, i.e., the first examination after MCAO had been induced. For those tests, in which significant treatment or treatment by time interaction effects were noticed, *post hoc* comparisons were performed for each time-point using unpaired *t*-tests with Bonferroni corrections. Western blotting and histochemical data were evaluated by one-way ANOVA followed by least significant differences tests (comparison between ≥ 3 groups) or unpaired *t*-tests (comparisons between 2 groups). *p*-Values < 0.05 were considered significant.

RESULTS

POST-ACUTE DELIVERY OF ROSUVASTATIN IMPROVES POST-ISCHEMIC NEUROLOGICAL RECOVERY

To evaluate if the HMG-CoA reductase inhibitor rosuvastatin influences neurological recovery, mice submitted to 30 min of MCAO were intraventricularly treated with vehicle or rosuvastatin (2 or 0.2 mg/kg/day) starting at 3 dpi, i.e., at a time-point, at which acute ischemic injury has already evolved (Reitmeir et al., 2011, 2012). LDF, which was recorded above the core of the middle cerebral artery territory using a flexible fiberoptic probe that was attached to the animals' skulls, did not show any differences between groups. In all experimental conditions, LDF decreased to ~ 15 – 20% of baseline during MCAO, followed by a rapid restoration of blood flow after reperfusion (Figure 1A).

Significant reductions of motor force of the contralesional right forepaw (Figure 1B) and motor coordination skills (Figure 1C) were detected in ischemic mice, as shown in grip strength and RotaRod tests. In vehicle-treated mice and in mice receiving rosuvastatin at the low dosage (0.2 mg/kg/day), grip strength, and coordination skills largely remained unchanged over the observation period of 42 days (Figures 1B,C). In animals treated with rosuvastatin at the higher dosage (2 mg/kg/day), progressive recovery of grip strength and motor coordination were observed, resulting in robust and significant improvement starting at 14 dpi (Figures 1B,C).



Whereas overall locomotor activity that was reduced by MCAO was mildly increased by rosuvastatin, as shown in open field tests (**Figure 2A**), rosuvastatin decreased the time spent in the open field wall zone (**Figure 2B**) and increased the time spent in the open field transition zone (**Figure 2C**) and center zone

(**Figure 2D**), indicating partial reversal of an anxious phenotype that was induced by the stroke. In line with this promotion of exploration behavior, the time spent in the unprotected zone of the elevated O maze (**Figure 2E**) and the time spent in the light zone of the light/dark transition test (**Figure 2F**) were significantly increased by rosuvastatin at a 2 mg/kg/day dosage. In view that effects on grip strength and coordination skills were noticed only when the higher dose of rosuvastatin was administered, the latter studies and all following studies were performed only in mice receiving vehicle or 2 mg/kg/day rosuvastatin.

ROSUVASTATIN PROMOTES PERI-LESIONAL TISSUE REMODELING

To clarify how the post-acute rosuvastatin delivery modifies the remodeling of ischemic brain tissue, we used two different approaches, i.e., conventional histochemical analysis and computer-based stereology and volumetry, always with consistent results in two different sets of mice. Rosuvastatin at a dose of 2 mg/kg/day significantly increased neuronal survival after the observation period of 42 days (**Figure 3A**; **Figure S2A** in Supplementary Material), preventing striatum (**Figure 3B**; **Figure S2B** in Supplementary Material) and corpus callosum (**Figure 3C**; **Figure S2C** in Supplementary Material) atrophy. Brain capillary density was increased in the lesion-sided striatum of rosuvastatin-treated as compared with vehicle-treated ischemic mice (**Figure 3D**; **Figure S2D** in Supplementary Material), but not the overlying parietal cortex (not shown). Glial scar formation was slightly reduced by rosuvastatin (1.76 ± 0.64 vs. 1.44 ± 0.60 mm³ in vehicle-treated compared with rosuvastatin-treated animals); yet, this effect failed significance.

ROSUVASTATIN PROMOTES CONTRALESIONAL CORTICORUBRAL TRACT PLASTICITY

Since the pyramidal tract crosses the middle cerebral artery territory, which was affected by ischemia, we examined how rosuvastatin influences pyramidal tract degeneration and plasticity. We administered two dextran conjugates, CB and BDA, into both motor cortices (**Figure 4A**). The analysis of injection sites revealed no relevant differences between groups. In all animals, injection sites covered the more caudal forelimb area and rostral hindlimb area of the primary motor cortex without relevant spreading of tracer deposits into subcortical structures. The size of the pyramidal tract, evaluated as area covered by the cerebral peduncle in coronal brain sections, was slightly lower in the ipsilesional ischemic, as compared to non-ischemic pyramidal tract, but was not influenced by rosuvastatin (10.8 ± 3.5 mm² in non-ischemic vehicle, 8.0 ± 1.8 mm² in ischemic vehicle, 8.0 ± 2.3 mm² in ischemic rosuvastatin; $p < 0.05$ for ischemic rosuvastatin and ischemic vehicle compared with non-ischemic vehicle).

Cascade blue- and BDA-stained fibers originating from the cerebral peduncle turned dorsomedially at mesencephalic levels, terminating as previously described in the parvocellular part of the ipsilateral red nucleus (**Figure 4A**) (Reitmeir et al., 2011). At this level, we quantified both the number of fibers crossing through the pyramidal tract and the number of fibers branching off the pyramidal tract and migrating across the midline in direction to the red nucleus in the other hemisphere. Our studies revealed that MCAO increased the number of CB-labeled fibers

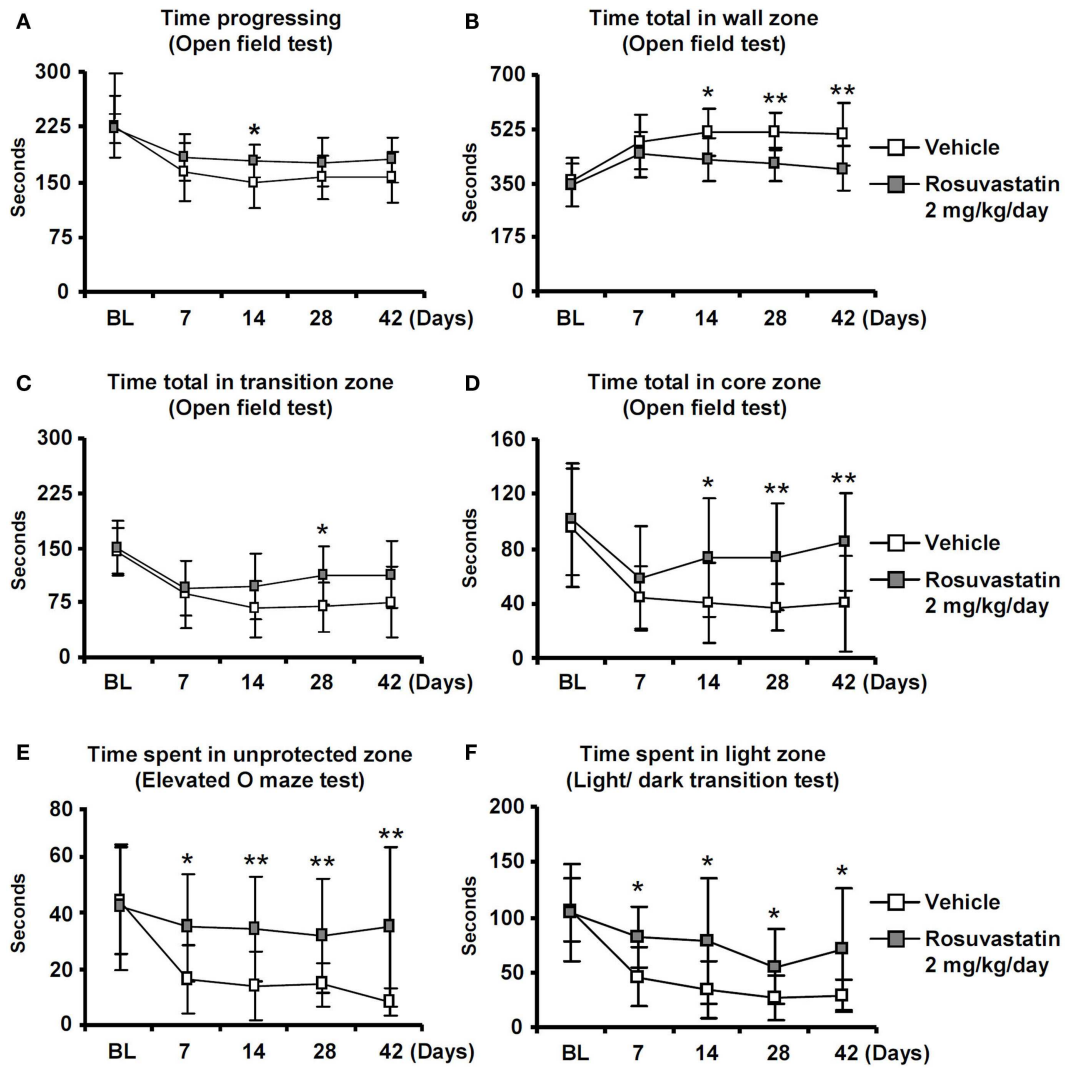


FIGURE 2 | Delayed delivery of rosuvastatin promotes post-ischemic spontaneous exploration behavior, thus, reducing anxiety. (A) Time progressing, **(B)** time spent in the wall zone, **(C)** time spent in the transition zone, and **(D)** time spent in the core zone of the open field test, as well as **(E)** time spent in the unprotected zone of the elevated O maze and **(F)** time spent in the light zone of the light/dark transition test of ischemic mice treated with vehicle or rosuvastatin (2 mg/kg/day i.c.v.) starting at 72 h post-ischemia. Note that while overall motor activity does

not differ between groups **(A)**, exploration activities of ischemic mice in the transition zone **(C)**, and core zone **(D)** of the open field are increased by rosuvastatin. Furthermore, note that the time spent in the unprotected zone of the elevated O maze **(E)** and the time spent in the light zone of the light/dark test **(F)** are increased by rosuvastatin, indicating that post-stroke anxiety is attenuated by HMG-CoA reductase inhibition BL, baseline. Data are mean values \pm SD ($n = 20$ animals/group). $**p < 0.01$ / $*p < 0.05$ compared with ischemic vehicle.

in the ipsilesional cerebral peduncle, whereas rosuvastatin delivery did not further elevate this number (19171 ± 6026 CB-labeled fibers in non-ischemic vehicle, 35942 ± 19114 CB-labeled fibers in ischemic vehicle, 38425 ± 11567 CB-labeled fibers in ischemic rosuvastatin; $p < 0.01$ for ischemic rosuvastatin and ischemic vehicle compared with non-ischemic vehicle). Conversely, neither MCAO nor rosuvastatin influenced the number of labeled fibers in the contralesional cerebral peduncle (48300 ± 19429 BDA-labeled fibers in non-ischemic vehicle, 55944 ± 17875 BDA-labeled fibers in ischemic vehicle, 55988 ± 14028 BDA-labeled fibers in ischemic rosuvastatin; n.s.). Hence, rosuvastatin did not induce the *de novo*

formation of proximal axons, neither ipsilateral nor contralateral to the stroke.

The percentage of midline-crossing fibers derived from the lesion-sided pyramidal tract, as revealed by CB, increased (though not significantly) upon MCAO (**Figures 4B,D**), whereas the percentage of BDA-labeled midline-crossing fibers originating from the contralesional pyramidal tract remained unchanged (**Figures 4C,D**). Importantly, rosuvastatin significantly increased the percentage of midline-crossing fibers originating from the BDA-labeled contralesional pyramidal tract, without influencing the percentage of CB-labeled ipsilesional pyramidal tract fibers

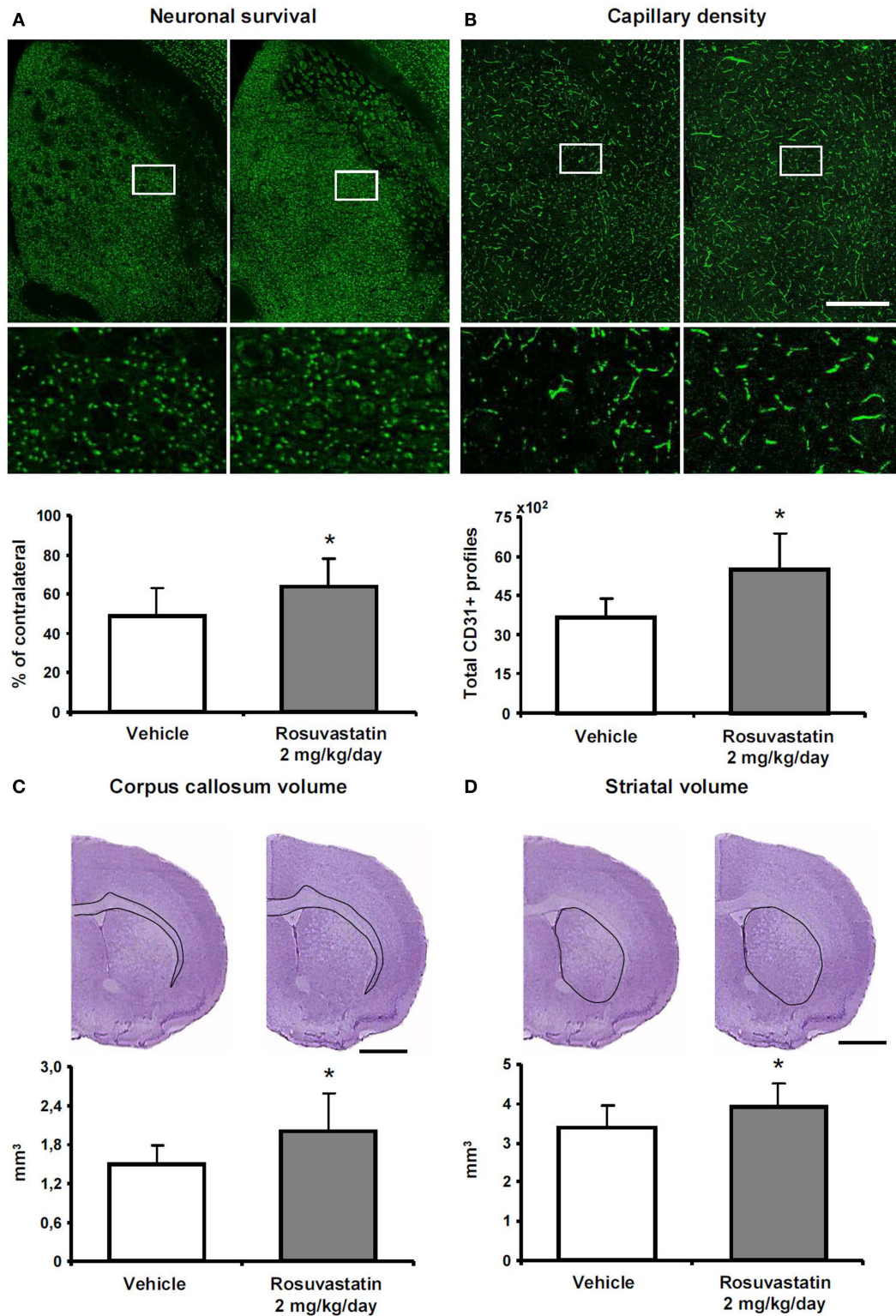
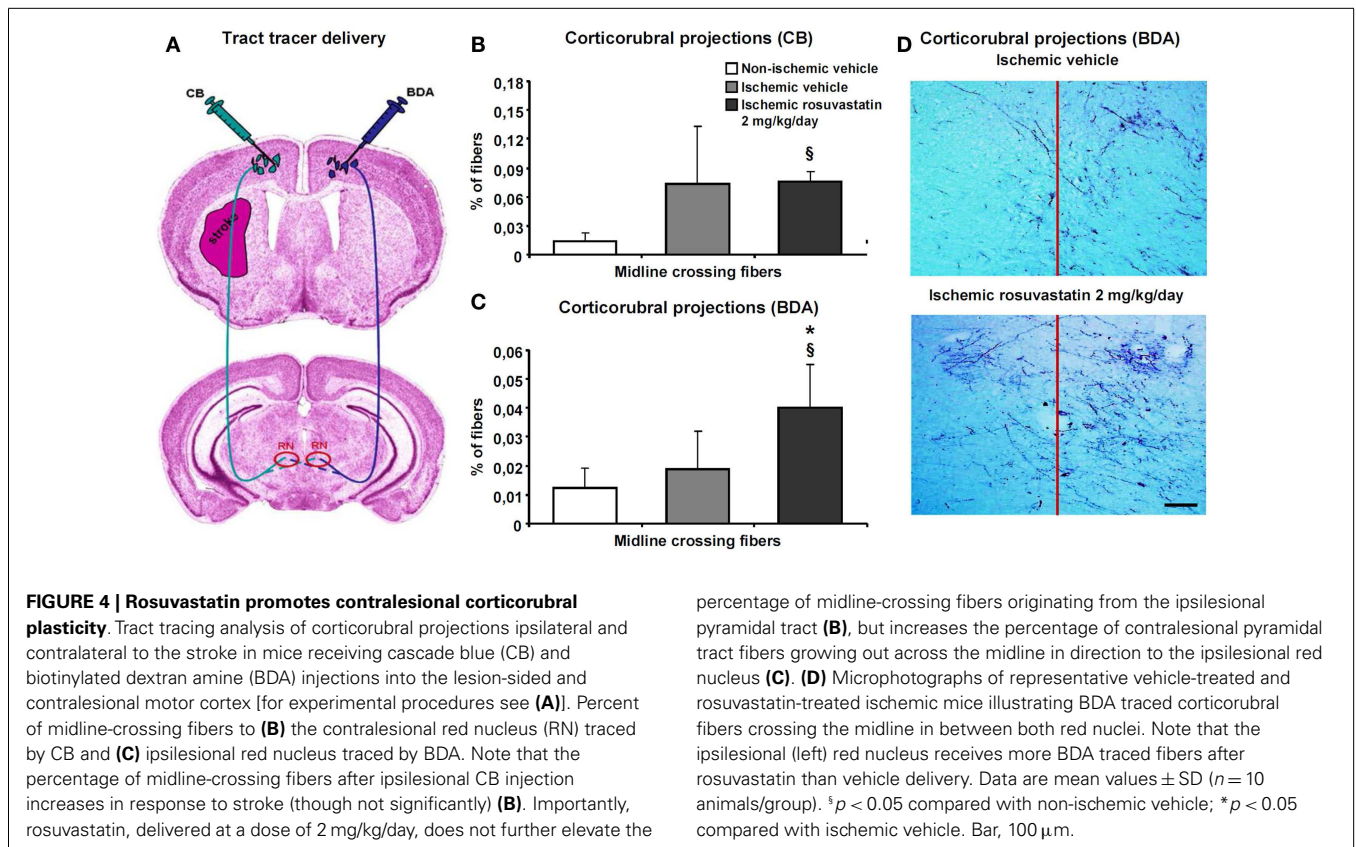


FIGURE 3 | Rosuvastatin promotes peri-lesional tissue remodeling. (A) Surviving neurons in ischemic striatum evaluated by NeuN immunohistochemistry, (B) striatum atrophy, and (C) corpus callosum atrophy examined by cresyl violet stainings, and (D) capillary number in the ischemic striatum assessed by CD31 immunohistochemistry at 42 dpi in ischemic mice receiving vehicle or rosuvastatin (2 mg/kg/day i.c.v.) starting at 72 h

post-ischemia. Data were analyzed using an investigator-independent computer-based stereology and volumetry approach. Note that rosuvastatin increases neuronal survival (A), diminishes progressive brain atrophy (B,C), and increases capillary survival (D). Representative microphotographs are also shown. Data are mean values ± SD (n = 10 animals/group). *p < 0.05 compared with ischemic vehicle. Bars, 1000 μm (A–D).



(Figures 4B–D). Thus, rosuvastatin enhanced the sprouting of terminal fibers originating from the contralateral, but not ipsilateral motor cortex.

HMG-CoA REDUCTASE IS UPREGULATED IN THE CONTRALESIONAL HEMISPHERE

Based on the observation that HMG-CoA reductase inhibition enhanced contralesional pyramidal tract plasticity, we finally analyzed how focal cerebral ischemia influences HMG-CoA reductase abundance both ipsilateral and contralateral to the stroke. In Western blots, we show that the abundance of HMG-CoA reductase increased in the contralateral hemisphere at 14 and 28 dpi in mice exposed to 30 min MCAO (Figure 5). In the ipsilesional hemisphere, HMG-CoA reductase abundance transiently decreased at 3 dpi.

DISCUSSION

We herein show that post-acute delivery of the HMG-CoA reductase inhibitor rosuvastatin, initiated at 72 h post-ischemia, that is a time-point far beyond classical neuroprotection, promotes neurological recovery, peri-lesional tissue remodeling, and contralesional pyramidal tract plasticity in mice submitted to MCAO. Robust correlates of recovery of motor function, coordination skills, and exploration behavior were noticed in functional neurological tests that were accompanied by decreased neuronal degeneration and brain atrophy, and increased capillary survival. Contralateral to the stroke, enhanced sprouting of midline-crossing motor cortical fibers was induced by

rosuvastatin, providing another structural correlate for the improved neurological recovery.

The observation of increased axonal plasticity in response to HMG-CoA reductase inhibitor delivery that occurs at distance to the lesion is new. It has previously been shown that HMG-CoA reductase inhibition promotes post-ischemic neuronal survival in the acute stroke phase (Sironi et al., 2003; Kilic et al., 2005), inhibit brain inflammation (Pahan et al., 1997; Kilic et al., 2005), restore endothelial function (Endres et al., 1998; Amin-Hanjani et al., 2001), and promote angiogenesis and neurogenesis (Chen et al., 2003). Following exposure of primary neurons that had undergone oxygen–glucose deprivation to the HMG-CoA reductase inhibitor simvastatin, increased neurite outgrowth has been reported, which was made responsible for the increased remodeling of Bielschowsky-labeled fiber tracts along the lesion border that was found by the same authors in simvastatin treated rats subjected to 2 h MCAO (Cui et al., 2012). These observations in the vicinity of the stroke lesion are in line with our findings of reduced striatum and corpus callosum atrophy. That corpus callosum atrophy is reduced by HMG-CoA reductase inhibition has to the best of our knowledge not yet been shown. Mechanistically, neuronal plasticity induced by HMG-CoA reductase inhibitors is thought to be mediated by prevention of geranylgeranylation, as previously shown *in vitro* in rat hippocampal neurons, in which inhibition of geranylgeranylation mimicked effects of the HMG-CoA reductase inhibitor pravastatin on neurogenesis (Pooler et al., 2006). Pravastatin significantly decreased levels of membrane-associated RhoA, suggesting that reduced

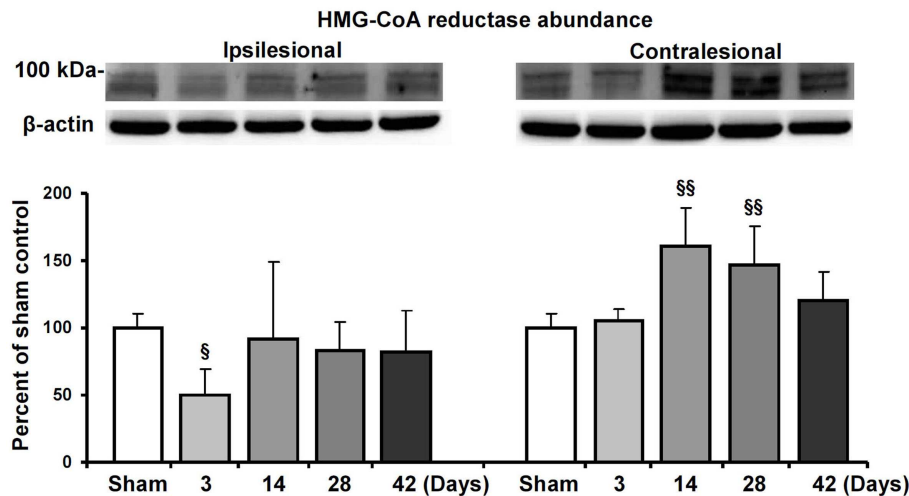


FIGURE 5 | HMG-CoA reductase abundance in the ischemic and contralesional hemisphere. Western blot analysis of the ~100 kDa double band of HMG-CoA reductase at various reperfusion times following 30 min MCAO. Representative blots are also shown. Note the

upregulation of HMG-CoA reductase in the contralesional hemisphere at 14 and 28 d.p.i. Data are mean values \pm SD ($n = 3$ independent blots/group). §§ $p < 0.01$ § $p < 0.05$ compared with corresponding samples from sham-operated mice.

geranylgeranylation of RhoA, which is required for membrane binding, was responsible (Pooler et al., 2006).

Studies in different models of MCAO using antibodies directed against axonal growth inhibitors [e.g., Nogo-A (Papadopoulos et al., 2002; Wiessner et al., 2003)], pleiotropic growth factors [e.g., erythropoietin, vascular endothelial growth factor (Reitmeir et al., 2011, 2012)], and neural precursor/stem cells (Andres et al., 2011) have in the meantime shown that contralesional pyramidal tract plasticity is a structural correlate of recovery in a variety of neurorestorative therapies. The present study shows that the HMG-CoA reductase inhibitor rosuvastatin shares this property. In contrast to antibodies, growth factors, and cell-based therapeutics, HMG-CoA reductase inhibitors may systemically be delivered without major side effects or complications. Unfortunately, HMG-CoA reductase inhibitors that are clinically used today are highly hydrophilic drugs, which poorly cross the blood–brain barrier. In order to ensure the brain access of rosuvastatin, which may still hamper in the post-ischemic brain despite blood–brain barrier opening, we used an i.c.v. delivery strategy and administered an effective drug dosage that was approximately an order of magnitude higher than that prescribed in human patients.

Since HMG-CoA reductase inhibitors are genuine pharmacological compounds that in contrast to growth factors, antibodies, or cells can easily be administered in stroke patients without concerns, more lipophilic HMG-CoA reductase inhibitors, which are able to enter the brain, might be useful neuronal plasticity-promoting drugs. Besides, HMG-CoA reductase inhibitors have very favorable effects on post-ischemic angiogenesis (Chen et al., 2003), which make them promising for restorative stroke therapy. We used a model of transient focal cerebral ischemia, in which the pyramidal tract is injured, while the motor cortex, which is located outside the middle cerebral artery territory, remains intact. Additional studies using a model, resulting in motor cortical infarcts (e.g., photothrombotic stroke) as well as studies using

systemic HMG-CoA reductase inhibitor delivery may be valuable, before the translational potential of HMG-CoA reductase inhibitor-induced neuronal plasticity may finally be evaluated.

ACKNOWLEDGMENTS

This work was supported by the German Research Council (HE3173/2-1, HE3173/2-2, and HE3173/3-1; to Dirk M. Hermann), Dr. Werner-Jackstädt Foundation (to Raluca Reitmeir), European Molecular Biology Organization (EMBO) (installation grant; to Ertugrul Kilic) and Turkish Academy of Sciences (TUBA/GEBIP; to Ertugrul Kilic).

SUPPLEMENTARY MATERIAL

The Supplementary Material for this article can be found online at <http://www.frontiersin.org/Journal/10.3389/fncel.2014.00422/abstract>

REFERENCES

- Amarenco, P., Bogousslavsky, J., Callahan, A. III, Goldstein, L. B., Hennerici, M., Rudolph, A. E., et al. (2006). High-dose atorvastatin after stroke or transient ischemic attack. *N. Engl. J. Med.* 355, 549–559. doi:10.1056/NEJMoa061894
- Amariglio, N., Hirshberg, A., Scheithauer, B. W., Cohen, Y., Loewenthal, R., Trakhtenbrot, L., et al. (2009). Donor-derived brain tumor following neural stem cell transplantation in an ataxia telangiectasia patient. *PLoS Med.* 6:e1000029. doi:10.1371/journal.pmed.1000029
- Amin-Hanjani, S., Stagliano, N. E., Yamada, M., Huang, P. L., Liao, J. K., and Moskowitz, M. A. (2001). Mevastatin, an HMG-CoA reductase inhibitor, reduces stroke damage and upregulates endothelial nitric oxide synthase in mice. *Stroke* 32, 980–986. doi:10.1161/01.STR.32.4.980
- Andres, R. H., Horie, N., Slikker, W., Keren-Gill, H., Zhan, K., Sun, G., et al. (2011). Human neural stem cells enhance structural plasticity and axonal transport in the ischaemic brain. *Brain* 134, 1777–1789. doi:10.1093/brain/awr094
- Bacigaluppi, M., Pluchino, S., Peruzzotti-Jametti, L., Kilic, E., Kilic, U., Salani, G., et al. (2009). Delayed post-ischaemic neuroprotection following systemic neural stem cell transplantation involves multiple mechanisms. *Brain* 132, 2239–2251. doi:10.1093/brain/awp174

- Chen, J., Zhang, Z. G., Li, Y., Wang, Y., Wang, L., Jiang, H., et al. (2003). Statins induce angiogenesis, neurogenesis, and synaptogenesis after stroke. *Ann. Neurol.* 53, 743–751. doi:10.1002/ana.10555
- Cui, X., Chopp, M., Shehadah, A., Zacharek, A., Kuzmin-Nichols, N., Sanberg, C. D., et al. (2012). Therapeutic benefit of treatment of stroke with simvastatin and human umbilical cord blood cells: neurogenesis, synaptic plasticity, and axon growth. *Cell Transplant.* 21, 845–856. doi:10.3727/096368911X627417
- Endres, M., Laufs, U., Huang, Z., Nakamura, T., Huang, P., Moskowitz, M. A., et al. (1998). Stroke protection by 3-hydroxy-3-methylglutaryl (HMG)-CoA reductase inhibitors mediated by endothelial nitric oxide synthase. *Proc. Natl. Acad. Sci. U.S.A.* 95, 8880–8885. doi:10.1073/pnas.95.15.8880
- Hermann, D. M., and Chopp, M. (2012). Promoting brain remodelling and plasticity for stroke recovery: therapeutic promise and potential pitfalls of clinical translation. *Lancet Neurol.* 11, 369–380. doi:10.1016/S1474-4422(12)70039-X
- Kilic, E., ElAli, A., Kilic, U., Guo, Z., Ugur, M., Uslu, U., et al. (2010). Role of Nogo-A in neuronal survival in the reperfused ischemic brain. *J. Cereb. Blood Flow Metab.* 30, 969–984. doi:10.1038/jcbfm.2009.268
- Kilic, E., Kilic, U., Bacigaluppi, M., Guo, Z., Abdallah, N. B., Wolfer, D. P., et al. (2008). Delayed melatonin administration promotes neuronal survival, neurogenesis and motor recovery, and attenuates hyperactivity and anxiety after mild focal cerebral ischemia in mice. *J. Pineal Res.* 45, 142–148. doi:10.1111/j.1600-079X.2008.00568.x
- Kilic, E., Kilic, U., Matter, C. M., Lüscher, T. F., Bassetti, C. L., and Hermann, D. M. (2005). Aggravation of focal cerebral ischemia by tissue plasminogen activator is reversed by 3-hydroxy-3-methylglutaryl coenzyme A reductase inhibitor but does not depend on endothelial NO synthase. *Stroke* 36, 332–336. doi:10.1161/01.STR.0000152273.24063.f7
- Kilic, E., Kilic, U., Wang, Y., Bassetti, C. L., Marti, H. H., and Hermann, D. M. (2006). The phosphatidylinositol-3 kinase/Akt pathway mediates VEGF's neuroprotective activity and induces blood brain barrier permeability after focal cerebral ischemia. *EASEB J.* 20, 1185–1187. doi:10.1096/fj.05-4829fje
- Orgogozo, J. M., Gilman, S., Dartigues, J. F., Laurent, B., Puel, M., Kirby, L. C., et al. (2003). Subacute meningoencephalitis in a subset of patients with AD after Abeta42 immunization. *Neurology* 61, 46–54. doi:10.1212/01.WNL.0000073623.84147.A8
- Pahan, K., Sheikh, F. G., Namboodiri, A. M., and Singh, I. (1997). Lovastatin and phenylacetate inhibit the induction of nitric oxide synthase and cytokines in rat primary astrocytes, microglia, and macrophages. *J. Clin. Invest.* 100, 2671–2679. doi:10.1172/JCI119812
- Papadopoulos, C. M., Tsai, S. Y., Alsbiet, T., O'Brien, T. E., Schwab, M. E., and Kartje, G. L. (2002). Functional recovery and neuroanatomical plasticity following middle cerebral artery occlusion and IN-1 antibody treatment in the adult rat. *Ann. Neurol.* 51, 433–441. doi:10.1002/ana.10144
- Pooler, A. M., Xi, S. C., and Wurtman, R. J. (2006). The 3-hydroxy-3-methylglutaryl co-enzyme A reductase inhibitor pravastatin enhances neurite outgrowth in hippocampal neurons. *J. Neurochem.* 97, 716–723. doi:10.1111/j.1471-4159.2006.03763.x
- Reitmeir, R., Kilic, E., Kilic, U., Bacigaluppi, M., ElAli, A., Salani, G., et al. (2011). Post-acute delivery of erythropoietin induces stroke recovery by promoting perilesional tissue remodelling and contralesional pyramidal tract plasticity. *Brain* 134, 84–99. doi:10.1093/brain/awq344
- Reitmeir, R., Kilic, E., Reinboth, B. S., Guo, Z., ElAli, A., Zechariah, A., et al. (2012). Vascular endothelial growth factor induces contralesional corticobulbar plasticity and functional neurological recovery in the ischemic brain. *Acta Neuropathol.* 123, 273–284. doi:10.1007/s00401-011-0914-z
- Sironi, L., Cimino, M., Guerrini, U., Calvio, A. M., Lodetti, B., Asdente, M., et al. (2003). Treatment with statins after induction of focal ischemia in rats reduces the extent of brain damage. *Arterioscler. Thromb. Vasc. Biol.* 23, 322–327. doi:10.1161/01.ATV.0000044458.23905.3B
- Wiessner, C., Bareyre, F. M., Allegrini, P. R., Mir, A. K., Frentzel, S., Zurini, M., et al. (2003). Anti-Nogo-A antibody infusion 24 hours after experimental stroke improved behavioral outcome and corticospinal plasticity in normotensive and spontaneously hypertensive rats. *J. Cereb. Blood Flow Metab.* 23, 154–165. doi:10.1097/00004647-200302000-00003
- Z'Graggen, W. J., Metz, G. A., Kartje, G. L., Thallmair, M., and Schwab, M. E. (1998). Functional recovery and enhanced corticofugal plasticity after unilateral pyramidal tract lesion and blockade of myelin-associated neurite growth inhibitors in adult rats. *J. Neurosci.* 18, 4744–4757.

Conflict of Interest Statement: The authors declare that the research was conducted in the absence of any commercial or financial relationships that could be construed as a potential conflict of interest.

Received: 05 August 2014; paper pending published: 22 October 2014; accepted: 23 November 2014; published online: 11 December 2014.

Citation: Kilic E, Reitmeir R, Kilic Ü, Caglayan AB, Beker MC, Kelestemur T, Ethemoglu MS, Ozturk G and Hermann DM (2014) HMG-CoA reductase inhibition promotes neurological recovery, peri-lesional tissue remodeling, and contralesional pyramidal tract plasticity after focal cerebral ischemia. *Front. Cell. Neurosci.* 8:422. doi: 10.3389/fncel.2014.00422

This article was submitted to the journal *Frontiers in Cellular Neuroscience*. Copyright © 2014 Kilic, Reitmeir, Kilic, Caglayan, Beker, Kelestemur, Ethemoglu, Ozturk and Hermann. This is an open-access article distributed under the terms of the Creative Commons Attribution License (CC BY). The use, distribution or reproduction in other forums is permitted, provided the original author(s) or licensor are credited and that the original publication in this journal is cited, in accordance with accepted academic practice. No use, distribution or reproduction is permitted which does not comply with these terms.



Valproic acid potentiates curcumin-mediated neuroprotection in lipopolysaccharide induced rats

Amira Zaky^{1*}, Mariam Mahmoud¹, Doaa Awad¹, Bassma M. El Sabaa², Kamal M. Kandeel¹ and Ahmad R. Bassiouny¹

¹ Department of Biochemistry, Faculty of Science, Alexandria University, Alexandria, Egypt

² Faculty of Medicine, Alexandria University, Alexandria, Egypt

Edited by:

Emmanuel Moyse, François Rabelais University, France

Reviewed by:

Hermona Soreq, The Hebrew

University of Jerusalem, Israel

Fatiha Chigr, Sultan Moulay Slimane

University, Morocco

Emmanuel Moyse, François Rabelais

University, France

*Correspondence:

Amira Zaky, Department of

Biochemistry, Faculty of Science,

Alexandria University, Moharram

Bake, P. O. Box 21511, Alexandria,

Egypt

e-mail: amzakyha@yahoo.com

The etiology of neuroinflammation is complex and comprises multifactorial, involving both genetic and environmental factors during which diverse genetic and epigenetic modulations are implicated. Curcumin (Cur) and valproic acid (VPA), histone deacetylase 1 inhibitor, have neuroprotective effects. The present study was designed with an aim to investigate the ability of co-treatment of both compounds (Cur or VPA, 200 mg/kg) for 4 weeks to augment neuroprotection and enhance brain recovery from intra-peritoneal injection of (250 μ g/kg) lipopolysaccharide-stimulated neuroinflammatory condition on rat brain cortex. Cortex activation and the effects of combined treatment and production of proinflammatory mediators, cyclooxygenase-2 (COX-2), APE1, and nitric oxide/inducible nitric oxide synthase (iNOS) were investigated. Neuroinflammation development was assessed by histological analyses and by investigating associated indices [β -secretase (BACE1), amyloid protein precursor (APP), presenilin (PSEN-1), and PSEN-2]. Furthermore we measured the expression profile of lethal-7 (let-7) miRNAs members a, b, c, e, and f in all groups, a highly abundant regulator of gene expression in the CNS. Protein and mRNA levels of neuroinflammation markers COX-2, BACE1, APP, and iNOS were also attenuated by combined therapy. On the other hand, assessment of the indicated five let-7 members, showed distinct expression profile pattern in the different groups. Let-7 a, b, and c disappeared in the induced group, an effect that was partially suppressed by co-addition of either Cur or VPA. These data suggest that the combined treatment induced significantly the expression of the five members when compared to rats treated with Cur or VPA only as well as to self-recovery group, which indicates a possible benefit from the synergistic effect of Cur-VPA combination as therapeutic agents for neuroinflammation and its associated disorders. The mechanism elucidated here highlights the particular drug-induced expression profile of let-7 family as new targets for future pharmacological development.

Keywords: neuroinflammation, lipopolysaccharide (LPS), curcumin (Cur), valproic acid (VPA), let-7 miRNA

INTRODUCTION

Lipopolysaccharide (LPS) is the most abundant component within the cell wall of Gram-negative bacteria that has been extensively used in models studying inflammation. LPS initiates cellular receptor transduction through Toll-like receptor 4 (TLR4), binding of LPS to TLR4 elicits a signaling network including the activation of NF- κ B through multiple mediators (Bode et al., 2012). NF- κ B plays a crucial role in regulating the transcription of genes related to innate immunity and inflammation responses and several studies indicate its activation is controlled by reactive oxygen species (ROS) in immune modulation in monocytes (Asehnoune et al., 2004 and Park et al., 2004). Oxidative stress is associated with virtually all central nervous system pathogenesis, infectious, inflammatory, or degenerative in nature. Since brain homeostasis largely depends on integrity of blood-brain barrier (BBB) and oxidative stress associates BBB permeability alteration, brain is endowed in numerous antioxidant effectors via orchestrated actions of immune cells, vascular cells, and neurons that constitute neuroinflammation, that control and prevent the

detrimental formation of ROS generated via different metabolic reactions (Dasuri et al., 2013; Xanthos and Sandkühler, 2014). Curcumin (Cur) has been shown to exhibit activity against various neurologic diseases; it is a potent inhibitor of reactive astrocyte expression and thus, prevents hippocampal cell death induced by kainic acid (Shin et al., 2007). Recent studies indicate that low doses of Cur is effectively disaggregate beta amyloid protein as well as prevents fibril and oligomer formation and hence has protective effect in treating Alzheimer's disease (AD; Kulkarni et al., 2009). Recent experimental researchers have shown protective effect of Cur in animal models of seizures (Du et al., 2009), and experimental model of epileptogenesis (Jyoti et al., 2009). Recently, Cur possess antidepressant activity and can modulate the release of serotonin and dopamine. Cur enhances the level of neurotrophic factors such as brain derived neurotrophic factor (BDNF; Wang et al., 2008)

Apurinic/aprimidinic endonuclease (APE1) is essential for cell survival in mammalian cells, APE1 is also essential in early embryonic development (Meira et al., 2001; Izumi et al., 2005). APE1 is

the second repair enzyme in base excision repair (BER)-pathway and hydrolyses the phosphodiester backbone immediately 5' to an AP site to produce 3' OH group and 5' deoxyribose-5-phosphate (Levin and Demple, 1990). APE1 knockdown in neurons accumulates significant oxidative DNA damage without efficient repair, which demonstrates that APE1 is essential for repair of oxidative DNA damage in neurons (Yang et al., 2010). In neurons, BER is the predominant mechanism for repair of oxidative DNA lesions. The major pathological features of AD are extracellular amyloid beta ($A\beta$) plaques and intracellular neurofibrillary tangles (NFTs). Moreover it has been reported that $A\beta$ level differentially modulates APE1, a key enzyme in BER pathway, expression which may contribute to selective neuronal vulnerability in AD (Mantha et al., 2012). We have previously reported that APE1 expression is significantly reduced during neuroinflammation progression and restored by resveratrol treatment (Zaky et al., 2013).

Histone deacetylase inhibitors (HDAC inhibitors) promote the acetylation of histones, which are generally associated with transcriptional activation. HDACs inhibitors also increase the acetylation status and modulate the activity of a wide range of histone as well as non-histone proteins. HDAC inhibitors have been shown to confer neuroprotection in experimental models of various neurodegenerative diseases (Camelo et al., 2005; Gardian et al., 2005; Petri et al., 2006) even though the exact mechanisms underlying their neuro-protective actions are still elusive.

Moreover, valproic acid (VPA; 2-propylpentanoic acid sodium salt), a drug commonly used to treat seizures, has been shown to exert neuro-protective effect at therapeutic levels in cellular and animal models. In cultured neurons, VPA protects from glutamate-induced excitotoxicity, thapsigargin-induced endoplasmic reticulum stress, and LPS-induced dopaminergic neuronal death (Phiel et al., 2001; Kanai et al., 2004). Recently, VPA was shown to inhibit LPS-induced, microglia-mediated inflammation in midbrain neuron-glia cultures as described by inhibition of TNF- α secretion and NO production (Peng et al., 2005).

Alzheimer's disease pathology is characterized by an accumulation of extracellular amyloid plaques composed of $A\beta$ peptide fragment and intracellular NFTs composed of hyperphosphorylated protein tau, as well as neuronal loss in the hippocampus, temporal, and frontal lobes, increased inflammation, and oxidative stress (Serrano-Pozo et al., 2011)

MirSVR is a new machine learning method for ranking microRNA (miRNA) target sites by a down-regulation score. In a large-scale evaluation, miRanda-mirSVR is competitive with other target prediction methods in identifying target genes and predicting the extent of their down-regulation at the mRNA or protein levels. Importantly, the method identifies a significant number of experimentally determined non-canonical and non-conserved sites (Betel et al., 2010).

Altered biogenesis and/or function of miRNA are implicated in the various pathological processes including inflammation and neurodegeneration. In Alzheimer's, miRNA profiling experiments have identified disease-specific miRNAs. Moreover a number of studies have linked differential miRNAs expression to pathology in AD such as deposition of amyloid plaques and NFTs, as well as more specific pathway interactions and regulatory functions

of the amyloid pathway, including regulation of amyloid protein precursor (APP) and beta-site APP cleaving enzyme 1 (β -secretase, BACE1; reviewed in Gustaw-Rothenberg et al., 2010; Geekiyanaage et al., 2012).

The aim of our study is to investigate the protective/therapeutic potential of Cur alone and in combination with histone deacetylase 1 (HDAC1) inhibitor, VPA, in LPS-induced rats. Also we are interested in studying the expression profiles of lethal-7 (let-7) miRNAs family members as signaling molecules in regulation of inflammatory enzymes cyclooxygenase-2 (COX-2) and inducible nitric oxide synthase (iNOS).

MATERIALS AND METHODS

ANIMALS AND ESTABLISHMENT OF NEUROINFLAMMATION EXPERIMENTAL MODEL

Fifty five male adult Sprague–Dawley (80–150 g) rats were used for the present study. The animals were supplied and maintained at medical research institute in which the European principles of laboratory animal ethics care were followed in all experimental protocols. Rats were maintained under controlled temperature ($25 \pm 2^\circ\text{C}$) and constant photoperiodic conditions (12:12-h daylight/darkness). The dams had free access to water and standard commercial chow containing 20% protein, 54% carbohydrate, 4.5% fiber, 4% lipids, 7% ash, and 10% moisture.

Neuroinflammation induction was established by LPS injection. Experimental design and rats classifications as indicated in **Figure 1**, included the following groups: (1) mock-treated rats (mock-Trx) that received empty vehicle, (2) LPS-induced rats that received intra-peritoneal (IP) injection of 250 $\mu\text{g}/\text{kg}$ LPS five times per week for 4 weeks, (3) Co Cur rats that received oral administration of 200 mg/kg Cur during LPS induction, (4) Co-VPA that were orally administered 200 mg/kg VPA in parallel to LPS. Treatment protocol involved oral administration of 200 mg/kg of Cur (Trx-Cur), VPA (Trx-VPA), or their combination (Trx-Cur + VPA) four times per week for 4 weeks. The Cur-VPA treated rats were administered the two doses at the same time. Moreover a group of LPS-induced rats were left untreated for the duration of 4-weeks in parallel to treated ones and referred as self-recovery to promote self-healing mechanism.

Samples collection

Blood was collected from each group at time intervals of 2 and 4 weeks of LPS administration and after treatment by retro-orbital bleeding or during sacrifice. From each group 4–6 rats were killed

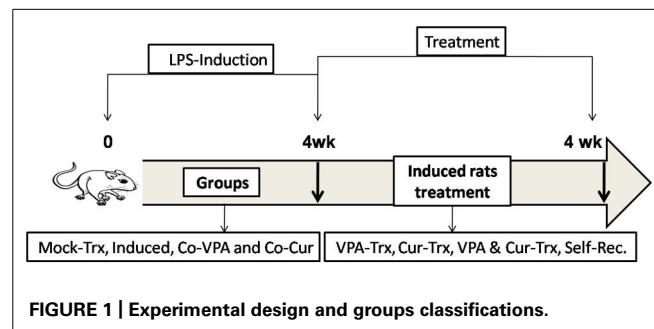


FIGURE 1 | Experimental design and groups classifications.

by cervical dislocation and sera were collected and stored at -80°C for further analyses. Brain tissues were removed, washed with cold 0.9% NaCl and dissected into different lobes; mid brains were stored in RNA later for extraction of total RNA and the remaining section was rapidly frozen with liquid nitrogen and stored at -80°C for preparation of total and nuclear extracts (NEs), and enzyme assays. A whole brain was removed for histochemical studies by fixation with 10% buffered-saline formalin.

Histopathological analysis

Formalin fixed brains were processed and cortex tissues were stained with hematoxylin and eosin (H&E) and examined for any histopathological changes. Pathological diagnosis of each brain specimen was assessed and analyzed by specialized histopathologist.

DETERMINATION OF OXIDATIVE STRESS MARKERS

Sera total antioxidant capacity

Blood was collected without using an anticoagulant, allowed to clot for 30 min at 25°C then centrifuged at 3000 rpm for 15 min at 4°C . Serum was collected and stored at -80°C if not assayed on the same day. The assay was performed according to method described before (Koracevic et al., 2001).

Reduced glutathione (GSH) level

Dissected parts of the brain cortex tissues (10% w/v) were washed with saline solution minced and homogenized in ice cooled homogenization buffer (1.15% KCl, 0.01 M sodium phosphate buffer pH 7.4). The homogenates were centrifuged at 10,000 rpm for 20 min at 4°C and the supernatants were used for determination of glutathione (GSH) and protein contents. GSH contents were determined as described by Ellman (1959). Briefly, Ellman's reagent [5,5', dithiobis (2-nitrobenzoic acid), DTNB] reacts with GSH to give 2-nitro-5-thiobenzoic acid, a yellow colored product with a maximum absorbance at 412 nm, GSH level is expressed as mg/g. tissue.

Lipid peroxidation

Frozen sections of brain tissues (10% w/v) were washed with saline solution, minced, and homogenized in ice cooled buffer (50 mM potassium phosphate pH 7.5), the homogenates were centrifuged at 10,000 rpm for 20 min at 4°C and the supernatants were used for the assay. Levels of lipid peroxidation were determined according to Ohkawa et al. (1979) colorimetric method. Thiobarbituric acid (TAB) reacts with malondialdehyde (MDA) in acidic medium at 95°C for 30 min to form TAB reactive product to give pink color that is measured at 534 nm and MDA content is expressed in nmol/g tissue.

Superoxide dismutase activity (SOD)

Brain tissue was homogenized in ice cooled buffer (100 mM potassium phosphate, pH 7.0 containing 2 mM EDTA) per gram tissue. Superoxide dismutase activity (SOD) was assayed according to Nishikimi et al. (1972). The assay depends on the ability of the enzyme to inhibit the phenazine methosulphate-mediated reaction of nitroblue tetrazolium dye. Phenazine methosulphate (0.1 mM/L) was diluted 500 times immediately before use in distilled water. In addition to working reagent was

freshly prepared by mixing phosphate buffer (50 mM/L) pH 8.5, nitroblue tetrazolium (1 mM/L), and NaOH (1 mM/L) in ratio of 10 + 1 + 1. Reaction mixture prepared by mixing the working reagent and samples, then initiated by addition of diluted phenazine methosulphate according to the protocol indicated ratios.

TOTAL RNA ISOLATION AND REVERSE TRANSCRIPTASE POLYMERASE REACTION (RT-PCR)

Total RNA was extracted from frozen brain tissues according to Chomczynski and Sacchi (1987) using GStruct™ RNA Isolation Kit II Guanidinium Thiocyanate Method (Maxim Biotech Inc., USA). Quality of RNA preparations were confirmed by calculating 260/280 ratio for detection of protein contamination and by running samples on agarose to confirm that the samples are DNA-free. Alterations in the target mRNA levels of genes relevant to microglia activation and neuroinflammation were determined using either semi-quantitative reverse-transcriptase PCR (semi-qRT-PCR) or quantitative real time RT-PCR (qRT-PCR).

Semi-quantitative RT-PCR

Semi-quantitative RT-PCR was performed using one-step RT-PCR (RT/PCR Master Mix Gold Beads, BIORON). The cDNA was synthesized and used for amplification of target gene(s). Briefly, total RNA (1–3 μg) and random primer (3 μM) mixture were denatured at 70°C for 5 min and placed on ice. The incubated mixture was added to the RT/PCR Gold mix that contains all the components necessary for cDNA synthesis and amplification in one tube. The cDNA synthesis reaction was performed at 42°C for 60 min then 5 min at 94°C for RTase inactivation. The primers then subjected to PCR cycles, each cycle consisting of denaturation, annealing, and extension. Annealing temperature and time was optimized for each primer/template combination. We investigated the expression of neuroinflammatory markers APP, BACE1, γ -secretase (presenilin; PSEN-1 and PSEN-2) and iNOS expressions using the following primers sets: APP; F-AGAGGTCTACCCTGAACTGC- R- ATCGCTTACAACTCACCAAC (154 bp), BACE1; F-CGGGAGTGGTATTATGAAGTG-R-AGGATGGTGATGCGGAAG (320 bp), PSEN-1; F- GGATGGG CAGCTAATCTATAC- R- CCTTCAGCCATATTCACCAAC (576), PSEN-2; F-GAG CAG AGC CAA ATC AAA GG- R- GGGAGAAAGAACAGCTCGTG (188 bp), iNOS; F-GTGTTCCACCAGGAGATGTTG- R-CTCCTGCCCACTGAGTTCGTC (576 bp) and for validation we used β -actin: F-GGC ATC CTG ACC CTG AAG TA- R-GCCGATAGTGATGACCTGACC (565 bp). Products of RT-PCR were separated on agarose gel, visualized and documented using ChemiDoc-It[®] 2 Imager then analyzed with VisionWorksLS Acquisition and Analysis Software for determinations of relative bands intensity.

Quantitative RT-PCR assay

Quantitative real time RT-PCR was used to measure the mRNA levels of APE1, let-7a, b, and c. analyses were performed using miScript II RT Kit (Qiagen) according to the manufacture guidelines. The primers for APE1 were F-GCTTGGATTGGGTAAAGGA, R-TTCTTTGTCTGATGGAGCTG, COX-2; F- AGGCCTCCATTG

ACCAGA- R- TCATGG TAGAGGGCTTTCAAC, β -actin; F-CCGACAGGATGCAGAAGG-3' and R-GGAGTACTTGCCTCAGGAG, let-7a; TGA GGT AGT AGG TTG TAT AGTT, let-7b; TGA GGT AGT AGG TTG TGT GTTT, let-7c; TGAGGTAGTAGTGTGTATGGTT and U6; F-GGAACGATACAGAGAAGATTAGC, R- AAATATGGAACGCTTCACGA. Gene expression results of indicated genes and miRNAs were normalized to β -actin and U6, respectively, fold difference calculated as described before (Livak and Schmittgen, 2001).

PREPARATION OF CYTOSOLIC AND NUCLEAR EXTRACTS AND WESTERN BLOTTING

The extraction of cytosolic and nuclear rich fractions was performed according to Dignam et al. (1983) procedure. Briefly brain tissues were homogenized using hypotonic buffer (10 mM HEPES buffer, pH 7.5 containing 10 mM KCl, 3 mM NaCl, 3 mM MgCl₂, 1 mM EDTA, 1 mM EGTA, 2 mM DTT, 2 mM PMSF, and protease inhibitor cocktail) and kept on ice for 15 min. The supernatants (cytoplasmic extracts) were collected by centrifugation then stored at -80°C and the pellets were washed in 200 μl of hypotonic buffer and re-centrifuged. The pellets nuclei were re-suspended in 100 μl of ice-cold NE buffer (20 mM HEPES buffer, pH 7.5 containing 25% glycerol, 500 mM KCl, 1 mM MgCl₂, 1% NP-40, 1 mM EDTA, 2 mM DTT, 2 mM PMSF, and protease inhibitor cocktail), and incubated on ice for 20 min, with occasional mixing, then centrifuged at $14,000 \times g$ for 15 min at 4°C . The resulting supernatants, nuclear extracts, were collected and stored at -80°C for further analysis. Primary antibody to APE1 (sc-17774) and COX-2 (sc-7951) were used and equal loading was confirmed by probing with β -Actin (sc-81178) monoclonal antibody.

STATISTICAL ANALYSIS

Experiments were repeated two or more times independently and graphs are represented as mean \pm SD. The difference between groups was analyzed by one-way analysis of variance (ANOVA) and the difference considered significant either at $p < 0.01$ or at $p < 0.001$ when compared to mock-treated group.

RESULTS

HISTOLOGICAL ANALYSES

Brain tissues of mock-treated, LPS-induced, Co-treated, and treated groups were examined using H&E staining as shown in (Figure 2) for confirmation of progression to neuroinflammation. The histopathology of cortex tissue from rats induced with LPS and co-treated with VPA and Cur showed some protection effect against neuroinflammation (Figures 2C,D). Although treatment with VPA exerted inhibitory effect on neuroinflammation but Cur showed more potent effect than VPA (Figures 3A,B). Interestingly combination of both Cur and VPA induced strong synergistic effect showing no significant neuroinflammation (Figure 3C) compared to self-recovery group (Figure 3D), which is consistent with the biochemical markers profile.

CURCUMIN COMBINATION WITH VALPROIC ACID AMELIORATES LPS-INDUCED OXIDATIVE STRESS

Oxidative stress is a hallmark of inflammatory mechanism. Herein we measured oxidative stress parameters represented by sera total

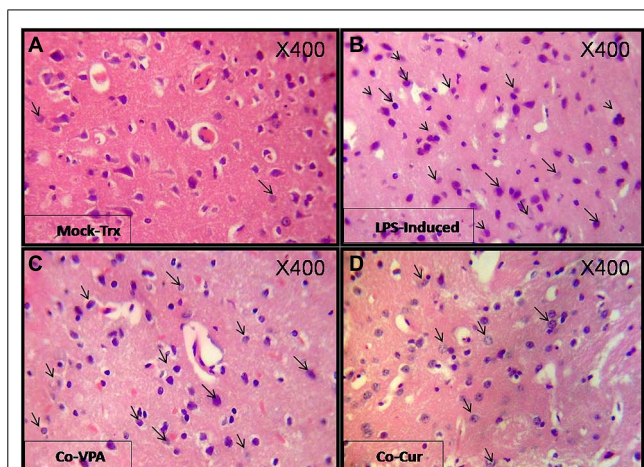


FIGURE 2 | Shows H&E (400X) staining of Cortex sections from different experimental groups: (A) shows photographs of mock-treated with normal parenchyma and architecture. (B) shows lipopolysaccharide (LPS)-induced cortex sections featuring an aggregate of mature lymphocytes an effect that was partially inhibited by co-administration of Valproic acid (VPA; C) and Curcumin (Cur; D). Apparently Co-Cur group showed sparse lymphocytic infiltrate compared to mock-treated. Arrows indicate the activated lymphocytes.

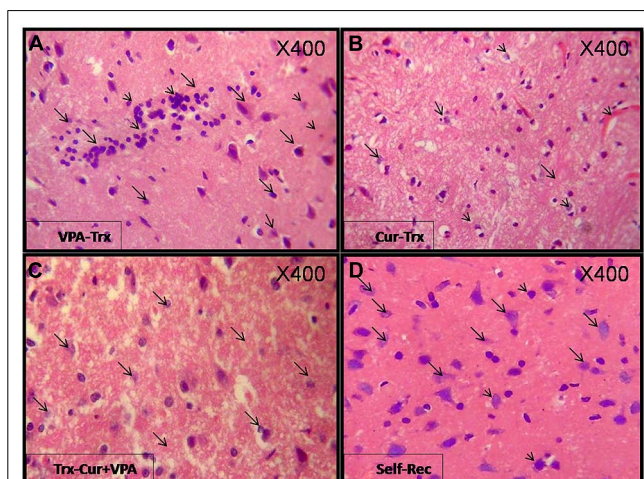


FIGURE 3 | Show H&E (400X) stained sections for the treated groups: Cur, VPA, and VPA-Cur as well as the self-recovery group that received no treatment for 1 month. The represented photographs indicate that VPA acid treated rats (A) featured moderately intense lymphocytic infiltrate and Cur treatment (B) induced suppression of the inflammatory response as depicted by negligible lymphocytic infiltrate as marked by the arrows. Moreover VPA-Cur combination (C) exerted the most anti-inflammatory effect by showing no inflammatory infiltrate compared to self-recovery group (D) that contain sparse lymphocytic infiltrate as indicated by the arrows.

antioxidant capacity (TAC), GSH, and MDA levels as well as SOD activity in the different experimental groups. Results are presented as fold change from the mock-treated group. An overall significant decline ($p < 0.01$) in the sera TAC, GSH level and SOD activity associated with significant elevation in MDA level ($p < 0.001$) were observed in LPS-induced brains (Figure 4). In

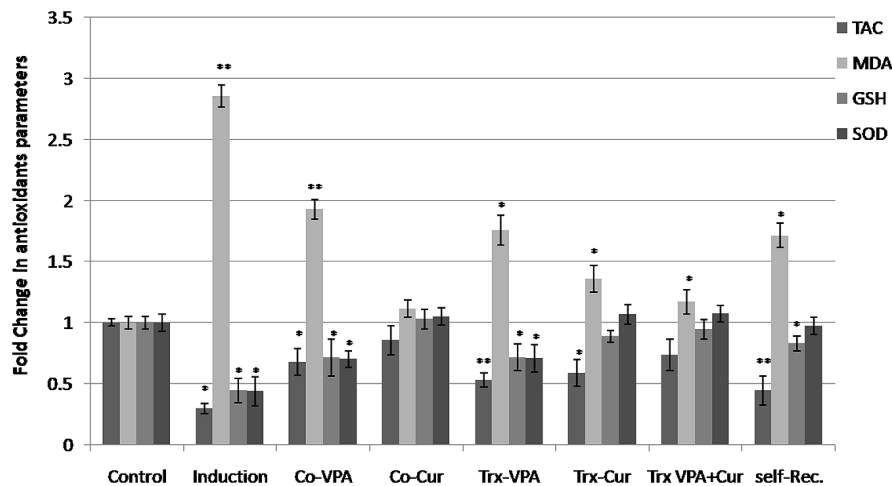


FIGURE 4 | Fold alterations in antioxidant capacity versus mock-treated rats. Oxidative stress related markers total antioxidant capacity (TAC), glutathione (GSH), and malondialdehyde (MDA) levels as well as superoxide dismutase activity (SOD) activity were measured in the different experimental groups. LPS-induced an overall reduction in antioxidant defense system as indicated by significant ($*p < 0.01$) decreases in TAC, GSH, and SOD and significant ($**p < 0.01$) elevation in MDA content versus mock-treated rats

(mock-Trx). Co-administration of VPA did not improve oxidative stress markers. On the contrary, Cur co-administration inhibited LPS-induced neurotoxicity markedly by maintaining all parameters near normal values. Moreover treating induced rats with cur but not with VPA restored GSH content and SOD activity. VPA addition to Cur exerted the most antioxidant effect on neuroinflamed rats. An improvement in GSH level and SOD activity was also observed in Self-Rec rats.

parallel to histological observations, co-administration of VPA or Cur ameliorated LPS-induced neurotoxicity with most prominent effect upon Cur co-administration. Furthermore Cur treatment markedly improved both GSH level and SOD activity (Figure 4). Obviously VPA treatment was not effective in inhibiting LPS-induced oxidative stress as indicated by significant elevation in MDA ($p < 0.01$) accompanied with significant reduction in TAC, GSH level, and SOD activity ($p < 0.001$ and $p < 0.01$, respectively; Figure 4). Interestingly, adding VPA to Cur potentiated Cur effect and restored the oxidative stress markers back to normal when compared to mock-Trx. Restoration of GSH level and SOD activity in the self-recovery group indicated that shifting the oxidative stress balance is essential during physiological wound healing process (Figure 4).

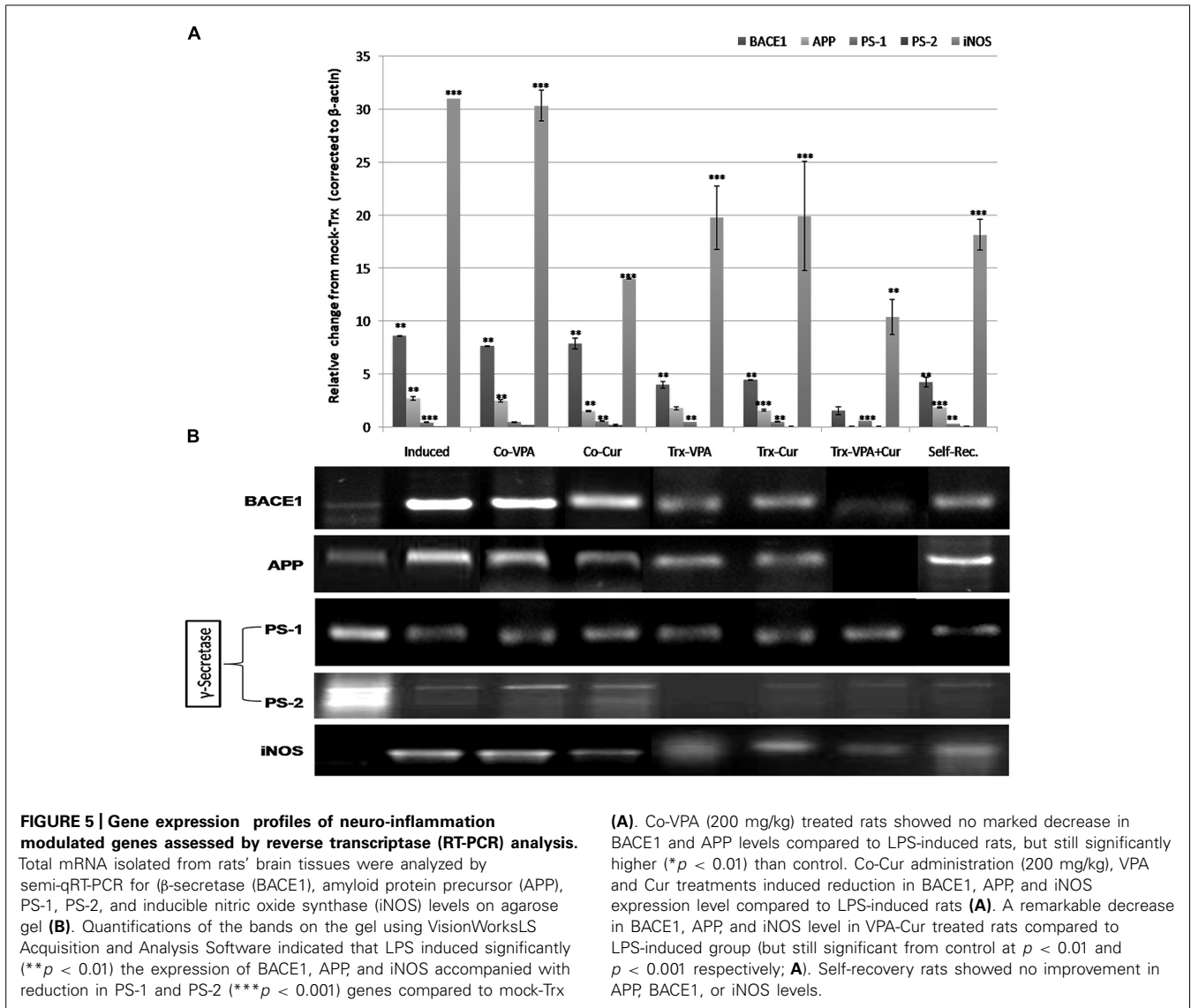
EXPRESSION PROFILE OF NEURO-INFLAMMATION MARKERS

The relevance of neuroinflammation to Alzheimer's pathology has been elucidated by different reports. Microglial activation has been shown in regions associated with A β deposition. In the current study we examined the expression of BACE1, APP, and γ -secretase subunits (PSEN-1 and PSEN-2) as the major factors implicated in A β deposition as well as the inflammatory enzymes iNOS, COX-2, and APE1. Total RNA from cortex tissues were extracted and mRNAs were analyzed by semi-qRT-PCR for the indicated genes. LPS-induced significantly BACE1 and APP along with the inflammatory enzyme iNOS expressions (around 8-, 2-, and 30-folds, respectively) when calculated in reference to the expression level in mock-Trx (Figures 5A,B). In addition, LPS reduced PSEN-1 and -2 expressions significantly ($p < 0.001$). Co-addition of either VPA or Cur ameliorated LPS effect by around 10 and 30% respectively (Figure 5B). Moreover treatment of induced rats with Cur is more effective than VPA

in reducing BACE1, APP, and iNOS expressions ($p < 0.01$) and increasing PSEN-1 and -2 levels (Figures 5A,B). We also show that adding VPA potentiates Cur-mediated anti-inflammatory properties and significantly reduced BACE1, APP ($p < 0.001$), and iNOS ($p < 0.01$) when compared to control and self-rec. groups (Figure 5B).

We have previously reported the involvement of APE1 down-regulation during the pathogenesis of neuroinflammation and maintaining high APE1 expression is associated with neuroprotection (Zaky et al., 2013). Cur has been reported to regulate COX-2 both at transcriptional and protein levels. In the current study we investigated APE1 and COX-2 as key inflammatory enzymes by real time-PCR (qRT-PCR) and western blotting. LPS induction for 4 weeks increased COX-2 expression by up to threefold and reduced APE1 by around 70% when compared to control (Figure 6A). Continuous administration of Cur with LPS inhibited significantly the brain toxicity by reducing COX-2 and maintaining high APE1 expressions. On the contrary, VPA co-administration did not improve COX-2 or APE1 levels. Although Cur treatment significantly inhibited COX-2 and induced APE1 expressions (up to normalization; Figure 6A), but VPA-Cur combination was more effective on inhibiting COX-2 and inducing APE1. In consistent with COX-2 gene expression results (qRT-PCR), western blotting analysis showed similar pattern of cytosolic COX-2 protein (Figure 6B).

Because LPS-induced neurotoxicity is associated with oxidative stress and DNA mutation that activate APE1 nuclear translocation, therefore we investigated nuclear versus cytosolic distribution of APE1 protein. The results showed high nuclear localization in LPS-induced and Co-VPA administered rats. In parallel to Cur effects on antioxidant capacity and



neuroinflammation markers, we observed marked reduction in nuclear APE1 level upon continuous supply of Cur during induction (Figure 6B). Likewise Cur only and in combination with VPA was shown to be effective in switching APE1 localization to cytoplasm versus VPA-treated and self-Rec groups (Figure 6B).

MODULATION OF FIVE MEMBERS OF let-7 FAMILY miRNAs

microRNAs are considered crucial regulators of cellular immunity and functions. Accumulating data from different studies have highlighted diverse alterations in miRNAs biogenesis and regulatory role in inflammatory diseases including neurodegeneration. miRNA let-7 family members are highly expressed in central nervous system and were shown to play crucial role in cell development and differentiation. Therefore we analyzed the expression profile of five members of let-7 family (a, b, c, e, and f) in the different experimental groups. The results show that let-7 a, b, and c were under detection level in LPS induced

rats, an effect that was countered by either co-VPA or co-Cur incorporation (Figure 7). We also observed unique pattern of drug-induced differential expression of the five miRNAs types. Moreover Cur or VPA treatment of induced rats exhibited the same pattern of inducing significantly let-7c and f compared to Cur-VPA treated rats that showed significant restoration in the expression of the five members (Figure 7). Evidently we observed significant elevations in let-7 a, c, and f in self-rec. group which confirms the implication of these let-7 members in self-healing mechanism.

DISCUSSION

In the present study, we observed the alteration of the inflammatory response in male adult Sprague–Dawley rats brain cortex and investigated the protective versus therapeutic effects of Cur alone or in combination with HDAC1 inhibitor, VPA on attenuating LPS-induced neuroinflammation in rats. We focused on Cur, which is used as a food additive, due to its diverse

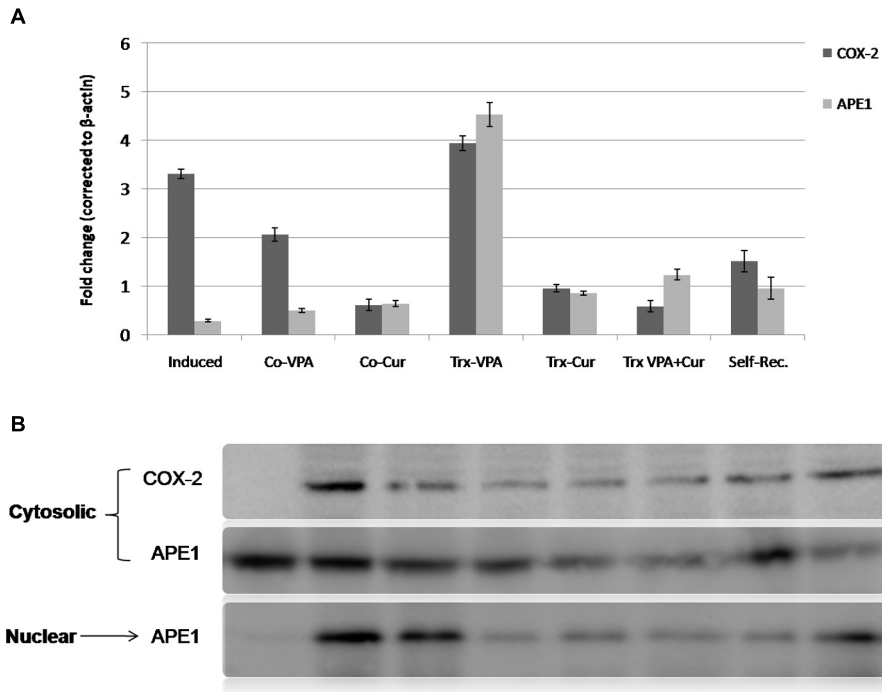


FIGURE 6 | Quantitative real time RT-PCR (qRT-PCR) and western blotting analysis of APE1 and COX-2 expressions. mRNA and total proteins extracts were prepared (as described in the methods section) from mock-treated and LPS-induced as well as co-treated and treated groups. **(A)** and **(B)** showed a significant elevation (** $p < 0.001$) in cyclooxygenase-2 (COX-2) level of LPS-induced group as well as VPA-treated and co-VPA treated groups in comparison with mock-treated

group versus reduction in COX-2 level in self-recovery group. A remarkable reduction ($*p < 0.01$) in COX-2 level in Co-Cur treated, Cur-Treated and VPA-Cur treated groups versus LPS-induced group. A remarkable reduction in APE1 in induced versus mock-treated group. Data revealed an elevation of APE1 in treated and Co-treated groups as well as self-recovery group but especially in VPA-treated group versus LPS-induced rats.

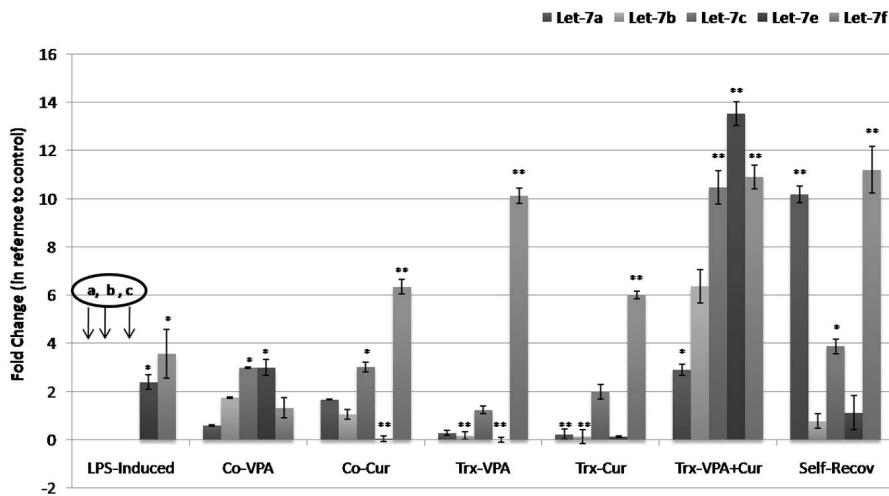


FIGURE 7 | Quantitative real time RT-PCR analyses of let-7 miRNAs family expression profile in different experimental groups. In our study we measured the alterations in the expression levels of five different types of let-7 miRNAs (Let-7 a, b, c, e, and f). Mock-treated, LPS-induced, co-treated and treated rat's miRNAs extracts were subjected to quantitative real time polymerase chain reaction (qRT-PCR)

of target genes expression. Completed reductions (under detection limit) in let-7a, b, and c levels were observed in LPS-induced rats, the effect that was ameliorated by co-administration of VPA or Cur (** $p < 0.001$). Moreover VPA+Cur combination for treating induced rats significantly ($*p < 0.01$) induced the five members of let-7 family in comparison to LPS-induced rats.

pharmacological activities, very low toxicity and widespread availability. The therapeutic potential of VPA in central nervous system diseases is also gaining support. We administered Cur and/or VPA (200 mg/kg) for 4 weeks and observed production of proinflammatory mediators, COX-2, APE1, and nitric oxide/iNOS. The combined therapy decreased the production and mRNA expression of the inflammatory TNF- α and interleukin (IL-6; data not shown). In addition, expression of iNOS and COX-2 were decreased by cotreatment with Cur and VPA. In conclusion, these results show that the anti-inflammatory properties of Cur and VPA potentially result from the inhibition of COX-2, iNOS, IL-6, TNF- α , and NO through activation of NF- κ B. These results impact the development of potential health products for preventing and treating inflammatory diseases.

Consistent with the inhibition of pro-inflammatory mediators by Cur and VPA, we observed an anti-inflammatory role of Cur via inhibition of NF- κ B pro-inflammatory pathways. Therefore, the NF- κ B pathway is potentially involved in the anti-inflammatory therapeutic effects of Cur in a variety of neuropathologies. In support of this, Cur has been found to block the LPS-mediated induction of COX-2 through inhibition of NF- κ B and STAT3 (Kim et al., 2003; Kang et al., 2004). Although the beneficial effects of combined therapy can be observed and conclusive under various experimental conditions, the effects of Cur and VPA in rat cortex cells exposed to LPS remain to be fully elucidated. Further experiments are required to explore the detailed mechanisms underlying this process. Regardless of the mechanism, the data presented in this study may assist future studies that aim to determine the therapeutic potential of Cur and VPA.

In a recent study, neuroinflammation was induced by bilateral intracerebroventricular (ICV) administration of LPS (Tyagi et al., 2008). They studied the proinflammatory cytokines (TNF- α and IL-1 β), acetylcholinesterase (AChE) activity, MDA, and reduced GSH as markers for neuroinflammation, cholinergic activity, and oxidative stress, respectively, in different brain regions at different time points after LPS injection. They found enhanced AChE activity with these inflammatory markers after LPS administration indicates a possible relationship between neuroinflammation and cholinergic system during the development of neurodegenerative diseases. It was found also that cholinergic agonists inhibit cytokine synthesis and protect against cytokine-mediated diseases (Tracey, 2007).

Findings from an experiment of selective serotonin reuptake inhibitors (SSRIs) by Waiskopf et al. (2014) suggested a possible interaction with both TLR4 responses and cholinergic signaling through as yet unclear molecular mechanism(s). They also demonstrated reduced LPS-induced pro-inflammatory IL-6 and TNF- α in human peripheral blood mononuclear cells preincubated with antidepressant fluoxetine. Furthermore, they showed that fluoxetine intercepts the LPS-induced decreases in intracellular AChE-S and that AChE-S interacts with the NF- κ B-activating intracellular receptor for activated C kinase 1 (RACK1). This interaction may prevent NF- κ B activation by residual RACK1 and its interacting protein kinase PKC β II. These

findings attribute the anti-inflammatory properties of SSRI to surface membrane interference with leukocyte TLR4 activation accompanied by intracellular limitation of pathogen-inducible changes in AChE-S, RACK1, and PKC β II (Waiskopf et al., 2014).

Also, Sailaja et al. (2012) reported that chromatin structure and histone modifications are causally involved in this transcriptional memory. Specifically, the AChE gene is known to undergo long-lasting transcriptional and alternative splicing changes after stress. Their findings provide further support and underscore the importance of better understanding for the notion that chromatin regulation is an important mechanism controlling long-term adaptive changes in the brain associated with complex psychiatric conditions.

In the present study we assessed the effect of the HDAC1 inhibitor VPA by measuring alterations at histological, biochemical, and molecular levels. The early stage of asymptomatic stage, reached by LPS with a modified dose (250 μ g/kg five times per week for 4 weeks) was established to explore the mechanism of action of Cur, VPA, and VPA-Cur combination on the attenuation of LPS-induced neuroinflammation. Histological analyses indicated that co-administration of either VPA or Cur inhibited LPS-induced lymphocyte infiltrations in the cortex tissues. However, treatment of induced rats with VPA, Cur or their combination for 4 weeks post LPS-induction, exerted neuronal recovery, but the most significant improvement was observed upon treatment with VPA-Cur combination as confirmed by H&E staining.

Altered oxidative stress levels determined in our experiments verify the neuroinflammation responses as explained by Ferger et al. (2010). Ngkelo et al. (2012) indicated the implication of ROS in the mechanism of TLR4 activation by LPS. The biological effects of Cur are mainly derived from its ability to either bind directly to various proteins such as COX-2 or its ability to modulate the intracellular redox state (Hong et al., 2004). In parallel, we investigated the anti-oxidant effect of VPA, Cur, and VPA-Cur combination by measuring tissues MDA and GSH levels as well as SOD activities. Our results clearly demonstrate that co-Cur administration inhibited significantly LPS-induced brain toxicity and oxidative stress compared to co-VPA group. In addition to, treatment with Cur alone or in combination with VPA restored oxidative stress balance significantly (close to normalization) compared to both VPA-treated and self-recovery groups.

Several lines of investigation support the notion that the pathogenesis of AD is related to progressive accumulation of A β protein, as a result of an imbalance between the levels of A β production, aggregation and clearance. It has been shown that the abnormal processing of APP by β and γ -secretase protease enzymes is a key event in the development of Alzheimer's disease (AD) neuropathology (Sastre et al., 2003), resulting in an increase in the generation of the 42 amino acid form of A β peptide which aggregates to form the insoluble amyloid plaques. Hauss-Wegrzyniak and Wenk (2002) demonstrated that LPS induced extracellular deposition of beta-amyloid fibrils into the hippocampus suggesting that there is a close connection between amyloidogenesis and LPS-induced neuro-inflammation and LPS-induced increase of APP level. The γ -secretase complex has not yet been fully characterized but minimally consists of

four individual proteins including PSEN. Therefore we detected the expression profile of neuroinflammation-related markers; APP, BACE1, and γ -secretase subunits (PSEN-1, PSEN-2) using semi-qRT-PCR in cortical region of rat's brain tissues. We observed marked induction of BACE1 and APP expressions in the cortex tissues of LPS-induced rats along with clear reduction in the expression levels of both γ -secretase subunits. Consistently, we observed marked suppression in BACE1 and APP expressions upon co-Cur administration, Cur-treatment and more significantly in VPA-Cur treated rats versus marked induction of PSEN-1 and PSEN-2 subunits levels in the same groups.

Several lines of investigation support the notion that the pathogenesis of AD is related to progressive accumulation of A β protein, as a result of an imbalance between the levels of A β production, aggregation, and clearance. It has been shown that the abnormal processing of APP by β and γ -secretase protease enzymes is a key event in the development of AD neuropathology (Sastre et al., 2003), resulting in an increase in the generation of the 42 amino acid form of A β peptide which aggregates to form the insoluble amyloid plaques. Hauss-Wegrzyniak and Wenk (2002) demonstrated that LPS induced extracellular deposition of beta-amyloid fibrils into the hippocampus suggesting that there is a close connection between amyloidogenesis and LPS-induced neuro-inflammation and LPS-induced increase of APP level. The γ -secretase complex has not yet been fully characterized but minimally consists of four individual proteins including PSEN. Therefore we detected the expression profile of neuroinflammation-related markers; APP, BACE1, and γ -secretase subunits (PSEN-1, PSEN-2) using semi-qRT-PCR in cortical region of rat's brain tissues.

We observed marked induction of BACE1 and APP expressions in the cortex tissues of LPS-induced rats along with clear reduction in the expression levels of both γ -secretase subunits. Consistently, we observed marked suppression in BACE1 and APP expressions upon co-Cur administration, Cur-treatment and more significantly in VPA-Cur treated rats versus marked induction of PSEN-1 and PSEN-2 subunits levels in the same groups.

Consistently in the present study, by investigating APE1 expression in LPS-neuroinflammation established model, the results revealed significant reduction of both APE1 mRNA level, and intracellular protein distribution (cytosolic versus nuclear) compared to mock-treated rats. Furthermore, we show that Cur co-administration maintained significantly elevated APE1 level during the course of LPS-induction compared to induced rats with more nuclear localization. Furthermore we found that VPA-Cur treatment was more effective than either Cur or VPA treatments alone in restoring high APE1 expression profile and inducing more cytosolic localization. The intracellular localization of the multifunctional APE1 has been closely correlated to its various functions, hence nuclear versus cytosolic distribution level reflects a vital role in BER or in redox co-activation of different transcription factors. This suggests that Cur and VPA-Cur combination actions are mediated, in part, by maintaining elevated APE1 level and shifting the intracellular balance to more cytosolic localization, a state that mimic normal condition.

In agreement with Peng et al. (2005) that showed that VPA may cause MKP-1 activation to dephosphorylate p38MAPK and JNK, leading to decrease in p65 and C/EBP β binding to the COX-2 promoter region and COX-2 down-regulation in LPS-stimulated bEnd.3 cells, our data established that co-expression of inflammatory proteins COX-2, iNOS and amyloid peptides were higher in the LPS-treated rats. However, Cur/VPA decreased the LPS-induced expressions of COX-2, iNOS, and amyloid peptides. Cur administered to rats either alone or in combination with VPA exhibited the most significant inhibitory effect on COX-2 and iNOS expressions in their brain tissues extracts.

Recently miRNAs have been identified as crucial regulators of immune cell development and function. Deregulated miRNAs contribute to the development of various diseases, for example, cancer, cardiovascular, or neurological diseases (Bonauer et al., 2010; Gascon and Gao, 2012; Thum, 2012).

Neurodegeneration is characterized by neuronal loss of specific neuronal circuits associated with cognitive and motor functions and by changes in miRNA levels in the nervous tissue and in the periphery. Recent reports of microRNA modulators of both neuronal and immune processes (termed NeurimmiRs) predict therapeutic potential for manipulating NeurimmiR levels in diseases affecting both the immune system and higher brain functions, such as AD, Parkinson's disease (PD), multiple sclerosis (MS), and anxiety-related disorders (Soreq and Wolf, 2011). Manipulating NeurimmiR control that function within both the nervous and the immune systems, over the immune contributions to cognitive pathways may offer new therapeutic targets. Amongst them let-7 family miRNA that were reported to be broadly expressed across all differentiated tissues and their expression is tightly controlled during embryonic stem cells differentiation. In our study, we screened in particular, five types of let-7 miRNAs family which are; let-7a, let-7b, let-7c, let-7e, and let-7f for possible modulation during the course of induction, protection, and treatment. Interestingly we observed an overall altered expression profile in the five types of let-7 miRNAs in induced versus protected and treated rats. However, let-7a, b, and c levels were undetectable when assessed using qRT-PCR in induced group, a significant expression was observed in Co-Cur and Co-VPA administered groups, which suggest their implication in neural protection. In addition, their levels were up-regulated up to 3, 6, and 11 folds consequently in VPA-Cur treated group which confirm their involvement in neural recovery of inflamed brain tissues.

A major question of our study was to delineate to what extent miRNA changes accompany disease and disease progression. miRNAs have recently been involved mostly in neurodegenerative disorders including AD (Lau et al., 2013). Their work reveal that most of the recorded expression changes in miRNAs are brain area specific, with 10 miRNAs deregulated in the hippocampus and prefrontal cortex in late onset AD. It is also likely that several miRNA changes recorded in our human brain samples are related to some neuroinflammatory changes occurring during disease, especially 132-3p which mediates anti-inflammatory signaling (Shaked et al., 2009). The targeting of acetylcholinesterase by miR-132-3p may

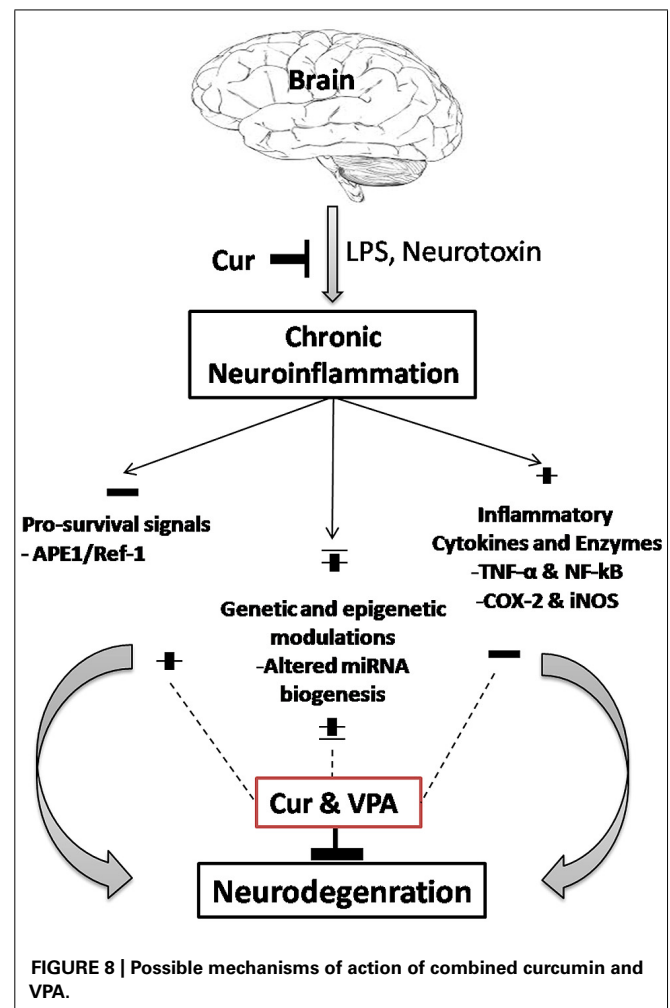
be indeed relevant for the association of the enzyme activity with amyloid load in late onset AD (Alkalay et al., 2013; Lau et al., 2013).

Consistent with obtained results of the five members of let-7 expression profile in the different experimental group, by applying mirSVR online data base for their mRNA targets prediction, we uncovered COX-2 gene (NM_011198) as a target for the five members while let-7b only regulates the expression of iNOS (NM_012611) gene. This explains the observation of let-7a, b, and c disappearance in induced group that was accompanied with threefold induction in COX-2 level as well as up to threefold induction in iNOS expression compared to mock-Trx. Our results suggest that microRNAs can function as signaling molecules and identify COX-2 as an essential element in a pathway that contributes to the spread of CNS damage.

Evidently the distinguished pattern of let-7 five members' expression in each group is directly correlated to the genetic remodeling activity that is exerted by LPS, Cur, or VPA. It is clearly demonstrated that LPS-induced neurotoxicity suppresses let-7 family miRNAs expression, an effect that is ameliorated by co-administration of either cur or VPA. Co-administration of either Cur or VPA a particular differential expression was observed in all investigated members of let-7 miRNAs confirming their function as important players in neuro-protection. Moreover a definite significant restoration of let-7-a, b, and c levels were observed in VPA-Cur treated rats versus self-recovery group that initiated self-healing for 4 weeks. Treatment of induced rats with VPA or Cur alone did not induce let-7 a, b, and c in the same pattern as their combination did which indicate the synergistic effect VPA-Cur treatment. The anti-inflammatory effect of Cur is most likely mediated through its ability to inhibit COX-2 and iNOS COX-2 as important enzymes that mediate inflammatory processes. Improper upregulation of COX-2 and/or iNOS has been associated with the pathophysiology inflammatory disorders. Since Cur was shown to modulate COX-2 by direct binding, adding VPA provide synergistic effect for COX-2 and iNOS down-regulation through its activity as epigenetic modulator.

The discovery and development of miRNA-based therapeutics, as well as the diverse range of molecular cascades they can regulate, offer a new approach for treating diseases with a heterogeneous or epigenetic origin. We provide strong evidence for meaningful changes in five let-7 members miRNA expression during induction, progression, and treatment with Cur and VPA as the most salient feature. Recently, alteration of miR- let-7 members expression has also been reported in several other neurodegenerative diseases including schizophrenia, AD and addiction (Beveridge et al., 2010; Hollander et al., 2010; Santarelli et al., 2011; Wang et al., 2011). Our work thus clearly indicates that miRNAs such as let-7 members deserve further functional exploration to deepen our understanding of molecular mechanisms driving not only neuroinflammation but also other neurodegenerative disorders. It is not unlikely that future studies might reveal part of those common molecular pathways that are relevant to these conditions.

The fine-tuning activity of miRNAs has been proven crucial in the regulation of differentiation of microglia allowing the maintenance of brain homeostasis. Since a single miRNA has the



capacity to target more than one protein involved in the same signaling pathway, their modulation can significantly change cell phenotypes that depend on the levels and activation of specific proteins. Such capacity reflects a molecular paradigm suitable for therapeutic intervention.

In conclusion, as shown in **Figure 8**, the antioxidant and the current study provides evidence for the potential neuro-protective and therapeutic effect of Cur through its anti-inflammatory and gene-remodeling activities. Furthermore we highlight the synergistic effect of VPA addition to Cur for treating neuroinflammation. Also we shed the light on the role of five let-7 family in VPA-Cur mediated mechanism of actions as novel therapeutic targets. Given their important role in the regulation of gene expression, we believe that miRNA-based therapies could constitute an interesting and attractive strategy to improve microglia activity, modulating signaling pathways linked with neuroinflammation.

ACKNOWLEDGMENTS

This work was supported partially by BA/CSSP-2010 grant, ISIS 510935-TEMPUS-1-2010-FR-TEMPUS-JPCR (Real time equipment) and NEUREN, International Research Staff Exchange Scheme (IRSES), FP7-People-2012-IRSES, grant number 318997.

We also would like to acknowledge the support of Faculty of Science and Alexandria University.

REFERENCES

- Alkalay, A., Rabinovici, G. D., Zimmerman, G., Agarwal, N., Kaufner, D., Miller, B. L., et al. (2013). Plasma acetylcholinesterase activity correlates with intracerebral beta-amyloid load. *Curr. Alzheimer Res.* 10, 48–56. doi: 10.1016/j.jalz.2010.05.1715
- Asehounne, K., Strassheim, D., Mitra, S., Kim, J. Y., and Abraham, E. (2004). Involvement of reactive oxygen species in Toll-like receptor 4-dependent activation of NF-kappa B. *J. Immunol.* 172, 3589–3593. doi: 10.4049/jimmunol.172.4.2522
- Betel, D., Koppal, A., Agius, P., Sander, C., and Leslie, C. (2010). Comprehensive modeling of microRNA targets predicts functional non-conserved and non-canonical sites. *Genome Biol.* 11, R90. doi: 10.1186/gb-2010-11-8-r90
- Beveridge, N. J., Gardiner, E., Carroll, A. P., Tooney, P. A., and Cairns, M. J. (2010). Schizophrenia is associated with an increase in cortical microRNA biogenesis. *Mol. Psychiatry* 15, 1176–1189. doi: 10.1038/mp.2009.84
- Bode, J. G., Ehrling, C., and Haussinger, D. (2012). The macrophage response towards LPS and its control through the p38(MAPK)-STAT3 axis. *Cell. Signal.* 24, 1185–1194. doi: 10.1016/j.cellsig.2012.01.018
- Bonauer, A., Boon, R. A., and Dimmeler, S. (2010). Vascular microRNAs. *Curr. Drug Targets* 11, 943–949. doi: 10.2174/138945010791591313
- Camelo, S., Iglesias, A. H., Hwang, D., Due, B., Ryu, H., Smith, K., et al. (2005). Transcriptional therapy with the histone deacetylase inhibitor trichostatin A ameliorates experimental autoimmune encephalomyelitis. *J. Neuroimmunol.* 164, 10–21. doi: 10.1016/j.jneuroim.2005.02.022
- Chomczynski, P., and Sacchi, N. (1987). Single-step method of RNA isolation by acid guanidinium thiocyanate-phenol-chloroform extraction. *Anal. Biochem.* 162, 156–159. doi: 10.1016/0003-2697(87)90021-2
- Dasuri, K., Zhang, L., and Keller, J. N. (2013). Oxidative stress, neurodegeneration, and the balance of protein degradation and protein synthesis. *Free Radic Biol. Med.* 62, 170–185. doi: 10.1016/j.freeradbiomed.2012.09.016
- Dignam, J. D., Lebovitz, R. M., and Roeder, R. G. (1983). Accurate transcription initiation by RNA polymerase II in a soluble extract from isolated mammalian nuclei. *Nucleic Acids Res.* 11, 1475–1489. doi: 10.1093/nar/11.5.1475
- Du, P., Li, X., Lin, H. J., Peng, W. F., Liu, J. Y., Ma, Y., et al. (2009). Curcumin inhibits amygdaloid kindled seizures in rats. *Chin. Med. J. (Engl.)* 122, 1435–1438.
- Ellman, G. (1959). Tissue sulfhydryl groups. *Arch. Biochem. Biophys.* 82, 70–77. doi: 10.1016/0003-9861(59)90090-6
- Ferger, A. I., Campanelli, L., Reimer, V., Muth, K. N., Merdian, I., Ludolph A. C., et al. (2010). Effects of mitochondrial dysfunction on the immunological properties of microglia. *J. Neuroinflammation* 7:45. doi: 10.1186/1742-2094-7-45
- Gardian, G., Browne, S. E., Choi, D. K., Klivenyi, P., Gregorio, J., Kubilus, J. K., et al. (2005). Neuroprotective effects of phenylbutyrate in the N171-82Q transgenic mouse model of Huntington's disease. *J. Biol. Chem.* 280, 556–563. doi: 10.1074/jbc.M410210200
- Gascon, E., and Gao, F. B. (2012). Cause or effect: misregulation of microRNA pathways in neurodegeneration. *Front. Neurosci.* 6:48. doi: 10.3389/fnins.2012.00048
- Geekyanage, H., Jicha, G. A., Nelson, P. T., and Chan, C. (2012). Blood serum miRNA: non-invasive biomarkers for Alzheimer's disease. *Exp. Neurol.* 235, 491–496. doi: 10.1016/j.expneurol.2011.11.026
- Gustaw-Rothenberg, K., Lerner, A., Bonda, D. J., Lee, H. G., Zhu, X., and Perry, G. (2010). Biomarkers in Alzheimer's disease: past, present and future. *Biomark. Med.* 4, 15–26. doi: 10.2217/bmm.09.86
- Hauss-Wegrzyniak, B., and Wenk, G. L. (2002). Beta-amyloid deposition in the brains of rats chronically infused with thiorphan or lipopolysaccharide: the role of ascorbic acid in the vehicle. *Neurosci. Lett.* 322, 75–78. doi: 10.1016/S0304-3940(02)00087-3
- Hollander, J. A., Im, H. I., Amelio, A. L., Kocerha, J., Bali, P., Lu, Q., et al. (2010). Striatal microRNA controls cocaine intake through CREB signalling. *Nature* 466, 197–202. doi: 10.1038/nature09202
- Hong, J., Bose, M., Ju, J., Ryu, J. H., Chen, X., Sang, S., et al. (2004). Modulation of arachidonic acid metabolism by curcumin and related beta-diketone derivatives: effects on cytosolic phospholipase A (2), cyclooxygenases and 5-lipoxygenase. *Carcinogenesis* 25, 1671–1679. doi: 10.1093/carcin/bgh165
- Izumi, T., Brown, D. B., Naidu, C. V., Bhakat, K. K., MacInnes, M. A., Saito, H., et al. (2005). Two essential but distinct functions of the mammalian a basic endonuclease. *Proc. Natl. Acad. Sci. U.S.A.* 102, 5739–5743. doi: 10.1073/pnas.0500986102
- Jyoti, A., Sethi, P., and Sharma, D. (2009). Curcumin protects against electrophysiological progression of seizures in the iron-induced experimental model of epileptogenesis. *Epilepsy Behav.* 14, 300–308. doi: 10.1016/j.yebeh.2008.11.011
- Kanai, H., Sawa, A., Chen, R. W., Leeds, P., and Chuang, D. M. (2004). Valproic acid inhibits histone deacetylase activity and suppresses excitotoxicity-induced GAPDH nuclear accumulation and apoptotic death in neurons. *Pharmacogenomics J.* 4, 336–344. doi: 10.1038/sj.tpj.6500269
- Kang, G., Kong, P. J., Yuh, Y. J., Lim, S. Y., Yim, S. V., Chun, W., et al. (2004). Curcumin suppresses lipopolysaccharide-induced cyclooxygenase-2 expression by inhibiting activator protein 1 and nuclear factor kappaB bindings in BV2 microglial cells. *J. Pharmacol. Sci.* 94, 325–328. doi: 10.1254/jphs.94.325
- Kim, H. Y., Park, E. J., Joe, E. H., and Jou, I. (2003). Curcumin suppresses Janus kinase-STAT inflammatory signaling through activation of Src homology 2 domain-containing tyrosine phosphatase 2 in brain microglia. *J. Immunol.* 171, 6072–6079. doi: 10.4049/jimmunol.171.11.6072
- Koracevic, D., Koracevic, G., Djordjevic, V., Andrejevic, S., and Cosic, V. (2001). Papers method for the measurement of antioxidant activity in human fluids. *J. Clin. Pathol.* 54, 356–361. doi: 10.1136/jcp.54.5.356
- Kulkarni, S., Dhir, A., and Akula, K. K. (2009). Potentials of curcumin as an antidepressant. *ScientificWorldJournal* 9, 1233–1241. doi: 10.1100/tsw.2009.137
- Lau, P., Bossers, K., Janky, R., Salta, E., Frigerio, C., Barbash, S., et al. (2013). Alteration of the microRNA network during the progression of Alzheimer's disease. *EMBO Mol. Med.* 5, 1613–1634. doi: 10.1002/emmm.201201974
- Levin, J. D., and Demple, B. (1990). Analysis of class II (hydrolytic) and class I (beta-lyase) apurinic/apyrimidinic endonucleases with a synthetic DNA substrate. *Nucleic Acids Res.* 18, 5069–5075. doi: 10.1093/nar/18.17.5069
- Livak, K. J., and Schmittgen, T. D. (2001). Analysis of relative gene expression data using real-time quantitative PCR and the 2(-Delta Delta C(T)) Method. *Methods* 25, 402–408. doi: 10.1006/meth.2001.1262
- Mantha, A. K., Dhiman, M., Taglialatela, G., Perez-Polo, R. J., and Mitra, S. (2012). Proteomic study of amyloid beta (25–35) peptide exposure to neuronal cells: impact on APE1/Ref-1's protein-protein interaction. *J. Neurosci. Res.* 90, 1230–1239. doi: 10.1002/jnr.23018
- Meira, L. B., Devaraj, S., Kisby, G. E., Burns, D. K., Daniel, R. L., Hammer, R. E., et al. (2001). Heterozygosity for the mouse Apex gene results in phenotypes associated with oxidative stress. *Cancer Res.* 61, 5552–5557.
- Ngkelo, A., Mejia, K., Yeadon, M., Adcock, I., and Kirkham, P. A. (2012). LPS induced inflammatory responses in human peripheral blood mononuclear cells is mediated through NOX4 and G12 dependent PI-3kinase signalling. *J. Inflamm.* 9, 1–7. doi: 10.1186/1476-9255-9-1
- Nishikimi, M., Roa, N. A., and Yogi, K. (1972). Measurement of superoxide dismutase. *Biochem. Biophys. Res. Commun.* 46, 849–854. doi: 10.1016/S0006-291X(72)80218-3
- Ohkawa, H., Ohishi, N., and Yagi, K. (1979). Assay of peroxides in animal tissues by thiobarbituric acid reaction. *Anal. Biochem.* 95, 351–358. doi: 10.1016/0003-2697(79)90738-3
- Park, H. S., Jung, H. Y., Park, E. Y., Kim, J., Lee, W. J., and Bae, Y. S. (2004). Cutting edge: direct interaction of TLR4 with NAD(P)H oxidase 4 isozyme is essential for lipopolysaccharide-induced production of reactive oxygen species and activation of NF-kappa B. *J. Immunol.* 173, 3589–3593. doi: 10.4049/jimmunol.173.6.3589
- Peng, G. S., Li, G., Tzeng, N. S., Chen, P. S., Chuang, D. M., Hsu, Y. D., et al. (2005). Valproate pretreatment protects dopaminergic neurons from LPS-induced neurotoxicity in rat primary midbrain cultures: role of microglia. *Mol. Brain Res.* 134, 162–169. doi: 10.1016/j.molbrainres.2004.10.021
- Petri, S., Kiaei, M., Kipiani, K., Chen, J., Calingasan, N. Y., Crow, J. P., et al. (2006). Additive neuroprotective effects of a histone deacetylase inhibitor and a catalytic antioxidant in a transgenic mouse model of amyotrophic lateral sclerosis. *Neurobiol. Dis.* 22, 40–49. doi: 10.1016/j.nbd.2005.09.013
- Phiel, C. J., Zhang, F., Huang, E. Y., Guenther, M. G., Lazar, M. A., and Klein, P. S. (2001). Histone deacetylase is a direct target of valproic acid, a potent anticonvulsant, mood stabilizer, and teratogen. *J. Biol. Chem.* 276, 36734–36741. doi: 10.1074/jbc.M101287200

- Sailaja, B. S., Cohen-Carmon, D., Zimmerman, G., Soreq, H., and Meshorer, E. (2012). Stress-induced epigenetic transcriptional memory of acetylcholinesterase by HDAC4. *Proc. Natl. Acad. Sci. U.S.A.* 109, E3687–E3695. doi: 10.1073/pnas.1209990110
- Santarelli, D. M., Beveridge, N. J., Tooney, P. A., and Cairns, M. J. (2011). Upregulation of dicer and microRNA expression in the dorsolateral prefrontal cortex Brodmann area 46 in schizophrenia. *Biol. Psychiatry* 69, 180–187. doi: 10.1016/j.biopsych.2010.09.030
- Sastre, M., Dewatcher, I., Landreth, G. E., Willson, T. M., Klockgether, T., van Leuven, F., et al. (2003). Nonsteroidal anti-inflammatory drugs and peroxisome proliferator-activated receptor-gamma agonists modulate immunostimulated processing of amyloid precursor protein through regulation of beta-secretase. *J. Neurosci.* 23, 9796–9804.
- Serrano-Pozo, A., Frosch, M. P., Masliah, E., and Hyman, B. T. (2011). Neuropathological alterations in Alzheimer disease. *Cold Spring Harb. Perspect. Biol.* 1, a006189. doi: 10.1101/cshperspect.a006189
- Shaked, I., Meerson, A., Wolf, Y., Avni, R., Greenberg, D., Gilboa-Geffen, A., et al. (2009). MicroRNA-132 potentiates cholinergic anti-inflammatory signaling by targeting acetylcholinesterase. *Immunity* 31, 965–973. doi: 10.1016/j.immuni.2009.09.019
- Shin, H. J., Lee, J. Y., Son, E., Lee, D. H., Kim, H. J., Kang, S. S., et al. (2007). Curcumin attenuates the kainic acid-induced hippocampal cell death in the mice. *Neurosci. Lett.* 416, 49–54. doi: 10.1016/j.neulet.2007.01.060
- Soreq, H., and Wolf, Y. (2011). NeurimmiRs: microRNAs in the neuroimmune interface. *Trends Mol. Med.* 17, 548–555. doi: 10.1016/j.molmed.2011.06.009
- Thum, T. (2012). MicroRNA therapeutics in cardiovascular medicine. *EMBO Mol. Med.* 4, 3–14. doi: 10.1002/emmm.201100191
- Tracey, K. (2007). Physiology and immunology of the cholinergic anti-inflammatory pathway. *J. Clin. Invest.* 117, 289–296. doi: 10.1172/JCI30555
- Tyagi, E., Agrawal, R., Nath, C., and Shukla, R. (2008). Influence of LPS-induced neuroinflammation on acetylcholinesterase activity in rat brain. *J. Neuroimmunol.* 5, 51–56. doi: 10.1016/j.jneuroim.2008.08.015
- Waiskopf, N., Ofek, K., Gilboa-Geffen, A., Bekenstein, U., Bahat, A., Bennett, E. R., et al. (2014). AChE and RACK1 promote the anti-inflammatory properties of fluoxetine. *J. Mol. Neurosci.* 53, 306–315. doi: 10.1007/s12031-013-0174-6
- Wang, R., Li, Y. B., Li, Y. H., Xu, Y., Wu, H. L., and Li, X. J. (2008). Curcumin protects against glutamate excitotoxicity in rat cerebral cortical neurons by increasing brain-derived neurotrophic factor level and activating TrkB. *Brain Res.* 1210, 84–91. doi: 10.1016/j.brainres.2008.01.104
- Wang, W. X., Huang, Q., Hu, Y., Stromberg, A. J., and Nelson, P. T. (2011). Patterns of microRNA expression in normal and early Alzheimer's disease human temporal cortex:white matter versus gray matter. *Acta Neuropathol.* 121, 193–205. doi: 10.1007/s00401-010-0756-0
- Xanthos, D. N., and Sandkühler, J. (2014). Neurogenic neuroinflammation: inflammatory CNS reactions in response to neuronal activity. *Nat. Rev. Neurosci.* 15, 43–53. doi: 10.1038/nrn3617
- Yang, J. L., Tadokoro, T., Keijzers, G., Mattson, M. P., and Bohr, V. A. (2010). Neurons efficiently repair glutamate-induced oxidative DNA damage by a process involving CREB-mediated upregulation of apurinic endonuclease 1. *J. Biol. Chem.* 285, 28191–28199. doi: 10.1074/jbc.M109.082883
- Zaky, A., Mohammad, B., Moftah, M., Kandeel, K. M., and Bassiouny, A. R. (2013). Apurinic/apurimidinic endonuclease 1 is a key modulator of aluminum-induced neuroinflammation. *BMC Neurosci.* 14:26. doi: 10.1186/1471-2202-14-26

Conflict of Interest Statement: The authors declare that the research was conducted in the absence of any commercial or financial relationships that could be construed as a potential conflict of interest.

Received: 15 July 2014; accepted: 01 October 2014; published online: 21 October 2014.

Citation: Zaky A, Mahmoud M, Awad D, El Sabaa BM, Kandeel KM and Bassiouny AR (2014) Valproic acid potentiates curcumin-mediated neuroprotection in lipopolysaccharide induced rats. *Front. Cell. Neurosci.* 8:337. doi: 10.3389/fncel.2014.00337

This article was submitted to the journal *Frontiers in Cellular Neuroscience*. Copyright © 2014 Zaky, Mahmoud, Awad, El Sabaa, Kandeel and Bassiouny. This is an open-access article distributed under the terms of the Creative Commons Attribution License (CC BY). The use, distribution or reproduction in other forums is permitted, provided the original author(s) or licensor are credited and that the original publication in this journal is cited, in accordance with accepted academic practice. No use, distribution or reproduction is permitted which does not comply with these terms.



Acquired equivalence associative learning in GTC epileptic patients: experimental and computational study

Radwa Khalil^{1,2,3*†}, Noha Abo Elfetoh⁴, Marie Z. Moftah⁵ and Eman M. Khedr⁴

¹ Department of Cognitive Biology, Otto-von-Guericke Universität, Magdeburg, Germany, ² Department of Developmental Physiology, Institute of Physiology, Otto-von-Guericke Universität, Magdeburg, Germany, ³ IMN - Institut des Maladies Neurodégénératives, University of Bordeaux, Bordeaux, France, ⁴ Department of Neurology, Faculty of Medicine, Assiut University, Assiut, Egypt, ⁵ Department of Zoology, Faculty of Science, Alexandria University, Alexandria, Egypt

OPEN ACCESS

Edited by:

Antonio Gambardella,
University Magna Graecia Catanzaro,
Italy

Reviewed by:

Marc Landry,
Bordeaux University, France
Marcel Carrère,
Aix Marseille Université, France

*Correspondence:

Radwa Khalil
radwakhil@hotmail.com

† Present Address:

Radwa Khalil,
Institute of Toxicology and
Neuropharmacology, Magdeburg,
Germany

Received: 02 May 2014

Accepted: 02 October 2015

Published: 27 October 2015

Citation:

Khalil R, Abo Elfetoh N, Moftah MZ
and Khedr EM (2015) Acquired
equivalence associative learning in
GTC epileptic patients: experimental
and computational study.
Front. Cell. Neurosci. 9:418.
doi: 10.3389/fncel.2015.00418

Previous cognitive behavioral studies based on Acquired Equivalence Associative learning Task (AEALT) showed a strong relation between hippocampus and basal ganglia in associative learning. However, experimental behavioral studies of patients with Generalized Tonic Clonic (GTC) epilepsy remained sparse. The aim of the present study is to integrate a classical behavioral cognitive analysis with a computational model approach to investigate cognitive associative learning impairments in patients with GTC epilepsy. We measured the accuracy of associative learning response performance in five GTC epileptic patients and five control subjects by using AEALT, all subjects were matched in age and gender. We ran the task using E-Prime, a neuropsychological software program, and SPSS for data statistical analysis. We tested whether GTC epileptic patients would have different learning performance than normal subjects, based on the degree and the location of impairment either in basal ganglia and/or hippocampus. With the number of patients that was available, our behavioral analysis showed no remarkable differences in learning performance of GTC patients as compared to their control subjects, both in the transfer and acquisition phases. In parallel, our simulation results confirmed strong connection and interaction between hippocampus and basal ganglia in our GTC and their control subjects. Nevertheless, the differences in neural firing rate of the connectionist model and weight update of basal ganglia were not significantly different between GTC and control subjects. Therefore, the behavioral analysis and the simulation data provided the same result, thus indicating that the computational model is likely to predict cognitive outcomes.

Keywords: generalized tonic clonic epilepsy, cognitive impairment, acquired equivalence associative learning task, basal ganglia, hippocampus, connectionist model

INTRODUCTION

Acquired Equivalence Associative learning Task (AEALT) is a psychological cognitive task for associative learning assessment (Moustafa et al., 2000; Myers et al., 2003; Herzallah et al., 2010; Moustafa and Gluck, 2011). Importantly, several behavioral and experimental studies based on AEALT provided evidence for a strong interaction between hippocampus and basal

ganglia in associative learning (Honey and Hall, 1991; Hall et al., 1993; Moustafa et al., 2000; Coutureau et al., 2002; Myers et al., 2003; Bodi et al., 2009). Moreover, it has been used to assess cognitive impairment in several brain regions, in particular the temporal lobe including the hippocampus and the frontal lobe including the basal ganglia (Moustafa et al., 2000; Myers et al., 2003; Herzallah et al., 2010; Moustafa and Gluck, 2011). Additionally, various cognitive profiles of different neurological and neuropsychological disorders have been also investigated using AEALT (Moustafa et al., 2000; Myers et al., 2003; Herzallah et al., 2010; Moustafa and Gluck, 2011). However, an AEALT-based behavioral study of Generalized Tonic Clonic (GTC) epilepsy remains sparse. In the present study; we applied AEALT (Moustafa et al., 2000; Myers et al., 2003; Herzallah et al., 2010; Moustafa and Gluck, 2011), to investigate cognitive impairments in GTC epileptic patients using combined experimental behavioral and computational approaches. Our main focus is to show how such computational approach could reproduce, at the functional level, the result obtained from the experimental analysis, thus validating the simulation protocol. Thus, our main purpose does not purely focusing on presenting a separate computational-theoretical study neither a segregated clinical case report independently but rather to validate the simulation approach by comparing our simulated results with the experimental behavioral results as measured in GTC-epileptic patients and controls. In other words, our attention was to test how our computational model (if correctly fed with experimental data from representative patients) could mimic the results of cognitive behavioral test.

Our neurobiological hypothesis is based on the fact that GTC is characterized by generalized seizures which invade most brain regions, in particular the temporal lobe also involving hippocampus and the frontal lobe, including basal ganglia. In parallel, the theoretical hypothesis of AEALT (Moustafa et al., 2000; Myers et al., 2003; Herzallah et al., 2010; Moustafa and Gluck, 2011), which is one of the classical cognitive learning tasks to measure the associative learning performance, relied on the idea that one region is associated with the acquisition while the other one with the transfer phase. This hypothesis suggests that this category of learning might be altered in GTC patients. Therefore, we measured associative learning performances in a group of GTC patients and in their matched healthy controls. For this purpose, AEALT (Moustafa et al., 2000; Myers et al., 2003; Herzallah et al., 2010; Moustafa and Gluck, 2011), was used for describing the connection between basal ganglia and hippocampus and their interaction in acquisition and transfer phases (Moustafa et al., 2000; Myers et al., 2003; Herzallah et al., 2010; Moustafa and Gluck, 2011). It is often difficult to identify the appropriate level of modeling for a particular problem and it is a frequent mistake to assume that a highly detailed model is necessarily superior. In the present study, we did not try to set a pure abstract cognitive model but, rather to feed this model with the output of the subjects' data. Accordingly, we used the actual experimental data collected from our groups, GTC-epileptic patients and controls, after performing AEALT (Moustafa et al., 2000; Myers et al., 2003; Herzallah et al., 2010; Moustafa and Gluck, 2011),

whereas these actual data represented the input values for our simulated model. In other word, the behavioral task, AEALT (Moustafa et al., 2000; Myers et al., 2003; Herzallah et al., 2010; Moustafa and Gluck, 2011), served as a read out for cognitive functions and documented the associative learning. In addition, the modeling approach explored the role of the temporal and frontal lobe, and more particularly of the hippocampus and basal ganglia in the AEALT associative learning task.

METHODOLOGY

Experimental Behavioral study Description of Acquired Equivalence Associative Learning Task (AEALT)

This task (adapted from Moustafa et al., 2000; Myers et al., 2003; Herzallah et al., 2010; Moustafa and Gluck, 2011) comprises of two sorts of stimuli; antecedent and consequent (see **Figure 1**). On one hand, the antecedent stimuli are represented by four drawings of human faces show distinctive ages, youthful and adult human, and genders, females and males; i.e., woman, boy, man, and girl. On the other hand, four drawings of fish with several colors, red, orange, purple, and pink, are related to the consequents. In general, this task incorporates two phases: (i) The acquisition phase, and (ii) The transfer phase. During the acquisition phase, both stimuli are associated with each other; the antecedent and the consequent one. Each subject has to associate a particular human face with a specific colored fish, by clicking on the keyboard arrow either right or left (see **Figure 1A**). In the training stage, two antecedent stimuli A1 and A2, are associated with the same consequent stimulus X1, while two antecedent stimuli B1 and B2 are associated with consequent Y1, i.e., subject has to guess which face is related to which fish. Immediately, the selected fish is circled and the correct feedback is given (**Figure 1B**). Next, A1 is associated with a new consequent X2 while B1 is associated with another novel consequent Y2. (ii) Finally, a transfer phase tests whether patients would show acquired equivalence and associate A2 with X2, and B2 with Y2, even though these particular stimulus pairings had never been trained. This phase corresponds to a new association that could be formed according to the principle of acquired equivalence.

Subjects

Neuropsychological background

We tested five subjects with GTC epilepsy ($n = 5$, Women, over 19 year old) and five controls. All subjects were matched on gender, age and education. Importantly, they were all matched in terms of educational levels and seizure onset. All GTC patients were on treatment since early age, between 12 and 16 years old. Their ages were above 19 and up to 41 years old and their controls are matching them. Additionally, we screened them for the absence of any neurological or psychiatric disorders that could interfere with epileptic symptoms. We allowed our subjects to perform AEALT (Moustafa et al., 2000; Myers et al., 2003; Herzallah et al., 2010; Moustafa and Gluck, 2011), after they passed the average scores of several Intelligence Quotient

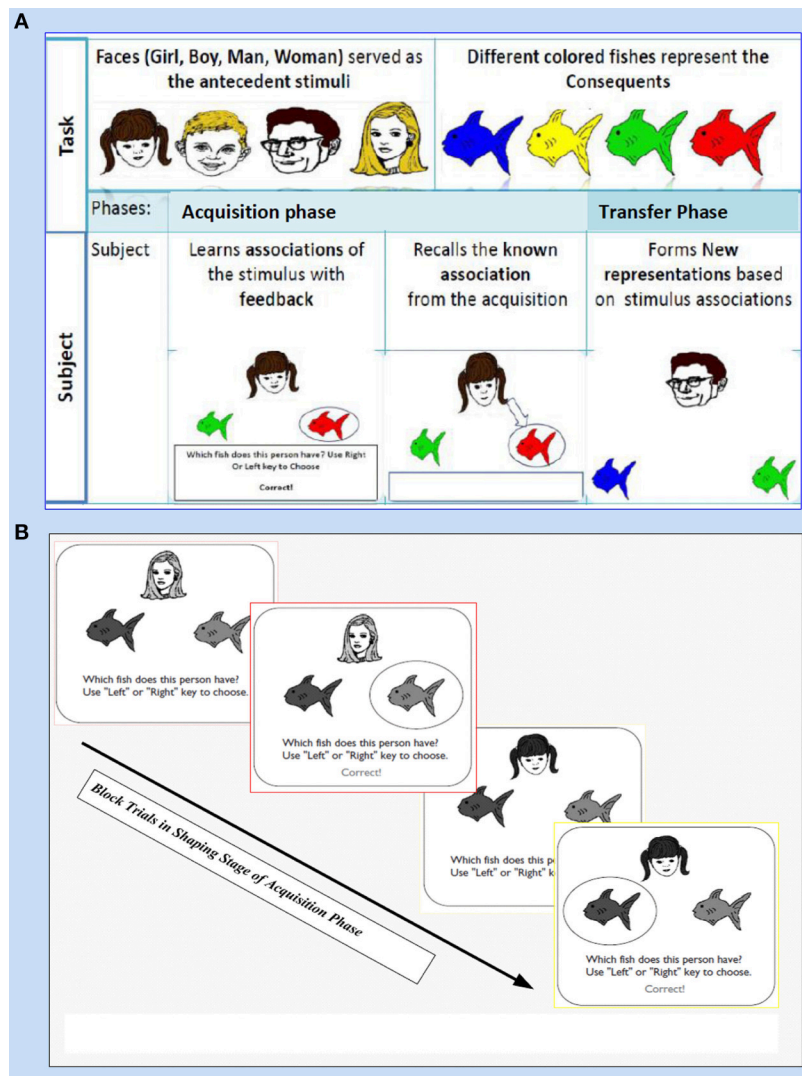


FIGURE 1 | It shows Acquired Equivalence Associative learning Task (AEALT); this task is (adapted from Moustafa et al., 2000; Myers et al., 2003; Herzallah et al., 2010; Moustafa and Gluck, 2011). (A) Represents the phases of AEALT; acquisition and transfer phases (see task description, Methodology Section), whilst (B) is a screen snapshot represents experimental trials in an early stage of acquisition phase which is considered as shaping and training stage. In this latter stage, the stimulus is represented as a human face appearing on the screen and subsequently, the subject responds by choosing one of the colored fish either by clicking left or right, only then, the correct feedback is given (see task description, Methodology Section).

(IQ) subtests, which represented Wechsler Intelligence Scale for Children (WISC). The original WISC (Wechsler, 1949) is an adaptation of several of the subtests used for the Wechsler Bellevue Intelligence Scale (Wechsler, 1939), which also proposed several specific subtests. These subtests were organized into Verbal and Performance scales, and provided scores for Verbal (VIQ), Performance (PIQ), and Full Scale IQ (FSIQ). We only selected the GTC patients who had a relatively high IQ score to ensure that they were able to go through the AEALT (Moustafa et al., 2000; Myers et al., 2003; Herzallah et al., 2010; Moustafa and Gluck, 2011). That was one of the reasons that made us ending up with small sample size, only five patients and five healthy controls. These averages of scores were in the following ranges (IQ = 60–79, VIQ = 62–80, PIQ = 63–77), we

observed that the level of IQ and its subtests decreased with the increasing the age.

Ethical approval for subjects’ participation

We performed this experimental behavioral study in accordance with the declaration of the medical university, after getting the official approval by Assiut Medical hospitals, Assiut, Egypt whereas all participant subjects gave written informed consent.

Statistical analyses

After task performance, we saved patients’ data and imported them directly into the SPSS, statistical software for analysis of the learning performance. Then, we performed a Mann–Whitney test to assess the significance level of learning response

accuracy between GTC epileptic patients and their healthy controls.

Computational Study

Computational Model Structure and Description

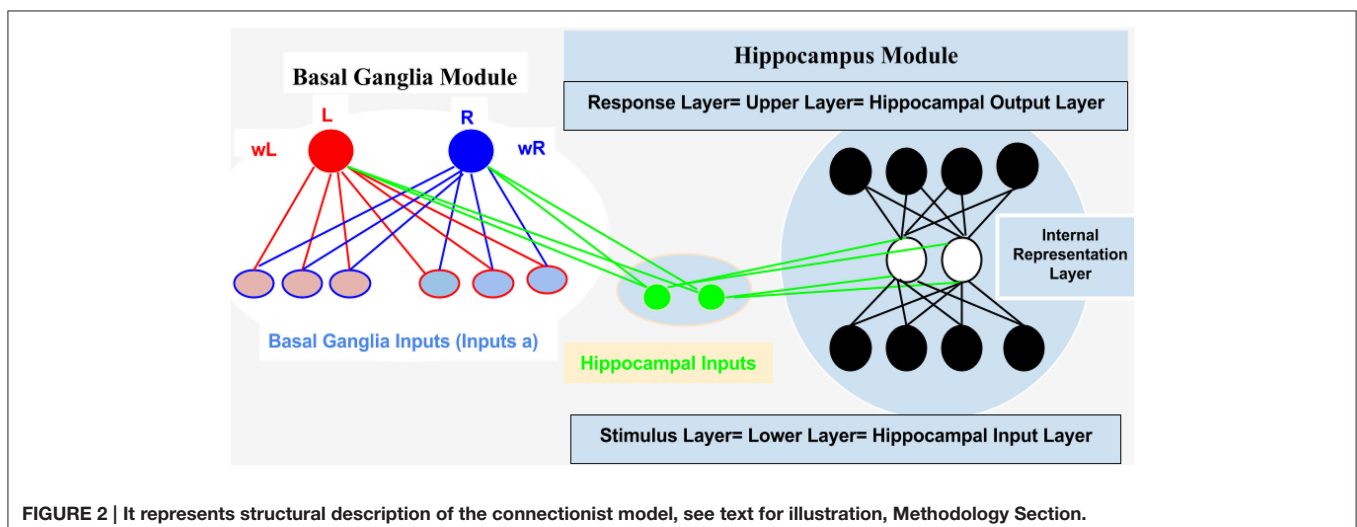
For computational and simulation study, we introduced an abstract connectionist model (for similar study; see Gluck and Rumelhart, 1990; Dayan and Abbott, 2001; Chapter 9 Classical Conditioning and Reinforcement Learning, and Moustafa et al., 2009), which is based on the structural analysis of AEALT (Moustafa et al., 2000; Myers et al., 2003; Herzallah et al., 2010; Moustafa and Gluck, 2011). We used it to explore the behavioral and cognitive significance of associative learning in GTC epileptic patients. We represented the connection between hippocampus and basal ganglia as two modules connected to each other by one-to-one connection (see **Figure 2**).

1. **Hippocampus Module:** It is a two layered network module consists of 10 patches and 20 nodes, each is considered to be a separate representation code of the input (Grossberg, 1988; Hemmen and Schulten, 1991; Hertz et al., 1991; Kearns and Vazirani, 1994; Miller and MacKay, 1994; Moustafa et al., 2009). We used winner-take-all for simulating the lateral inhibitory connections among neurons in each patch, which are connected to the basal ganglia module (Barto, 1995; Berns and Sejnowski, 1996; Schultz et al., 1997; Suri and Schultz, 1998; Moustafa et al., 2009). Additionally, weight update of the hippocampus was based on soft max probability (see Equations 1.0 and 1.1, Mathematical Appendix).
2. **Basal Ganglia Module:** It is based on a trial by trial learning rule known as the Rescorla-Wagner rule (Rescorla and Wagner, 1972). This rule relies on a simple linear prediction of the reward associated with a stimulus. We used a binary input variable (u) as an indication of the presence or absence of the stimulus ($u = 1$ in case the stimulus is present while $u = 0$ in case of its absence), (see Equations 2 and 3, Mathematical Appendix). The basal ganglia input represents the learning rate value; enabling to assess the association between all the

possible input stimuli with the reward (see Equations 3, 4.0, 4.1, 4.2, 5.1, and 5.2, Mathematical Appendix).

Model Fitting to AEALT

We specified the pattern of inputs in term of task stimuli (antecedent and consequent) which were randomly assigned in AEALT (see task description and **Figure 1**). Therefore, we considered a stochastic policy, which means that when subject used to choose a particular colored fish associated with a specific human face, it would be associated with probabilities of choice either left or right (see Equations 1.0, 1.1, and 3, Mathematical Appendix). We adjusted the values of such probabilities during the associative learning process on the basis of the reward provided for the subject according to the slope of soft max probability (β). For large β ; the probability of an action was either raised rapidly to 1 or fallen rapidly to 0, as the difference between the action values increased or decreased, then, the action choice of the subject almost a deterministic choice action. When β is small, the soft max probability is approaching to 1 or 0 more slowly, and the subject's actions are more variable and random. In our model, we adjusted β of soft-max function in each simulation time step of the hippocampus weight update, whereas we represented action selection using soft-max function, which was responsible for hippocampus weight updates. All possible inputs for AEALT (Moustafa et al., 2000; Myers et al., 2003; Herzallah et al., 2010; Moustafa and Gluck, 2011), consists of 16 input from antecedent and consequent stimuli and four inputs from the hippocampus. The 16 inputs represent four different human faces; each one is associated with four different colored fishes, only two are appearing on the screen for each face per trial. For hippocampus inputs; they represent the hippocampus strength having value in the ranges of 0, 1, 2, 3, 4. We considered the direct actor as a simple method for solving the subject' learning response performance in AEALT (Moustafa et al., 2000; Myers et al., 2003; Herzallah et al., 2010; Moustafa and Gluck, 2011), since we focused on static action choice where the reward immediately was followed by the taken action (Montague et al., 1995; Dayan and Abbott, 2001; Chapter 9 Classical Conditioning



and Reinforcement Learning; see Equations 3, 4.0, 4.1, and 4.2, Mathematical Appendix). Accordingly, the choice of actions was based directly on maximizing the expected average reward. On the other hand, we represented this reward value using stimulus index associated with choosing actions, where we represented a list of rewards for each stimulus in rows featuring all possible inputs, and columns featuring left or right choosing action. Accordingly, we computed Q -values for direct actor for this chosen action. Also, we represented the learning rate value as basal ganglia input and the connection between both modules by one-to-one connection. By the end, we computed the mean and variance of the accuracy, correct performance of the subject. Importantly, we fitted the model with the average of experimental block trials that GTC epileptic and control subjects performed during each phase of AEALT (see Figure 3), before running the simulation for each subject.

Mathematical Appendix

(I) Parameterization of choice probabilities either left or right using softmax distribution:

$$p[r] = \frac{\exp(\beta m_r)}{(\exp(\beta m_r) + \exp(\beta m_l))},$$

$$p[l] = \frac{\exp(\beta m_l)}{(\exp(\beta m_l) + \exp(\beta m_r))}. \quad (1.0)$$

Where $P[r]$ and $P[l]$ represent the probability of right and left choices, respectively, both probabilities are similar to a sigmoid function of $\beta (m_r - m_l)$ and $\beta (m_l - m_r)$. β represents the slope of soft max function. The parameters m_r and m_l determine the frequency at which corresponding face is chosen. $P[r] + P[l] = 1$, indicates the fact that the model invariably makes one of the two choices, either left or right. The values of $P[r]$ and $P[l]$ are adjusted during AEALT on the basis of the reward provided. For large β , the probability of an action rises rapidly to one, or falls rapidly to zero, as the difference between the action values increase or decrease. This makes the chosen action of the subject almost a deterministic function of the m variables. If β is small, then, the softmax probability approaches one or zero more slowly, and the action choices of the subject are more variable and random. We adjusted β -value over simulation trials, according to the value of the hippocampus input, which represented the hippocampus strength.

$$P[a] = \frac{\exp(\beta m_a)}{\sum_{\hat{a}=1}^2 \exp(\beta m_{\hat{a}})}. \quad (1.1)$$

Where $P[a]$ is the probability vector m of choosing action a , which controls the decision process. $\hat{a} = 1, 2$ represents the possibility of choices between two actions; right or left.

(II) The Rescola-Wagner learning rule(a version of delta rule):

$$w \rightarrow w + \varepsilon \delta u \text{ with } \delta = r - v. \quad (2)$$

Where w represents the weight update, δ represents the prediction error. U is a binary variable which indicates the

presence or absence of the stimulus, if $u = 1$, then the stimulus is present and $u = 0$ in case of its absence. v is the expected reward. ε is a coefficient which indicates balancing state of the weight update; if it is sufficiently small, the rule changes w systematically until the average value of δ reaches to zero, at this point w fluctuates about the equilibrium value in approximation.

(III) Direct Actor Equations:

$$\langle r \rangle = P[r] \langle r_r \rangle + P[l] \langle r_l \rangle. \quad (3)$$

Where $\langle r \rangle$ is the expected average of the reward, $P[r]$ is the probability of choosing the right choice. $\langle r_r \rangle$ is the average of reward based on choosing the right choice. $P[l]$ is the probability of choosing the left choice. $\langle r_l \rangle$ is the average of reward based on choosing the left choice. In the Direct Actor method, the choice of actions is based directly on maximizing the expected average of the reward.

$$m_{\hat{a}} \rightarrow m_{\hat{a}} + \varepsilon(\delta_{a\hat{a}} - P[\hat{a}]) (r_a - \hat{r}). \quad (4.0)$$

Where $m_{\hat{a}}$ is an action, which is taken for all value of \hat{a} .

$$m_{\hat{a}}(u) \rightarrow m_{\hat{a}}(u) + \varepsilon(\delta_{a\hat{a}} - P[\hat{a}; u]) \delta. \quad (4.1)$$

Where u is a binary stimuli input.

$$m = M \cdot u(u) \text{ or } m_a = \sum_b M_{ar} u_r(u). \quad (4.2)$$

In Equations (4.1) and (4.2); the update of action probability depends on value of δ , when $\delta > 0$ is taken, which increases the probability of the action and when $\delta < 0$ is taken, this value decreases the probability of the action. This means increasing the chance that the subject makes the correct accurate response. Then, the actor learning rule is modified to make use of the information provided by the state vector through generalizing the action from value vector m to action matrix M . M has as many columns as there are components of u (binary stimuli input) and as many rows as there are actions (reward). Given a binary stimuli input u , action a is chosen at location u with the soft max probability of Equations (1.0) and (1.1), using component a of the action value vector.

These previous equations show how to change the elements of the action matrix (M), when action a is chosen at location u with state vector $u(u)$, leading to location u .

(IV) Policy Actor learning rule equations:

$$m_r \rightarrow m_r + \varepsilon(\delta_{ar} - P[r]) (r_a - \hat{r}). \quad (5.1)$$

$$m_l \rightarrow m_l + \varepsilon(\delta_{al} - P[l]) (r_a - \hat{r}). \quad (5.2)$$

Where r_a is the selected action; either right or left. δ_{ar} and δ_{al} are the Kronecker delta, $\delta_{ar} = 1$ if $a = r$ and $\delta_{ar} = 0$

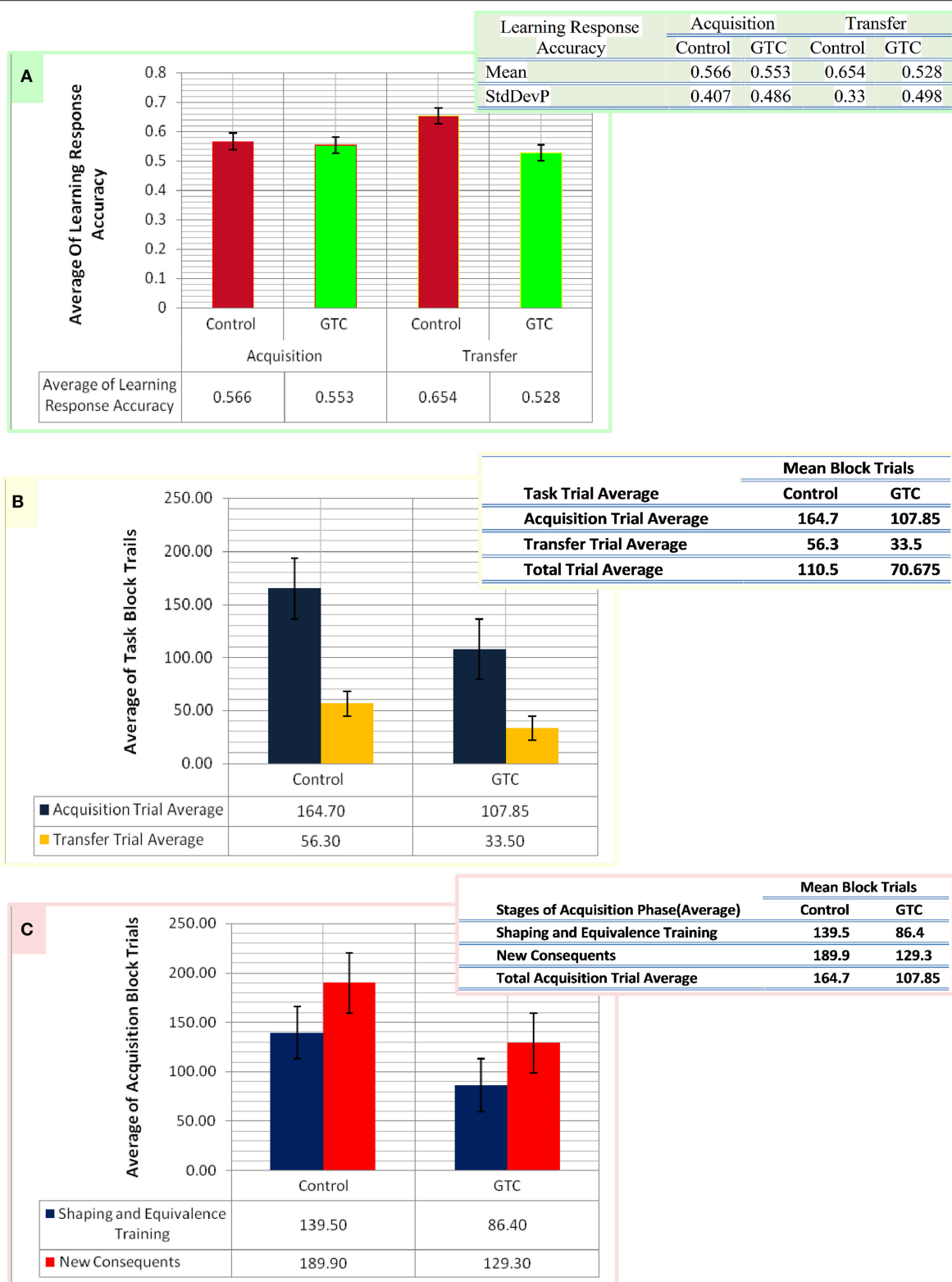


FIGURE 3 | This figure represents the data of our subjects which considered as an input for our computational model. Panel (A) shows the average of the accurate response in associative learning in GTC epileptic patients and their healthy controls during both phases of AEALT; acquisition and transfer phases of whilst the associated table to (A) represents the mean and the standard deviation of the average accuracy responses. (B) Represents the average of block trials which were (Continued)

FIGURE 3 | Continued

performed by the GTC epileptic patients and their healthy controls during acquisition and transfer phase, whereas these values, which are represented in the associated table to **(B)**, were required as input for our simulated model. **(C)** Indicates the average of block trials which were performed by the GTC epileptic patients and their healthy controls during the stages of shaping and equivalence training, and in the new consequent one, which resemble the acquisition phase, whereas these values, which are shown in the adjacent table to **(C)**, were required as inputs for our simulated model.

if $a = l$ and $\delta_{al} = 1$ if $a = l$ and $\delta_{al} = 0$ if $a \neq l$. \bar{r} is the mean of the reward under the specified policy. These equations perform the stochastic gradient ascent on the average reward, whatever the value of \bar{r} (the mean of the reward). Different values of \bar{r} lead to different variation of the stochastic gradient terms, and thus different speeds of learning.

Model Implementation

The algorithms had been adjusted from Dayan and Abbott (2001), Chapter 9 Classical Conditioning and Reinforcement Learning whilst the code was implemented using Python (Python Software Foundation. Python Language Reference, version 2.7; van Rossum, 1995), BRIAN, neurosimulator based Python Library (Stimberg et al., 2014) and Mat Lab (MATLAB 8.0 and Statistics Toolbox 8.1, The Math Works, Inc., Natick, Massachusetts, United States) softwares.

RESULTS**Experimental Behavior**

Our experimental behavioral results showed no considerable differences in the average of accuracy in learning response performance of GTC epileptic patients and controls during acquisition and transfer phases of AEALT. In the acquisition phase; the average accurate performance of associative learning in GTC was not significantly different ($p = 0.68$, two-tailed test) from controls. Similarly, in the transfer phase the difference was not strong either ($p = 0.97$, two-tailed test) (see **Figure 3**). These results indicated that AEALT did not reveal cognitive impairment in GTC epileptic patients, neither in hippocampus (associated with the transfer (Tamminga et al., 1992; Buchanan et al., 1993; Bunsey and Eichenbaum, 1995; Henke et al., 1997; Heckers et al., 1999; Myers et al., 2003; Polgár et al., 2010; Moustafa and Gluck, 2011), nor in basal ganglia (associated with the acquisition; Tamminga et al., 1992; Buchanan et al., 1993; Moustafa et al., 2000; Myers et al., 2003; Polgár et al., 2010; Moustafa and Gluck, 2011).

Computational Modeling

Our abstract model-based analysis of AEALT (Moustafa et al., 2000; Myers et al., 2003; Herzallah et al., 2010; Moustafa and Gluck, 2011), showed a strong connection between hippocampus and basal ganglia in GTC epileptic patients. This connection was represented in our connectionist model by two modules (hippocampus and basal ganglia), which connected to each other by one-to-one connection. We introduced different values of hippocampus input representing differential states hippocampus strength. Then, we associated each of these values with different values of the basal ganglia input representing the learning rate

values. In our simulation, we considered two different conditions based on the strength of hippocampus (hippocampus input) while fixing the values of basal ganglia input (the learning rate values) to have range of values in each condition between 0, 0.1, 0.2, 0.3, 0.4, 0.5, 0.6, 0.7, 0.8, 0.9, and 1. In each condition, we measured the changes in the neural firing rate and observed the evaluation of the basal ganglia weight update in response to the changes in the inputs of hippocampus and basal ganglia. For the first condition, the hippocampus strength was equal to zero while the second one represented it to be above zero, with values ranging between 1, 2, 3, and 4. In the first condition, we observed that the percentage of the neural firing rate in GTC epileptic patients and controls was below 55%. Additionally, the weight update evaluation of the basal ganglia was in the same range as the neural firing rate (below 55%). Thus, the learning rate of basal ganglia had an impact on scaling the average of neural firing rate and also a robust role in guiding the choosing action either left or right when hippocampus strength was zero (see **Figure 4** and **Table 1**).

In the second condition, we observed that the percentage of the neural firing rate in our subjects was increasing to be above 50%. Also, the weight update evaluation of the basal ganglia was in the same range as the neural firing rate in this condition (above 50%), (see **Figure 4** and **Table 1**), which means that the neural firing rate was increasing with increasing hippocampus strength (hippocampus input). GTC epileptic patients showed less neural firing rate as compared to controls in each state of hippocampus strength (i.e.; different hippocampus input values). Additionally, changes in such neural firing rate were sensitive to the changes in the basal ganglia inputs. All together indicated that the learning rate values of the basal ganglia were critical for modulating the neural firing rate of the connectionist model by stabilizing it as long as its' increase remained comprised between 68 and 81%. In general, there was a reasonable correlation between the percentage of the neural firing rate (see **Figure 4** and **Table 1**), and evaluation of weight update in GTC epileptic patients and controls in each condition. For example, when hippocampus strength was above zero, the percentage of weight update was above 50% for both GTC epileptic patients and controls. Moreover, the weight update of the basal ganglia was increasing with increasing in the hippocampus strength, i.e.; the weight update of the basal ganglia was very sensitive to hippocampus strength. For example, the evaluation of weight update of the basal ganglia was increasing rapidly when the hippocampus strength was large (values 3 and 4) while this increase was slow when the hippocampus strength was less (values 1 and 2). This observation suggested a strong influence of the hippocampus strength on weight update evaluation of the basal ganglia and hence strong connection between them.

TABLE 1 | It represents the values of the neural firing rate in GTC epileptic patients and their controls in our connectionist simulated model which are shown in Figure 4.

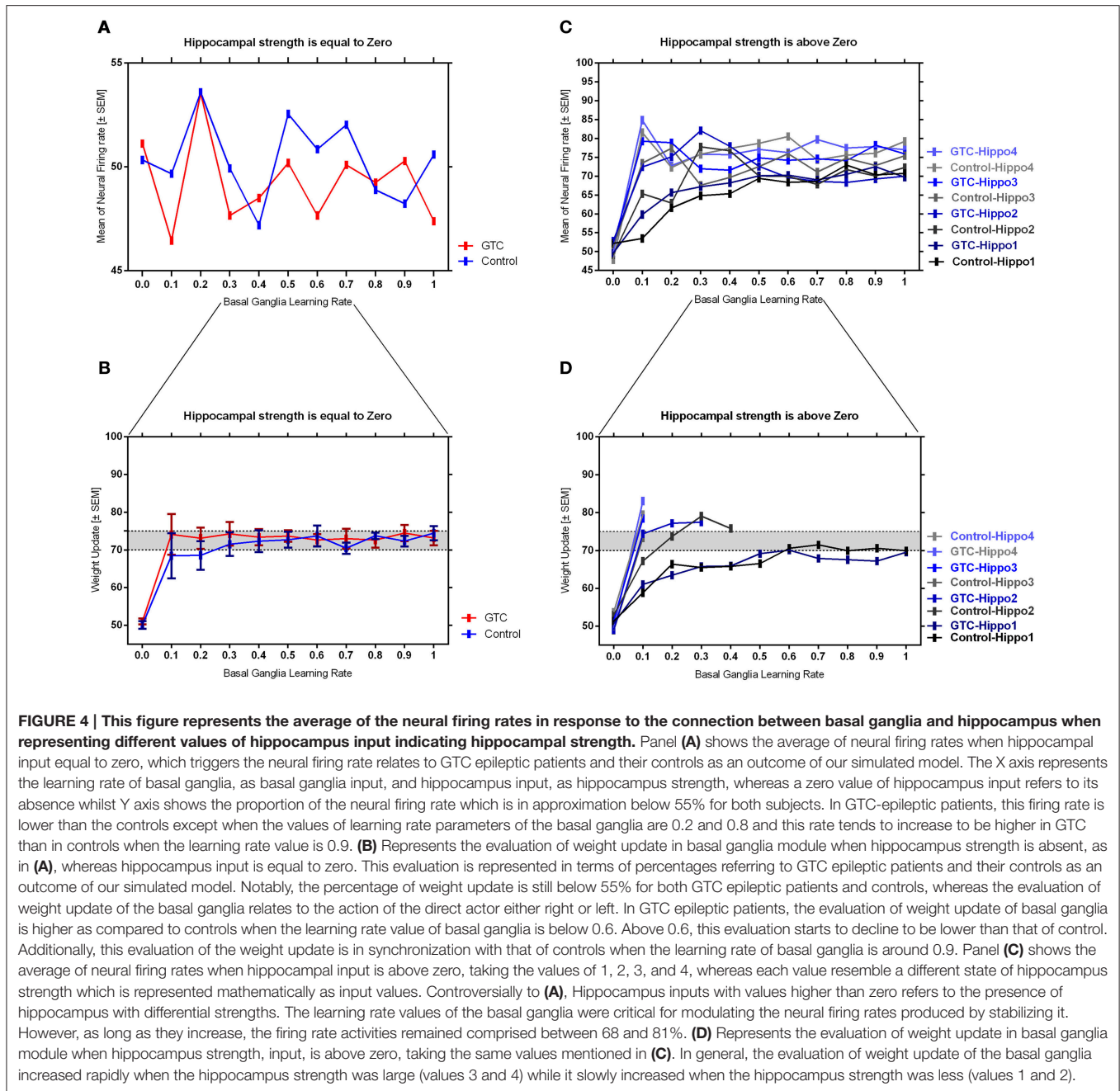
Learning rate values			0	0.1	0.2	0.3	0.4	0.5	0.6	0.7	0.8	0.9	1.0
(A) Mean firing rate values													
Control			50.33	49.67	53.59	49.93	47.19	52.55	50.85	52.03	48.89	48.23	50.59
GTC			51.12	46.45	53.55	47.66	48.50	50.19	47.66	50.09	49.25	50.28	47.38
(B) Mean weight update values													
Control			50.85	48.13	48.37	50.85	50.2	49.15	53.46	46.41	49.54	48.89	52.94
GTC			50.37	51.21	50.28	50.37	50.8	52.24	49.99	48.04	47.85	49.25	52.15
(C) Mean firing rate values													
Control	Hippocampus strength	1	52.17	53.46	61.57	64.84	65.36	69.41	68.37	68.6	72.94	70.33	70.72
GTC		1	49.63	59.81	65.61	67.2	68.22	70.09	70.28	69	70.47	72.52	69.72
Control		2	49.15	65.36	62.88	77.78	76.73	70.06	69.93	67.8	71.76	70.06	72.29
GTC		2	52.8	72.43	75.14	82.06	77.94	72.62	69.63	68.6	68.32	69.25	69.99
Control		3	51.24	73.46	77.39	67.58	69.67	72.55	75.95	71.1	74.77	72.81	75.42
GTC		3	51.87	79.25	78.88	71.96	71.59	74.86	74.21	74.6	74.11	78.22	75.89
Control		4	47.84	81.57	72.29	75.82	77.38	78.69	80.52	74.3	75.55	76.08	79.22
GTC		4	49.81	84.86	72.8	75.79	75.7	77.1	76.26	79.7	77.48	77.85	77.01
(D) Mean weight update values													
Control	Hippocampus strength	1	51.37	58.82	66.4	65.49	65.8	66.54	70.59	71.5	69.93	70.59	69.93
GTC		1	50.75	61.03	63.46	65.79	65.9	69.16	70.09	67.9	67.57	67.2	69.53
Control		2	52.94	67.19	73.72	79.08	75.8						
GTC		2	49.06	74.39	77.2	77.48							
Control		3	48.89	73.33									
GTC		3	51.59	78.41									
Control		4	53.72	79.48									
GTC		4	49.53	83.08									

Panel (A) is linked to **Figure 4A** whilst panels (B–D) are associated to **Figures 4B–D**, respectively.

DISCUSSION

To our knowledge, this present study is the first to assess AEALT (Moustafa et al., 2000; Myers et al., 2003; Herzallah et al., 2010; Moustafa and Gluck, 2011), in patients with the GTC epilepsy. We measured the accuracy of associative learning in GTC epileptic patients through AEALT. We relied on using combined experimental behavioral and computational study to link our experimental findings with associative acquired equivalence principles; neurobiological, psychologically and theoretically. One clear limitation of our study is the low number of GTC patients and their healthy subjects that was studied. Therefore, our results will need to be confirmed by further complementary studies at larger scale in the near future. However, our approach allowed to design a computational model that can be fed from actual subjects' data. Therefore, this model will be useful to test the role of the connectivity between the frontal and temporal lobes in cognitive functions, and its possible alterations in epilepsy. Importantly, most of the studies dealing with epilepsy used a low number of subjects due to the difficulty to recruit large populations, in particular in a case of cognitive and behavioral studies. Even within the largest postoperative cognitive study in adult, Helmstaedter and Witt (2008) included only 39 patients and the largest pediatric study of Gleissner included only 15 patients (Gleissner et al., 2008). Even the study with the most

comprehensive neuropsychological testing and the largest sample ($n = 11$) (Picard and Craig, 2009) had only 5 patients in the sample having IEDs on EEG, and the IEDs. In addition, these studies are composed of highly heterogeneous groups of patients, including wide age ranges, divergent seizure characteristics and, in some cases, even different surgical procedures (e.g., cortical reactions, lesions and/or multiple transactions). In order to be more consistent, we paid a special attention to investigate homogenous group made of healthy subjects and matched GTC patients, that is of patients suffering from a specific type of epilepsy. Due to the limited size of our sample groups, it was difficult to draw a robust statistical significance from our results, whereas; we focused on testing the validation of this connectionist model through using our patients' data as an input for the model. Our experimental behavioral results showed that the accuracy of learning performance was not different in GTC patients as compared to controls (see **Figure 3**). This result indicated no impairments neither in hippocampus (associated to transfer phase; Tamminga et al., 1992; Buchanan et al., 1993; Bunsey and Eichenbaum, 1995; Henke et al., 1997; Heckers et al., 1999; Myers et al., 2003; Polgár et al., 2010; Moustafa and Gluck, 2011), nor in basal ganglia (associated with acquisition phase; Tamminga et al., 1992; Buchanan et al., 1993; Moustafa et al., 2000; Myers et al., 2003; Polgár et al., 2010; Moustafa and Gluck, 2011). On the other hand, our



computational simulation findings confirmed our experimental behavioral results since they showed strong connection between hippocampus and basal ganglia modules. We segregated our simulation into two conditions based on the strength of the hippocampus (hippocampus input); either equal or above zero. In each condition, we fixed the values of the basal ganglia inputs, which represented the learning rate values, to be in the ranges of 0, 0.1, 0.2, 0.3, 0.4, 0.5, 0.6, 0.7, 0.8, 0.9, and 1. Then, we measured the average of the neural firing rate and weight update evaluation of the basal ganglia in response to the changes of the input of the hippocampus referring to hippocampus strength. In the

first condition, when hippocampus strength was equal to zero, the average of the neural firing rate in both GTC and controls was below 55%. In addition, the weight update evaluation of the basal ganglia was similar to this range (below 55%); this observation indicated the robust role of the basal ganglia input in guiding the direct actor either left or right. All together approved the considerable impact of hippocampus strength, hippocampus input, and the learning rate of basal ganglia, basal ganglia input, on modulating of the neural firing rate of our connectionist model (see Figures 4A,B and Table 1). On the other hand, in the second condition, when hippocampus strength was above

zero, taking ranges of 1, 2, 3, and 4, the average of the neural firing rate in GTC and controls was above 50% and the weight update evaluation of basal ganglia was in line with this range of the neural firing rate (above 50%), (see **Figures 4C,D** and **Table 1**). In this case, changes in the basal ganglia inputs were sensitive to the changes in the hippocampus input (differential state of hippocampus strength). However, this sensitivity was observed only when hippocampus strength had a value of 1, with increasing hippocampus inputs; the influence of basal ganglia inputs was decreasing. For example, the average of the neural firing rate reached to the highest peak when hippocampus input was in the range of 4 and 3 although the value of basal ganglia input was very small or nearly absent (around 0–0.1). Then, there was no need for increasing the value of basal ganglia input above 0.1 to enhance the neural firing rate of our model. This observation indicated that learning rate values of basal ganglia had a role in modulating and stabilizing the mean neural firing rate of the model only when hippocampus strength was around 1. Additionally, weight update of the basal ganglia increased rapidly and immediately when hippocampus strength was larger (values 3 and 4) while it increased slowly and regularly when hippocampus strength was smaller (values 1 and 2). Generally, GTC epileptic patients showed less neural firing rate as compared to controls in each state of hippocampus strength. In conclusion, the two conditions that we explored in our study explained how the interactive connection between basal ganglia and hippocampus module influenced the neural activity after changing the learning rate of both, the basal ganglia, representing in basal ganglia input, and the hippocampus strength, which resembles hippocampus input. We did not include Temporal Difference (TD) learning Algorithm (Dayan and Abbott, 2001; Chapter 9 Classical Conditioning and Reinforcement Learning) to measure the temporal differences in GTC epileptic patients within both phases of acquired equivalence task; acquisition and transfer. Alternatively, We relied on using direct actor method and Rescorla Wagner rule instead of TD since we preferred to use this simple method in the beginning of our study with GTC epileptic patients, aiming to extend this study with GTC epileptic patients further in the future studies. While cognitive impairments, and especially memory disruption (Henke et al., 1997), are prominent comorbidity in patients with epilepsy, their path physiology remains unknown (Bell et al., 2011). Recent studies concluded that cognitive impairment in epilepsy results from a network disorder in which the micro-structures as well as the functionality can be disturbed (Braakman et al., 2012). In this present study, however, we did not find any considerable

difference in associative learning between GTC patients and control subjects. This lack of impairment may be due to several factors. First, the number of our subjects remained small and the study should be extended to a larger number of subjects, which we are planning to do in the future studies. No doubt, including more GTC epileptic patients with different ages and/or sex will enable us to detect possible correlation between ages and/or sex in shaping the acquired learning performance in GTC epileptic patients. Second, the age of the patients seems to be a critical factor. Indeed, a very recent study found no difference in neuropsychological performances in children with temporal lobe epilepsy (Mankinen et al., 2014) whilst a study with animal models has shown that early-life seizures are key events that contribute to deficits in learning (Lugo et al., 2014). In this current study, our patients did not experience a long history of seizures, which can explain the absence of associative learning impairment. Despite lack of differences with AEALT (Moustafa et al., 2000; Myers et al., 2003; Herzallah et al., 2010; Myers et al., 2003), the GTC patients may show fine structural and/or functional alterations of the brain networks, which could be involved, besides, the relatively small sample size examined here may limit the representativeness of patients with GTC. Therefore, additional numbers of patients with GTC will be added in further future studies as a continuation of the present work. Moreover, to address this question further, we will need to complement these behavioral and model studies with imaging studies aiming to describe the functional connectivity between basal ganglia and hippocampus in the future. Regarding the methodological aspect of our study, independently of the functional result, our main aim was to validate a modeling approach. Importantly, our simulation protocol proved a reasonable efficiency to reproduce the results obtained with a cognitive behavioral task. In summary, the main result of the present work was to provide a simulation method that permits to analyses functionally the network (i.e., basal ganglia and hippocampus) underlying cognitive processes within the context of a neurological pathology.

ACKNOWLEDGMENTS

We are extremely grateful to N€uroMed project (EU FP7) which funded a collaboration between the Faculty of Science, Alexandria University and the Faculty of Medicine, Assiut University. We particularly thank Professor Peter Dayan for providing extensive discussion and advice on developing the model during ACCN course; IBRO summer school for Advanced Courses in Computational Neuroscience (ACCN, 2011).

REFERENCES

- Barto, A. G. (1995). "Adaptive critics and the basal ganglia," in *Models of Information Processing in the Basal Ganglia* (pp. xii), eds J. C. Houk, J. L. Davis, and D. G. Beiser (Cambridge, MA: MIT Press), 382.
- Bell, B., Lin, J. J., Seidenberg, M., and Hermann, B. (2011). The neurobiology of cognitive disorders in temporal lobe epilepsy. *Nat. Rev. Neurol.* 7, 154–164. doi: 10.1038/nrneurol.2011.3
- Berns, G. S., and Sejnowski, T. J. (1996). "How the basal ganglia make decisions," in *The Neurobiology of Decision Making*, eds A. Damasio, H. Damasio, and Y. Christen (Berlin: Springer-Verlag), 101–113.
- Bodi, N., Csibri, E., Myers, C. E., Gluck, M. A., and Keri, S. (2009). Associative learning, acquired equivalence, and flexible generalization of knowledge in mild Alzheimer disease. *Cogn. Behav. Neurol.* 22, 89–94. doi: 10.1097/WNN.0b013e318192ccf0
- Braakman, H. M., van der Kruijs, S. J., Vaessen, M. J., Jansen, J. F., Debeij-van Hall, M. H., Vles, J. S., et al. (2012). Microstructural and functional MRI

- studies of cognitive impairment in epilepsy. *Epilepsia* 53, 1690–1699. doi: 10.1111/j.1528-1167.2012.03624.x
- Buchanan, R. W., Breier, A., Kirkpatrick, B., Elkashef, A., Munson, R. C., Gellad, F., et al. (1993). Structural abnormalities in deficit and nondeficit schizophrenia. *Am. J. Psychiatry* 150, 59–65. doi: 10.1176/ajp.150.1.59
- Bunsey, M., and Eichenbaum, H. (1995). Selective damage to the hippocampal region blocks long-term retention of a natural and nonspatial stimulus-stimulus association. *Hippocampus* 5, 546–556. doi: 10.1002/hipo.450050606
- Coutureau, E., Killcross, A. S., and Good, M. (2002). Acquired equivalence and distinctiveness of cues: II. Neural manipulations and their implications. *J. Exp. Psychol. Anim. Behav. Process.* 28, 388–396. doi: 10.1037/0097-7403.28.4.388
- Dayan, P., and Abbott, L. F. (2001). *Theoretical Neuroscience: Computational and Mathematical Modeling of Neural Systems*. Cambridge, MA: MIT Press.
- Gleissner, U., Kuczaty, S., Clusmann, H., Elger, C. E., and Helmstaedter, C. (2008). Neuropsychological results in pediatric patients with epilepsy surgery in the parietal cortex. *Epilepsia* 49, 700–704. doi: 10.1111/j.1528-1167.2007.01497.x
- Gluck, M. A., and Rumelhart, D. E. (eds.). (1990). *Neuroscience and Connectionist Theory*. Hillsboro, NY: Lawrence Erlbaum.
- Grossberg, S. (eds.). (1988). *Neural Networks and Natural Intelligence*. Cambridge, MA: MIT Press.
- Hall, G., Ray, E., and Bonardi, C. (1993). Acquired equivalence between cues trained with a common antecedent. *J. Exp. Psychol. Anim. Behav. Process.* 19, 391–399. doi: 10.1037/0097-7403.19.4.391
- Heckers, S., Goff, D., Schacter, D. L., Savage, C. R., Fischman, A. J., Alpert, N. M., et al. (1999). Functional imaging of memory retrieval in deficit vs. nondeficit schizophrenia. *Arch. Gen. Psychiatry* 56, 1117–1123. doi: 10.1001/archpsyc.56.12.1117
- Helmstaedter, C., and Witt, J. A. (2008). The effects of levetiracetam on cognition: a non-interventional surveillance study. *Epilepsy Behav.* 13, 642–649. doi: 10.1016/j.yebeh.2008.07.012
- Hemmen, E., and Schulken, K. (eds.). (1991). *Models of Neural Networks, I. I. I.* New York, NY: Springer-Verlag.
- Henke, K., Buck, A., Weber, B., and Wieser, H. G. (1997). Human hippocampus establishes associations in memory. *Hippocampus* 7, 249–256. doi: 10.1002/(SICI)1098-1063(1997)7:3<249::AID-HIPO1>3.0.CO;2-G
- Hertz, J., Krogh, A., and Palmer, R. G. (1991). *Introduction to the Theory of Neural Computation*. Redwood City, CA: Addison-Wesley.
- Herzallah, M. M., Moustafa, A. A., Misk, A. J., Al-Dweib, L. H., Abdelrazeq, S. A., Myers, C. E., et al. (2010). Depression impairs learning whereas anticholinergics impair transfer generalization in Parkinson patients tested on dopaminergic medications. *Cogn. Behav. Neurol.* 23, 98–105. doi: 10.1097/WNN.0b013e3181df3048
- Honey, R. C., and Hall, G. (1991). Acquired equivalence and distinctiveness of cues using a sensory-preconditioning procedure. *Q. J. Exp. Psychol.* 43B, 121–135.
- Kearns, M. J., and Vazirani, U. V. (1994). *An Introduction to Computational Learning Theory*. Cambridge, MA: MIT Press.
- Lugo, J. N., Swann, J. W., and Anderson, A. E. (2014). Early-life seizures result in deficits in social behavior and learning. *Exp. Neurol.* 256, 74–80. doi: 10.1016/j.expneurol.2014.03.014
- Mankinen, K., Harila, M. J., Rytty, S. I., Pokka, T. M., and Rantala, H. M. (2014). Neuropsychological performance in children with temporal lobe epilepsy having normal MRI findings. *Eur. J. Paediatr. Neurol.* 18, 60–65. doi: 10.1016/j.ejpn.2013.08.005
- Miller, K. D., and MacKay, D. J. C. (1994). The role of constraints in hebbian learning. *Neural Comput.* 6, 100–126. doi: 10.1162/neco.1994.6.1.100
- Montague, P. R., Dayan, P., Person, C., and Sejnowski, T. J. (1995). Bee foraging in uncertain environments using predictive hebbian learning. *Nature* 377, 725–728. doi: 10.1038/377725a0
- Moustafa, A. A., Gluck, M. A., and Myers, C. E. (2009). A neurocomputational model of classical conditioning phenomena: a putative role of the parahippocampal region. *Brain Res.* 1276, 180–195. doi: 10.1016/j.brainres.2009.04.020
- Moustafa, A. A., and Gluck, M. A. (2011). Computational cognitive models of prefrontal-striatal-hippocampal interactions in Parkinson's disease and schizophrenia. *Neural Netw.* 24, 575–591. doi: 10.1016/j.neunet.2011.02.006
- Moustafa, A. A., Keri, S., Herzallah, M. M., Myers, C. E., and Gluck, M. A. (2000). Acquisition and transfer on an acquired equivalence task in patients with Parkinson's disease. *Cogn. Neurosci. Soc. Annu. Meet. Abstr.*
- Myers, C., Shohamy, D., Gluck, M., Grossman, S., Kluger, A., Ferris, S., et al. (2003). Dissociating hippocampal versus basal ganglia contributions to learning and transfer. *J. Cogn. Neurosci.* 15, 185–193. doi: 10.1162/089892903321208123
- Picard, F., and Craig, A. D. (2009). Ecstatic epileptic seizures: a potential window on the neural basis for human self-awareness. *Epilepsy Behav.* 16, 539–546. doi: 10.1016/j.yebeh.2009.09.013
- Polgár, P., Réthelyi, J. M., Bálint, S., Komlósi, S., Czobor, P., and Bitter, I. (2010). Executive function in deficit schizophrenia: what do the dimensions of the Wisconsin card sorting test tell us? *Schizophr. Res.* 122, 85–93. doi: 10.1016/j.schres.2010.06.007
- Rescorla, R. A., and Wagner, A. R. (1972). “A theory of Pavlovian conditioning: the effectiveness of reinforcement and non-reinforcement,” in *Classical Conditioning II: Current Research and Theory*, eds A. H. Black and W. F. Prokasy (New York, NY: Aleton-Century-Crofts), 64–69.
- Schultz, W., Dayan, P., and Montague, P. R. (1997). A neural substrate of prediction and reward. *Science* 275, 1593–1599. doi: 10.1126/science.275.5306.1593
- Stimberg, M., Goodman, D. F. M., Benichoux, V., and Brette, R. (2014). Equation-oriented specification of neural models for simulations. *Front. Neuroinform.* 8:6. doi: 10.3389/fninf.2014.00006
- Suri, R. E., and Schultz, W. (1998). Learning of sequential movements by neural network model with dopamine-like reinforcement signal. *Exp. Brain Res.* 121, 350–354. doi: 10.1007/s002210050467
- Tammimga, C. A., Thaker, G. K., Buchanan, R., Kirkpatrick, B., Alphs, L. D., Chase, T. N., et al. (1992). Limbic system abnormalities identified in schizophrenia using positron emission tomography with fluorodeoxyglucose and neocortical alterations with deficit syndrome. *Arch. Gen. Psychiatry* 49, 522–530. doi: 10.1001/archpsyc.1992.01820070016003
- van Rossum, G. (1995). *Python Tutorial*. Technical Report, CS-R9526, Centrum voor Wiskunde en Informatica (CWI), Amsterdam.
- Wechsler, D. (1939). *Wechsler-Bellevue Intelligence Scale*. New York, NY: The Psychological Corporation.
- Wechsler, D. (1949). *Wechsler Intelligence Scale for Children*. New York, NY: The Psychological Corporation.

Conflict of Interest Statement: The Review Editor Marc Landry declares that, despite being affiliated to the same institution as author Radwa Khalil, the review process was handled objectively and no conflict of interest exists. The authors declare that the research was conducted in the absence of any commercial or financial relationships that could be construed as a potential conflict of interest.

Copyright © 2015 Khalil, Abo Elfetoh, Mofiah and Khedr. This is an open-access article distributed under the terms of the Creative Commons Attribution License (CC BY). The use, distribution or reproduction in other forums is permitted, provided the original author(s) or licensor are credited and that the original publication in this journal is cited, in accordance with accepted academic practice. No use, distribution or reproduction is permitted which does not comply with these terms.



Developmental dynamics of neurotensin binding sites in the human hypothalamus during the first postnatal year

Mohamed Najimi^{1*}, Alain Sarrieau², Nicolas Kopp³ and Fatiha Chigr¹

¹ Biological Engineering Laboratory, Life Sciences, Sultan Moulay Slimane University, Beni-Mellal, Morocco

² Unité de Formation et de Recherche de Biologie, Université de Bordeaux 1, Talence, France

³ Lyon 1 University, Lyon, France

Edited by:

Marie Z. Moftah, Alexandria University, Egypt

Reviewed by:

Youssef Aboussaleh, Ibn Tofail University, Morocco

Valérie Compan, Université de Nîmes, France

*Correspondence:

Mohamed Najimi, Biological Engineering Laboratory, Life Sciences, Sultan Moulay Slimane University, P. O. Box 523, Beni-Mellal 23000, Morocco
e-mail: mnajimi1@fstbm.ac.ma

The aim of the present study was to determine a detailed mapping of neurotensin (NT) in the human hypothalamus, during the first postnatal year using an *in vitro* quantitative autoradiography technique and the selective radioligand monoiodo-Tyr³-NT. Ten human postmortem hypothalami obtained from control neonates and infants (aged from 2 h to 1 year of postnatal age) were used. The biochemical kinetics of the binding in all obtained in this study revealed that the binding affinity constants were of high affinity (in the nanomolar range) and did not differ significantly between all cases investigated. Furthermore, competition experiments show insensitivity to levocabastine and were in favor of the presence of the high affinity site of NT receptor. Autoradiographic distribution showed that NT binding sites were widely distributed throughout the rostrocaudal extent of the hypothalamus. However, the distribution of NT binding sites was not homogenous and regional variations exist. In general, the highest densities were mainly present in the anterior hypothalamic level, particularly in the preoptic area. High NT binding site densities are also present at the mediobasal hypothalamic level, particularly in the paraventricular, parafoveolar, and dorsomedial nuclei. At the posterior level, low to very low densities could be observed in all the mammillary complex subdivisions, as well as the posterior hypothalamic area. Although this topographical distribution is almost identical during the postnatal period analyzed, age-related variations exist in discrete structures of the hypothalamus. The densities were higher in neonates/less aged infants than older infants in preoptic area (medial and lateral parts). The developmental profile is characterized by a progressive decrease from the neonate period to 1 year of postnatal age with a tendency to reach adult levels. On the other hand, the low levels of NT binding sites observed in posterior hypothalamus did not vary during the first postnatal year. They contrast in that with the very high levels we reported previously in adult. In conclusion, the present study demonstrates the occurrence of high NT binding sites density in various structures in many regions in the human neonate/infant hypothalamus, involved in the control of neuroendocrine and/or neurovegetative functions.

Keywords: neurotensin receptor, human hypothalamus, newborn brain, infant brain development, autoradiography

INTRODUCTION

The brain-gut peptide neurotensin (NT) is a neurotransmitter and neuromodulator in the central nervous system (CNS), and acts as a hormone in the gastrointestinal tract (Hermans and Maloteaux,

1998). Previous studies have shown that NT has a role, in both central and peripheral nervous systems. NT-producing neurons and their projections are widely distributed in the CNS, which explains the wide range of effects of this peptide (for review see Rostène and Alexander, 1997). The neuropeptide acts via three recognized receptors: NT1, NT 2, and NT3 (Vita et al., 1993; Mazella et al., 1996; Martin et al., 2003; Dicou et al., 2004). NT1 and NT2, are seven transmembrane domain G protein-coupled receptors, whereas NT3 has a single transmembrane domain sorting receptor that is predominantly associated with vesicular organelles and shares 100% homology with gp95/sortilin (Vincent et al., 1999). From a neuroendocrine/ endocrine perspective, the neuropeptide and its receptors are mainly located in neuronal synaptic vesicles of hypothalamus (Rostène and Alexander, 1997), in adenohipophys cells (Reyes et al., 2008) and in neuroendocrine cells of the small bowel where they are involved in enteric digestive processes,

Abbreviations: AA, anterior hypothalamic area; Ac, anterior commissure; DA, dorsal hypothalamic area; DBBh, diagonal band of Broca horizontalis; DBBv, diagonal band of Broca verticalis; DM, dorsomedial nucleus; F, Fornix; I, infundibular nucleus; Ic, intercalates nucleus; LH, lateral hypothalamic area; LM, lateral mammillary nucleus; LP, lateral preoptic area; Lt, lateral tuberal nucleus; MM, medial mammillary nucleus; MP, medial preoptic area; Mt, medial tuberal nucleus; Oc, optic chiasma; Ot, optic tract; Ovl, organum vasculosum of amina terminalis; PA, posterior hypothalamic area; Pe, periventricular nucleus; Pf, parafoveolar nucleus; PM, paramammillary nucleus; Pva, paraventricular nucleus, anterior part; Pvp, paraventricular nucleus, posterior part; Sb, Subthalamic nucleus; Sc, suprachiasmatic nucleus; Sh, septohypothalamic nucleus; SM, supramammillary nucleus; So, Supraoptic nucleus; St, Septothalamic nucleus; TCA, tubero cinereum area; Tm, tuberomammillary nucleus; Vm, ventromedial nucleus; Z, zona incerta.

gut motility and intestinal inflammatory mechanisms (for review see Evers, 2006). Previous studies have shown the role of the peptide in the regulation of the hypothalamo–pituitary–adrenal gland axis (Geisler et al., 2006). The hypothalamic region is of particular interest in the study of neuroendocrine regulation and related endocrine and autonomic disorders due to its role in the control of hormonal release, funneling converging inputs from widely distributed vegetative/autonomic regions. Thus, intracerebroventricular or local NT injections in hypothalamus have been associated with dramatic alterations of the plasma levels of most anterior pituitary hormones (Alexander and Leeman, 1992; Vijayan et al., 1994; Rostène and Alexander, 1997; Sicard et al., 2005). Of interest, the hypothalamus, as reported in laboratory animals and human is especially enriched in endogenous peptide and NT receptors (Sarrieau et al., 1985; Kanba et al., 1986; Mai et al., 1987; Sakamoto et al., 1987; Rostène and Alexander, 1997; Najimi et al., 2014). The human hypothalamus is not completely mature at birth and its maturation continues during the postnatal period with relation to the maturation of peptidergic factors regulating pituitary function (Swaab, 1995). Transient nature of hormone levels seems to prevail for most of the first postnatal life. The stabilization of their rates and their hypothalamic regulatory systems is observed well after this period (Donovan, 1980) which makes postnatal period highly sensitive to structural or neurochemical alterations. These changes could perturb not only neuroendocrine circuits subserving the anterior pituitary, but indirectly disrupt widespread hypothalamic autonomic functions as well. Indeed, previous studies have shown that events on early life may have long-term effects on physiology (Contreras et al., 2013). Dysregulation of NT neuro-modulation in many brain systems notably during development has been hypothesized to be involved in the pathogenesis of several insults. Changes in levels of NT and its cognate receptors have been reported in victims of sudden infant death syndrome (SIDS; Chigr et al., 1992; Coquerel et al., 1992). The relevance of the neurotensinergic system activity in the correct development and function of the human brain seems to be of great importance.

Developmental aspects of neurotensinergic system in human hypothalamo–pituitary complex are scarce and concerned particularly the endogenous NT in developing human hypothalamus (Sakamoto et al., 1987) and pituitary (Reyes et al., 2008). Developmental principles in NT and NT receptors have been extensively reported in laboratory animals notably in murine brain (Palacios et al., 1988; Sato et al., 1991, 1992; Lépée-Logeoux et al., 2000). This relevant literature about the neuroanatomy of central NT and its receptors indicate the presence of different developmental profiles. Moreover, it has been suggested that NT could promote and sustain survival, and be involved in neuronal migration pattern and synapse formation (O’Leary and Koester, 1993). In addition, NT has been shown to promote dendrite elongation and dendritic spine maturation (Gandou et al., 2010). Finally, studies in non-neuronal cells have shown that NT exerts mitogenic and trophic effects in normal and cancer cells in liver, pancreas, lung, and prostate (Hasegawa et al., 1994; Sehgal et al., 1994). Although well studied in animals, the developmental characteristics of NT receptors have been poorly investigated in humans

and no investigations have concerned the hypothalamus. As far as NT receptors are known to be important in the function of the neuropeptide, only few studies have specifically examined NT receptor development in human brain (the whole hemisphere: Zsürger et al., 1992 and medulla oblongata: Mailleux et al., 1990; Chigr et al., 1992). In this study, we investigated the developmental distribution of NT binding sites in normal post mortem human hypothalamus obtained from newborns and infants.

MATERIALS AND METHODS

SOURCE AND PREPARATION OF HUMAN TISSUES

We studied NT binding sites in the hypothalami of ten neonates and infants, autopsied at the Edouard Herriot and Lyon Sud Hospitals (Lyon, France) in accordance with written consent from the next of kin and local ethical approval (Ethics Committee of the two French laboratories). None of these subjects died as a result of neurologic, neuroendocrine, or endocrine disease (Table 1) and no pathological lesions were observed after macroscopic and microscopic examination of the brains. Ante mortem variables as age and sex were also summarized in Table 1. Furthermore, available information relating to tissue donor ante-mortem variables does not indicate the presence of agonal state or the presence of specific medication. At autopsy, the brains were removed from the cranium and the hypothalami were dissected out at 4°C by taking the parallel plane joining the optic chiasma and the anterior commissure as frontal plane and the caudal plane just behind the mammillary complex. The hypothalamus samples were immediately frozen at –80°C and stored at the same temperature until mounted on cryostat chucks. The frozen hypothalami were then sliced as 20 µm thick coronal sections at –20°C (Frigocut 2800, Reichert Jung, Heidelberg, Germany). Sections were collected onto chrome alum gelatin coated slides (Mentzel-Gläser, Braunschweig, Germany) and stored at –20°C until use. For the anatomical localization of the hypothalamic nuclei and areas, sections adjacent to those used

Table 1 | Source of brain tissues.

Cases	Sex	Age	Post-mortem delay (h)	Cause of death
A	F	2 h	14	Pulmonary hypoplasia
B	M	35 h	34	Amniotic inhalation with gastric regurgitation
C	M	1 day	10	Oedematic alveolitis with Refractory hypoplasia
D	M	3 days	15	Diaphragmatic hernia
E	M	1 month	20	Liver lesions
F	M	1 month	5	Enterocolitis
G	F	2 months	24	Pulmonary hemorrhage
H	F	4 months	24	Kidney medullar invagination
I	M	6 months	22	Pneumopathy
J	F	1 year	7	Hepatic necrosis

for autoradiography were stained with cresyl violet. We adopted conventional nomenclature we used in our previous investigations (Najimi et al., 2001, 2006, 2014).

IN VITRO QUANTITATIVE AUTORADIOGRAPHY

The slides containing the sections of the hypothalamus were first warmed to room temperature and then incubated at 4°C for 2 h, with 0.1 nM monoiodo ¹²⁵I-Tyr-NT (2000 Ci/mmol) in 50 mM Tris-HCl buffer (pH 7.5) containing 5 mM MgCl₂, 0.2% bovine serum albumin and 0.02 mM bacitracin (New England Nuclear: NEN, Wellesley, MA, USA). Non-specific binding was determined as the binding of ¹²⁵I-NT in the presence of 1 μM of unlabelled NT_{1–13}. After incubation, the slides were washed with ice cold buffer four times for 2 min each and rapidly dried with cold air. Labeled sections and iodinated standards (Amersham, Courtaboeuf Cedex, France) were then apposed to 3H sensitive Ultrofilm (Amersham) in Amersham exposure cassettes. After 2 weeks exposure in dark conditions at 4°C, the film was developed in Kodak D19 (Eastman Kodak, Rochester, NY, USA) for 3 min, dipped in water and fixed with Kodak rapid fixer for 10 min.

Competition experiments were performed by incubating serial sections from the anterior and mediobasal hypothalamic levels in the same medium containing graded concentrations of unlabelled NT (10⁻¹² to 10⁻⁶ M). IC₅₀ values were calculated from inhibition curves as peptide concentrations inhibiting 50% of monoiodo ¹²⁵I-Tyr-NT binding. Kinetics (IC₅₀ and K_D) analysis was computed by the method of Parker and Waud (1971).

Densitometric analysis of ¹²⁵I-NT binding was carried out according to the methods described previously (Chigr et al., 1992) using a computer assisted image analysis system (Biocom 2000, les Ulis, France) and the standards coexposed. Values for total and non-specific binding of ¹²⁵I-NT were obtained for each region by averaging four to eight readings for each hypothalamic nucleus and area on an individual autoradiograph.

Statistics

Results were expressed as means ± SEM. The differences of ¹²⁵I-NT binding site densities between the different age periods analyzed were evaluated using the analysis of variance (ANOVA) with 99% significant level. When necessary, *post hoc* tests were performed and the data were analyzed using the Scheffe' *F* test of the Stat View 512⁺⁺™ computer program.

RESULTS

We firstly assessed the binding characteristics of the ¹²⁵I-NT in the hypothalami of the cases examined. Computer analysis of binding isotherms showed that the apparent constant K_d and IC₅₀ are in the range of 0.88–1.40 nM and 1.96–2.8 Nm, respectively (Table 2).

AUTORADIOGRAPHIC LOCALIZATION OF ¹²⁵I-NT BINDING

The autoradiographic labeling was present throughout the rostro-caudal extent of the hypothalamic region in both neonates and infants. In all hypothalamic nuclei and areas analyzed, the non-specific binding, as determined in the presence of 1 μM NT_{1–13} was small throughout the concentration range (<10% of total binding). The distribution of NT binding sites throughout the

Table 2 | K_d values of [¹²⁵I]-neurotensin 1–13 binding and IC₅₀ values (Inhibition of specific ¹²⁵I-NT binding to hypothalamic sections by unlabeled NT) in different human individuals during the peri- and postnatal period.

Cases	Sex	Age	PMD	K _d (nM)	IC ₅₀ (nM)
A	F	2 h	14	1.40	1.9
B	M	35 h	34	0.91	2.6
C	M	1 day	10	0.88	2.7
D	M	3 days	15	1.45	2.3
E	M	1 month	20	0.98	2.8
F	M	1 month	5	1.10	2.6
G	F	2 months	24	1.20	2.6
H	F	4 months	24	0.96	1.9
I	M	6 months	22	1.30	2.4
J	F	1 year	7	1.10	2.4

Note that neither sex nor age influence on the values obtained.

human neonate/infant hypothalamus is shown in Figure 1 and the corresponding drawings are reported in Figure 2. The detailed mapping has been realized in the three anatomical hypothalamic levels, i.e., anterior, mediobasal, and posterior hypothalamus. Quantification of ¹²⁵I-NT binding site densities in the different hypothalamic structures is presented in the three histograms representing the comparison of NT binding sites density during the first postnatal year in the three hypothalamic levels (Figure 3).

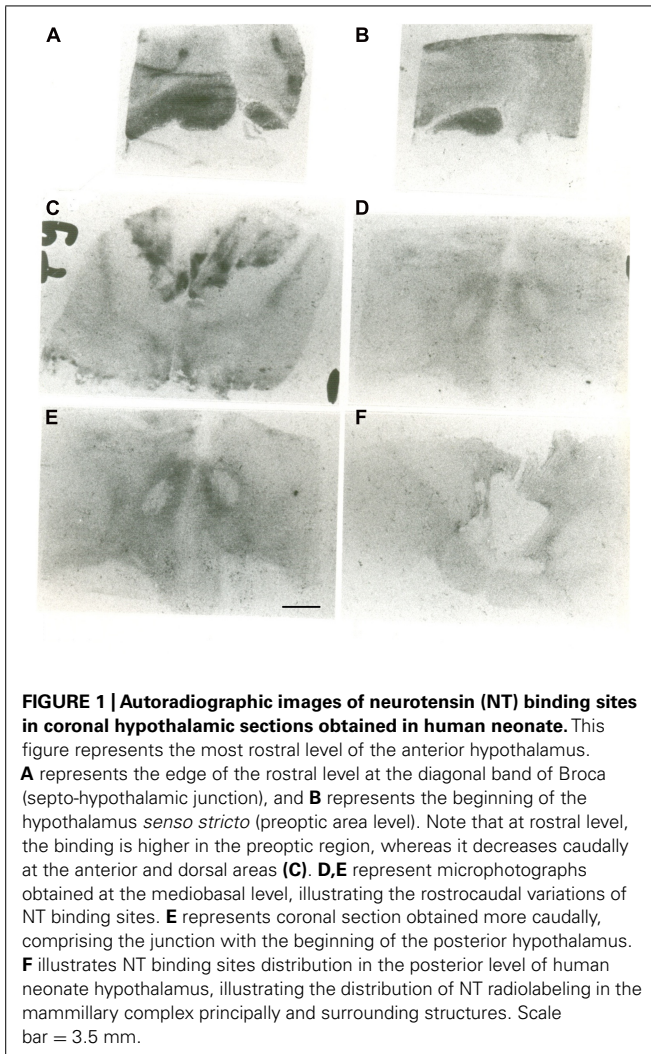
NEONATE

Anterior hypothalamus

The highest densities observed in the anterior hypothalamic level were present in the diagonal band of Broca and the medial and lateral preoptic areas (Figures 1A and 3A). Dorsally, low to moderate autoradiographic labeling was revealed in the septo-hypothalamic nucleus, whereas the nucleus of the stria terminalis displayed a dense binding (Figures 1A,B and 3A). At this level, low binding sites density is present in the anterior, dorsal and lateral hypothalamic areas as well as the organum vasculosum of lamina terminalis (Figures 1B,C and 3A) whereas the suprachiasmatic nucleus shows moderate binding site densities (Figures 1C and 3A) and the autoradiographic labeling was present throughout the entire structure. At the median level, low densities of NT binding sites were detected in the periventricular and paraventricular nuclei (Figures 1D and 3A). The supraoptic nucleus presented a relatively moderate autoradiographic binding, mainly in the ventrolateral part (Figures 1C,D and 3A). Finally, the fornix column which emerged at this level as well as the anterior commissure, showed no binding (Figures 1A–D).

Mediobasal hypothalamus

Generally, the mediobasal hypothalamic level presented relatively low autoradiographic labeling throughout its whole extent, particularly in the ventral portion. The infundibular, the ventromedial and the dorsomedial nuclei displayed equivalent low pattern of labeling (Figures 1D,E and 3B). In contrast to the anterior



hypothalamic level, the mediobasal part of the paraventricular nucleus as well as in the periventricular nucleus showed moderate NT binding site densities as (**Figures 1E** and **3B**). The parafornical nucleus also displayed moderate densities. In the posterior hypothalamic area, NT binding site density was moderate, existing principally in both its ventral and medial parts. The tuberal nuclei displayed low to moderate NT binding site density (**Figures 1D,E** and **3B**), the autoradiographic labeling was homogenous in both the medial and lateral portions. At the mediobasal hypothalamic level, the labeling present in the lateral hypothalamic area tended to relatively increase but remained in the low density average. Finally, no significant labeling was detected in the median eminence.

Posterior hypothalamus

In the transition zone between the mediobasal and the posterior hypothalamus, only low but significant NT binding site densities were detected in the premammillary nucleus and the surrounding areas (**Figures 1E** and **3C**). At the posterior level, the mammillary complex presented a diffuse and heterogeneous distribution of NT

binding (**Figures 1F** and **3C**) with a low labeling in all the anatomical components: the lateral mammillary nucleus, the intercalatus nucleus, and the supramammillary nucleus (**Figures 1F** and **3C**). Dorsally, the posterior hypothalamic area, the subthalamic nucleus and the zona incerta displayed very low densities (**Figures 1F** and **3C**), while the mamillothalamic tract and the Vicq d'Azyr fibers tract surrounding the medial mammillary nucleus were devoid of binding.

INFANT

Anterior hypothalamus

The pattern of ^{125}I -NT binding was quite similar to that observed for the neonate with binding sites density being in equivalent range for all anatomical components except for preoptic region where the densities were relatively moderate compared to neonate (20.1 ± 1.8 to 18.7 ± 1.4 in infants aged 1–2 months, vs. 25.1 ± 2.4 to 22.7 ± 2.1 in neonates, $p < 0.001$; 12.8 ± 2.0 to 13.1 ± 1.1 in infants aged 4–12 months, vs. 25.1 ± 2.4 to 22.7 ± 2.1 in neonates, $p < 0.001$; **Figure 3A**).

Mediobasal hypothalamus

All the structures analyzed in infant presented similar anatomical distribution of the autoradiographic labeling and equivalent densities of NT binding sites (**Figure 3B**).

Posterior hypothalamus

Similar topography of NT binding sites distribution was also present for this hypothalamic level in infant and neonate. In all the structures, the densities were slightly but not significantly, higher in infant than in neonate (**Figure 3C**).

No significant differences related to gender have been seen in all hypothalamic nuclei and areas in all the postnatal period investigated.

DISCUSSION

To the best of our knowledge, there is no information concerning the developmental dynamics of NT binding sites in normal human hypothalamus. We investigated in the present study, the autoradiographic distribution and quantitation of NT receptors in hypothalamus of postmortem normal human hypothalamus during development. This completes our previous study, analyzing the overall distribution of NT binding sites in the adult human hypothalamus (Najimi et al., 2014). To date, three NT receptors with distinct functional and pharmacological properties have been identified: NT1, NT2, and nts3 (for review, see Le et al., 1996; Vincent et al., 1999). NT binds to all three receptors (Vincent et al., 1999). NT has lower affinity for the NT2 receptor compared with the NT1 receptor (Schotte et al., 1986; Mazella et al., 1996; Vita et al., 1998). In our study, biochemical characteristics of binding carried out on different hypothalamic levels, showed that ^{125}I -NT bind to a high-affinity site with a K_d value varying from 0.88 to 1.40 nM ($n = 10$). Interestingly, the affinity of the binding sites labeled for the radiolabeled ligand was very close to that reported previously for NT1 receptors in many species including human (Sarriveau et al., 1985; Szigethy et al., 1990; Benzing et al., 1992; Chigr et al., 1992; Zsürger et al., 1992). Furthermore, levocabastine, which has affinity for the NT2 receptor, did not inhibit specific binding of ^{125}I -NT

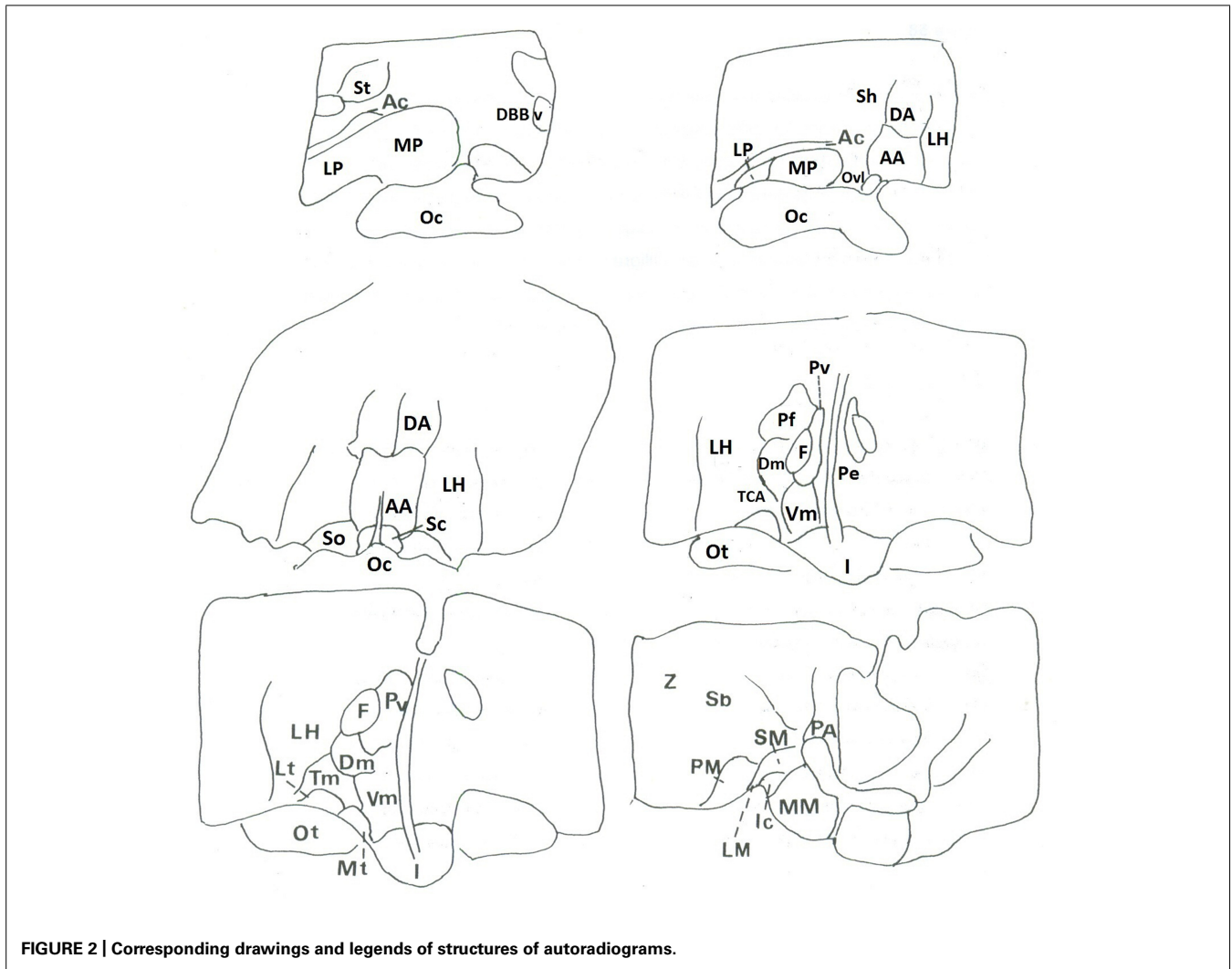


FIGURE 2 | Corresponding drawings and legends of structures of autoradiograms.

in competition experiments and autoradiographic studies. This insensitivity was observed for all hypothalamic nuclei and areas in all cases investigated. This is in favor of the presence of the high affinity subtype (NT1) in the human hypothalamus and particularly during the first postnatal year. Zsürger et al. (1992) reported the presence only of the high affinity type during the first postnatal year. The low affinity binding sites were absent during this period and they were first detected in 15-month-old human brain. Thus, from their investigations made on hemispheric membrane preparations containing also the hypothalamic region, it appears clearly that the high affinity NT1 is the most abundant receptor subtype in fetuses and early postnatal stages, whereas later in development, the low affinity NT2 receptor is successively expressed during definite periods. Therefore, we could assume that under our experimental conditions and the postnatal period we investigated, that the binding sites of NT we observed; belong to the high affinity NT receptor subtype, commonly called NT1. In rodent brain, NT1 and NT2 exhibit markedly different patterns of expression during development. NT1 expression in most subcortical areas is detectable during

the first postnatal week and increases progressively to reach adult levels by the third week (Palacios et al., 1988; Sato et al., 1992) whereas NT2 expression is detectable during the second postnatal week and increases to reach adult levels between the fourth and eighth weeks after birth (Schotte and Laduron, 1987; Sarret et al., 1998).

The NT binding sites we identified in the human hypothalamus were detected throughout the entire first postnatal period investigated and did not display different affinities for NT and analogs. Furthermore, individual kinetic affinities did not vary significantly, arguing for a stability of NT binding sites affinity during development. Interestingly, kinetics of NT binding, were equivalent to those we reported in adult hypothalamus (Najimi et al., 2014) suggesting that they are not age related. Such stability during postnatal development for NT binding sites has been reported previously in other human brain structures (Chigr et al., 1992; Zsürger et al., 1992).

Autoradiographic studies conducted in the developing hypothalamus have demonstrated that NT receptors are present in the entire rostrocaudal extent of the hypothalamic region and

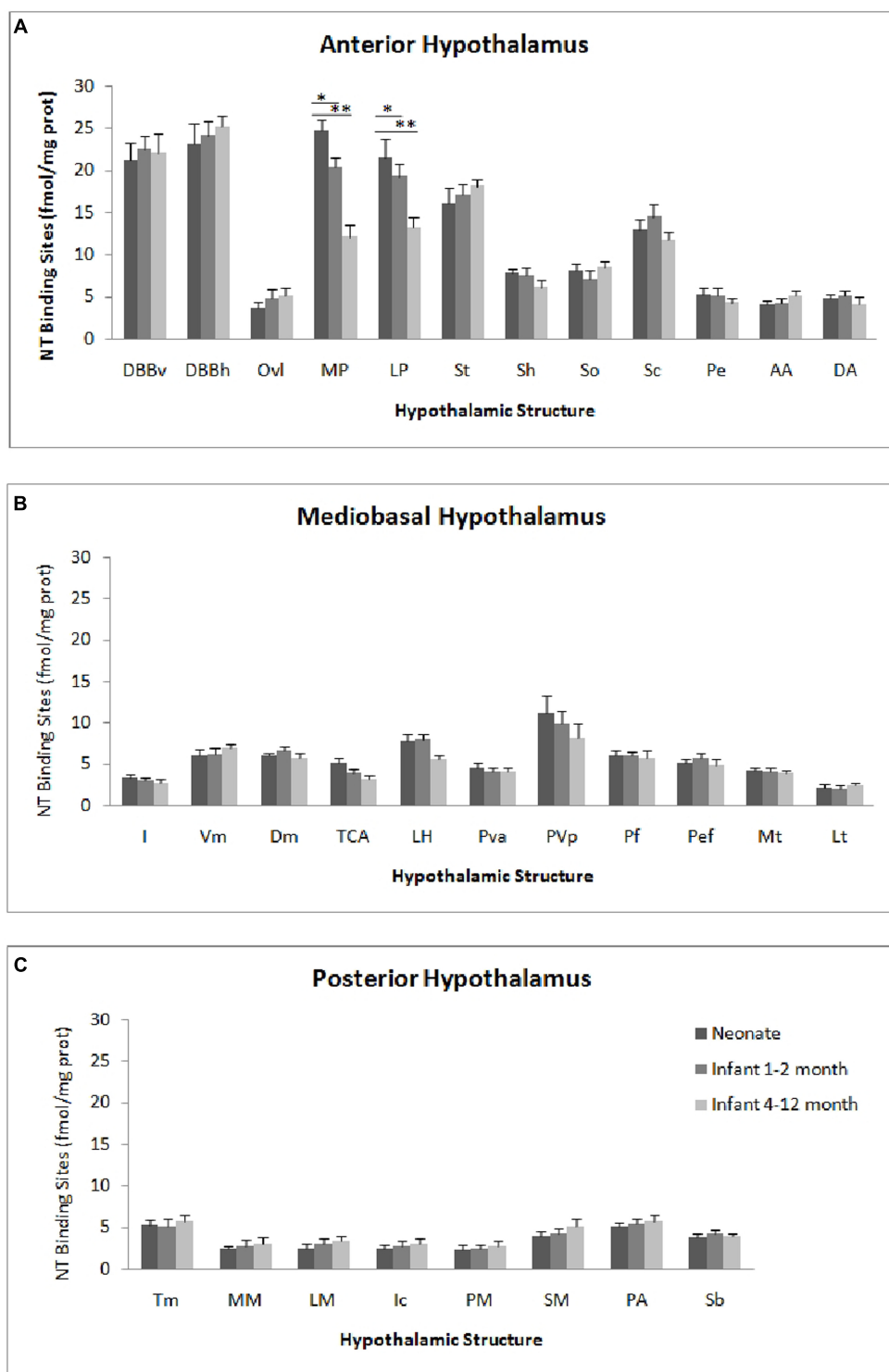


FIGURE 3 | Age comparison of NT receptor densities in the human hypothalamus during the peri- and the postnatal periods in the three hypothalamic levels: anterior (A), mediobasal (B) and posterior (C). The densities of binding sites are expressed as mean ± SEM of femtomoles of specifically bound per mg of

protein (fmole/mg protein). ****p* < 0.001 neonate vs. infant (1–2 months) and neonate vs. infant 4–12 months respectively for medial preoptic area (MP). ****p* < 0.001 neonate vs. infant (1–2 months) and infant (1–2 months) vs. infant 4–12 months respectively for lateral preoptic area (LP).

were exclusively present in gray matter. However, the labeling of NT binding sites across the hypothalamic region revealed somewhat several waves of receptors expression during development. Thus, the comparison of data obtained in preoptic region, at three age stages studied, from the neonate period to the 1 year postnatal age, showed gradual and significant decrease in NT binding sites density (24.2 ± 2.1 to 22.7 ± 2.1 in the neonate period vs. 12.8 ± 1.9 to 13.1 ± 1.1 in infant, $p < 0.001$). This progressive decrease, in density of NT binding sites, starts probably from the age of 23 weeks post-conceptional (presence of high densities in a fetus of 23 weeks of conceptional age, equivalent to the neonatal period, data not shown). This phenomenon continues throughout the first postnatal year and the densities decrease considerably to reach adult levels, but it is difficult with the sample we used to accurately determine the precise age when densities reach the level found in adults. Previous radioautographic studies have also highlighted the presence of more important densities of NT binding sites during the peri- and postnatal periods, in different brain structures in humans (Mailleux et al., 1990; Chigr et al., 1992; Zsürger et al., 1992). These differences in densities observed during the first postnatal period, could not be due to variation in the affinity. As discussed above, the affinity characteristics were remarkably stable during the first postnatal year. Also, the altered receptor binding, could not be due to differences in the postmortem delays (PMD). In accordance of this, previous studies in human brain with PMD's up to 42 h (Palacios et al., 1991) or rat brain up to 48 h (Sadoul et al., 1984) showed no significant negative effect of PMD's on NT binding. Furthermore, our previous studies in human did not relate any influence of this factor on NT receptor density (Sarrieau et al., 1985; Chigr et al., 1992; Najimi et al., 2014). Finally, the higher PMD of the sample investigated (34 h, case B) belong to the neonate group expressing high densities as well as for the lowest PMD (7 h, case J).

These differences in density observed with age (in the sense of decreasing density) could be the consequence of neuronal death involving these binding sites (Stanfield et al., 1982). This regressive process cell death occurs frequently during development in rat CNS is responsible for decreased levels of certain proteins in neurons after birth (Cowan et al., 1984). It has been postulated that these occurring changes may also result from elimination of neuronal connections during the fetal and the postnatal periods, leading to a differential stability of functional synaptic contacts. The elimination period modifying synaptic intercellular signals could lead to a repression of gene expression of NT receptor in hypothalamic neurons. The high expression of NT₁ receptor early in development suggests that it may play a specific role in the establishment of neuronal circuitry (Boudin et al., 2000). The physiological significance of this transient expression of NT binding sites during neuronal maturation remains unknown. It may be suggested that NT acts as a regulatory peptide during ontogeny. Thus, the presence of NT receptor before the full establishment of neural networks suggests that it is involved in the regulation of developmental processes and maturation of these structures in the human hypothalamus. The high binding levels observed may be a consequence of the low levels of NT release and a compensatory up-regulation of

receptors. In accordance of this, previous data report on the presence of relatively moderate amounts of NT immunoreactivity in human infant preoptic region, during the first postnatal month (Sakamoto et al., 1987).

As mentioned above and recall here, low binding sites density is observed during all the first postnatal year period in mammillary bodies compared to adults (Najimi et al., 2014). This is similar to that reported previously for somatostatin and benzodiazepine binding sites (Najimi et al., 1991, 2001). These results suggest an incomplete maturation of NT binding sites in these structures during the first postnatal period. We cannot exclude also that these hypothalamic structures have not yet completed their neuronal maturation (Kopp et al., 1992). Studies on older ages should reveal the precise period wherein the densities of binding sites begin to rise and reach levels observed in adults. It is also possible that these relatively low densities of NT binding sites are due to inhibitory control of NT on the endogenous expression of its correspondent receptor. Indeed, it has been shown in rat, that a blockade of neurotransmission for 5–9 days after the birth, with SR 48692 (NT antagonist), increases greatly the number of NT binding sites (Lépée-Lorgeoux et al., 1999). As previous studies reporting high and low amounts of endogenous NT in the human mammillary bodies of infant (Sakamoto et al., 1987) and adult (Langevin and Emson, 1982), respectively, one may speculate that endogenous NT levels would be responsible, at least in part, for the expression of NT binding, in the human hypothalamus, during peri- and postnatal phases. If in fact the reduced NT binding represents a physiologically relevant process, one plausible explanation would be that NT receptors in the hypothalamus during the postnatal period are down-regulated. Alternatively, the observed low levels of these binding sites could be explained by the fact that the synthesis of high-affinity NT receptors in fetuses and newborns is delayed in the posterior hypothalamus as has been reported for somatostatin receptors (Bologna and Leroux, 2000).

Taken together, it is tempting to postulate that the complex spatiotemporal pattern of NT binding sites expression in the developing hypothalamus in human, presumably results, at least partially, from the action of endogenous NT (Sakamoto et al., 1987) leading to an up or down regulation of NT receptors, as has been reported for rat brain (Palacios et al., 1988; Lépée-Lorgeoux et al., 2000). Nevertheless, and despite the well established modulatory role of the peptide on NT₁ receptors in mature brain in rat (Azzi et al., 1996), it does not play a major role in establishing their developmental profile during the early postnatal period (Lépée-Lorgeoux et al., 2000). This could suggest that peptide release during this period, as well as connection formation, are probably not sufficient for the regulation of NT₁ receptors by the endogenous ligand. It is therefore possible that other unknown mechanisms may explain these developmental changes. Thus, the progressive reduction in NT₁ receptors density during the postnatal period in the human hypothalamus could coincide with normal maturational events characterized by programmed cell death of neurons bearing N receptors, or the influence of hypothalamic inputs on the expression of NT₁ receptors. A reduction in NT binding may simply reflect a loss of synaptic connectivity (Stanfield et al., 1982; Cowan et al., 1984; Zecevic et al., 1989).

On the contrary, in the posterior hypothalamus, the NT could be more involved in the maturational process of NT1 receptor. This could be corroborated by *in vitro* and *in vivo* experiments which have demonstrated a variety of effects of NT in the developmental processes such as the facilitation of dendritic outgrowth (Gandou et al., 2010), the regulation of growth factor secretion by astrocytes (Camby et al., 1996), the modulation of neuron sensitivity to glutamate (Ferraro et al., 2008) as well as important role during the onset of neuritic ingrowth (Staecker et al., 1996).

The characteristic of postnatal autoradiographic pattern of ¹²⁵I-NT binding in the human hypothalamus is not unique to the neurotransmitter/neuromodulator receptor studied to date. Such a short-lasting expression of a particular receptor has been shown for vasoactive intestinal peptide (VIP) and benzodiazepine receptors in the hypothalamus during the first postnatal year (Najimi et al., 2001, 2006).

The actions of NT as a regulator of anterior pituitary secretions and food intake has been well characterized (Rostène and Alexander, 1997; Kalafatakis and Triantafyllou, 2011). Interestingly, the presence of considerable amounts of the peptide (Sakamoto et al., 1987) as well as NT binding sites (this study) is in favor of the direct control or modulation (by finely tuning feeding regulation; Brunetti et al., 2005) of these autonomic function in neonate/infant. This function is highly vital for the survival of the body during this sensitive period of life. Indeed, neonatal nutrition during critical periods plays a key role in the development of obesity and related metabolic pathologies such as cardiovascular disease and type II diabetes (McMillen and Robinson, 2005).

In summary, the results obtained in this study sustain the concept that the NTergic system participates in the development, differentiation, and maintenance of the human hypothalamus. As perspectives, the present work should be extended, by investigating, firstly the characteristics of NT binding sites during the other postnatal years (particularly the second postnatal year) to examine the eventual dynamics in binding site levels notably in the posterior hypothalamus. Secondly, as the sensitive levocabastine subtype is expressed at the 15th postnatal month in human brain, it would be very interesting to examine in these postnatal ages, if these binding sites subtype are present in the human hypothalamus.

ACKNOWLEDGMENTS

The authors thank Dr. N. Hamamouch for his critical review of the paper. This work is supported by Grant from the TWAS 2003 (Mohamed Najimi) and the financial support of GDRI NEURO (CNRS/INSERM/CNRST) France–Morocco.

REFERENCES

- Alexander, M. J., and Leeman, S. E. (1992). Neurotensin gene expression in the rat preoptic area. implications for the regulation of reproduction. *Ann. N. Y. Acad. Sci.* 668, 70–89. doi: 10.1111/j.1749-6632.1992.tb27340.x
- Azzi, M., Boudin, H., Mahmudi, N., Pélaprat, D., Rostène, W., and Berod, A. (1996). In vivo regulation of neurotensin receptors following long-term pharmacological blockade with a specific receptor antagonist. *Mol. Brain Res.* 42, 213–221. doi: 10.1016/S0169-328X(96)00124-6
- Benzing, W. C., Mufson, E. J., Jennes, L., Stopa, E. G., and Armstrong, D. M. (1992). Distribution of neurotensin immunoreactivity within the human amygdaloid complex: a comparison with acetylcholinesterase- and Nissl-stained tissue sections. *J. Comp. Neurol.* 317, 283–297. doi: 10.1002/cne.903170306
- Bologna, E., and Leroux, P. (2000). Identification of multiple somatostatin receptors in the rat somatosensory cortex during development. *J. Comp. Neurol.* 420, 466–480.
- Boudin, H., Lazaroff, B., Bachelet, C. M., Pelaprat, D., Rostène, W., and Beaudet, A. (2000). Immunologic differentiation of two high-affinity neurotensin receptor isoforms in the developing rat brain. *J. Comp. Neurol.* 425, 45–57. doi: 10.1002/1096-9861(20000911)425:13.3.CO;2-0
- Brunetti, L., Di Nisio, C., Orlando, G., Ferrante, C., and Vacca, M. (2005). The regulation of feeding: a cross talk between peripheral and central signalling. *Int. J. Immunopathol. Pharmacol.* 18, 201–212.
- Camby, I., Salmon, I., Bourdel, E., Nagy, N., Danguy, A., Brotch, I. J., et al. (1996). Neurotensin-mediated effects on astrocytic tumor cell proliferation. *Neuropeptides* 30, 133–139. doi: 10.1016/S0143-4179(96)90080-3
- Chigr, F., Jordan, D., Najimi, M., Denoroy, L., Sarrieau, A., de Broca, A., et al. (1992). Quantitative autoradiographic study of somatostatin and neurotensin binding sites in medulla oblongata of SIDS. *Neurochem. Int.* 20, 113–118. doi: 10.1016/0197-0186(92)90134-D
- Contreras, C., Novell, M. G., Leis, R., Diéguez, C., Skrede, S., and Lopez, M. (2013). Effects of neonatal programming on hypothalamic mechanisms controlling energy balance. *Horm. Metabol. Res.* 45, 935–944. doi: 10.1055/s-0033-1351281
- Coquerel, A., Buser, M., Tayot, J., Pfaff, F., Matray, F., and Proust, B. (1992). Beta-endorphin and neurotensin in brainstem and cerebrospinal fluid in the sudden infant death syndrome. *Neurochem. Int.* 20, 97–102. doi: 10.1016/0197-0186(92)90131-A
- Cowan, W. M., Fawcett, J. W., O'Leary, D. D. M., and Stanfield, B. B. (1984). Regressive events in neurogenesis. *Science* 255, 1258–1265. doi: 10.1126/science.6474175
- Dicou, E., Vincent, J. P., and Mazella, J. (2004). Neurotensin receptor-3/sortilin mediates neurotensin-induced cytokine/chemokine expression in a murine microglial cell line. *J. Neurosci. Res.* 78, 92–99. doi: 10.1002/jnr.20231
- Donovan, B. T. (1980). "The role of hormones in perinatal brain differentiation", in *The Endocrine Functions of the Brain*, ed. M. Motta (New York: Raven Press), 117–141.
- Evers, B. M. (2006). Neurotensin and growth of normal and neoplastic tissues. *Peptides* 27, 2424–2433. doi: 10.1016/j.peptides.2006.01.028
- Ferraro, L., Tomasini, M. C., Mazza, R., Fuxe, K., Fournier, J., Tanganelli, S., et al. (2008). Neurotensin receptors modulators of glutamatergic transmission. *Brain Res. Rev.* 58, 365–373. doi: 10.1016/j.brainresrev.2007.11.001
- Gandou, C., Ohtani, A., Senzaki, K., and Shiga, T. (2010). Neurotensin promotes the dendrite elongation and the dendritic spine maturation of the cerebral cortex in vitro. *Neurosci. Res.* 66, 246–255. doi: 10.1016/j.neures.2009.11.007
- Geisler, S., Béro, A., Zahm, D. S., and Rostène, W. (2006). Brain neurotensin, psychostimulants, and stress—emphasis on neuroanatomical substrates. *Peptides* 27, 2364–2384. doi: 10.1016/j.peptides.2006.03.037
- Hasegawa, K., Kar, S., and Carr, B. (1994). Stimulation of hepatocyte DNA synthesis by neurotensin. *J. Cell. Physiol.* 158, 215–222. doi: 10.1002/jcp.1041580202
- Hermans, E., and Maloteaux, J. M. (1998). Mechanisms of regulation of neurotensin receptors. *Pharmacol. Ther.* 79, 89–104. doi: 10.1016/S0163-7258(98)00009-6
- Kanba, K. S., Kanba, S., Okazaki, H., and Richelson, E. (1986). Binding of [³H]neurotensin in human brain: properties and distribution. *J. Neurochem.* 46, 946–952. doi: 10.1111/j.1471-4159.1986.tb13061.x
- Kalafatakis, K., and Triantafyllou, K. (2011). Contribution of neurotensin in the immune and neuroendocrine modulation of normal and abnormal enteric function. *Regul. Pept.* 170, 7–17. doi: 10.1016/j.regpep.2011.04.005
- Kopp, N., Najimi, M., Champier, J., Chigr, F., Charnay, Y., Epelbaum, J., et al. (1992). Ontogeny of peptides in human hypothalamus in relation to sudden infant death syndrome (SIDS). *Prog. Brain Res.* 93, 167–188. doi: 10.1016/S0079-6123(08)64571-9
- Langevin, H., and Emson, P. C. (1982). Distribution of substance P, somatostatin and neurotensin in the human hypothalamus. *Brain Res.* 246, 65–69. doi: 10.1016/0006-8993(82)90142-1
- Le, F., Cusack, B., and Richelson, E. (1996). The neurotensin receptor: is there more than one subtype? *Trends Pharmacol. Sci.* 17, 1–3. doi: 10.1016/0165-6147(96)81561-6
- Lépée-Lorgeoux, I., Betancur, C., Rostène, W., and Pélaprat, D. (1999). Differential ontogenetic patterns of levocabastine-sensitive neurotensin NT2 receptors and of NT1 receptors in the rat brain revealed by in situ hybridization. *Dev. Brain Res.* 113, 115–131. doi: 10.1016/S0165-3806(99)00009-7

- Lépée-Loigeux, I., Betancur, C., Souazé, F., Rostène, W., Béro, A., and Pélaprat, D. (2000). Regulation of the neurotensin NT1 receptor in the developing rat brain following chronic treatment with the antagonist SR 48692. *J. Neurosci. Res.* 60, 362–369. doi: 10.1002/(SICI)1097-4547(20000501)60:3<362::AID-JNR11>3.0.CO;2-F
- Mai, J. K., Triepel, J., and Metz, J. (1987). Neurotensin in the human brain. *Neuroscience* 22, 499–524. doi: 10.1016/0306-4522(87)90349-6
- Mailleux, P., Pelaprat, D., and Vanderhaeghen, J. J. (1990). Transient neurotensin high-affinity binding sites in the human inferior olive during development. *Brain Res.* 508, 345–348. doi: 10.1016/0006-8993(90)90422-8
- Martin, S., Vincent, J. P., and Mazella, J. (2003). Involvement of the neurotensin receptor-3 in the neurotensin-induced migration of human microglia. *J. Neurosci.* 23, 1198–1205.
- Mazella, J., Botto, J. M., Guillemare, E., Coppola, T., Sarret, P., and Vincent, J. P. (1996). Structure, functional expression, and cerebral localization of the levocabastine-sensitive neurotensin/neuromedin N receptor from mouse brain. *J. Neurosci.* 16, 5613–5620.
- McMillen, I. C., and Robinson, J. S. (2005). Developmental origins of the metabolic syndrome: prediction, plasticity and programming. *Physiol. Rev.* 85, 571–633. doi: 10.1152/physrev.00053.2003
- Najimi, M., Bennis, M., Moysé, E., Miachon, S., Kopp, N., and Chigr, F. (2001). Regional distribution of benzodiazepine binding sites in the human newborn and infant hypothalamus. A quantitative autoradiographic study. *Brain Res.* 895, 129–138. doi: 10.1016/S0006-8993(01)02060-1
- Najimi, M., Jordan, D., Chigr, F., Champier, J., Kopp, N., Slama, A., et al. (1991). Regional distribution of somatostatin binding sites in the human hypothalamus: a quantitative autoradiographic study. *Neuroscience* 40, 321–335. doi: 10.1016/0306-4522(91)90123-6
- Najimi, M., Rachidi, F., Afif, A., and Chigr, F. (2006). Developmental pattern of VIP binding sites in the human hypothalamus. *Ann. N. Y. Acad. Sci.* 1070, 462–467. doi: 10.1196/annals.1317.062
- Najimi, M., Sarrieau, A., Kopp, N., and Chigr, F. (2014). An autoradiographic study of neurotensin receptors in the human hypothalamus. *Acta Histochem.* 116, 382–389. doi: 10.1016/j.acthis.2013.09.008
- O'Leary, D. D., and Koester, S. E. (1993). Development of projection neuron types, axon pathways, and patterned connections of the mammalian cortex. *Neuron* 10, 991–1006. doi: 10.1016/0896-6273(93)90049-W
- Palacios, J. M., Chinaglia, G., Rigo, M., Ulrich, J., and Probst, A. (1991). Neurotensin receptor binding levels in basal ganglia are not altered in Huntington's chorea or schizophrenia. *Synapse* 7, 114–122. doi: 10.1002/syn.890070205
- Palacios, J. M., Pazos, A., Dietl, M. M., Schlumpf, M., and Lichtensteiger, W. (1988). The ontogeny of brain neurotensin receptors studied by autoradiography. *Neuroscience* 25, 307–317. doi: 10.1016/0306-4522(88)90028-0
- Parker, R. B., and Waud, D. R. (1971). Pharmacological estimation of drug-receptor dissociation constants. Statistical evaluation. I. Agonists. *J. Pharmacol. Exp. Ther.* 177, 1–12.
- Reyes, R., Valladares, E., Gutiérrez, R., González, M., and Bello, A. R. (2008). Immunohistochemical distribution of regulatory peptides in the human fetal adenohypophysis. *J. Anat.* 212, 817–826. doi: 10.1111/j.1469-7580.2008.00906.x
- Rostène, W. H., and Alexander, M. J. (1997). Neurotensin and neuroendocrine regulation. *Front. Neuroendocrinol.* 18:115–173. doi: 10.1006/frne.1996.0146
- Sadoul, J. L., Kitabgi, P., Rostene, W., Javoy-Agid, F., Agid, Y., and Vincent, J. P. (1984). Characterization and visualization of neurotensin binding to receptor sites in human brain. *Biochem. Biophys. Res. Commun.* 120, 206–213. doi: 10.1016/0006-291X(84)91434-7
- Sakamoto, N., Michel, J. P., Kopp, N., and Pearson, J. (1987). Neurotensin immunoreactive neurons in the human infant diencephalon. *Brain Res.* 403, 31–42. doi: 10.1016/0006-8993(87)90119-3
- Sarret, P., Beaudet, A., Vincent, J. P., and Mazella, J. (1998). Regional and cellular distribution of low affinity neurotensin receptor mRNA in adult and developing mouse brain. *J. Comp. Neurol.* 394, 344–356. doi: 10.1002/(SICI)1096-9861(19980511)394:3<344::AID-CNE6>3.0.CO;2-1
- Sarrieau, A., Javoy-Agid, F., Kitabgi, P., Dussailant, M., Vial, M., Vincent, J. P., et al. (1985). Characterization and autoradiographic distribution of neurotensin binding sites in the human brain. *Brain Res.* 348, 375–380. doi: 10.1016/0006-8993(85)90461-5
- Sato, M., Kiyama, H., and Tohyama, M. (1992). Different postnatal development of cells expressing mRNA encoding neurotensin receptor. *Neuroscience* 48, 137–149. doi: 10.1016/0306-4522(92)90344-2
- Sato, M., Kiyama, H., Yoshida, S., Saika, T., and Tohyama, M. (1991). Postnatal ontogeny of cells expressing prepro-neurotensin/neuromedin N mRNA in the rat forebrain and midbrain: a hybridization histochemical study involving isotope-labeled and enzyme-labeled probes. *Neurosci. Lett.* 128, 85–89. doi: 10.1016/0304-3940(91)90765-L
- Schotte, A., and Laduron, P. M. (1987). Different postnatal ontogeny of two [3H]neurotensin binding sites in rat brain. *Brain Res.* 408, 326–328. doi: 10.1016/0006-8993(87)90398-2
- Schotte, A., Leysen, J. E., and Laduron, P. M. (1986). Evidence for a displaceable non-specific [3H]neurotensin binding site in rat brain. *Naunyn Schmiedeberg's Arch. Pharmacol.* 333, 400–405. doi: 10.1007/BF00500016
- Sehgal, I., Powers, S., Huntley, B., Powis, G., Pittelkow, M., and Maihle, N. J. (1994). Neurotensin is an autocrine trophic factor stimulated by androgen withdrawal in human prostate cancer. *Proc. Natl. Acad. Sci. U.S.A.* 91, 4673–4677. doi: 10.1073/pnas.91.11.4673
- Sicard, F., De Groot, D., Gras, M., Leprince, J., Conlon, J. M., Roubos, E. W., et al. (2005). Neuroendocrine regulation of frog adrenocortical cells by neurotensin. *Ann. N. Y. Acad. Sci.* 1040, 200–205. doi: 10.1196/annals.1327.025
- Stanfield, B. B., O'Leary, D. D., and Fricks, C. (1982). Selective collateral elimination in early postnatal development restricts cortical distribution of rat pyramidal tract neurons. *Nature* 298, 371–373. doi: 10.1038/298371a0
- Staecker, H., Van De Water, T. R., Lefebvre, P. P., Liu, W., Moghadasi, M., Galinovic-Schwartz, V., et al. (1996). NGF, BDNF and NT-3 play unique roles in the in vitro development and patterning of innervation of the mammalian inner ear. *Brain Res.* 508, 345–348. doi: 10.1016/0006-8993(90)90422-8
- Swaab, D. F. (1995). Development of the human hypothalamus. *Neurochem. Res.* 20, 509–519. doi: 10.1007/BF01694533
- Szigethy, E., Quirion, R., and Beaudet, A. (1990). Distribution of 125I-neurotensin binding sites in human forebrain: comparison with the localization of acetylcholinesterase. *J. Comp. Neurol.* 297, 487–498. doi: 10.1002/cne.902970403
- Vijayan, E., Carraway, R., Leeman, S. E., and Mc Cann, S. M. (1994). Physiological significance of neurotensin in pituitary glycoprotein hormone release as revealed by in vivo and in vitro studies with neurotensin antiserum. *Neuroendocrinology* 60, 157–64. doi: 10.1159/000126746
- Vincent, J. P., Mazella, J., and Kitabgi, P. (1999). Neurotensin and neurotensin receptors. *Trends Pharmacol. Sci.* 20, 302–309. doi: 10.1016/S0165-6147(99)01357-7
- Vita, N., Laurent, P., Lefort, S., Chalou, P., Dumont, X., Kaghad, M., et al. (1993). Cloning and expression of a complementary DNA encoding a high affinity human neurotensin receptor. *FEBS Lett.* 317, 139–142. doi: 10.1016/0014-5793(93)81509-X
- Vita, N., Oury-Donat, E., Chalou, P., Guillemot, M., Kaghad, M., Bachy, A., et al. (1998). Neurotensin is an antagonist of the human neurotensin NT2 receptor expressed in Chinese hamster ovary cells. *Eur. J. Pharmacol.* 360, 265–272. doi: 10.1016/S0014-2999(98)00678-5
- Zecevic, N., Bourgeois, J. P., and Rakic, P. (1989). Changes in synaptic density in motor cortex of monkey during fetal and postnatal life. *Dev. Brain Res.* 50, 11–32. doi: 10.1016/0165-3806(89)90124-7
- Zsürger, N., Chabry, J., Coquerel, A., and Vincent, J.-P. (1992). Ontogenesis and binding properties of high affinity neurotensin receptors in human brain. *Brain Res.* 586, 303–310. doi: 10.1016/0006-8993(92)91640-Z

Conflict of Interest Statement: The reviewer, Dr. Valérie Compañ declares that despite having collaborated with the authors, the review process was handled objectively. The authors declare that the research was conducted in the absence of any commercial or financial relationships that could be construed as a potential conflict of interest.

Received: 30 April 2014; accepted: 07 August 2014; published online: 10 September 2014.

Citation: Najimi M, Sarrieau A, Kopp N and Chigr F (2014) Developmental dynamics of neurotensin binding sites in the human hypothalamus during the first postnatal year. *Front. Cell. Neurosci.* 8:251. doi: 10.3389/fncel.2014.00251

This article was submitted to the journal *Frontiers in Cellular Neuroscience*.

Copyright © 2014 Najimi, Sarrieau, Kopp and Chigr. This is an open-access article distributed under the terms of the Creative Commons Attribution License (CC BY). The use, distribution or reproduction in other forums is permitted, provided the original author(s) or licensor are credited and that the original publication in this journal is cited, in accordance with accepted academic practice. No use, distribution or reproduction is permitted which does not comply with these terms.



Modulation of orexigenic and anorexigenic peptides gene expression in the rat DVC and hypothalamus by acute immobilization stress

Fatiha Chigr^{1*}, Fatima Rachidi¹, Catherine Tardivel², Mohamed Najimi¹ and Emmanuel Moyse³

¹ Life Sciences, Biological Engineering, Faculty of Sciences and Techniques, Sultan Moulay Slimane University, Beni Mellal, Morocco

² Faculté des Sciences et Techniques, Aix-Marseille Université, PPSN, Marseille, France

³ Biologie Animale et de Génétique, Université François, Rabelais, INRA, Tours, Nouzilly, France

Edited by:

Marie Z. Mofteh, Alexandria University, Egypt

Reviewed by:

Liana Fattore, CNR, National Research Council, Italy
Slavica Krantic, CNRS, France

*Correspondence:

Fatiha Chigr, Life Sciences, Biological Engineering, Faculty of Sciences and Techniques, Sultan Moulay Slimane University, Building A, Rte Mghila, PO. Box: 523, Beni Mellal, Morocco
e-mail: f.chigr@usms.ma

We studied the long term effects of a single exposure to immobilization stress (IS) (1 h) on the expression of anorexigenic (Pro-opiomelanocortin: POMC and cocaine amphetamine related transcript: CART) and orexigenic (neuropeptide Y:NPY, Agouti related peptide: AgRP) factors in hypothalamus and dorso vagal complex (DVC). We showed, by using RT-PCR that in the hypothalamus, that the mRNAs of POMC and CART were up-regulated at the end of IS and up to 24 h. This up regulation persists until 48–72 h after IS for CART only. In the DVC, their expressions peak significantly at 24 h post stress and decline afterwards; CART mRNA is down regulated after 48 h post stress. NPY and AgRP mRNAs show a gradual increase just after the end of IS. The up regulation is significant only at 24 h after stress for AgRP but remains significantly higher for NPY compared to controls. In DVC, the mRNAs of the two factors show generally a similar post stress pattern. A significant increase just after the end of IS of rats which persists up to 24 h after is firstly noticed. The levels tend then to reach the basal levels although, they were slightly but significantly higher up to 72 h after stress for mRNA NPY. The comparison between the expression profiles of anorexigenic and the two orexigenic peptides investigated shows the presence of a parallelism between that of POMC and AgRP and that of CART and NPY when each brain region (hypothalamus and DVC) is considered separately. It seems that any surge in the expression of each anorexigenic factor stimulates the expression of those of corresponding and appropriated orexigenic one. These last reactions from orexigenic peptides tend to attenuate the anorexigenic effects of CART and POMC and by consequent to abolish the anorexia state generated by stress.

Keywords: stress, psychological, POMC, CART, AgRP, NPY, hypothalamo-hypophyseal system, DVC

INTRODUCTION

Stress is well established as a serious health problem in industrialized human societies, since it favors several major pathologies such as cardiovascular failure (Manni et al., 2008; Wirtz et al., 2008), cancer (Quick et al., 2008) and depression (Chaplin et al., 2008). Other emerging deleterious effects of stress include feeding disorders and body weight (BW) dysregulations (Harris et al., 2002; Hamer and Stamatakis, 2008). In animals, many studies reported that different paradigms of stress produce a significant reduction in food intake (FI), unless access to food is given after the stress period. In human, psychological stress paradigms are more effective in producing such manifestations (Vallès et al., 2000; Charrier et al., 2006; Adam and Epel, 2007; Laurent et al., 2013).

FI regulation in adult Mammals is integrated mainly by two brain structures: the hypothalamus and the dorsal vagal complex (DVC), and involves an array of neuroendocrine communications (Schwartz et al., 2000; Berthoud et al., 2006; Morton

et al., 2006). Short-term regulation, which consists in reflex arrest of FI under stomachal filling or satiety reflex, is triggered by vagus nerve afferents to the DVC. Long-term regulation consists essentially in satiety reflex threshold modulation by “adiposity signals”, i.e., the peripheral hormones signaling metabolic storage levels like leptin or insulin, which involves the hypothalamus and its reciprocal projection on the DVC (Haupt, 2000; Schwartz et al., 2000; Morton et al., 2006). In the hypothalamus, adiposity signals are integrated into the balance between two mutually antagonistic pathways from the arcuate nucleus: the orexigenic neurons expressing neuropeptide Y (NPY) and the agouti-related peptide (AgRP) as co-neurotransmitters, and the anorexigenic neurons emitting pro-opiomelanocortin (POMC)-derived alpha-melanocyte stimulating hormone (α -MSH) and cocaine and amphetamine regulated Peptide (CART; Schwartz et al., 2000; Cone, 2005; Morton et al., 2006). Both neuron sub-populations are receptive to leptin and display signal-dependent plasticity (Bouret et al., 2004; Pinto et al., 2004).

The receptors and downstream effectors of the orexigenic and anorexigenic neuromediators, like brain-derived neurotrophic factor (BDNF), as well as receptors of leptin and other metabolically relevant systemic messengers, are expressed in specific neuronal populations of the DVC (Cone, 2005). Their involvement in FI regulation is hardly known, except for BDNF (Bariohay et al., 2005; Charrier et al., 2006) and melanocortin-ergic signaling (Ellacott et al., 2006). Such redundancy supports a distributed, rather than hierarchical model of brain center involvement in feeding regulation (Berthoud et al., 2006; Lebrun et al., 2006). However, actual involvement of DVC peptidergic signaling in FI regulation remains largely unaddressed. Anorexigenic challenges by cholecystokinin or leptin were shown to elicit parallel changes of anorexigenic BDNF expression in DVC and hypothalamus (Fan et al., 2004; Bariohay et al., 2005; Ellacott et al., 2006). Conversely, anorexia-inducing immobilization stress (IS) triggered different BDNF recruitment patterns between DVC and hypothalamus (Charrier et al., 2006). Furthermore, in the framework of hypothalamus-DVC relationships, the precise mechanism by which stress affects energy metabolism as well as FI and BW control is not well understood, notably at the gene expression level. Furthermore, stress could have long lasting effects, depending on the paradigm used. The post stress effects, of acute stress, are less well known, however emerging evidence shows that it can impact later, depending on stress paradigm (Vallès et al., 2000; Charrier et al., 2006). Thus, to further understand the interplay between the central appetite-stimulating and stress signals in the regulation of FI, we examined the post stress dynamics of NPY, AgRP, POMC and CART gene expressions in microdissected hypothalamic and DVC from adult rats submitted to immobilization stress.

MATERIALS AND METHODS

ANIMALS

Twenty-five male Wistar rats (Charles River, Les Oncins, France) weighing 220–250 g were used in this study. The rats were divided into five groups, four stressed groups ($n = 5$ for each group) and a control group ($n = 5$). The four stressed groups consisted of rats sacrificed just after the termination of stress (0 h), 24, 48 and 72 h following the termination of 1 h immobilization. All the rats were housed under a 12:12 h dark:light cycle and constant temperature with water and standard rat chow (pellets A04, Scientific Animal Food and Engineering, Augy, France) *ad libitum*. Animals were handled and cared for in accordance with the *Guide for the Care and Use of Laboratory Animals* (NRC, 1996) and the European Communities Council Directive of 24 November 1986 (86/609/EEC). Experimental protocols were carried out in compliance with institutional Ethical Committee guidelines for animal research. Rats were housed 3–6 per cage, and allowed to acclimatize for at least 5 days after their arrival. All animals were then handled daily for 5 days before the experiment. Some rats were subjected to acute immobilization stress according to a well-established protocol (Kvetnansky and Mikulaj, 1970; Benyassi et al., 1993): each rat was attached on a wooden board in prone position by taping their limbs and shoulders to metal mounts at 9:30 a.m. for 60 min, and returned to its cage. Rats were sacrificed by decapitation at 0, 24, 48 or 72 h after stress; control

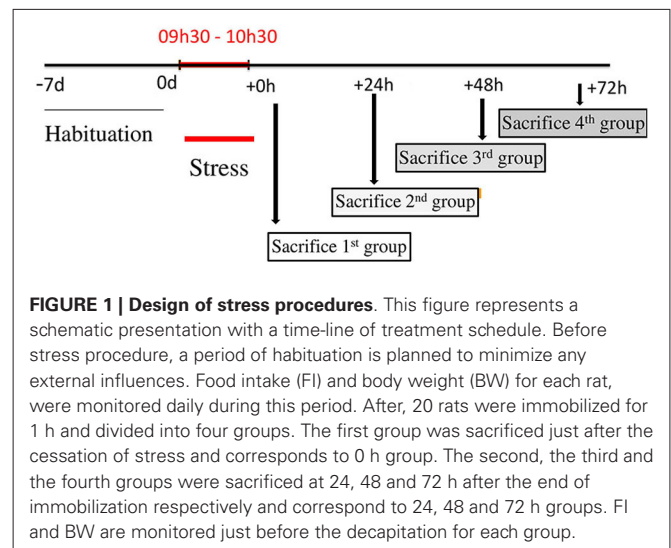


FIGURE 1 | Design of stress procedures. This figure represents a schematic presentation with a time-line of treatment schedule. Before stress procedure, a period of habituation is planned to minimize any external influences. Food intake (FI) and body weight (BW) for each rat, were monitored daily during this period. After, 20 rats were immobilized for 1 h and divided into four groups. The first group was sacrificed just after the cessation of stress and corresponds to 0 h group. The second, the third and the fourth groups were sacrificed at 24, 48 and 72 h after the end of immobilization respectively and correspond to 24, 48 and 72 h groups. FI and BW are monitored just before the decapitation for each group.

rats were sacrificed at identical times of day (Figure 1). Tissue blocks of DVC and hypothalamus were microdissected from each rat brain, dropped in sterile tubes and immediately frozen in liquid nitrogen. BW of each animal was measured daily, beginning 1 week before stress and up to sacrifice.

CONTROL OF FOOD INTAKE

FI was measured daily both in controls and stressed animals. Rats were given in excess a known quantity of chow and the amount of food eaten was calculated by subtracting the remaining amount of chow from the original amount provided to the rats. Chow spillage was carefully calculated and accounted for in the measurements. The measurements were made just before stress, 24, 48 and 72 h after stress.

CONTROL OF BODY WEIGHT GAIN

After 1 week of accommodation, experimental animals were assigned to *ad libitum* feeding, BWs of both control and rats destined to be stressed, were assessed daily, 72, 48 and 24 h before stress application. The BWs of all rats were measured at the same time of the day, and just before the stress session on the day of immobilization stress, 24, 48 and 72 h after stress.

FECAL PELLETT

The number of fecal pellets production during immobilization session has been counted and compared to production in controls.

RNA EXTRACTIONS

Total RNA were extracted from different tissue samples obtained from hypothalamus and DVC. Each frozen tissue block was homogenized on ice in 500 μ L TRIzol^R reagent (Life Technologies, Cergy-Pontoise, France) and RNA was extracted according to the manufacturer's instructions. Extracted RNA was resuspended in 20 μ L DEPC-treated distilled water. RNA concentration and purity were evaluated by spectrometry at 260 and 280 nm on 1 μ L aliquots and RNA extracts were kept frozen until use. For protein extraction, each frozen sample was homogenized on ice in

Table 1 | PCR parameters for amplification of NPY, AgRP, POMC, CART mRNAs under basal conditions.

Transcript	Sequence (3'-5') forward (f) and reverse (r)	Product size (bp)	[Mg ²⁺] (mM)	Annealing temperature	Number of cycles	Genbank accession number
NPY	f: gcc atg atg cta ggt aac aaa r: tct ctt gcc ata tct ctg tct	214	1.5	55°C	30	M20373
AgRP	f: gct gca gaa ggc aga agc r: tga aga agc gg v agt agc ac	152	1.5	58°C	35	AF206017
POMC	f: cgg ccc cag aaa cag cag cag t r: ggg ccc gtc ggc ctt ctc g	304	1.5	66°C	30	NM_139226
CART	f: gat cgg gaa gct gtg tga ct r: att ttg aag cag cag gga aa	208	1.5	56°C	31	NM_017110

100 μ l lysis buffer (137 mM NaCl, 20 mM TrisHCl, 1 mM sodium orthovanadate, 1% Triton X100, 10% glycerol, 1 mM EDTA, 1 mM PMSF, protease inhibitor cocktail, pH 8) and incubated for 30 min on ice. Homogenates were then cleared by centrifugation (10,000 rpm for 30 min at 4°C). Proteins were quantified using the Bradford assay (BioRad, Marnes-la-Coquette, France), and each sample was adjusted to 1 μ g/ μ l with ultra-pure water, mixed to equal volumes of 2X Laemmli buffer. Extracted proteins were denatured by heat at 70°C for 3 min and then kept frozen until use.

RT-PCR

Single-stranded cDNAs were synthesized using 2 μ g of total RNA of tissue samples by reverse transcription in a total volume of 20 μ L using 200U of M-MLV reverse transcriptase (Promega, Madison, WI, USA), 5 μ M random hexanucleotide (Promega), 0.2 mM dNTP (Amersham, Saclay, France), and 1X manufacturer's RT buffer. Specific genes were amplified in a 20 μ L reaction mixture containing 2.5 U/ μ L Taq polymerase (Promega), 0.1 μ M dNTP (Amersham), 1.5–2.5 mM MgCl₂ (see **Table 1**), 1 μ M specific primer pair (Invitrogen, Cergy-Pontoise, France, **Table 1**) 1X manufacturer's Taq buffer, and 1 μ l cDNA through a PCR program including one DNA denaturation step (4 min at 95°C), 30–35 cycles consisting of DNA denaturation (45 s at 95°C)—primer hybridization (30 s at optimal temperature)—elongation (1 min 30 s at 72°C), and a final elongation step (10 min at 72°C). Primers and PCR program used in the amplification of genes are presented in **Table 1**. PCR products were separated by electrophoresis on 1% agarose gel stained with ethidium bromide and then visualized under UV light connected to a computer-assisted analyzer (GelDoc, Biorad, Marnes-la-Coquette, France). Optical densities (OD) of PCR products were measured and normalized to OD values from β -actin PCR of the corresponding cDNAs.

STATISTICAL ANALYSIS

The results are expressed as mean \pm standard error of the means (S.E.M). The results were analyzed by one-way ANOVA followed by post-hoc analysis using Tukey tests. $p < 0.05$ was considered statistically significant.

RESULTS

EFFECTS OF 1 H IMMOBILIZATION ON FOOD INTAKE

Cumulated daily FI was reduced significantly following 24 h after the cessation of stress (16.2 ± 0.8 vs. 20.4 ± 1.3 , $p < 0.001$;

Figure 2A). This relative hypophagia in stressed rats was no longer observed after 48 h of stress (**Figure 2A**).

EFFECTS OF 1 H IMMOBILIZATION ON RAT'S BODY WEIGHT

As depicted in **Figure 2B**, no differences were seen in BW gain levels between unstressed and stressed rats, over the course of the period preceding the experiment. Both groups of rats gained weight at a steady rate. However, as expected, during the 24 h following the stress application, the stressed animals showed a significant decrease in their BW gain (-2.2 ± 0.7 g; $n = 5$; $p < 0.001$) compared with the important BW gain recorded for control rats (8.1 ± 0.6 g; $n = 5$). However, at 48 h post stress period, a slight increase in BW was observed in stressed animals but below control values (**Figure 1B**).

EFFECTS OF STRESS ON FECAL PELLETS

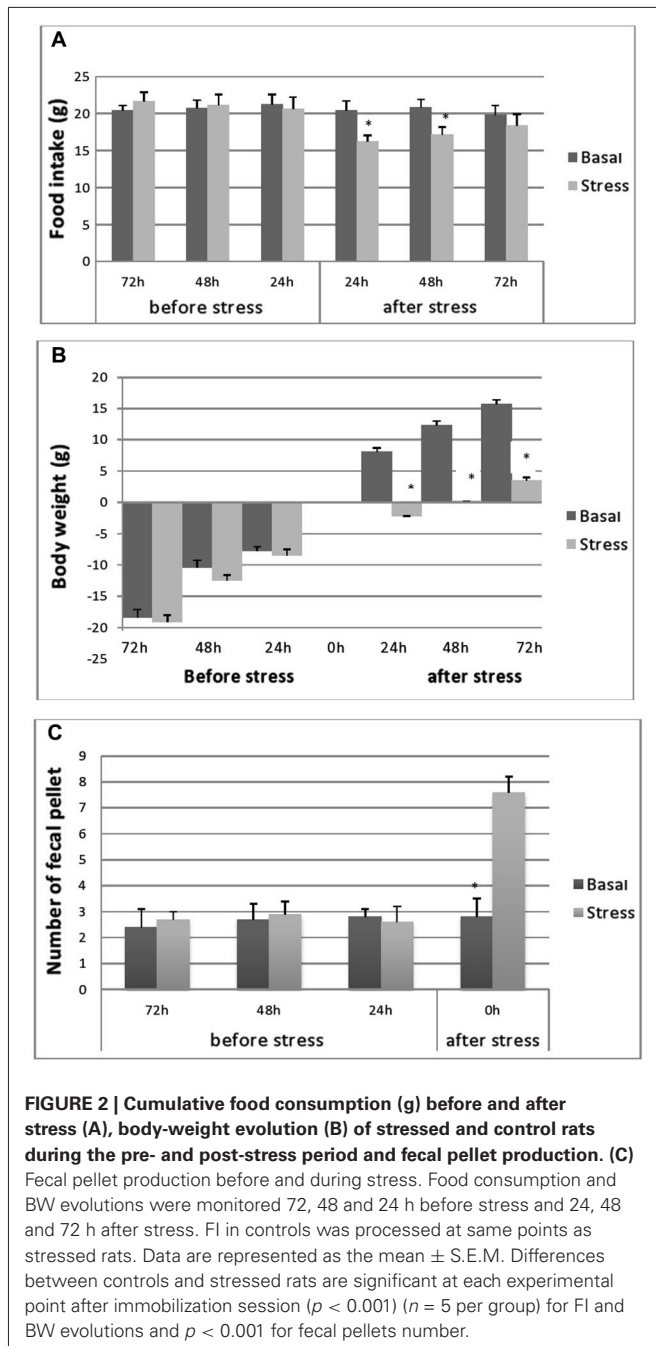
Fecal pellet output (i.e., the number of fecal pellets produced) during each stress session was significantly higher in immobilized rats (7.25 ± 1.01) compared to controls (2.59 ± 0.66) ($p < 0.01$) (**Figure 2C**).

DIFFERENT REGULATION OF OREXIGENIC AND ANOREXIGENIC PEPTIDES

To evaluate eventual variations in the expression of genes encoding the different peptides after stress exposure, their levels were determined relative to that of β -actin mRNA. In all groups, significant amounts of each peptide (NPY, AgRP, POMC and CART) mRNA were detected in the adult rat hypothalamus (**Figure 3**). Furthermore, we show the presence of important levels of peptides mRNA in the microdissected DVC of adult rat (**Figure 4**).

In general, the effect of stress on the expression level of four peptides, showed similar patterns especially, in the hypothalamus. A significant increase in gene expression was observed for hypothalamic NPY and CART gene. This increase was observed immediately after the termination of the stress session and up to 72 h post stress. However, the NPY transcript levels in stressed animals were not significantly different from the controls (**Figure 3**). Hypothalamic POMC mRNA profile mimics partially the two precedent patterns, a significant increase in POMC transcript was observed up to 24 h post stress (**Figure 3**; $p < 0.05$). Finally, the AgRP expression increased significantly at 24 h and to a lesser extent at 72 h post stress (**Figure 3**; $p < 0.05$).

With regard to DVC, a general similar pattern post stress evolution of the mRNA peptides level was observed for the peptides analyzed. A substantial and significant increase was observed



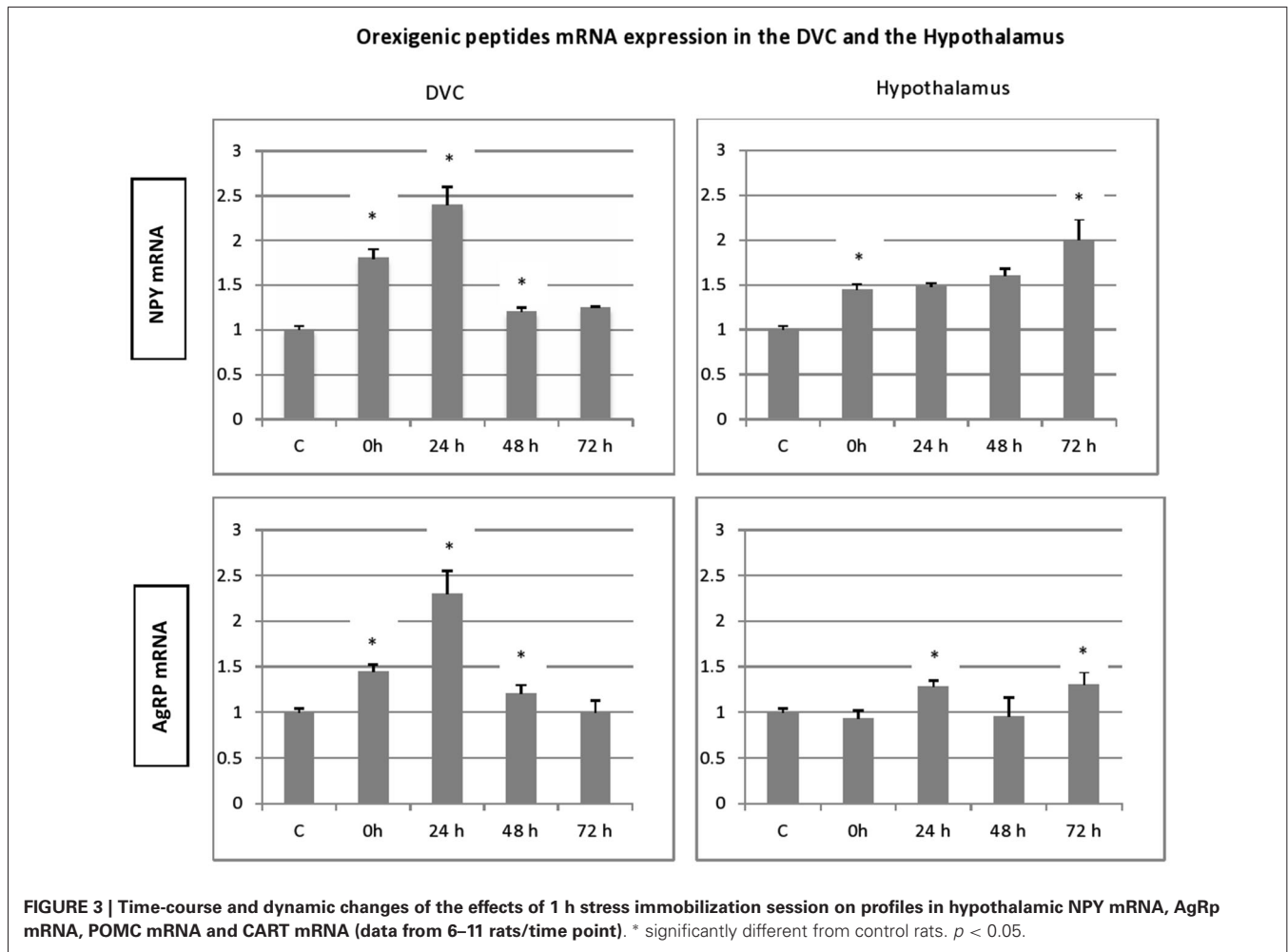
particularly at 24 h post stress, and a decline in the up regulation was noticed at 48 and 72 h post stress. A striking similarity between the patterns of expression of the genes encoding the two orexigenic peptides was observed (Figure 3). The mRNA of both NPY and AgRP increase significantly just after the end of 1 h immobilization session and the increase became more important at 24 h after stress (Figure 3; $p < 0.01$). In contrast to NPY and AgRP, the expression of POMC failed to increase after the end of stress but showed a strong and significant elevation at 24 h, the highest one of the four peptides analyzed (Figure 4; $p < 0.01$). CART expression respects the general post stress mRNA peptides

evolution in that it increases at 0 and 24 ($p < 0.01$ at 24 h). However, at 48 and 72 h post stress period, the profile differs from that observed for the other peptides. Indeed, there was a clear and significant down regulation of CART expression compared to NPY, AgRP and POMC (Figure 4; $p < 0.01$ at 48 h and $p < 0.001$ at 72 h).

DISCUSSION

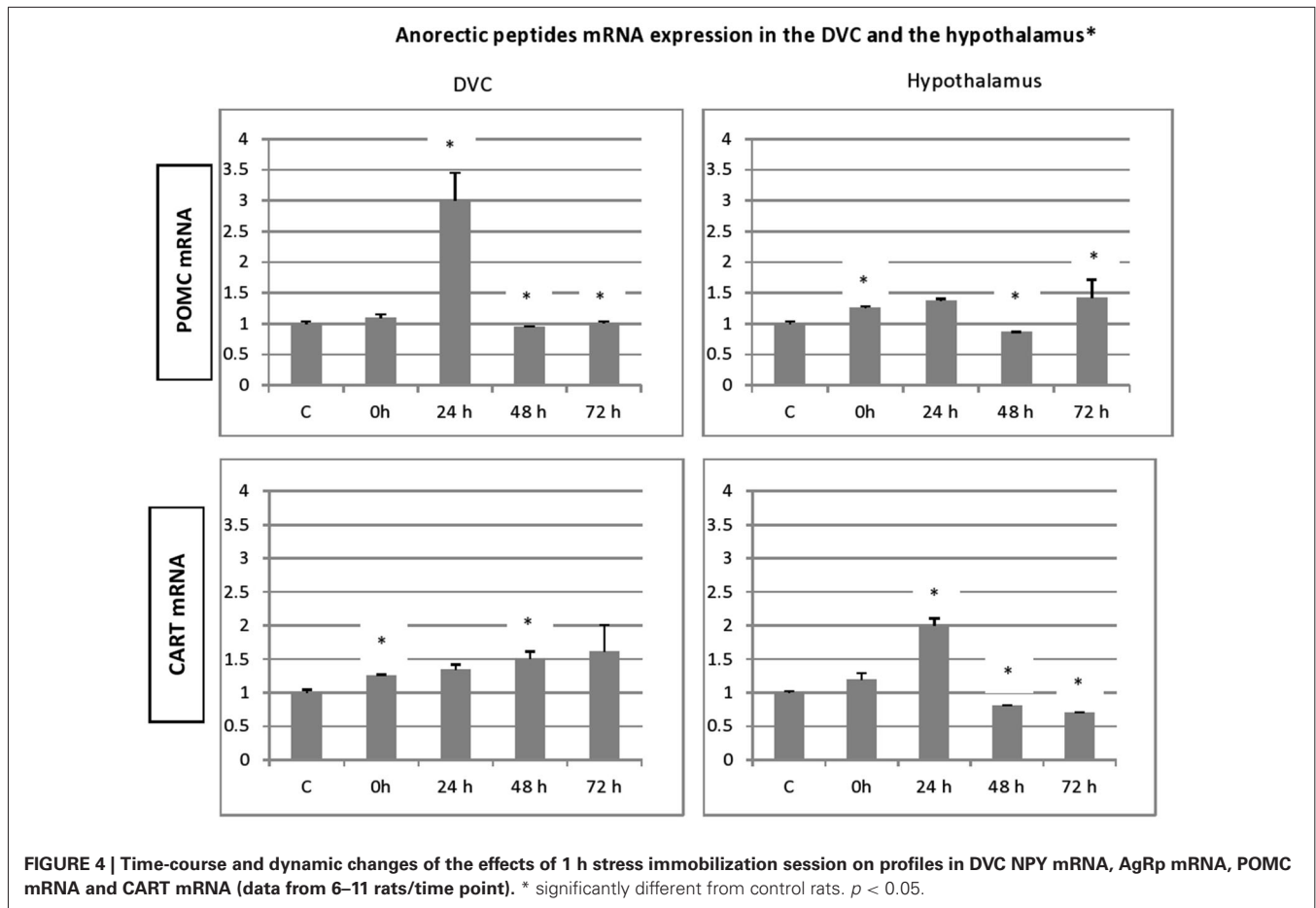
The aim of the present study was to evaluate if acute immobilization stress in adult rat has long lasting effects on FI regulation. The results demonstrated that the application of acute immobilization stress (1 h) increased significantly the expression level of the four peptides studied in the hypothalamus and DVC regions. Both orexigenic (NPY and AgRP) and anorexigenic (CART and POMC) genes were up regulated principally at 24 h post stress. Concomitantly, acutely immobilized rats showed a substantial decrease in BW and FI, especially at 24 h post stress. These two parameters were monitored in order to determine whether these FI indicators were related to the expression of the genes encoding the orexigenic and anorexigenic peptides. Taken together, the differences in signaling and behavior suggest that systems involved in the regulation of the stress response and of energy balance are highly integrated. We assessed the post stress period as this phase shows high sensitivity to environmental changes, a long-lasting sensitisation of the hypothalamo-pituitary-adrenal (HPA) axis and corresponds to the recovery period (Dal-Zotto et al., 2004). The present observations showing significant variations in the tissue contents of orexigenic and anorexigenic peptides were related specifically to acute immobilization stress. Indeed, the protocol schedules we used have minimized the effects of handling and eliminated any other artifacts by standardizing the experiments before brain dissection.

Our results showed that 1 h immobilization stress affects differentially the amplitude and the direction of gene expression changes depending on the post period point and the brain region investigated, although in all cases, an up regulation of the gene expression of each peptide was observed 24 h after the cessation of stress session. This may indicate that at this experimental point corresponding to the “day after”, profound changes occur in the regulatory control of FI, in support of this assertion the marked decrease in BW gain and FI amount recorded. Nevertheless, hypothalamus and DVC display different responses to stress. The hypothalamus is more sensitive to stress effect as just after the termination of immobilization and except for AgRP, the gene expressions of NPY, POMC and CART are up regulated. In DVC, only the expressions of orexigenic peptides investigated are up regulated. This stress sensitivity in hypothalamus could be explained at least in part by the mobilization of the HPA axis notably via the actions of glucocorticoids (GCs). This system also regulates feeding responses as the neural circuits regulating FI converge on the PVN containing corticotrophin releasing hormone (CRH) neurons (the primary target for initiating a stress response). CRH is not only the major regulator of pituitary-adrenal axis, but it is also involved in energy homeostasis, processing catabolic effects, restraining FI and activating sympathetic nervous system (Fulton et al., 2002; Guillemin, 2005). Interestingly, the interaction between



GCs and feeding related neuropeptides such as NPY, CART, AgRP and POMC has been well documented (Savontaus et al., 2002; Germano et al., 2007). Thus, a surge of GCs results in an increase in the expression of these neuropeptides at least in hypothalamus. Furthermore, the presence of GC receptors within NPY/AgRP and POMC/CART neurons suggest a direct role of corticosterone on these neurons. It is known that GCs levels rise at 15 min after the beginning of the immobilization stress (Rage et al., 2002; Marmigère et al., 2003) and this peak could be sufficient to stimulate the expression of peptides during or at the end of stress session giving an explanation to the rise of gene expression observed. The delayed effect on AgRP gene expression could be a result of differential sensitivity of AgRP neurons although, co-localized exclusively with NPY in the arcuate nucleus (Broberger et al., 1998). AgRP is more important during conditions of high energy requirements under which it has been shown to be more highly expressed (Sorensen et al., 2002) as in the period of 24 h post stress, where an anorexia-like state has been occurred. Of interest, stimulation of AgRP neurons profoundly increased FI and decreased energy expenditure (Aponte et al., 2011), leading to a recovery of control conditions. Furthermore, stimulation of AgRP in the absence of food increased locomotor

activity indicating that the neuropeptide could be involved in the regulation of motivations associated with food-seeking behaviors (Sohn and Williams, 2012). Another alternative explanation is the possible involvement of the melanocortin pathway as it has been shown that AgRP suppression of POMC-derived melanocortin signaling has been widely considered as a pathway through which these neurons could rapidly increase feeding behavior (Cowley, 2003). Thus, the increase of DVC AgRP gene expression just after the termination of stress up to 24 h before POMC gene expression suggests that AgRP system drive the expression of the POMC to attenuate the ongoing established anorexia state. Another discrepancy between hypothalamus and DVC is illustrated by the post-stress pattern of gene expressions in the two structures. Whereas they show a marked peak in the DVC at 24 h post stress followed by a gradual decrease, they display a gradual increase up to 72 h post stress in the hypothalamus, particularly for NPY and CART expressions. This could reflect a stress neuroendocrine regulation as we stressed above about GCs action on these two neuropeptides which in turn have been reported to stimulate CRF and increase plasma ACTH and corticosterone following stress (Suda et al., 1993; Stanley et al., 2001). This last situation underlies behavioral adaptation,



storage of energy and information processing to prepare for future events (De Kloet, 2004). The increase in NPY expression may be also a response to the anxiogenic-like effects on stress response (Kim et al., 2003) as the peptide is negatively correlated with anxiety symptoms (Heilig et al., 1989). In this sense, NPY will act as a stress buffer to counteract anxiogenic effects of stress (Heilig et al., 1994). Of interest, single intranasal NPY infusion attenuates development Post-Traumatic Stress Disorder: PTSD-like symptoms to traumatic stress in rat (Serova et al., 2013). The fact that the magnitude of up regulation is more marked in hypothalamus than in the DVC, could be explained by the occurrence of high peptide containing neurons levels in the hypothalamus compared to the brainstem structure (Heilig and Widerlöv, 1995), although these project to the CRH hypothalamic paraventricular neurons (Liposits et al., 1988). Taken together, the resemblance of NPY expression responses observed in these two structures could indicate that the severe physiologic stress used in these investigations appears to trigger brainstem/circumventricular organ systems that project directly to the paraventricular nucleus.

With regard to CART, an equivalent pattern to that observed for NPY gene expression is present in hypothalamus. This continuous vigorous over-expression could reflect a strong response of the anorexigenic peptide to stress (notably via their stimulation by GCs), establishing an anorexia-like state by inhibiting FI.

An elevation in hypothalamic CART gene expression has also been reported to coincide with the onset of short day anorexia in hibernating Siberian hamster (Adam et al., 2000). In line of this, central administration of CART has been reported previously to inhibit FI (Vrang et al., 1999). For this, it would seem logical that the actions of CART following stress are anorectic and trigger in turn equivalent reaction of NPY to counteract these effects. On the other hand, it is noteworthy that important increase in CART expression (48–72 h post stress) is associated with a recovery of normal BW and FI suggesting the involvement of the peptide in energy homeostasis (Smith et al., 2008) and possible orexigenic role (Abbott et al., 2001; Kong et al., 2003). This passes via an interaction with CB1 receptors (Cota et al., 2003; Yu et al., 2008). With regard to DVC signaling responses following stress, peptide expression pattern differs significantly from that observed in the hypothalamus. Stress leads to a down regulation observed at 48 h post stress time following a rapid up regulation period, which may suggest that acute CART induction might trigger immobilization-induced anorexia principally at the hypothalamus, as a FI regulation center and at a lesser degree at the satiety-reflex-integrating DVC. This phase of down regulation could correspond to the inhibition of a tonic satiety-enhancing mechanism as suggested for another anorexigenic peptide the BDNF (Lebrun et al., 2006). Therefore, immobilization-induced modulations of CART expression

in hypothalamus and DVC would not be a downstream effect of peripheral stress response, but would more likely result from an intracerebral pathway upstream of the neuroendocrine axis, which seems in accordance with the psychological quality of immobilization.

It is certain that NPY and CART interact with other factors to modulate stress responses. In this sense, it is interesting to note that expressions of AgRP (an orexigenic peptide) and POMC (an anorexigenic peptide) were also up regulated following immobilization in the hypothalamus although they do not exceed 24 h post stress. Thus, it is not excluded that AgRP could potentiate NPY action as POMC could do to CART action. These concomitant actions in anorexigenic and orexigenic peptides could contribute to the fine tuning of homeostasis regulation. Thus, any deregulation of these actions, by an excess simultaneous secretion of the components or a non adequate integration of NPY and AgRP signals (Kas et al., 2005) for example, could lead to a blurred signal which could be fatal during the recovery period and may lead to an irreversible pathological state as the installation of anorexia nervosa (Inui, 2001).

In summary, differences in neuropeptides expression in response to stress could reflect gene function regulation as adaptive behavioral responses to environmental events. Any disturbance at this level could contribute to the development of eating disorders. It remains to be investigated whether similar changes will be observed at the protein level and neuropeptide release.

ACKNOWLEDGMENTS

This work was supported by GDRI NEURO CNRS/INSERM/CNRST (France/Morocco), NEUROMED FP7 Project and PICS CNRS/CNRST (Marseille/Beni-Mellal).

REFERENCES

- Abbott, C. R., Rossi, M., Wren, A. M., Murphy, K. G., Kennedy, A. R., Stanley, S. A., et al. (2001). Evidence of an orexigenic role for cocaine- and amphetamine-regulated transcript after administration into discrete hypothalamic nuclei. *Endocrinology* 142, 3457–3463. doi: 10.1210/en.142.8.3457
- Adam, T. C., and Epel, E. S. (2007). Stress, eating and the reward system. *Physiol. Behav.* 91, 449–458. doi: 10.1016/j.physbeh.2007.04.011
- Adam, C. L., Moar, K. M., Logie, T. J., Ross, A. W., Barrett, P., Morgan, P. J., et al. (2000). Photoperiod regulates growth, puberty and hypothalamic neuropeptide and receptor gene expression in female Siberian hamsters. *Endocrinology* 141, 4349–4356. doi: 10.1210/en.141.12.4349
- Aponte, Y., Atasoy, D., and Sternson, S. M. (2011). AGRP neurons are sufficient to orchestrate feeding behavior rapidly and without training. *Nat. Neurosci.* 14, 351–355. doi: 10.1038/nn.2739
- Bariohay, B., Lebrun, B., Moysé, E., and Jean, A. (2005). Brain-derived neurotrophic factor plays a role as an anorexigenic factor in the dorsal vagal complex. *Endocrinology* 146, 5612–5620. doi: 10.1210/en.2005-0419
- Benyassi, A., Gavalda, A., Armario, A., and Arancibia, S. (1993). Role of somatostatin in the acute immobilization stress-induced GH decrease in rat. *Life Sci.* 52, 361–370. doi: 10.1016/0024-3205(93)90149-W
- Berthoud, H. R., Sutton, G. M., Townsend, R. L., Patterson, L. M., and Zheng, H. (2006). Brainstem mechanisms integrating gut-derived satiety signals and descending forebrain information in the control of meal size. *Physiol. Behav.* 89, 517–524. doi: 10.1016/j.physbeh.2006.08.018
- Bouret, S. G., Draper, S. J., and Simerly, R. B. (2004). Trophic action of leptin on hypothalamic neurons that regulate feeding. *Science* 304, 108–110. doi: 10.1126/science.1095004
- Broberger, C., Johansen, J., Johansson, C., Schalling, M., and Hokfelt, T. (1998). The neuropeptide Y/agouti gene-related protein (AGRP) brain circuitry in normal, anorectic and monosodium glutamate-treated mice. *Proc. Natl. Acad. Sci. U S A* 95, 15043–15048. doi: 10.1073/pnas.95.25.15043
- Chaplin, T. M., Hong, K., Bergquist, K., and Sinha, R. (2008). Gender differences in response to emotional stress: an assessment across subjective, behavioral and physiological domains and relations to alcohol craving. *Alcohol. Clin. Exp. Res.* 32, 1242–1250. doi: 10.1111/j.1530-0277.2008.00679.x
- Charrier, C., Chigr, F., Tardivel, C., Mahaut, S., Jean, A., Najimi, M., et al. (2006). BDNF regulation in the rat dorsal vagal complex during stress-induced anorexia. *Brain Res.* 1107, 52–57. doi: 10.1016/j.brainres.2006.05.099
- Cone, R. D. (2005). Anatomy and regulation of the central melanocortin system. *Nat. Neurosci.* 8, 571–578. doi: 10.1038/nn1455
- Cota, D., Marsicano, G., Lutz, B., Vicennati, V., Stalla, G. K., Pasquali, R., et al. (2003). Cannabinoid system as a modulator of food intake. *Int. J. Obes. Relat. Metab. Disord.* 27, 289–301. doi: 10.1038/sj.ijo.0802250
- Cowley, M. A. (2003). Hypothalamic melanocortin neurons integrate signals of energy state. *Eur. J. Pharmacol.* 480, 3–11. doi: 10.1016/j.ejphar.2003.08.087
- Dal-Zotto, S., Martí, O., Delgado, R., and Armario, A. (2004). Potentiation of glucocorticoid release does not modify the long-term effects of a single exposure to immobilization stress. *Psychopharmacology (Berl)* 177, 230–237. doi: 10.1007/s00213-004-1939-y
- De Kloet, E. R. (2004). Hormones and the stressed brain. *Ann. N Y Acad. Sci.* 1018, 1–15. doi: 10.1196/annals.1296.001
- Ellacott, K. L., Halatchev, I. G., and Cone, R. D. (2006). Interactions between gut peptides and the central melanocortin system in the regulation of energy homeostasis. *Peptides* 27, 340–349. doi: 10.1016/j.peptides.2005.02.031
- Fan, W., Ellacott, K. L., Halatchev, I. G., Takahashi, K., Yu, P., and Cone, R. D. (2004). Cholecystokinin-mediated suppression of feeding involves the brainstem melanocortin system. *Nat. Neurosci.* 7, 335–336. doi: 10.1038/nn1214
- Fulton, S., Richard, D., Woodside, B., and Shizgal, P. (2002). Interaction of CRH and energy balance in the modulation of brain stimulation reward. *Behav. Neurosci.* 116, 651–659. doi: 10.1037//0735-7044.116.4.651
- Germano, C. M., de Castro, M., Rorato, R., Laguna, M. T., Antunes-Rodrigues, J., Elias, C. F., et al. (2007). Time course effects of adrenalectomy and food intake on cocaine- and amphetamine-regulated transcript expression in the hypothalamus. *Brain Res.* 1166, 55–64. doi: 10.1016/j.brainres.2007.05.077
- Guillemin, R. (2005). Hypothalamic hormones a.k.a. hypothalamic releasing factors. *J. Endocrinol.* 184, 11–28. doi: 10.1677/joe.1.05883
- Hamer, M., and Stamatakis, E. (2008). Inflammation as an intermediate pathway in the association between psychosocial stress and obesity. *Physiol. Behav.* 94, 536–539. doi: 10.1016/j.physbeh.2008.03.010
- Harris, R. B., Mitchell, T. D., Simpson, J., Redmann, S. M. Jr., Youngblood, B. D., and Ryan, D. H. (2002). Weight loss in rats exposed to repeated acute restraint stress is independent of energy or leptin status. *Am. J. Physiol. Regul. Integr. Comp. Physiol.* 282, R77–R88.
- Heilig, M., Koob, G. F., Ekman, R., and Britton, K. T. (1994). Corticotropin-releasing factor and neuropeptide Y: role in emotional integration. *Trends Neurosci.* 17, 80–85. doi: 10.1016/0166-2236(94)90079-5
- Heilig, M., Söderpalm, B., Engel, J. A., and Widerlöv, E. (1989). Centrally administered neuropeptide Y (NPY) produces anxiolytic-like effects in animal anxiety models. *Psychopharmacology (Berl)* 98, 524–529. doi: 10.1007/bf00441953
- Heilig, M., and Widerlöv, E. (1995). Neurobiology and clinical aspects of neuropeptide Y. *Crit. Rev. Neurobiol.* 9, 115–136.
- Houpt, T. A. (2000). Molecular neurobiology of ingestive behavior. *Nutrition* 16, 827–836. doi: 10.1016/s0899-9007(00)00420-2
- Inui, A. (2001). Eating behavior in anorexia nervosa—an excess of both orexigenic and anorexigenic signalling? *Mol. Psychiatry* 6, 620–624. doi: 10.1038/sj.mp.4000944
- Kas, M. J., Bruijnzeel, A. W., Haanstra, J. R., Wiegant, V. M., and Adan, R. A. (2005). Differential regulation of agouti-related protein and neuropeptide Y in hypothalamic neurons following a stressful event. *J. Mol. Endocrinol.* 35, 159–164. doi: 10.1677/jme.1.01819
- Kim, H., Whang, W. W., Kim, H. T., Pyun, K. H., Cho, S. Y., Hahm, D. H., et al. (2003). Expression of neuropeptide Y and cholecystokinin in the rat brain by chronic mild stress. *Brain Res.* 983, 201–208. doi: 10.1016/s0006-8993(03)03087-7
- Kong, W. M., Stanley, S., Gardiner, J., Abbott, C., Murphy, K., Seth, A., et al. (2003). A role for arcuate cocaine and amphetamine-regulated transcript in hyperphagia, thermogenesis and cold adaptation. *FASEB J.* 17, 1688–1690. doi: 10.1096/fj.02-0805fe

- Kvetnansky, R., and Mikulaj, L. (1970). Adrenal and urinary catecholamines in rats during adaptation to repeated immobilization stress. *Endocrinology* 87, 738–743. doi: 10.1210/endo-87-4-738
- Laurent, L., Jean, A., Manrique, C., Najimi, M., Chigr, F., and Compan, V. (2013). “Anorexia and drugs of abuse abnormally suppress appetite, the result of a shared molecular signal foul-up,” in *Animal Model Of Eating Disorders*, ed N. M. Avena (Philadelphia, PA: Springer Book, Humana Press), 319–331.
- Lebrun, B., Bariohay, B., Moysé, E., and Jean, A. (2006). Brain-derived neurotrophic factor (BDNF) and food intake regulation: a minireview. *Auton. Neurosci.* 126–127, 30–38. doi: 10.1016/j.autneu.2006.02.027
- Liposits, Z., Sievers, L., and Paull, W. K. (1988). Neuropeptide-Y and ACTH-immunoreactive innervation of corticotropin releasing factor (CRF)-synthesizing neurons in the hypothalamus of the rat. An immunocytochemical analysis at the light and electron microscopic levels. *Histochemistry* 88, 227–234.
- Manni, L., Di Fausto, V., Fiore, M., and Aloe, L. (2008). Repeated restraint and nerve growth factor administration in male and female mice: effect on sympathetic and cardiovascular mediators of the stress response. *Curr. Neurovasc. Res.* 5, 1–12. doi: 10.2174/156720208783565654
- Marmigère, F., Givalois, L., Rage, F., Arancibia, S., and Tapia-Arancibia, L. (2003). Rapid induction of BDNF expression in the hippocampus during immobilization stress challenge in adult rats. *Hippocampus* 13, 646–655. doi: 10.1002/hipo.10109
- Morton, G. J., Cummings, D. E., Baskin, D. G., Barsh, G. S., and Schwartz, M. W. (2006). Central nervous system control of food intake and body weight. *Nature* 443, 289–295. doi: 10.1038/nature05026
- Pinto, S., Roseberry, A. G., Liu, H., Diano, S., Shanabrough, M., Cai, X., et al. (2004). Rapid rewiring of arcuate nucleus feeding circuits by leptin. *Science* 304, 110–115. doi: 10.1126/science.1089459
- Quick, S. K., Shields, P. G., Nie, J., Platek, M. E., McCann, S. E., Hutson, A. D., et al. (2008). Effect modification by catalase genotype suggests a role for oxidative stress in the association of hormone replacement therapy with postmenopausal breast cancer risk. *Cancer Epidemiol. Biomarkers Prev.* 17, 1082–1087. doi: 10.1158/1055-9965.epi-07-2755
- Rage, F., Givalois, L., Marmigère, F., Tapia-Arancibia, L., and Arancibia, S. (2002). Immobilization stress rapidly modulates BDNF mRNA expression in the hypothalamus of adult male rats. *Neuroscience* 112, 309–318. doi: 10.1016/s0306-4522(02)00072-6
- Savontaus, E., Conwell, I., and Wardlaw, S. (2002). Effects of adrenalectomy on AGRP, POMC, NPY and CART gene expression in the basal hypothalamus of fed and fasted rats. *Brain Res.* 958, 130–138. doi: 10.1016/s0006-8993(02)03674-0
- Schwartz, M. W., Woods, S. C., Porte, D. Jr., Seeley, R. J., and Baskin, D. G. (2000). Central nervous system control of food intake. *Nature* 404, 661–671. doi: 10.1038/35007534
- Serova, L. I., Laukova, M., Alaluf, L. G., and Sabban, E. L. (2013). Intranasal infusion of melanocortin receptor four (MC4R) antagonist to rats ameliorates development of depression and anxiety related symptoms induced by single prolonged stress. *Behav. Brain Res.* 250, 139–147. doi: 10.1016/j.bbr.2013.05.006
- Smith, K. L., Gardiner, J. V., Ward, H. L., Kong, W. M., Murphy, K. G., Martin, N. M., et al. (2008). Overexpression of CART in the PVN increases food intake and weight gain in rats. *Obesity (Silver Spring)* 16, 2239–2244. doi: 10.1038/oby.2008.366
- Sohn, J. W., and Williams, K. W. (2012). Functional heterogeneity of arcuate nucleus pro-opiomelanocortin neurons: implications for diverging melanocortin pathways. *Mol. Neurobiol.* 45, 225–233. doi: 10.1007/s12035-012-8240-6
- Sorensen, A., Adam, A. L., Findlay, P. A., Marie, M., Thomas, L., Travers, M. T., et al. (2002). Leptin secretion and hypothalamic neuropeptide and receptor gene expression in sheep. *Am. J. Physiol. Regul. Integr. Comp. Physiol.* 282, R1227–R1235. doi: 10.1152/ajpregu.00595.2001
- Stanley, S. A., Small, C. J., Murphy, K. G., Rayes, E., Abbott, C. R., Seal, L. J., et al. (2001). Actions of cocaine- and amphetamine-regulated transcript (CART) peptide on regulation of appetite and hypothalamo-pituitary axes in vitro and in vivo in male rats. *Brain Res.* 893, 186–194. doi: 10.1016/s0006-8993(00)03312-6
- Suda, T., Tozawa, F., Iwai, I., Sato, Y., Sumitomo, T., Nakano, Y., et al. (1993). Neuropeptide Y increases the corticotropin-releasing factor messenger ribonucleic acid level in the rat hypothalamus. *Brain Res. Mol. Brain Res.* 18, 311–315. doi: 10.1016/0169-328x(93)90094-6
- Vallès, A., Martí, O., García, A., and Armario, A. (2000). Single exposure to stressors causes long-lasting, stress-dependent reduction of food intake in rats. *Am. J. Physiol. Regul. Integr. Comp. Physiol.* 279, R1138–R1144.
- Vrang, N., Tang-Christensen, M., Larsen, P. J., and Kristensen, P. (1999). Recombinant CART peptide induces c-Fos expression in central areas involved in control of feeding behaviour. *Brain Res.* 818, 499–509. doi: 10.1016/s0006-8993(98)01349-3
- Wirtz, P. H., Redwine, L. S., Baertschi, C., Spillmann, M., Ehlert, U., and von Känel, R. (2008). Coagulation activity before and after acute psychosocial stress increases with age. *Psychosom. Med.* 70, 476–481. doi: 10.1097/psy.0b013e31816e03a5
- Yu, Y., South, T., Wang, Q., and Huang, X. F. (2008). Differential expression of hypothalamic CART mRNA in response to body weight change following different dietary interventions. *Neurochem. Int.* 52, 1422–1430. doi: 10.1016/j.neuint.2008.03.003

Conflict of Interest Statement: The authors declare that the research was conducted in the absence of any commercial or financial relationships that could be construed as a potential conflict of interest.

Received: 30 April 2014; accepted: 01 July 2014; published online: 18 July 2014.

Citation: Chigr F, Rachidi F, Tardivel C, Najimi M and Moysé E (2014) Modulation of orexigenic and anorexigenic peptides gene expression in the rat DVC and hypothalamus by acute immobilization stress. *Front. Cell. Neurosci.* 8:198. doi: 10.3389/fncel.2014.00198

This article was submitted to the journal *Frontiers in Cellular Neuroscience*.

Copyright © 2014 Chigr, Rachidi, Tardivel, Najimi and Moysé. This is an open-access article distributed under the terms of the Creative Commons Attribution License (CC BY). The use, distribution or reproduction in other forums is permitted, provided the original author(s) or licensor are credited and that the original publication in this journal is cited, in accordance with accepted academic practice. No use, distribution or reproduction is permitted which does not comply with these terms.



Effects of cold exposure on behavioral and electrophysiological parameters related with hippocampal function in rats

Hajar Elmarzouki¹, Youssef Aboussaleh^{1*}, Soner Bitiktas², Cem Suer², A. Seda Artis³, Nazan Dolu² and Ahmed Ahami¹

¹ Laboratory of Nutrition and Health, Department of Biology, Faculty of Science, Ibn Tofail University, Kenitra, Morocco

² Department of Physiology, Erciyes University School of Medicine, Kayseri, Turkey

³ Department of Physiology, Medeniyyet University School of Medicine, İstanbul, Turkey

Edited by:

Marie Z. Mofteh, Alexandria University, Egypt

Reviewed by:

Mohamed Najimi, Sultan Moulay Slimane University, Morocco
Wael Mohamed, Menoufia Medical School, Egypt

*Correspondence:

Youssef Aboussaleh, Laboratory of Nutrition and Health, Department of Biology, Faculty of Science, Ibn Tofail University, Street Bir Rami Est, Kenitra 14000, Morocco
e-mail: abou_85@yahoo.fr

Aim: Behavioral and mental changes may occur in people exposed to cold stress by decreasing their work efficiency and their mental capacity while increasing the number of accidents on the job site. The goal of this study was to explore the effect of cold stress in spatial learning performance excitability and LTP.

Materials and Methods: Three to four month old rats were randomly divided into four groups to form a control group and a cold stress group for each sex. The groups of cold stressed animals were placed in a cold room ambient temperature of 4°C for 2 h day. Adrenal glands and body weight (g) were recorded in control and stressed rats during the cold exposure. Spatial learning (acquisition phase) and memory (probe trial) were tested in the Morris water maze (MWM) immediately after daily exposure. Latency to locate the hidden platform, distance moved (DM), mean distance to platform, swim speed (SS) and time spent in the platform quadrant were compared between genders and treatments. Field potential recordings were made, under urethane anesthesia, from the dentate gyrus (DG) granule-cell layer, with stimulation of the medial perforant pathway 2 h after the probe trial. This study examined spatial memory as measured by MWM performance and hippocampal long-term potentiation (LTP) in the DG after exposure to cold in a repeated stress condition for 2 h/day for 5 days.

Results: The cold-exposed female rats needed less time to find the hidden platform on day 1 (43.0 ± 13.9 s vs. 63.2 ± 13.2 s), day 2 (18.2 ± 8.4 s vs. 40.9 ± 12.2 s) and on day 4 (8.0 ± 2.1 s vs. 17.2 ± 7.0 s) while cold-exposed male rats showed a decreased escape latency (EL) on day 1 only (37.3 ± 12.5 s vs. 75.4 ± 13.1 s). Cold-exposed male rats spent less time in the target quadrant (30.08 ± 6.11%) than the control male rats (37.33 ± 8.89%). Two hour cold exposure decreased population spike (PS) potentiation during both induction (218.3 ± 21.6 vs. 304.5 ± 18.8%) and maintenance intervals (193.9 ± 24.5 vs. 276.6 ± 25.4%) in male rats. Meanwhile cold exposure did not affect the body weight (C: 221 ± 2.5 vs. S: 222 ± 1.7) but it impacts the adrenal gland relative weight (S: 27.1 ± 1.8 mg vs. C: 26.2 ± 1.4 mg).

Conclusion: Overall, the results show that repeated cold exposure can selectively improve spatial learning in adult female rats, but impaired retention memory for platform location in male rats. It is possible that impaired LTP underlies some of the impaired retention memory caused by cold exposure in the male rats.

Keywords: stress, hippocampus, long-term potentiation (LTP), Morris water maze test (MWM), rat

INTRODUCTION

People who live mainly in cold countries and outdoor workers are exposed to hazardous cold stress. Indeed cold may decrease mental capacity attentiveness, work efficiency and increase the number of accidents on the jobsite. Other behavioral alterations

like a reduced mental alertness, craziness and confused behavior were also reported.

From a psychological point of view, cold causes unpleasant thermal sensations or even cold-induced pain, which is experienced as stress. Exposure to stress is associated with an alteration

in learning and memory formation in experimental animals and human subjects (Zheng et al., 2008). Although the performance of stressed animals in a learning task critically depends on the type of stressor, cold as a stressor has been relatively less used. Apart from metabolic stressors such as hypoglycemia, glucopenia, and emotional stressors, which cause adrenaline release by activating the sympatho-adrenomedullary system, cold exposure (as well as pain) causes noradrenaline release from the sympathetic terminals (Kvetnanský et al., 1997; Kvetnansky et al., 2009). Afferent nerves from cold receptors, located in the skin, terminate in the hypothalamus and then multisynaptic pathways reach limbic areas, especially the hippocampus, leading to noradrenaline release (Rintamaki, 2005; Kvetnansky et al., 2009). Considerable evidence supports a close interaction between stress and the noradrenergic system in the hippocampus (Nisenbaum et al., 1991; Britton et al., 1992; Sandi et al., 2005).

The existence of sex differences in the standard rat and mouse models of learning and memory is a controversial topic in the literature. Although a few studies used females to examine the influence of stress on hippocampal functions focusing on gender difference in learning and memory, findings indicate male advantage for rats in radial maze and water maze protocols (Jonasson, 2005). As a general observation, the larger adrenaline responses to stress found in females than in males can be explained by the different hippocampal cognitive ability in both sexes in response to stress. However a similar difference in noradrenaline is rarely observed.

To the best of our knowledge, there is no study examining the effect of intermittent cold stress from behavioral and/or electrophysiological aspects. In the present study we measured the spatial memory performance of adult male and female rats using the Morris water maze (MWM). We also recorded Long-Term Potentiation (LTP) from the dentate gyrus (DG), a model of synaptic plasticity that is thought to underlie learning and memory processes (Bliss and Collingridge, 1993), as an electrophysiological correlate of behavior. Both tests used in this study require hippocampal integrity (Morris et al., 1982; Sutherland et al., 1982) and has been extensively employed in studying the relationship between hippocampal function and spatial learning and memory in rodents (Rosenzweig and Barnes, 2003).

The goal of our study was to explore the effect of cold stress in spatial learning performance excitability and LTP, and the results obtained may explain the behavioral and mental changes that may occur in people exposed to cold.

MATERIALS AND METHODS

ANIMAL CARE

The experiments were conducted in compliance with the guiding principles for the care and use of laboratory animals approved by Erciyes University. In this study, thirty-six male and female rats (3–4 months old) weighing 200–250 g, were randomly divided into four groups to form a control group and a cold stress group for each sex. The groups of cold stressed animals were placed in a cold room (ambient temperature of 4°C) for 2 h/day between 8:00 a.m. and 10:00 a.m. to avoid corticosterone circadian rhythm. The acclimation

of control animals was according to standard animal laboratory conditions (12 h/12 h light/dark cycle, temperature 22°C).

BODY WEIGHT AND ADRENAL GLAND WEIGHT

In order to determine the effect of cold stress procedures, the body weight and the adrenal gland weight were measured in control and stressed rats.

RECTAL TEMPERATURE

We examined changes in rectal temperature due to stress. Rectal temperature was digitized for 1-min with a probe (Biopac) immediately after cold exposure in the stress groups. The mean temperature of 1 min for each rat was averaged.

BEHAVIORAL TESTING

Morris water maze testing

The evaluation of performance in the MWM was used to measure spatial memory. The experiments were realized in a circular, galvanized steel maze (2 m in diameter and 75 cm in depth), which was filled with water at a depth of 50 cm and kept at 22°C. A blue non-toxic dye was added to the water to make it opaque. The maze was placed in a large quiet test room, surrounded by many visual cues external to the maze (some A3 sized posters), which were visible from within the pool and could be used by the rats for spatial orientation. There was no change in the locations of the cues during the period of testing. Four equal quadrants were divided in the pool. In one of the quadrants, a platform (10 cm in diameter) was placed centrally and fixed in a position which was kept constant during the acquisition trials.

An automated video-tracking system (Noldus) recorded the position of the rat in the tank. A camera (TOTA-450III, Japan) was mounted 1.5 m above the surface of the water and was connected to a computer. Light was provided by four 40-W fluorescent lamps, mounted in a square pattern, 1.4 m above the surface of the water (Liu et al., 2006). Each trial was started manually and ended automatically when the rat escaped on the platform. All the trials were completed between 10.00 to 12.00 h (after cold exposure) and the experimenter always stood at the same position to avoid technical bias.

Reference memory. These trials have trained the rats to find a hidden platform and have helped them to remind their constant position throughout the training days; within 120 s. Rats underwent four trials per day for four consecutive days in the reference memory version of the MWM test.

The launch of each rat in the water was slow, and at a random quadrant except the target one that contained the platform. After reaching the platform, the rat was allowed to stay on it for 15 s and was then put back into its cage. If they could not escape to the platform within 120 s by themselves, the rat was placed on the platform by hand for 15 s. The rats were kept in a dry home cage for 60 s during the inter-trial intervals.

Memory consolidation. A probe test was carried out the day after the acquisition phase. The platform was removed and the rats were allowed to swim freely in the pool for 60 s. The degree of memory consolidation acquired after learning was indicated

by the time in seconds spent in the target quadrant, which had contained the hidden platform.

Electrophysiology

Stimulation and recording. Electrophysiological responses are recorded at room temperature (approximately 22°C). The Urethane (1.5 g/kg, ip) was used to anesthetize the rats and they were placed in a stereotaxic frame (Kopf Instruments, Tujunga, CA, USA). The stimulation of the medial perforant path (from bregma, in mm: AP: -7.0, ML: 4.2, DV: 2–2.5 below dura) of the right hemisphere was performed by a bipolar tungsten electrode (stainless steel, Teflon coated, 127 μ m in diameter, insulated except at its tips). The output of a stimulus isolator (World Precision Instruments, USA) was connected to the Stimulating electrode. 3 M NaCl (tip resistance: 2–10 M) was used to fill a glass micropipette (Borosilicate, o.d.: 1.5 mm, 10 cm length, World Precision Instruments). For recording field excitatory postsynaptic potentials (fEPSPs), the glass micropipette was inserted in the granule cell layer of the ipsilateral DG (in mm: AP: 3.5, ML: 2.15, DV: 2.5–3 mm below dura). The reference electrode was positioned under the neck skin (An Ag-AgCl disc electrode).

A head-stage was used to connect the recording and reference electrodes to an amplifier (VCC600 single channel epithelial voltage/current clamp system, Physiological Instruments). A Faraday cage was used to shield the entire system. To obtain a large positive fEPSP, the depth of recording electrode was adjusted, and a superimposed negative-going population spike (PS) was evoked with a 0.1 mm step. After recording a typical response, the final depth of the stimulating electrode was adjusted to maximize the PS amplitude in response to the perforant path stimulation.

To control stimulation and recording the “Scope” program (ADInstruments, Colorado Springs, CO, USA) was used. Monophasic 10 V and 0.175-ms pulses were generated by the A/D board (Powerlab/8SP, ADInstruments, Colorado Springs, CO, USA) of a computer and triggered to a stimulator which was connected to an isolator (Suer et al., 2009). Biological signals were amplified (1000 \times). A pre-amplifier allowed to amplify the biological signals (1000 \times) at a bandwidth of 0.1–10 kHz. Waveforms were digitized on-line at a rate of 40 kHz for 20 ms, displayed on a computer monitor, and stored using Scope for off-line analysis.

Input—Output (I/O) Curve. The stimulation consisting of 175 μ s duration monophasic constant current pulses was delivered once every 20 s for 15 min after electrode placement, and it allowed to obtain an I/O curve. The stimulation current ranged from 0.1 to 1.5 mA. There was an average of three evoked responses for each current value. A sigmoidal curve described the relation between stimulus intensity and the fEPSP slope or PS amplitude; the half maximal stimulus intensity was determined from this curve. The stimulus intensity that produced 50% of the maximum response (i.e., test pulse) was used in subsequent experiments.

Long-term potentiation. Then, after a 15 min baseline recording of the fEPSPs, four sets of tetanic trains (high frequency stimulation: HFS, 100 Hz, 1 s), separated by 5 min intervals at 15, 20, 25 and 30 min, were administered to induce LTP. Following delivery

of the last tetanic train, test stimuli were repeated every 30 s for up to 80 min (Artis et al., 2012).

Data analysis and statistics. The PS amplitude was measured from the first positive peak to the negative peak. The slope of the fEPSP was calculated as the amplitude change at 20–80 t% of the voltage difference between the start of the waveform and the fEPSP amplitude at the onset of PS. During the I/O experiments the maximum value of the fEPSP slope or PS amplitude was evaluated as 100 percent, the EPSP and PS was expressed as the percentage of this value. Analysis of two-way (Treatment: 22°C vs. 4°C \times Gender: male vs. female) ANOVA with repeated measures (Stimulus intensity) was conducted on the EPSP slope and on the PS amplitude.

The mean value of the fEPSP slope or PS amplitude during the first 15-min period (30 sweeps) was evaluated as 100 percent and was defined as the baseline. Each EPSP and each PS was expressed as the percentage of the baseline value (Artis et al., 2012). The increase in EPSP slope and spike amplitude during HFS application (0–15 min) was considered as a measure of the induction of LTP. The remainder of the experiment (15–80 min) serves for the maintenance of LTP. A repeated-measures ANOVA with two between (Treatment \times Gender) and one within (Interval: baseline, induction, and maintenance) subject factor was conducted on the EPSP slope and spike amplitude separately.

Escape latency (EL) was measured as the time in seconds between being placed in the water and finding the hidden platform. Distance moved (DM) was the distance of the swim path between the start location and the hidden platform (Liu et al., 2006). Mean distance from the platform (MDP) was also measured as an indicator of reference memory error, and swim speed (SS) as an indicator of the rat's motor ability over 4 days. Results from the four trials for each training day were averaged for every rat and used for the statistical analysis. Analysis of two-way (Treatment \times Gender) ANOVA with repeated measures (Day) was conducted on the EL, DM, MDP, and SS. Shortened EL, and decreased DM and MDP without changing SS across days was evaluated as outperformed learning performance.

A two factor ANOVA (Treatment \times Gender) was conducted on the means of day 5 (probe trial) in terms of the time spent in the target quadrant and rectal temperature. The degree of memory consolidation which had taken place after learning was indicated by the time spent in the target quadrant.

The comparison between two independent groups was made using an least square difference (LSD) *Post hoc* test. The SPSS statistical software package version 10.0 (SPSS Inc., Chicago, Illinois, USA) performed all statistical analysis.

RESULTS

COLD EXPOSURE DECREASED THE RECTAL TEMPERATURE IN BOTH MALE AND FEMALE RATS

Since we used a 2-h cold exposure to elicit the changes in spatial memory, we measured rectal temperature to determine whether such a stress protocol exerts a similar effect in both sexes. The rectal temperatures of the control male ($n = 9$) and female ($n = 9$) rats were $36.3 \pm 0.31^\circ\text{C}$ and $36.21 \pm 0.29^\circ\text{C}$, respectively. After 2 h exposure to cold, the temperature of the male rats decreased

to $32.73 \pm 1.07^\circ\text{C}$, and that of the female dropped to $32.79 \pm 0.97^\circ\text{C}$. An ANOVA showed significant Treatment Effect ($F_{(1,35)} = 173.261$; $p < 0.001$) with non significant main effect of gender ($F_{(1,35)} = 0.004$; $p = 0.950$) and non significant Interaction Gender \times Treatment ($F_{(1,35)} = 0.047$; $p = 0.787$).

COLD EXPOSURE EFFECT ON BODY WEIGHT AND ADRENAL GLAND WEIGHT

The body weight on the day before cold stress exposure was 210 ± 2.3 g in the control group and 214 ± 2.9 g in the stressed group. Data are represented as the mean S.E.M. of body-weight measured at 09:00 h daily before the cold exposure. Differences between controls and stressed rats are not statistically significant at each experimental ($P < 0.07$; $n = 7$ per group; **Figure 1**; Day 1: 216 ± 2.1 vs. 218 ± 2.5 ; Day 2: 221 ± 2.5 vs. 222 ± 1.7 ; Day 3: 228 ± 1.6 vs. 227 ± 3.3 ; Day 4: 234 ± 2.1 vs. 232 ± 2.4 ; Day 5: 241 ± 2.7 vs. 236 ± 2.2 ; Day 6: 247 ± 2.9 vs. 242 ± 2.8). This p nearing 0.05 however seem to suggest that increasing the number of observations the difference could be relevant.

Daily exposure to 2 h cold for 5 days resulted in an insignificant increase in adrenal weight in the stressed animals (27.1 ± 1.8 mg vs. 26.2 ± 1.4 mg, $n = 7$ per group, $P < 0.06$). However the analysis with one-way ANOVA revealed a significant effect of stress on adrenal gland/body weight ratio at the time of autopsy ($P < 0.009$; 0.07 ± 0.01 mg organ/g of body weight S: 0.1 ± 0.02 mg organ/g of body weight).

BEHAVIORAL MEASUREMENTS

Cold exposure improved acquisition performance in female rats, but, disrupted retrieval performance in male rats

In the MWM, which requires the integrity of the dorsal hippocampus, all groups successfully learned to find the hidden platform as shown by shortened ELs, DMs and MDPs (Day

Effects: $F_{S(3,525)} = 70.336, 78.515, 78.938$; $P < 0.001$) over the four training days. The SS did not change within each group, showing similar motor ability ($F_{(3,525)} = 1.729$; $P > 0.05$) during the training period. A Repeated-Measures ANOVA showed significant Treatment Effect on EL, DM, MDP and SS ($F_{S(1,172)} = 33.662, 19.531, 47.709$ and 30.026 ; $P_s < 0.001$). Significant Gender Effect was found on SS only ($F_{(1,172)} = 17.340$; $P = 0.001$) and significant Interaction Effects were found on MDP ($F_{(1,172)} = 4.666$; $P = 0.032$) and SS ($F_{(1,172)} = 20.786$; $P = 0.001$). LSD *post hoc* tests showed that 2-h cold exposure decreased EL (**Figure 2A**; 75.4 ± 13.1 vs. 37.3 ± 12.5 ; $P = 0.001$), DM (**Figure 2B**; 914.6 ± 118.0 vs. 697.5 ± 183.8 ; $P = 0.034$), and MDP (**Figure 2C**; 58.2 ± 2.5 vs. 49.6 ± 4.1 ; $P = 0.001$) on the first day of training in male rats.

During the remaining days of the training period no difference was observed between cold-exposed male and control male rats in any learning measurement, with observed trends on EL ($P_s = 0.058$ and 0.052 on 2nd and 4th day, respectively) and MDP ($P_s = 0.077$ and 0.054 on 3rd and 4th day, respectively). SS was faster in cold-exposed males than in control male rats on all training days (**Figure 2D**; Day 1: 20.3 ± 1.2 vs. 23.4 ± 1.6 ; Day 2: 21.1 ± 1.5 vs. 23.4 ± 1.2 ; Day 3: 19.2 ± 1.2 vs. 24.4 ± 1.3 ; Day 4: 18.2 ± 1.4 vs. 26.2 ± 2.8 ; $P_s < 0.02$). However cold-exposed female rats outperformed the task on the 1st day [as shown by EL (**Figure 2A**; 63.2 ± 13.2 vs. 43.0 ± 13.9 ; $P = 0.035$), DM (**Figure 2B**; 909.6 ± 126.2 vs. 639.8 ± 142.8 ; $P = 0.009$), and MDP (**Figure 2C**; 58.3 ± 2.8 vs. 48.4 ± 2.7 ; $P < 0.001$)], on the 2nd day [as shown by EL (40.9 ± 12.2 vs. 18.2 ± 8.4 ; $P = 0.002$) and DM (662.5 ± 139.3 vs. 317.8 ± 100.4 ; $P = 0.001$) and; MDP (53.7 ± 3.4 vs. 42.0 ± 3.3 ; $P < 0.001$)], on the 3rd day [as shown by MDP (44.5 ± 3.2 vs. 38.3 ± 3.4 ; $P = 0.010$)] and on the 4th day [as shown by EL (17.2 ± 7.0 vs. 8.0 ± 2.1 ; $P = 0.006$) and MDP (45.7 ± 3.6 vs. 35.4 ± 3.1 ;

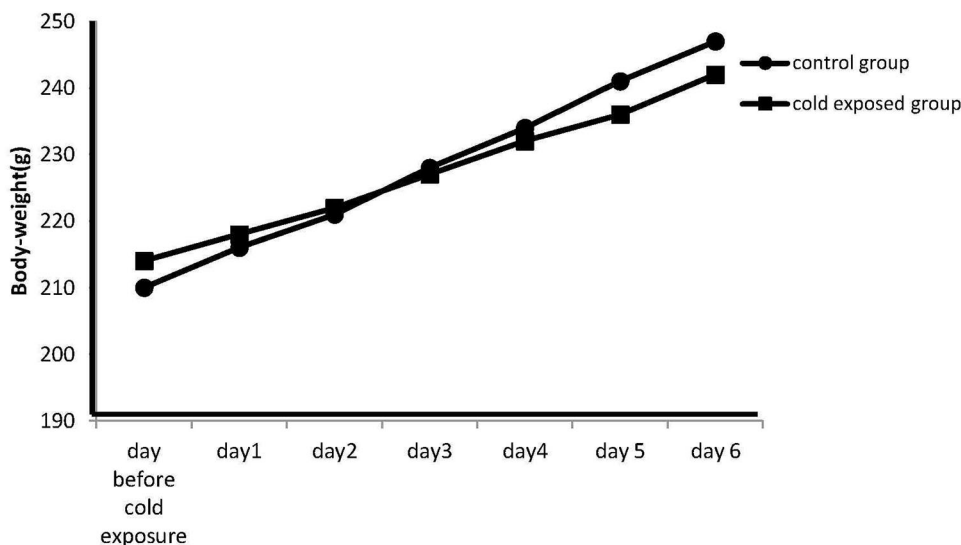
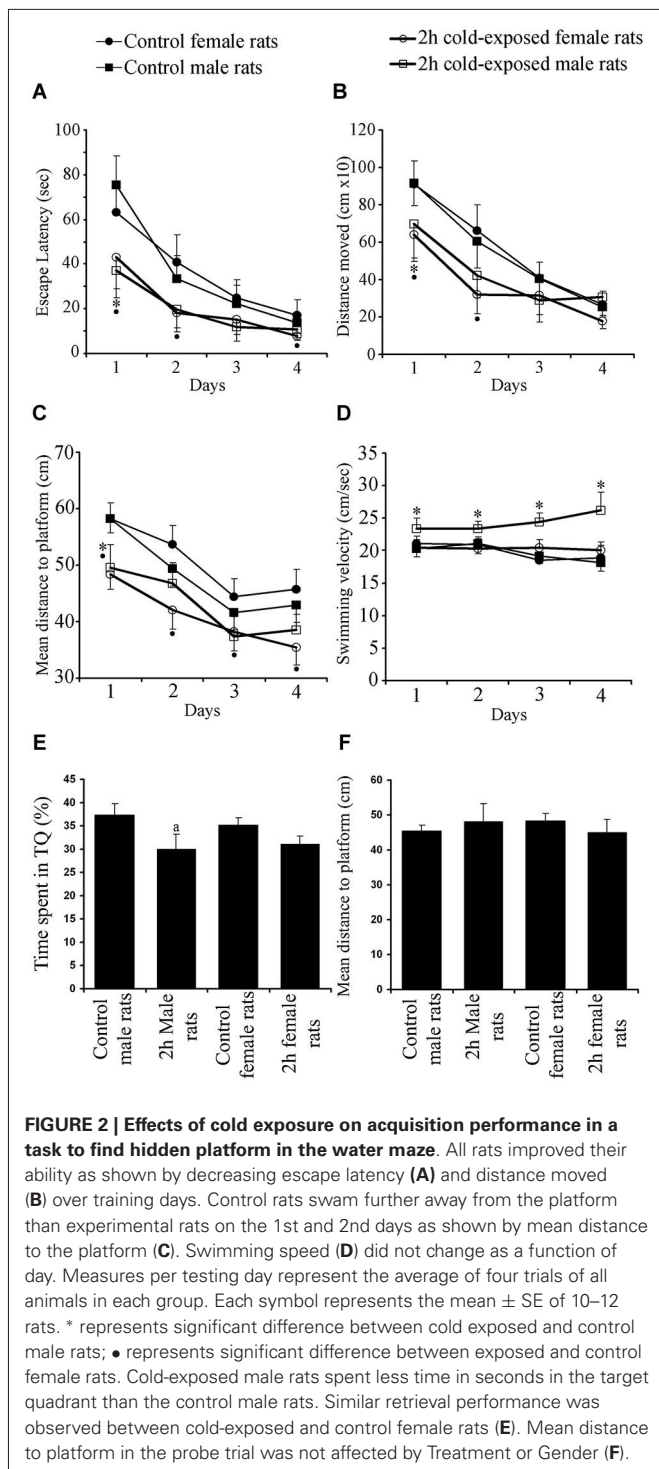


FIGURE 1 | Effect of cold stress on the body weight. Data are represented as the mean S.E.M. of body-weight measured at 09:00 h daily before the exposure. Differences in body weight gain between controls and stressed rats are not statistically significant during any time period of the study ($P < 0.07$; $n = 7$ per group). However the p nearing 0.05 seem to suggest that increasing the number of observation the difference could be relevant.



$P < 0.001$]. Swim speed was not different between cold-exposed female and control female rats, except for that on the 3rd day ($P = 0.038$). Significant differences between control male and female rats were not observed in any learning parameter measured. Under cold stress gender difference was found in DM on the 4th day ($P < 0.015$) and SS on each day ($P_s < 0.003$). Summed up, these data demonstrate that adult female rats are more sensitive

to cold exposure in hippocampus-dependent spatial learning task than male rats.

Regarding spatial accuracy and the ability to remember the location of the hidden platform, the results showed that the time spent by the rat in the target quadrant (TS) was significantly above the 25% chance level for male controls ($37.33 \pm 8.89\%$; $t_{(11)} = 4.800$, $P = 0.001$; one-sample T test), female control rats ($35.17 \pm 11.03\%$; $t_{(11)} = 3.194$; $P = 0.009$), cold-exposed male rats ($30.08 \pm 6.11\%$; $t_{(9)} = 2.628$, $P = 0.027$) and cold-exposed female rats ($31.11 \pm 5.19\%$; $t_{(9)} = 3.719$, $P = 0.005$; **Figure 2E**).

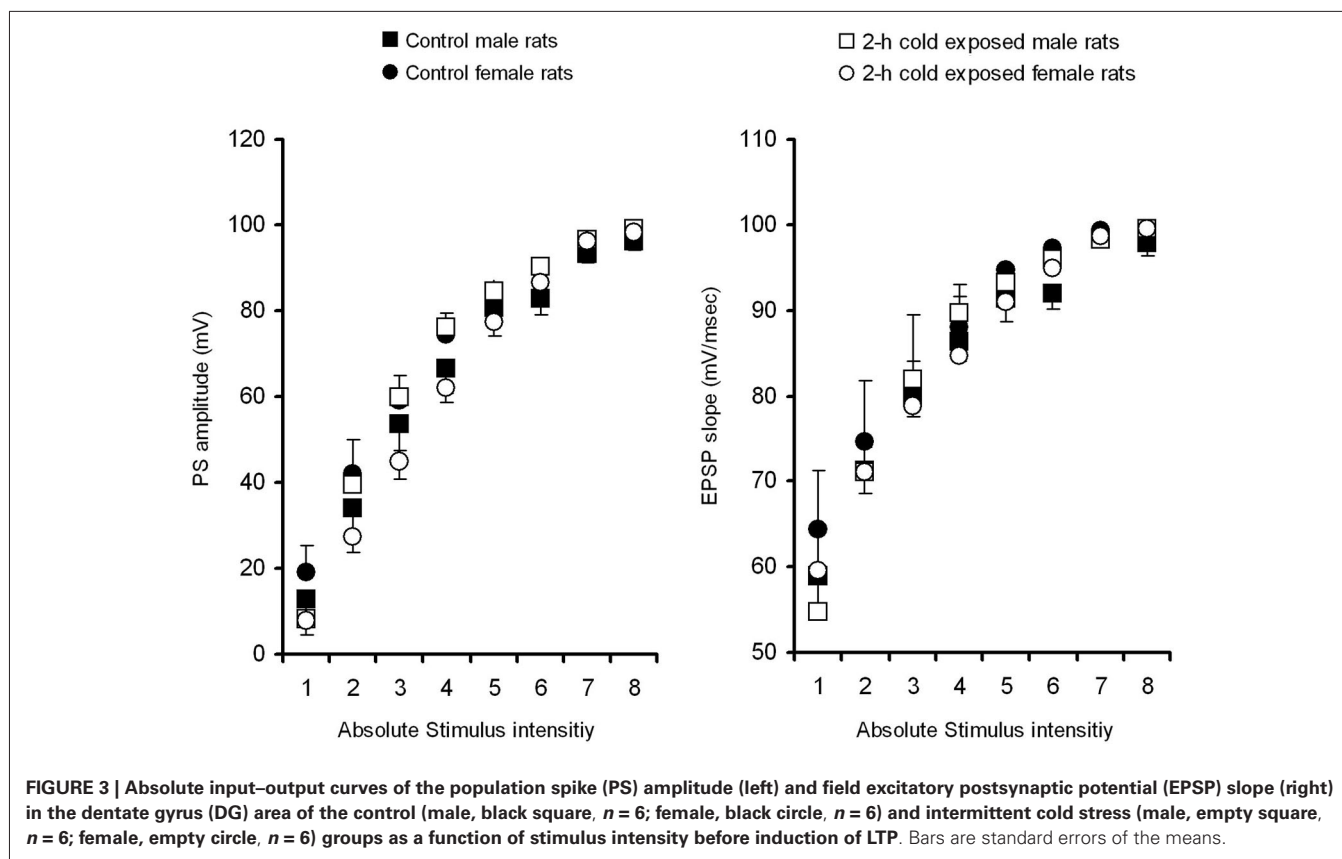
The time spent in the target quadrant (**Figure 2E**) and mean distance to the platform point origin was previously located are used as a measurement of the retrieval performance of a rat (**Figure 2F**). Two factor ANOVA showed a significant Treatment Effect ($F_{(1,43)} = 5.004$; $p = 0.031$) with non significant Gender Effect ($F_{(1,43)} = 0.049$; $p = 0.826$) or Interaction Gender \times Treatment ($F_{(1,43)} = 0.396$; $p = 0.533$). The LSD *post hoc* test showed that cold-exposed male rats spent less time in the target quadrant than control male rats ($P = 0.049$). A significant difference between cold-exposed and control female rats was not found ($P > 0.05$). Globally, cold exposure caused a minimal impairment in hippocampus-dependent spatial memory in male rats as shown by less time spent in the target quadrant. Mean distance to platform, the other retrieval parameter, however, was not affected by Treatment ($F_{(1,43)} = 0.067$; $p = 0.797$), Gender ($F_{(1,43)} = 0.013$; $p = 0.909$) or Interaction Treatment \times Gender ($F_{(1,43)} = 2.619$; $p = 0.114$).

ELECTROPHYSIOLOGY

To determine whether behavioral changes in response to cold stress are parallel with neuronal activity, we investigated the baseline and stimulated activity of the DG. In order to verify if the exposure to intermittent cold stress influenced the basal circuitry properties of the DG, average EPSP slopes and PS amplitudes were plotted against stimulus intensities of 100–1500 μ A (I/O curves, **Figure 3**). Repeated-measures ANOVAs with Treatment and Gender as between-subjects factors showed that neither cold exposure ($F_{(7,140)} = 1.638$ and 1.049) nor gender ($F_{(7,140)} = 0.122$ and 1.015) had a significant effect on PS amplitude across the stimulus intensity range ($p > 0.05$). Moreover, Interaction effect Treatment \times Gender ($F_{(7,140)} = 1.168$ and 1.113) did not reach a significant level. These results show that cold stress does not change I/O curves, indicating no overall change in the baseline transmission of the Perforant Pathway—DG synapsis.

Cold exposure impairs PS-LTP in male rats

High frequency stimulation-induced potentiation of basal PSs (**Figure 4A**) and EPSPs (**Figure 4B**) lasted at least 60 min in LTP recordings from all groups *in vivo*. This potentiation of PS amplitude was lower in the stress groups than in the control groups. Graphical summaries of PS and EPSP slope potentiation are shown in **Figures 4C,D**, respectively. Repeated-measures ANOVAs showed a significant Treatment Effect ($F_{(1,20)} = 9.500$; $P = 0.006$) and over intervals ($F_{(2,40)} = 181.151$; $P < 0.001$) on PS amplitude, and a significant Gender Effect ($F_{(1,20)} = 8.159$; $P = 0.010$) on the fEPSP slope. LSD *post hoc* tests showed that 2-h



cold exposure decreased PS potentiation during both induction ($218.3 \pm 21.6\%$ vs. $304.5 \pm 18.8\%$; $P = 0.004$) and maintenance intervals ($193.9 \pm 24.5\%$ vs. $276.6 \pm 25.4\%$; $P = 0.015$) in male rats, in contrast to the female rats. There was no difference in PS-LTP between both sexes; however, the fEPSP slope was more potentiated in control male rats in the induction interval ($P = 0.026$) and there was a trend ($P = 0.061$) in the maintenance interval. Under cold exposure, this gender dependency in the fEPSP slope was not observed (induction $P = 0.072$ and maintenance $P = 0.262$). We also observed, in the maintenance interval that cold exposure decreased EPSP slope potentiation in female rats when compared with male control rats (0.030). These results suggest that cold exposure has a negative effect on the synaptic plasticity of the DG neurons to the detriment of the male gender.

DISCUSSION

BODY WEIGHT AND ADRENAL GLAND WEIGHT

Body weight loss or a reduction in body weight gain in growing rats may be an indication of disease, pain, stress or discomfort in an animal (Morton and Hau, 2002).

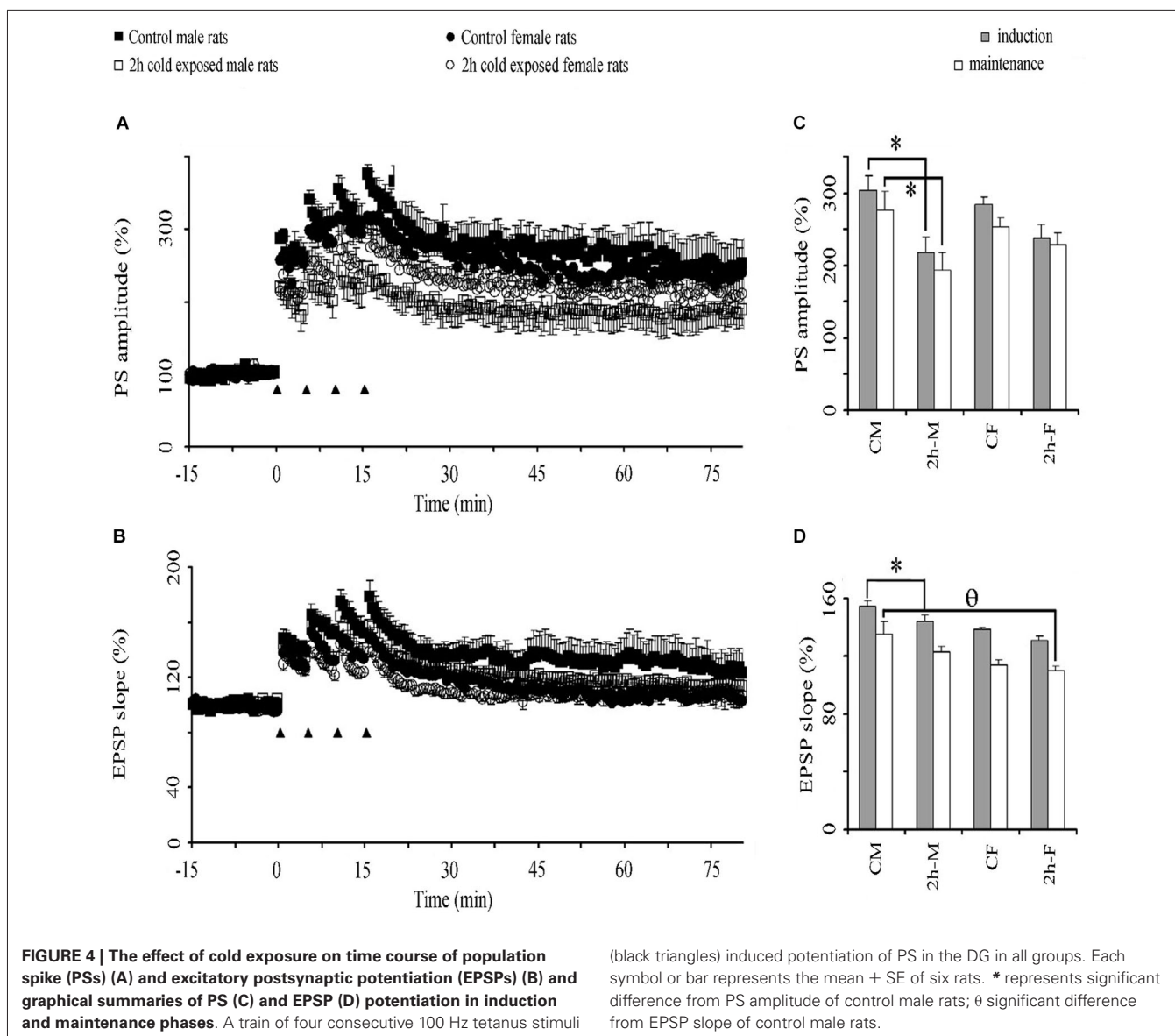
In the present study there were no significant differences in body weight gain between groups during any time period of the study. It explains that the environmental changes that the rats were exposed to had no impact on their body weight. Likewise, for the adrenal glands weight, there is no significant enlargement of these ones in stressed rats although a tendency is shown ($0.07 \pm$

0.01 (mg organ/g of body weight); stressed group: 0.1 ± 0.02 (mg organ/g of body weight) $p < 0.03$). This may indicate that this kind of stress does not engage glucocorticoids as other stress paradigms.

Even though the noradrenergic system is postulated to play a primary role in an organism's response to stress (Stanford, 1995). In fact in some studies it was well established that acute stress exposure can increase the discharge activity and norepinephrine (NE) release from noradrenergic locus coeruleus (LC) neurons (Korf et al., 1973; Abercrombie and Jacobs, 1987; Abercrombie et al., 1988). Furthermore, chronic exposure to stress can alter the response of LC neurons to subsequent stress exposure. However, to show the involvement of the Noradrenaline system in hippocampal pathway and also to explain its role in an organism's response to stress we need to make a second study about Noradrenaline release in rats during prolonged cold-stress.

GENDER DIFFERENCE IN BEHAVIORAL PERFORMANCE IN COLD-EXPOSED RATS

The results of the present study suggest that intermittent cold exposure impairs hippocampal-dependent spatial memory in male rats but facilitates it in female rats. This is similar to the previous findings in restraint stress (Conrad et al., 2004). In the present study, cold-exposed female rats, significantly outperformed control female rats in the learning task to locate a hidden platform in a water maze on four consecutive days of testing;



cold-exposed male rats, however, underperformed in the retrieval task on the probe trial. Female superiority in response to stress has been also reported in object recognition tasks (Beck and Luine, 2002) and in radial maze tests (Bowman et al., 2002).

To the best of our knowledge no study has yet reported the effects of cold stress on learning and memory in female rats. As the first study, we show that when a female rat is subjected to cold, spatial learning is improved. On the other hand there is a general agreement on impaired memory retrieval in males, rats (Panakhova et al., 1984; Nuñez et al., 2000) and humans (Coleshaw et al., 1983; O'Brien et al., 2007). Improved (Palinkas et al., 2005; Zheng et al., 2008) or unaffected (Baddeley et al., 1975) performance which was reported after cold exposure causing hypothermia is probably related to the variability in study designs, type (water or air), duration and intensity of cold exposure. Performance in spatial tasks seems to be correlated with the intensity

of hypothermia. It was reported that spatial memory retrieval is resistant to mild hypothermia (30°C), but that it is severely impaired at body temperatures below 25°C (Panakhova et al., 1984). Since we found similar hypothermia after cold exposure in adult male and female rats, non significant decrease in time spent in the target quadrant observed in cold-exposed female rats suggests their resistance to hypothermia.

The results of the present study suggest a sex difference in motor ability to stress in rats as shown by faster swimming velocity in cold-exposed male rats. Since differences in SS create the possibility of a significant bias of ELs as measures of spatial learning, swim distance is the most appropriate measure of cognitive function in the MWM task (Liu et al., 2006). Therefore, increased swimming ability can explain the significant decrease on the first day and insignificant decreases on the remaining days in EL according to the control male rats in cold-exposed male rats.

Water temperature can be a confounding factor that might influence the acquisition rate of this task (Morris et al., 1982). For this reason we preferred not to let the rats swim in cold water. The present results are somewhat different from the experiment in which rats were exposed to cold during training trials. A quicker rate of acquisition observed in the rats trained at 19°C than in rats trained at 25°C water (Sandi et al., 1997) supports the present study; however better long-term retention is in contrast to the study.

Several studies demonstrated that exposure to 2°C ambient temperature did not decrease rectal temperature (Ahlers et al., 1991; Thomas et al., 1991). However, the results of the present study suggest that a longer lasting 4°C cold exposure procedure may be effective to produce hypothermia. Rectal temperature was measured as 32.7°C showing moderate hypothermia in the present study. Although not measured in the present study, it has been shown that exposure to ambient cold resulted in decreases in both memory and hippocampal temperature, suggesting that central cooling may be responsible for performance decrements (Ahlers et al., 1991). It may be suggested that a decrease in brain temperature slows hippocampal synaptic transmission, which would impair spatial memory (Moser and Andersen, 1994). Therefore hypothermia may be a possible explanation for impaired spatial memory performance after cold exposure in male rats. However, hypothermia could not be responsible for enhanced acquisition performance in female rats. We believe that neurohormonal response to stress should overcome the depressive effect of hypothermia on the hippocampus.

GENDER DIFFERENCE IN BEHAVIORAL PERFORMANCE IN ADULT CONTROL RATS

Numerous studies have suggested that sexual dimorphism may exist in learning and memory, particularly in types involving the hippocampus (Williams and Meck, 1991; Maren et al., 1994). Male rats outperformed female rats in tasks such as the radial-arm maze (Maren et al., 1994; Diamond et al., 1999) and the MWM (Brandeis et al., 1989; Maren et al., 1994), both of which require hippocampal spatial learning. However, no spatial superiority in male rats within Morris water task (MWT) was noted (Berger-Sweeney et al., 1995; Nicolle et al., 2003). Two studies have considered that female rats and mice are superior to males in learning some aspects of a working /reference memory version of the radial arm maze (Bimonte et al., 2000; Hyde et al., 2000). The present results suggest an equivalent performance in male and female rats tested at adult ages.

According to hormonal theory, higher testosterone levels lead to better spatial performance in males whereas varying estrogen levels result in variation in spatial learning and memory in females (Healy et al., 1999). In the present study we did not take into account the estrous cycle in female rats. One may presume that the changing number of female rats could be at any phase of the estrous cycle in all the trials of the MWM in our study; thus the effect of variations in gonadal hormone levels could be minimal in the MWM test. Moreover as the number of animal used is only nine, it is possible that the different phase of the estrous cycle could indeed influence the results.

GENDER DIFFERENCE IN THE DENTATE GYRUS LTP IN COLD-EXPOSED RATS

Since hippocampus-dependent memory is mediated, at least in part, by hippocampal synaptic plasticity we also studied the electrophysiological properties of the Perforant Pathway—DG synapses. The examination of I/O functions across a range of stimulus strengths characterizes the efficiency of excitatory synaptic transmission. We found that cold exposure results in non-shifting I/O curves in adult anesthetized rats of both sexes indicating unaffected baseline transmission of Perforant Pathway—DG synapses. Although even short episodes of stress were reported to reduce the number of newly generated neurons in the DG (Schwabe and Wolf, 2013), acute cold stress (4 h, 4°C) was reported not to affect in synaptic efficacy in the DG of freely moving adult male rats (Bramham et al., 1998).

The PS-LTP induction was impaired in cold-exposed male rats, but not in female rats, in spite of similar I/O curves and similar drop in rectal temperature. Taken together with behavioral data, stress-induced memory disruption may therefore be related to suppression of LTP in male rats. Impaired LTP and poor retrieval performance in cold-exposed male rats are parallel. Therefore LTP in the DG seems to be intracellular correlates of retrieval performance in response to cold exposure. The association with LTP and the MWM is difficult, because the electrophysiological part of the study was carried out in urethane anesthetized rats. Indeed acute cold stress (1 time, 4°C and 90 min) leading to elevated serum corticosterone levels did not impair tetanus-evoked LTP in the DG of freely moving male rats (Bramham et al., 1998). The difference in the total exposure time of the two studies (90 min vs. 10 h) should be considered when interpreting these results. Although not measured in the present study, higher corticosterone levels would be expected in rats exposed to cold for a longer time. It is well-established that levels of corticosterone sufficient to occupy Type II glucocorticoid receptors produce a decrement in LTP, which is prevented by dehydroepiandrosterone (DHEA) in the DG of the hippocampus in male rats (Kaminska et al., 2000). Although the effects of cold exposure on histological changes in the DG were not investigated in the present studies, it was reported that chronically raised corticosterone reduced neurogenesis in the DG of the hippocampal formation (Karishma and Herbert, 2002; Wong and Herbert, 2006).

GENDER DIFFERENCE IN THE DENTATE GYRUS LTP IN CONTROL RATS

A limited number of studies has examined sex difference in the LTP at the synapses of the rat hippocampus. A robust sex difference in the magnitude of LTP induced at the perforant path synapses was also reported in the CA1 region of hippocampal slices (Yang et al., 2004). As an earlier study these gender differences in LTP were specific to the EPSP component of the DG field potentials (Maren et al., 1994). Significant sex differences in EPSP amplitude were also observed, with slices from males having larger EPSP amplitudes than those from females (Zheng et al., 2008). However we did not find any difference either in baseline synaptic strength or in LTP between male and female adult rats in the DG. The results found here suggested that the LTP amplitude is not different depending on the gender.

CONCLUSION

Overall, the results show that repeated cold exposure can selectively improve spatial learning in adult female rats, but impaired retention memory for platform location in male rats. It is possible that impaired LTP underlies some of the impaired retention memory caused by cold exposure in the male rats.

Cold exposure decreased the rectal temperature in both male and female rats. Nevertheless, there were no significant differences in body weight gain between groups during any time period of the study. It explains that the environmental changes that the rats were exposed to had no impact on their body weight.

We have followed the experimental protocol used in several studies on stress and the test of the levels of the principal sexual hormones was not explored here but could be assessed in further studies.

Data from the present study demonstrate that cold-exposed male rats show worse spatial memory performance and impaired PS-LTP, while cold-exposed female rats show enhanced learning ability and unaffected LTP. Detailed studies are needed to understand the gender dependent exact mechanism of the effects of cold stress on hippocampal pathways for learning and memory.

AUTHOR AND CONTRIBUTORS

Hajar Elmarzouki has done the core experiments and the reports; Youssef Aboussaleh has submitted the project and planned the study; Cem Suer has supervised the work; Soner Bitiktas has assisted in animals models; Seda Artis has revised and did some data analysis; Nazan Dolu has followed the work; Ahmed Ahami has read the report and provided good advices.

ACKNOWLEDGMENTS

This study was supported by Neuromed Project of the FP7 European Commission and the Erciyas University Research Foundation Grant TSY-11-3770 and TSY-11-3768.

REFERENCES

- Abercrombie, E. D., and Jacobs, B. L. (1987). Single-unit response of noradrenergic neurons in the locus coeruleus of freely moving cats. I. Acutely presented stressful and nonstressful stimuli. *J. Neurosci.* 7, 2837–2843.
- Abercrombie, E. D., Keller, R. W. Jr., and Zigmond, M. J. (1988). Characterization of hippocampal norepinephrine release as measured by microdialysis perfusion: pharmacological and behavioral studies. *Neuroscience* 27, 897–904. doi: 10.1016/0306-4522(88)90192-3
- Ahlers, S. T., Thomas, J. R., and Berkey, D. L. (1991). Hippocampal and body temperature changes in rats during delayed matching-to-sample performance in a cold environment. *Physiol. Behav.* 50, 1013–1018. doi: 10.1016/0031-9384(91)90430-v
- Artis, A. S., Bitiktas, S., Taşkın, E., Dolu, N., Liman, N., and Suer, C. (2012). Experimental hypothyroidism delays field excitatory post-synaptic potentials and disrupts hippocampal long-term potentiation in the dentate gyrus of hippocampal formation and y-maze performance in adult rats: hypothyroidism delays fEPSP and disrupts spatial memory. *J. Neuroendocrinol.* 24, 422–433. doi: 10.1111/j.1365-2826.2011.02253.x
- Baddeley, A. D., Thomson, N., and Buchanan, M. (1975). Word length and the structure of short-term memory. *J. Verbal Learning Verbal Behav.* 14, 575–589. doi: 10.1016/S0022-5371(75)80045-4
- Beck, K. D., and Luine, V. N. (2002). Sex differences in behavioral and neurochemical profiles after chronic stress: role of housing conditions. *Physiol. Behav.* 75, 661–673. doi: 10.1016/s0031-9384(02)00670-4
- Berger-Sweeney, J., Arnold, A., Gabeau, D., and Mills, J. (1995). Sex differences in learning and memory in mice: effects of sequence of testing and cholinergic blockade. *Behav. Neurosci.* 109, 859–873. doi: 10.1037/0735-7044.109.5.859
- Bimonte, H. A., Hyde, L. A., Hoplight, B. J., and Denenberg, V. H. (2000). In two species, females exhibit superior working memory and inferior reference memory on the water radial-arm maze. *Physiol. Behav.* 70, 311–317. doi: 10.1016/s0031-9384(00)00259-6
- Bliss, T. V. P., and Collingridge, G. L. (1993). A synaptic model of memory: long-term potentiation in the hippocampus. *Nature* 361, 31–39. doi: 10.1038/361031a0
- Bowman, R. E., Ferguson, D., and Luine, V. N. (2002). Effects of chronic restraint stress and estradiol on open field activity, spatial memory and monoaminergic neurotransmitters in ovariectomized rats. *Neuroscience* 113, 401–410. doi: 10.1016/s0306-4522(02)00156-2
- Bramham, C. R., Southard, T., Ahlers, S. T., and Sarvey, J. M. (1998). Acute cold stress leading to elevated corticosterone neither enhances synaptic efficacy nor impairs LTP in the dentate gyrus of freely moving rats. *Brain Res.* 789, 245–255. doi: 10.1016/s0006-8993(97)01265-1
- Brandeis, R., Brandys, Y., and Yehuda, S. (1989). The use of the Morris Water Maze in the study of memory and learning. *Int. J. Neurosci.* 48, 29–69. doi: 10.3109/00207458909002151
- Britton, K. T., Segal, D. S., Kuczenski, R., and Hauger, R. (1992). Dissociation between in vivo hippocampal norepinephrine response and behavioral/neuroendocrine responses to noise stress in rats. *Brain Res.* 574, 125–130. doi: 10.1016/0006-8993(92)90808-m
- Coleshaw, S. R., Van Someren, R. N., Wolff, A. H., Davis, H. M., and Keatinge, W. R. (1983). Impaired memory registration and speed of reasoning caused by low body temperature. *J. Appl. Physiol. Respir. Environ. Exerc. Physiol.* 55(1 Pt. 1), 27–31. doi: 10.1097/00132586-198408000-00077
- Conrad, C. D., Jackson, J. L., Wiczorek, L., Baran, S. E., Harman, J. S., Wright, R. L., et al. (2004). Acute stress impairs spatial memory in male but not female rats: influence of estrous cycle. *Pharmacol. Biochem. Behav.* 78, 569–579. doi: 10.1016/j.pbb.2004.04.025
- Diamond, D. M., Park, C. R., Heman, K. L., and Rose, G. M. (1999). Exposing rats to a predator impairs spatial working memory in the radial arm water maze. *Hippocampus* 9, 542–552. doi: 10.1002/(sici)1098-1063(1999)9:5<542::aid-hipo8>3.0.co;2-n
- Healy, S. D., Braham, S. R., and Braithwaite, V. A. (1999). Spatial working memory in rats: no differences between the sexes. *Proc. Biol. Sci.* 266, 2303–2308. doi: 10.1098/rspb.1999.0923
- Hyde, L. A., Sherman, G. F., and Denenberg, V. H. (2000). Non-spatial water radial-arm maze learning in mice. *Brain Res.* 863, 151–159. doi: 10.1016/s0006-8993(00)02113-2
- Jonasson, Z. (2005). Meta-analysis of sex differences in rodent models of learning and memory: a review of behavioral and biological data. *Neurosci. Biobehav. Rev.* 28, 811–825. doi: 10.1016/j.neubiorev.2004.10.006
- Kaminska, M., Harris, J., Gijbbers, K., and Dubrovsky, B. (2000). Dehydroepiandrosterone sulfate (DHEAS) counteracts decremental effects of corticosterone on dentate gyrus LTP. Implications for depression. *Brain Res. Bull.* 52, 229–234. doi: 10.1016/s0361-9230(00)00251-3
- Karishma, K. K., and Herbert, J. (2002). Dehydroepiandrosterone (DHEA) stimulates neurogenesis in the hippocampus of the rat, promotes survival of newly formed neurons and prevents corticosterone-induced suppression. *Eur. J. Neurosci.* 16, 445–453. doi: 10.1046/j.1460-9568.2002.02099.x
- Korf, J., Aghajanian, G. K., and Roth, R. H. (1973). Increased turnover of norepinephrine in the rat cerebral cortex during stress: role of the locus coeruleus. *Neuropharmacology* 12, 933–938. doi: 10.1016/0028-3908(73)90024-5
- Kvetnanský, R., Pacák, K., Sabban, E. L., Kopin, I. J., and Goldstein, D. S. (1997). Stressor specificity of peripheral catecholaminergic activation. *Adv. Pharmacol.* 42, 556–560. doi: 10.1016/s1054-3589(08)60811-x
- Kvetnansky, R., Sabban, E. L., and Palkovits, M. (2009). Catecholaminergic systems in stress: structural and molecular genetic approaches. *Physiol. Rev.* 89, 535–606. doi: 10.1152/physrev.00042.2006
- Liu, C. Z., Yu, J. C., Cheng, H. Y., Jiang, Z. G., Li, T., Zhang, X. Z., et al. (2006). Spatial memory performance and hippocampal neuron number in osteoporotic SAMP6 mice. *Exp. Neurol.* 201, 452–460. doi: 10.1016/j.expneurol.2006.04.025
- Maren, S., De Oca, B., and Fanselow, M. S. (1994). Sex differences in hippocampal long-term potentiation (LTP) and Pavlovian fear conditioning in rats: positive correlation between LTP and contextual learning. *Brain Res.* 661, 25–34. doi: 10.1016/0006-8993(94)91176-2

- Morris, R. G., Garrud, P., Rawlins, J. N., and O'Keefe, J. (1982). Place navigation impaired in rats with hippocampal lesions. *Nature* 297, 681–683. doi: 10.1038/297681a0
- Morton, D. B., and Hau, J. (2002). "Welfare assessment and humane endpoints," in *Handbook of Laboratory Animal Science* (Vol. 1), eds J. Hau and L. Van Hoosier Jr. (Boca Raton: CRC Press), 457–486.
- Moser, E. I., and Andersen, P. (1994). Conserved spatial learning in cooled rats in spite of slowing of dentate field potentials. *J. Neurosci.* 14, 4458–4466.
- Nicolle, M. M., Prescott, S., and Bizon, J. L. (2003). Emergence of a cue strategy preference on the water maze task in aged C57B6 x SJL F1 hybrid mice. *Learn. Mem.* 10, 520–524. doi: 10.1101/lm.64803
- Nisenbaum, L. K., Zigmond, M. J., Sved, A. F., and Abercrombie, E. D. (1991). Prior exposure to chronic stress results in enhanced synthesis and release of hippocampal norepinephrine in response to a novel stressor. *J. Neurosci.* 11, 1478–1484.
- Núñez, J. L., Koss, W. A., and Juraska, J. M. (2000). Hippocampal anatomy and water maze performance are affected by neonatal cryoanesthesia in rats of both sexes. *Horm. Behav.* 37, 169–178. doi: 10.1006/hbeh.2000.1572
- O'Brien, C., Mahoney, C., Tharion, W. J., Sils, I. V., and Castellani, J. W. (2007). Dietary tyrosine benefits cognitive and psychomotor performance during body cooling. *Physiol. Behav.* 90, 301–307. doi: 10.1016/j.physbeh.2006.09.027
- Palinkas, L. A., Mäkinen, T. M., Pääkkönen, T., Rintamäki, H., Leppäluoto, J., and Hassi, J. (2005). Influence of seasonally adjusted exposure to cold and darkness on cognitive performance in circumpolar residents. *Scand. J. Psychol.* 46, 239–246. doi: 10.1111/j.1467-9450.2005.00453.x
- Panakhova, E., Burešová, O., and Bures, J. (1984). The effect of hypothermia on the rat's spatial memory in the water tank task. *Behav. Neural Biol.* 42, 191–196. doi: 10.1016/s0163-1047(84)91059-8
- Rintamäki, H. (2005). "Protective clothing and performance in cold environments", in *Proceeding of the Third International Conference on Human-Environment System* (Tokyo, Japan).
- Rosenzweig, E. S., and Barnes, C. A. (2003). Impact of aging on hippocampal function: plasticity, network dynamics and cognition. *Prog. Neurobiol.* 69, 143–179. doi: 10.1016/s0301-0082(02)00126-0
- Sandi, C., Loscertales, M., and Guaza, C. (1997). Experience-dependent facilitating effect of corticosterone on spatial memory formation in the water maze. *Eur. J. Neurosci.* 9, 637–642. doi: 10.1111/j.1460-9568.1997.tb01412.x
- Sandi, C., Woodson, J. C., Haynes, V. F., Park, C. R., Touyarot, K., Lopez-Fernandez, M. A., et al. (2005). Acute stress-induced impairment of spatial memory is associated with decreased expression of neural cell adhesion molecule in the hippocampus and prefrontal cortex. *Biol. Psychiatry* 57, 856–864. doi: 10.1016/j.biopsych.2004.12.034
- Schwabe, L., and Wolf, O. T. (2013). Stress and multiple memory systems: from 'thinking' to 'doing'. *Trends Cogn. Sci.* 17, 60–68. doi: 10.1016/j.tics.2012.12.001
- Stanford, S. C. (1995). Central noradrenergic neurones and stress. *Pharmacol. Ther.* 68, 297–342. doi: 10.1016/0163-7258(95)02010-1
- Suer, C., Dolu, N., Artis, S., and Aydogan, S. (2009). Effects of carnosine on long-term plasticity of medial perforant pathway/dentate gyrus synapses in urethane-anesthetized rats: an in vivo model. *Exp. Brain Res.* 197, 135–142. doi: 10.1007/s00221-009-1899-x
- Sutherland, R. J., Whishaw, I. Q., and Regehr, J. C. (1982). Cholinergic receptor blockade impairs spatial localization by use of distal cues in the rat. *J. Comp. Physiol. Psychol.* 96, 563–573. doi: 10.1037/h0077914
- Thomas, J. R., Ahlers, S. T., and Schrot, J. (1991). Cold-induced impairment of delayed matching in rats. *Behav. Neural Biol.* 55, 19–30. doi: 10.1016/0163-1047(91)80124-w
- Williams, C. L., and Meck, W. H. (1991). The organizational effects of gonadal steroids on sexually dimorphic spatial ability. *Psychoneuroendocrinology* 16, 155–176. doi: 10.1016/0306-4530(91)90076-6
- Wong, E. Y. H., and Herbert, J. (2006). Raised circulating corticosterone inhibits neuronal differentiation of progenitor cells in the adult hippocampus. *Neuroscience* 137, 83–92. doi: 10.1016/j.neuroscience.2005.08.073
- Yang, D. W., Pan, B., Han, T. Z., and Xie, W. (2004). Sexual dimorphism in the induction of LTP: critical role of tetanizing stimulation. *Life Sci.* 75, 119–127. doi: 10.1016/j.lfs.2003.12.004
- Zheng, G., Chen, Y., Zhang, X., Cai, T., Liu, M., Zhao, F., et al. (2008). Acute cold exposure and rewarming enhanced spatial memory and activated the MAPK cascades in the rat brain. *Brain Res.* 1239, 171–180. doi: 10.1016/j.brainres.2008.08.057

Conflict of Interest Statement: The Reviewer Dr. Mohamed Najimi declares that, despite having collaborated with the authors, the review process was handled objectively and no conflict of interest exists. The authors declare that the research was conducted in the absence of any commercial or financial relationships that could be construed as a potential conflict of interest.

Received: 18 February 2014; accepted: 10 August 2014; published online: 01 September 2014.

Citation: Elmarzouki H, Aboussaleh Y, Bitiktas S, Suer C, Artis AS, Dolu N and Ahami A (2014) Effects of cold exposure on behavioral and electrophysiological parameters related with hippocampal function in rats. *Front. Cell. Neurosci.* 8:253. doi: 10.3389/fncel.2014.00253

This article was submitted to the journal *Frontiers in Cellular Neuroscience*.

Copyright © 2014 Elmarzouki, Aboussaleh, Bitiktas, Suer, Artis, Dolu and Ahami. This is an open-access article distributed under the terms of the Creative Commons Attribution License (CC BY). The use, distribution or reproduction in other forums is permitted, provided the original author(s) or licensor are credited and that the original publication in this journal is cited, in accordance with accepted academic practice. No use, distribution or reproduction is permitted which does not comply with these terms.



Distribution of nitric oxide-producing cells along spinal cord in urodeles

Mayada A. Mahmoud¹, Gehan H. Fahmy^{2*}, Marie Z. Moftah² and Ismail Sabry²

¹ Faculty of Medicine, Institut de Neurosciences des Systèmes, Unités Mixtes de Recherche Institut National de la Santé et de la Recherche Médicale 1106, Aix-Marseille University, Marseille, France

² Zoology Department, Faculty of Science, Alexandria University, Alexandria, Egypt

Edited by:

Emmanuel Moyse, University
Francois Rabelais, France

Reviewed by:

Marc Landry, Bordeaux University,
France

Emmanuel Moyse, University
Francois Rabelais, France

*Correspondence:

Gehan H. Fahmy, Zoology
Department, Faculty of Science,
Alexandria University, 21151
Alexandria, Egypt
e-mail: gfahmy2014@yahoo.com

Nitric oxide is a unique neurotransmitter, which participates in many physiological and pathological processes in the organism. There are little data about the neuronal nitric oxide synthase immunoreactivity in the spinal cord of amphibians. In this respect, the present study aims to investigate the distribution of nitric oxide producing cells in the spinal cord of urodele and to find out the possibility of a functional locomotory role to this neurotransmitter. The results of the present study demonstrate a specific pattern of NADPH-d labeling in the selected amphibian model throughout the spinal cord length as NADPH-d-producing cells and fibers were present in almost all segments of the spinal cord of the salamander investigated. However, their number, cytological characteristics and labeling intensity varied significantly. It was noticed that the NO-producing cells (NO-PC) were accumulated in the ventral side of certain segments in the spinal cord corresponding to the brachial and sacral plexuses. In addition, the number of NO-PC was found to be increased also at the beginning of the tail and this could be due to the fact that salamanders are tetrapods having bimodal locomotion, namely swimming and walking.

Keywords: nitric oxide, spinal cord, urodeles, NADPH-d labeling, neurotransmitter agents

INTRODUCTION

Nitric oxide (NO) was recognized as the first gaseous neurotransmitter with a very short half-life time (2–6 s) (Greenwood and Earnshaw, 1997; Barañano et al., 2001; González-Soriano et al., 2002) and it has been implicated as a non-adrenergic non-cholinergic (NANC) inhibitory neurotransmitter at various sites in the nervous system (Grozdanovic et al., 1994; Schuman and Madison, 1994; Sharma et al., 2005).

Anatomical studies have linked NO to developing brain regions associated with locomotion in the rat (Terada et al., 1996), fish (Villani, 1999) and even insects (Wildemann and Bicker, 1999). In addition, it is widely accepted that NO plays a major role in sensory and motor systems (Funakoshi et al., 1999), neurogenesis (Estrada and Murillo-Carretero, 2005) and neuroendocrine and autonomic nervous activities (Gerstberger, 1999; Guo and Longhurst, 2003). There is vast evidence that NO is also involved in spinal functions. Its effects include the regulation of cardiovascular function and the mediation of nociception (Chowdhary and Townend, 1999; Osuka et al., 2008), and it is well accepted that NO is involved in nociceptive processing and persistent pain as intracellular and intercellular messengers in the spinal cord (Ito et al., 2001; Chung et al., 2005; Dagi et al., 2011).

NO is a typical neurotransmitter which is a typical in chemical nature, biosynthesis, mechanism of action, and cellular localization as they are neither stored in synaptic vesicles nor released by exocytosis. They nearly diffuse into adjacent neurons (Barañano et al., 2001) where they block cellular enzymes required in metabolism and activate soluble guanylate cyclase (sGC)—an insoluble enzyme—in an inactive form, present in the

cells cytoplasm. The activation occurs via interaction of NO with Fe⁺² in the heme portion of the molecule, thereby altering its conformation and activating it, this causes conversion of guanosine triphosphate (GTP) to cyclic guanosine monophosphate (cGMP), which mediates many of the physiological actions of NO in mammalian cells (McCann et al., 2005). In aldehyde fixed tissue, nitric oxide synthase (NOS) is able to selectively catalyze a histochemically detectable Golgi-like dense staining of reactive neurons produced by Nicotinamide Adenine Dinucleotide Phosphate diaphorase (NADPH-d) histochemistry (González-Soriano et al., 2002). This is known as NADPH-diaphorase activity, which is used as a histochemical detection method for neuronal NO-producing structures (Bredt et al., 1991).

Nitroergic elements have been inferred from cells positive to NADPH-d histochemistry and/or to the neuronal nitric oxide synthase (nNOS) immunohistochemistry in different species of vertebrates (Giraldez-Perez et al., 2008). Thus, the distribution of neuronal elements that express NOS in the brain of the amphibian *Dermophis mexicanus*, by means of immunohistochemistry, with specific antibodies against NOS, and enzyme histochemistry for NADPH-diaphorase were equally demonstrated by both techniques (González et al., 2002).

The most important and attractive reason, for which neuroanatomists were interested in the technique of detecting NADPH-d by histochemistry, arose when NADPH was identified as a marker for nNOS (Hope et al., 1991). It has been repeatedly corroborated that in the nervous system, NADPH activity and NOS immunoreactivity widely colocalize in distinct sets of neurons (Briñon et al., 1998; Giraldez-Perez et al., 2008). The relative

simple NADPH-d histochemical technique was widely used to identify NO-producing elements in the brain of representatives of all vertebrate classes (Arévalo et al., 1995; Munoz et al., 1996; Smeets et al., 1997; Alonso et al., 2000).

While several studies have described the localization of NO-PC in the developing brains of birds and mammals including human brain (Vincent, 1994; Samama et al., 1995; Takemura et al., 1996; Terada et al., 1996; Iwase et al., 1998), the distribution of NO-positive cell population has not been well characterized in the amphibian central nervous system. In fact, the spinal cord (Thomas and Pearse, 1964)—which has extensive distribution of NOS-containing cells and fibers—and the brain of amphibians have been demonstrated for several species of anurans (Lázár and Losonczy, 1999; López and González, 2002) and urodeles (González et al., 1996; Moreno et al., 2002). Salamanders (a urodele amphibian animal) is a perfect animal model for studying the relation between spinal cord and movements, as they do not lose their tails after metamorphosis and thereby conceives the ability for both axial and limb-based locomotion in adulthood.

There is little data about the neuronal nitric oxide synthase immunoreactive (nNOS-ir) neurons of amphibian spinal cord. In this respect, the aims of this study were to demonstrate the presence of NO in neurons of salamanders' spinal cord, to describe its light microscope morphology and distribution, to verify whether the NO-producing neurons have specific patterns of organization throughout the spinal cord and to investigate whether this transmitter has a certain relation with movement or not.

MATERIALS AND METHODS

HISTOLOGICAL PREPARATION

A group of four salamanders were anesthetized by immersion in a 0.1% aqueous solution Tricaine methane sulphonate (MS-222; Sigma, Saint Quentin Fallavier, France). Vertebral columns were separated and fixed in Bouin's solution for two h at room temperature. The spinal cord was dissected out by cutting the vertebral column after each two constitutive vertebrae starting from the Atlas except vertebra number 9 and withdrawing it anteriorly. It has been thus divided anatomically into five segments. As for segment V, it represents the part of the spinal cord present within vertebra number 9 (sacral).

Collected spinal cord specimens were dehydrated in an ascending series of ethanol (60 m for each), cleared twice in xylene (60 m each), impregnated in wax and xylene for 10 m (1:1), embedded twice in paraffin wax (1 h. each), then finally embedded in paraffin wax. Specimens were then sectioned (5 μ m thick) by using a traditional microtome (American Optical Scientific Instrument Division, Buffalo, NY, USA), then stained with hematoxylin and eosin for microscopic histological study. Cell profiles were confirmed by adjusting the focal depth of the objective.

NADPH-d HISTOCHEMISTRY

Salamanders were perfused transcardially with oxygenated urodele Ringer's solution as previously tested (Chevallier et al., 2004) and then by 4% paraformaldehyde in 0.1 M phosphate buffer (pH 7.4). The dorsal half of the vertebrae was removed (laminectomy). The spinal cord was separated from the opened

vertebrae and divided into five segments for histological preparations. Specimens were post-fixed in 4% paraformaldehyde for 2 h at room temperature then immersed in a solution of 12% sucrose in PB overnight at 4°C. Specimens were transferred into tissue Tek and kept in -80°C until processed. Blocks were transferred to -20°C for 2 h before being cut on a cryostat at 15 μ m. Sections were collected in phosphate buffer (PB) as free-floating sections. They were rinsed in fresh PB then treated according to previously published method (Moreno et al., 2002). In brief, free-floating sections were incubated in a medium containing 1 mM β -NADPH, 0.8 mM nitro blue tetrazolium and 0.06% triton X-100 in PB, at 37°C for 1–2 h. The reaction was stopped by successive rinses in cold PB. Some sections were incubated in a medium without β -NADPH to be used as controls. All sections were then mounted using 0.25% gelatin in 0.1 M Tris buffer, pH 7.6 then dried overnight and cover slipped.

IMAGE ACQUISITION

The distribution of nitric oxide positive cells (NO-PC) in the spinal cord was charted in a series of transverse sections along the rostrocaudal axis of the animal by using camera Lucida and the image of each segment was recorded with a digital camera wide zoom operating on a microscope, and reversed on a computer by the Analysis Life Science Series (Soft Imaging System, Japan) and Life View software (Animation Technologies Inc, Taiwan).

QUANTIFICATION

Quantification procedures have been done by drawing all sections using camera lucida, then manually counting all stained cells. All neurons that contained violet stain (strong stain = dark violet color, weak stain = light violet color) in all sections incubated in NADPH-d were expressed as mean \pm SE.

STATISTICAL ANALYSIS

All data were represented as means \pm s.e.m. and were statistically analyzed with One-Way ANOVA by using "Statistical Package for the Social Sciences" SPSS software and student's two-tailed *t*-test to compare each two groups together.

RESULTS

In the salamander's spinal cord, the gray matter was composed of unspecialized primitive cells (Figures 1A,B). They were arranged in 9–10 concentric rows surrounding the central canal. Although not specialized, the first internal row of cells lining the central canal was oriented toward its cavity, hence referred to as ependymal cells.

NO-PC and fibers were found to be present in almost all segments of the spinal cord. They could also be divided into two classes: (1) heavily stained indicating large quantity of NO production and (2) lightly stained neurons indicating less quantity of NO production. For the latter, only cell bodies were observed, whereas for the former, cell bodies and their dendrites were both visible. NADPH-d labeling clearly revealed discrete populations of pear-shaped cells, which may be unipolar and/or bipolar neurons (Figures 2A,B).

Mapping and distribution of labeled cells in representative transverse sections have been charted at different regions of the spinal cord as follows (Table 1):

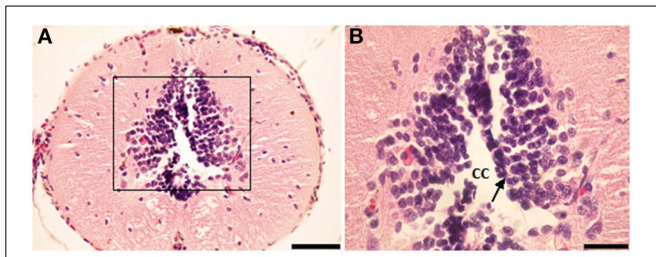


FIGURE 1 | Photomicrograph showing transverse sections through the spinal cord segment IA. (B) is enlargement of the framed area in (A), note the shape of ependymal cells (arrow). CC, central canal. Scale bar in (A) is 100 μ m and in (B) is 50 μ m.

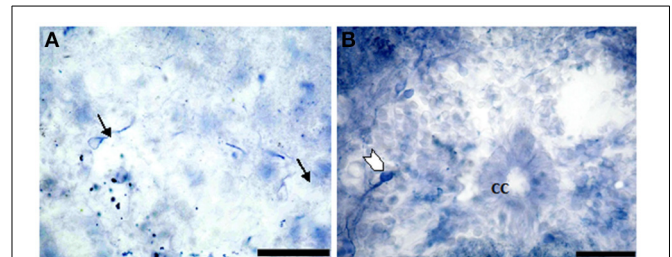


FIGURE 3 | Photomicrograph showing the distribution of NO-PC in segment IA (arrows in A) and IP (arrowhead in B) in salamanders. Note the difference in stained neurons (weak: arrows in A and strong: arrowhead in B). Scale bar is 50 μ m.

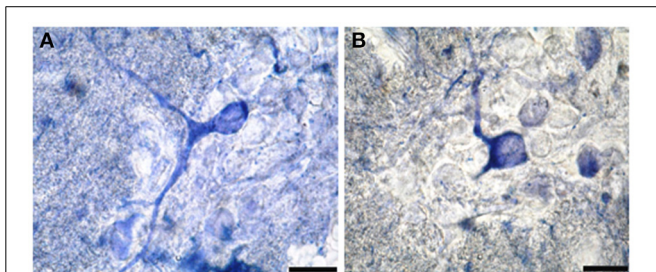


FIGURE 2 | Photomicrograph showing different shapes of NO-PC in the spinal cord of salamanders. (A) Unipolar neuron. Note the axon extending from the cell body toward the white matter. (B) Bipolar neuron. Scale bar: 20 μ m.

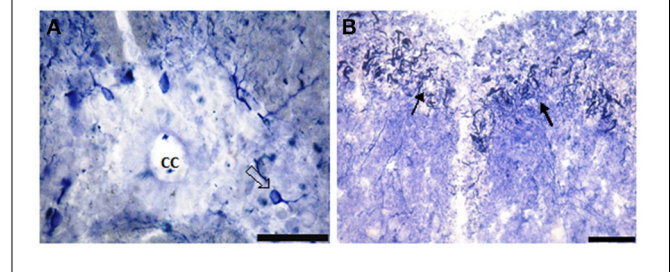


FIGURE 4 | Photomicrograph showing NO-PC distribution in spinal cord segment II of salamanders. Note the presence of the densely-packed multipolar neurons and moderate staining pear-shaped neurons (B: arrows). Scale bar in (A) is 50 μ m and in (B) is 100 μ m.

Table 1 | Showing total number of NO-PC in different segments of salamander's spinal cord.

Segment	Mean number of cells/section	Mean number of cells/section in ventral side
IA	2.03 \pm 0.276	0.33 \pm 0.05
IP	7.3 \pm 0.38	2.53 \pm 0.01
II	5.5 \pm 1.08	0.86 \pm 0.03
III	2.9 \pm 0.28	0.63 \pm 0.01
IV	1.2 \pm 0.20	1.0 \pm 0.06
V	3.5 \pm 0.57	2.8 \pm 0.2

Mean \pm SE.
p \leq 0.05 vs. IA.

Segment IA represented the anterior part of the spinal cord. Nitric oxide positive cells (NO-PC) was scarce and their number did not exceed 2 cells/section (Figure 3A). These cells were mainly found in the ventral side of the spinal cord and they were weakly labeled (arrows in Figure 3A). In segment IP, NO-PC significantly increased in number to reach the maximum cell number among all segments (7 cells/section) (Figure 3B). Some of these cells were highly stained compared to others; they were generally located in the periphery of the gray matter whereas long nerve fibers were ventrally directed (arrowhead in Figure 3B).

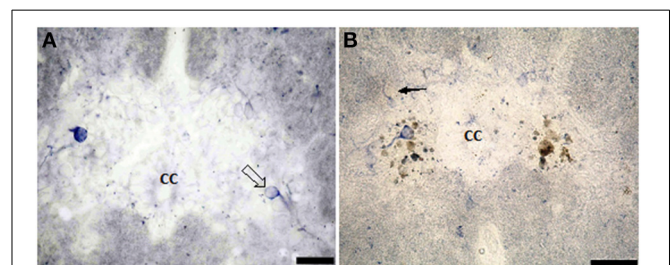


FIGURE 5 | Photomicrograph showing the distribution of NO-PC in segment III (A) and segment IV (B) in salamanders. Scale bar is 50 μ m.

In segment II, NO-PC showed slight decrease in number (average 5 cells/section) compared to the previous one and almost all recognizable cells were highly labeled with NADPH-d (Figures 4A,B). In segment III, NO-PC showed more decline in number of positive cells (2 cells/section), that had different degree of labeling intensity. The cells with higher NADPH-d stain intensity were located in the ventral side of the spinal cord (Figure 5A). The axons of these cells had no specific direction. The least number of NO-PC was found in segment number IV (1 cell/section) (Figure 5B), where the intensity of NADPH-d labeling was faint and the cells axons were ventrally directed. In segment V, the number of NO-PC significantly increased again (3 cells/section), in which they had higher NADPH-d staining intensity than in the previous segments (Figure 6). Most of these cells axons were also ventrally directed.

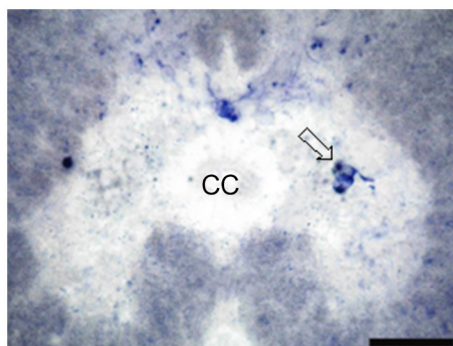


FIGURE 6 | Photomicrograph showing the distribution of NO-PC in the last studied segment of salamanders spinal cord, namely segment V. Scale bar is 50 μ m.

Comparing the distribution of NADPH-d positive neurons along spinal cord segments of pleurodeles, we found that the segment that had the most significant increase in number of NADPH-d positive cells was the IP segment (7.3 ± 0.38), then it gradually decreased posteriorly till it reached its minimum in segment IV (1.2 ± 0.2), then it started to increase again at the last segment (3.5 ± 0.57) (**Figure 7**).

A Camera Lucida drawing (**Figure 8**) showed NO-PC mapping through spinal cord segments. In segment IA, NO-PC appeared to have light staining and were located around the central canal. Their number was low compared to the following segment. In segment IP, more NO-PC were seen, some of which had dark and high NADPH-d stain ability. Their dendrites were mostly directed toward the ventral side, while other cells had faint staining. In segment II, the number of NO-PC was less than the previous one and all cells had a faint stain ability. Their dendrites were mostly directed toward the dorsal side. In segment III, some NO-PC got dark staining and others had lighter staining. Some of their dendrites were directed toward the dorsal side of the spinal cord while others were directed toward the ventral side. In segment IV, the number of NO-PC was less than any other segment of the spinal cord and cells had faint NADPH-d staining. Their dendrites were directed toward the ventral side of the cord. In the fifth segment, it was noticed that the number of NO-PC increased and their dendrites were mainly directed toward the ventral side.

In addition, it was noticed that NO-PC were accumulated in the ventral region of certain segments in the spinal cord, we counted the labeled cells in this region (**Table 1**). It was found that the segment that had the highest number of NO-PC was the IP segment (2.5 cells/section), then it gradually decreased along the rostrocaudal axis till segment number III, where it reached its minimum (0.6 cells/section) (**Figure 9**). Then, the NO-PC significantly increased again in segments IV and V reaching 2.8 cells/section.

DISCUSSION

The results of the present study provide a detailed map of the distribution of NADPH-d-containing neurons in the spinal cord

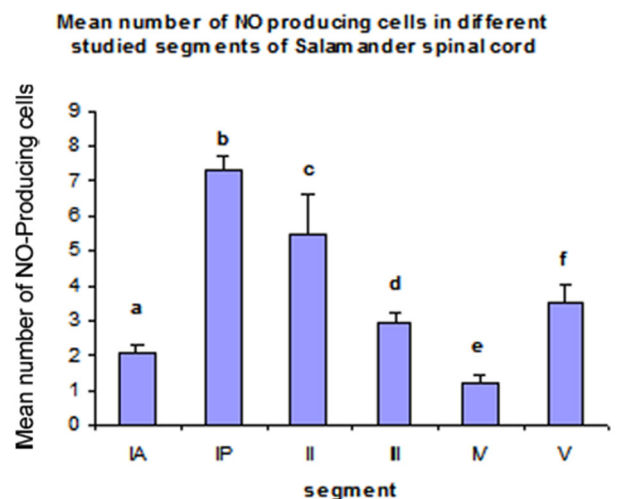
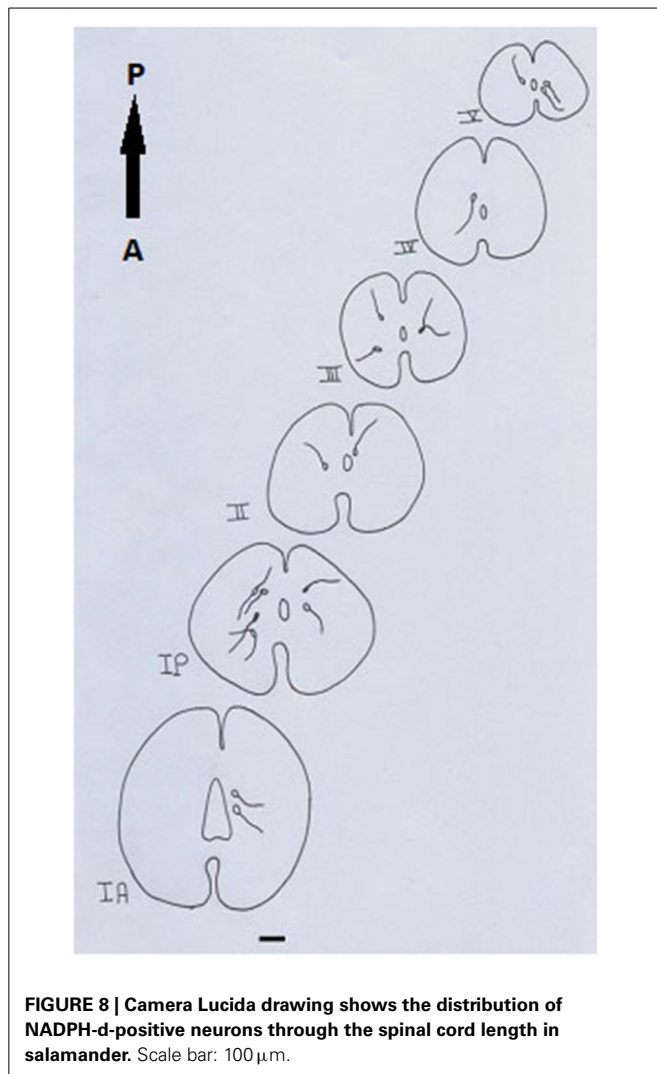


FIGURE 7 | Histograms illustrating the differences in the distribution of NO-PC along the spinal cord segments in salamanders. ^a $P < 0.05$ vs. segments IP, II, III and V; ^b $P < 0.05$ vs. all other segments; ^c $P < 0.05$ vs. all other segments; ^d $P < 0.05$ vs. segments IP, IV and V; ^e $P < 0.05$ vs. all other segments except IA; ^f $P < 0.05$ vs. all other segments except III.

of salamanders to localize NO, since the relative simplicity of the amphibian tadpole nervous system has been used as a model for the mechanisms underlying the generation and development of vertebrate locomotion (McLean et al., 2000).

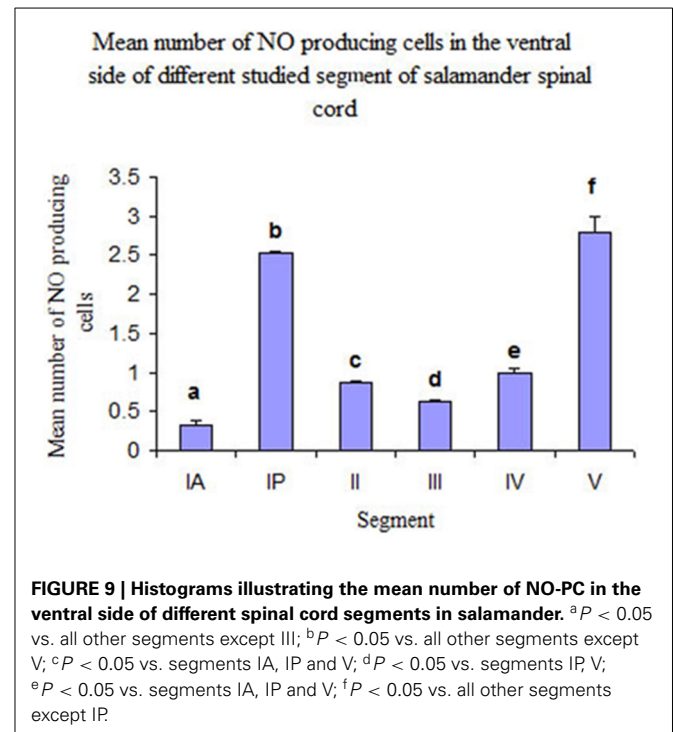
From histochemistry experiments on salamanders, it was observed that the number of NO-PC per section was gradually decreasing toward the posterior end of the spinal cord; however, it suddenly increased just before the caudal region. Moreno et al. (2002) indicated that most, if not all nitergic neurons in the spinal cord of amphibians are interneurons. Thus, we suggest that the NO-producing cells are interneurons especially in segments IP and V.

The highest immunoreactivity of NADPH-d was found in segment IP and this segment is at the forelimbs level. It was also found that NO-PC were mainly accumulated in the ventral region of the spinal cord, where it contains the somatic motoneurons of the spinal cord. The present data are in agreement with previous research (Crowe et al., 1995) where NADPH-d was present in neuronal populations within *Xenopus leavis* spinal cord, such as the fore and hind limb motoneuron pools. NO has also been reported to play a role in motoneuron development. Abundance of NADPH-d in certain segments of spinal cords, which are parallel to the fore and hind limb, implicates that NO has an important role as neuronal messenger in these regions of the spinal cord. Collectively, from previous and present findings we may conclude that NO-producing cells are the control keys for locomotion. Furthermore, we found that NO-PC were also mainly located in the intermediate gray area of spinal segments corresponding to the thoracic region. According to Crowe et al. (1995), this intermediate area corresponds to the location of autonomic preganglionic neuronal cell bodies. Consequently, we may conclude that the positive neurons in this area of the cord may have an autonomic function. In addition, the present



results were in accordance with those of Dun et al. (1992), who stated that immunoreactivity for nNOS were present in neurons in regions of the rodent spinal cord that were associated primarily with autonomic and sensory functions. However, it is not excluded that NO-PC might be glial cells. A double labeling for astrocytic markers and NADPH-d would be necessary to clarify this possibility.

Fox (1992) stated that during metamorphosis the movement of anuran amphibians gradually switches from undulatory oscillation of the trunk and tail during tadpole swimming to limb-based propulsion in frog and toad, necessitating a complete remodeling of their locomotory system as limbs grow and the tail regresses. In this respect, results obtained herein could be discussed as the number of NO-producing cells is higher in the ventral side of the spinal cord segments corresponding to brachial and sacral plexuses. In our work, the number of NO-PC were increased in the spinal cord segments corresponding to brachial and sacral plexuses and also at the beginning of the tail and this could be due to the fact that salamanders are tetrapods capable of both swimming and walking (ten Donkelaar et al.,



2001). Our finding is antagonistic with Ramanathan et al. (2006), who showed that during early stages of metamorphosis, nitroergic neurons were excluded from regions where spinal limb circuits were forming. As metamorphosis progressed, NOS expression became distributed along the length of the spinal cord together with an increase in the number and intensity of labeled cells and fibers.

The analysis of NADPH-d-expressing and/or NOS-immunoreactive neurons in the spinal cord of different animal species (Vizzard et al., 1994b, 1995) have shown a morphologically heterogeneous pattern of NADPH-d-expressing neuronal pools ranging from bipolar, poorly branched NADPH-d-exhibiting neurons in the superficial dorsal horn to highly differentiated neurons in the pericentral region (lamina X), deep dorsal horn (laminae IV–V), and dorsal gray commissure containing widely branching NADPH-d-exhibiting neurons (Vizzard et al., 1994a; Burnett et al., 1995; Maršala et al., 1998). In general, NADPH-d staining has been seen in neurons and fibers in the superficial dorsal horn, in neurons around the central canal at all levels of the spinal cord, in the dorsal commissure, in the sacral parasympathetic nucleus (SPN), and in the intermediolateral cell column (IML) of the thoracolumbar segments. In addition, large numbers of NADPH-d stained neurons were found in the superficial dorsal horn and around the central canal of rabbit spinal cord (Maršala et al., 2007). On the contrary, our finding was antagonistic to the previous two researches, NO-PC were seen mostly accumulated in the ventral parts of the spinal cord. The differences between these two findings could be due taxa differences.

The distribution of neuronal nitric oxide synthase-immunoreactive (nNOS-ir) system was described in man

(Egberongbe et al., 1994) and rat's (Bredt et al., 1991) brain as well as in cat and mouse's spinal cord (Dun et al., 1993). Moreover, the system was described in more limited cerebral regions, as the hippocampus, the striatum, or the hypothalamus in the rat (Ng et al., 1999). NADPH-d-positive elements have been described within the brain and spinal cord of rat (Vincent and Kimura, 1992; Freire et al., 2004), the spinal cord of rabbit and mouse (Kluchova et al., 2000), and the mouse cerebellum (Brüning, 1993). Recently, Bombardi et al. (2013) suggested that NO may be involved in spinal sensory and visceral circuitries. Giraldez-Perez et al. (2008) found a wide distribution of double labeled cells co-localizing NADPH-d and NOS in brain and spinal cord of goldfish.

NADPH-d-labeled cells were consistently seen in the regions of the intermediate gray matter in the spinal cord of *Xenopus laevis* (Crowe et al., 1995). A similar study of Maršala et al. (1999) has shown that the segmental distribution of NADPH-d-expressing neurons in the rabbit is comparable to that described in the spinal cord of other species such as rat, mouse, cat, dog, squirrel, and monkey with certain differences consisting in an increasing number of NADPH-d-expressing neurons along the rostrocaudal axis of the spinal cord and accumulation of NADPH-d-positive somata in the lower lumbar and sacral segments. A considerable increase in the cell body size of large, multipolar, pericentrally located NADPH-d-expressing neurons was seen. McLean et al. (2000) found that NO appears to be located in three distinct clusters of neurons in the brain stem of *Xenopus* larva where they may function as a modulator, which is released with other conventional transmitters.

In conclusion, NADPH-d stain along the rostrocaudal spinal cord segments of salamanders has shown quantitative and qualitative heterogeneous appearance of NO-PC. These findings raise the possibility that NO synthesized by bipolar neurons and large multipolar NADPH-d expressing neurons located in the ventral horn may be involved in the motor control. In addition, the present work revealed the accumulation of NO-PC at specific segments in the spinal cord that are related to fore- and hindlimb movement and stepping.

ACKNOWLEDGMENTS

This work was supported by STDF project number 513. Fixed blocks, β -NADPH and nitro blue tetrazolium were generously offered by Prof. Jean-Marie Cabelguen (INSERM U862) and Prof. Marc Landry (IINS, CNRS UMR 5297), Bordeaux, France.

REFERENCES

- Alonso, J. R., Arévalo, R., Weruaga, E., Porteros, J. G., Briñón, J. G., and Aijón, J. (2000). "Comparative and developmental neuroanatomical aspects of the NO system," in *Functional Neuroanatomy of the Nitric Oxide System*, eds H. W. M. Stein busch, J. Devente, and S. R. Vincent (Amsterdam: Elsevier), 51–109.
- Arévalo, R., Alonso, J. R., Garcia-Ojeda, E., Briñón, J. G., Crespo, C., and Aijón, J. (1995). NADPH-diaphorase in the central nervous system of the tench (*Tinca tinca* L., 1758). *J. Comp. Neurol.* 352, 398–420.
- Barañano, D. E., Ferris, C. D., and Snyder, S. H. (2001). Atypical neural messengers. *Trends Neurosci.* 24, 99–106. doi: 10.1016/S0166-2236(00)01716-1
- Bombardi, C., Grandis, A., Gardini, A., and Cozzi, B. (2013). Nitroergic neurons in the spinal cord of the bottlenose dolphin (*Tursiops truncatus*). *Anat. Rec. (Hoboken)* 296, 1603–1614. doi: 10.1002/ar.22766
- Bredt, D. S., Glatt, C. E., Hwang, P. M., Fotuhi, M., Dawson, T. M., and Snyder, S. H. (1991). Nitric oxide synthase protein and mRNA are discretely localized in neuronal populations of the mammalian CNS together with NADPH diaphorase. *Neuron* 7, 615–624. doi: 10.1016/0896-6273(91)90374-9
- Briñón, J. G., Crespo, C., Weruaga, E., Alonso, J., Sobreviela, T., Aijón, J., et al. (1998). NADPH-diaphorase/nitric oxide synthase-positive elements in the human olfactory bulb. *Neuroreport* 9, 3141–3146. doi: 10.1097/00001756-199810050-00004
- Brüning, G. (1993). Localization of NADPH-diaphorase in the brain of the chicken. *J. Comp. Neurol.* 334, 192–208. doi: 10.1002/cne.903340204
- Burnett, A. L., Saito, S., Maguire, M. P., Yamaguchi, H., Chang, T. S. K., and Hanley, D. F. (1995). Localization of nitric oxide synthase in spinal nuclei innervating pelvic ganglia. *J. Urol.* 153, 212–217. doi: 10.1097/00005392-199501000-00079
- Chevallier, S., Landry, M., Nagy, E., and Cabelguen, J. M. (2004). Recovery of bimodal locomotion in the spinal-transected salamander, *Pleurodeles waltlii*. *Eur. J. Neurosci.* 20, 1995–2007. doi: 10.1111/j.1460-9568.2004.03671.x
- Chowdhary, S., and Townend, J. N. (1999). Role of nitric oxide in the regulation of cardiovascular autonomic control. *Clin. Sci.* 97, 5–17. doi: 10.1042/CS19980399
- Chung, Y. H., Kim, D., Lee, K. J., Kim, S. S., Kim, Y. K., Cho, D. Y., et al. (2005). Immunohistochemical study on the distribution of neuronal nitric oxide synthase-immunoreactive neurons in the spinal cord of aged rat. *J. Mol. Histol.* 36, 325–329. doi: 10.1007/s10735-005-9001-x
- Crowe, M. J., Brown, T. J., Bresnahan, J. C., and Beattie, M. S. (1995). Distribution of NADPH-diaphorase reactivity in the spinal cord of metamorphosing and adult *Xenopus laevis*. *Dev. Brain Res.* 86, 155–166. doi: 10.1016/0165-3806(95)00021-5
- Dagci, T., Sengul, G., Keser, A., and Onal, A. (2011). NADPH-d and Fos reactivity in the rat spinal cord following experimental spinal cord injury and embryonic neuronal stem cell transplantation. *Life. Sci.* 88, 746–752. doi: 10.1016/j.lfs.2011.02.013
- Dun, N. J., Dun, S. L., Förstermann, U., and Tseng, L. F. (1992). Nitric oxide synthase immunoreactivity in rat spinal cord. *Neurosci. Lett.* 147, 217–220. doi: 10.1016/0304-3940(92)90599-3
- Dun, N. J., Dun, S. L., Wu, S. Y., Förstermann, U., Schmidt, H. H., and Tseng, L. F. (1993). Nitric oxide synthase immunoreactivity in the rat, mouse, cat and squirrel monkey spinal cord. *Neuroscience* 54, 845–857. doi: 10.1016/0306-4522(93)90579-5
- Egberongbe, Y. I., Gentleman, S. M., Falkai, P., Bogerts, B., Polak, J. M., and Roberts, G. W. (1994). The distribution of nitric oxide synthase immunoreactivity in the human brain. *Neuroscience* 59, 561–578. doi: 10.1016/0306-4522(94)90177-5
- Estrada, C., and Murillo-Carretero, M. (2005). Nitric oxide and adult neurogenesis in health and disease. *Neuroscientist* 11, 294–307. doi: 10.1177/1073858404273850
- Fox, H. (1992). Figures of Eberth in the amphibian larval epidermis. *J. Morphol.* 212, 87–97. doi: 10.1002/jmor.1052120109
- Freire, M. A. M., Gomes-Leal, W., Carvalho, W. A., Guimarães, J. S., Franca, J. G., Picanço-Diniz, C. W., et al. (2004). Amorphometric study of the progressive changes on NADPH diaphorase activity in the developing rat's barrel field. *Neurosci. Res.* 50, 55–66. doi: 10.1016/j.neures.2004.05.009
- Funakoshi, K., Kadota, T., Atobe, Y., Nakano, M., Goris, R. C., and Kishida, R. (1999). Nitric oxide synthase in the glossopharyngeal and vagal afferent pathway of a teleost, *Takifugu niphobes*. The branchial vascular innervation. *Cell Tissue Res.* 298, 45–54. doi: 10.1007/s004419900078
- Gerstberger, R. (1999). Nitric oxide and body temperature control. *News Physiol. Sci.* 14, 30–36.
- Giraldez-Perez, R. M., Gaytan, S. P., Ruano, D., Torres, B., and Pasaro, R. (2008). Distribution of NADPH-diaphorase and nitric oxide synthase reactivity in the central nervous system of the goldfish (*Carassius auratus*). *J. Chem. Neuroanat.* 35, 12–32. doi: 10.1016/j.jchemneu.2007.05.007
- González, A., Moreno, N., and López, J. M. (2002). Distribution of NADPH-diaphorase/nitric oxide synthase in the brain of the caecilian *Dermophis mexicanus* (amphibia: gymnophiona): comparative aspects in amphibians. *Brain Behav. Evol.* 60, 80–100. doi: 10.1159/000065204
- González, A., Muñoz, M., Marín, O., Arévalo, R., Porteros, A., and Alonso, J. R. (1996). Nitric oxide synthase in the brain of a urodele amphibian (*Pleurodeles waltli*) and its relation to catecholaminergic neuronal structures. *Brain Res.* 727, 49–64. doi: 10.1016/0006-8993(96)00354-X
- González-Soriano, J., Contreras-Rodríguez, J., Martínez-Sainz, P., Martín-Palacios, S., Marín-García, P., and Rodríguez-Veiga, E. (2002). NADPH-diaphorase

- distribution in the rabbit superior colliculus and co-localization with calcium-binding proteins. *J. Anat.* 200, 297–308. doi: 10.1046/j.1469-7580.2002.00025.x
- Greenwood, N. N., and Earnshaw, A. (1997). *Chemistry of the Elements, 2nd Edn.* Oxford: Butterworth-Heinemann.
- Grozdanovic, Z., Brünig, G., and Baumgarten, H. G. (1994). Nitric Oxide a novel autonomic neurotransmitter. *Acta Anat.* 150, 16–24. doi: 10.1159/000147598
- Guo, Z. L., and Longhurst, J. C. (2003). Activation of nitric oxide producing neurons in the brain stem during Cardiac sympathoexcitatory reflexes in the cat. *Neuroscience* 116, 167–178. doi: 10.1016/S0306-4522(02)00707-8
- Hope, B. T., Michael, G. F., Knigge, K. M., and Vincent, S. R. (1991). Neuronal NADPH-diaphorase is anitric oxide synthase. *Proc. Natl. Acad. Sci. U.S.A.* 88, 2811–2814. doi: 10.1073/pnas.88.7.2811
- Ito, S., OkudaAshtaka, E., and Minami, T. (2001). Central and peripheral roles of prostaglandin in pain and their interactions with novel neuropeptides nociceptin and nocistatin. *Neurosci. Res.* 41, 299–332. doi: 10.1016/S0168-0102(01)00289-9
- Iwase, K., Takemura, M., Shimada, T., Wakisaka, S., Nokubi, T., and Shigenaba, Y. (1998). Ontogeny of NADPH-diaphorase in the rat fore brain and mid brain. *Anat. Embryol.* 197, 229–247. doi: 10.1007/s004290050134
- Kluchova, D., Schmidtova, K., Rybarova, S., Lovasova, K., Pomfy, M., Prosova, T., et al. (2000). Partial colocalization of NADPH-diaphorase and acetylcholinesterase positivity in spinal cord neurons. *Physiol. Res.* 49, 151–155. Available online at: http://www.biomed.cas.cz/physiolres/pdf/49/49_151.pdf
- Lázár, G., and Losonczy, A. (1999). NADPH-diaphorase-positive neurons and pathways in the brain of the frog *Rana esculenta*. *Anat. Embryol.* 199, 185–198. doi: 10.1007/s004290050219
- López, J. M., and González, A. (2002). Ontogeny of NADPH diaphorase/nitric oxide synthase reactivity in the brain of *Xenopus laevis*. *J. Comp. Neurol.* 445, 59–77. doi: 10.1002/cne.10163
- Maršala, J., Marsala, M., Vanicki, I., and Taira, Y. (1999). Localization of NADPH-d exhibiting neurons in the spinal cord of the rabbit. *J. Comp. Neurol.* 406, 263–284
- Maršala, J., Orendáčová, J., Lukáčová, N., and Vanický, I. (2007). Traumatic injury of the spinal cord and nitric oxide. *Prog. Brain Res.* 161, 171–183. doi: 10.1016/S0079-6123(06)61011-X
- Maršala, J., Vanický, I., Maršala, M., Jalč, P., Orendáčová, J., and Taira, Y. (1998). Reduced nicotinamide adenine dinucleotide phosphate diaphorase in the spinal cord of dogs. *Neuroscience* 85, 847–862. doi: 10.1016/S0306-4522(97)00690-8
- McCann, S. M., Mastronardi, C., de Laurentiis, A., and Rettori, V. (2005). The nitric oxide theory of aging revisited. *Ann. N.Y. Acad. Sci.* 1057, 64–84. doi: 10.1196/annals.1356.064
- McLean, D. L., Merrywest, S. D., and Sillar, K. T. (2000). The development of neuromodulatory systems and the maturation of motor patterns in amphibian tadpoles. *Brain Res. Bull.* 53, 595–603. doi: 10.1016/S0361-9230(00)00393-2
- Moreno, N., López, J. M., Sánchez-Camacho, C., and González, A. (2002). Development of NADPH-diaphorase/nitric oxide synthase in the brain of urodele amphibian *Pleurodele waltl*. *J. Chem. Neuroanat.* 23, 105–121. doi: 10.1016/S0891-0618(01)00146-6
- Munoz, M., Munoz, A., Marín, O., Alonso, J. R., Arévalo, R., Porteros, A., et al. (1996). Topographical distribution of NADPH-diaphorase activity in the central nervous system of the frog *Rana perezi*. *J. Comp. Neurol.* 367, 54–69.
- Ng, Y. K., Xue, Y. D., and Wong, P. T. (1999). Different distribution of nitric oxide synthase-containing neurons in the mouse and rat hypothalamus. *Nitric Oxide* 3, 383–392. doi: 10.1006/niox.1999.0247
- Osuka, K., Watanabe, Y., Takagi, T., Usuda, N., Atsuzawa, K., Yoshida, J., et al. (2008). Activation of endothelial nitric oxide synthase following spinal cord injury in mice. *Neurosci. Lett.* 436, 265–268. doi: 10.1016/j.neulet.2008.03.039
- Ramanathan, S., Combes, D., Molinari, M., Simmers, J., and Sillar, K. T. (2006). Developmental and regional expression of NADPH-diaphorase/nitric oxide synthase in spinal cord neurons correlates with the emergence of limb motor networks in metamorphosing *Xenopus laevis*. *Eur. J. Neurosci.* 24, 1907–1922. doi: 10.1111/j.1460-9568.2006.05057.x
- Samama, B., Chateau, D., and Boehm, N. (1995). Expression of NADPH-diaphorase in the rat fore brain during development. *Neurosci. Lett.* 184, 204–207. doi: 10.1016/0304-3940(94)11207-Y
- Schuman, E. M., and Madison, D. V. (1994). Nitric Oxide and synaptic function. *Ann. Rev. Neurosci.* 17, 153–183. doi: 10.1146/annurev.ne.17.030194.001101
- Sharma, H. S., Badgaiyan, R. D., Alm, P., Mohanty, S., and Wiklund, L. (2005). Neuroprotective effects of nitric oxide synthase inhibitors in spinal cord injury-induced pathophysiology and motor functions: an experimental study in the rat. *Ann. N.Y. Acad. Sci.* 1053, 422–434. doi: 10.1196/annals.1344.037
- Smeets, W., Alonso, J. R., and González, A. (1997). Distribution of NADPH-diaphorase and nitric oxide synthase in relation to catecholaminergic neuronal structures in the brain of lizard *Gekko gekko*. *J. Comp. Neurol.* 377, 121–141.
- Takemura, M., Wakisaka, S., Iwase, K., Yabuta, N. H., Nakagawa, S., Chen, K., et al. (1996). NADPH-diaphorase in the developing rat: lower brain stem and cervical spinal cord, with special reference to the trigemino-solitary complex. *J. Comp. Neurol.* 365, 511–525.
- ten Donkelaar, H. J., Lammens, M., Wesseling, P., Thijssen, H. O., Renier, W. O., and Gabreëls, F. J. (2001). Development and developmental disorders of the human brain. III. Neuronal migration disorders of the cerebrum. *Ned. Tijdschr. Geneesk.* 145, 466–474.
- Terada, H., Nagai, T., Kimura, H., Kitahama, K., and Okada, S. (1996). Distribution of nitric oxide synthase-immunoreactive neurons in fetal rat brains at embryonic day 15 and day 19. *J. Chem. Neuroanat.* 10, 273–278. doi: 10.1016/0891-0618(96)00141-X
- Thomas, E., and Pearce, A. G. E. (1964). The solitary active cells. Histochemical demonstration of damage-resistant nerve cells with a TPN-diaphorase reaction. *Acta Neuropathol.* 3, 238–249. doi: 10.1007/BF00684399
- Villani, L. (1999). Development of NADPH-diaphorase activity in the central nervous system of the Cichlid fish, *Tilapia mariae*. *Brain Behav. Evol.* 54, 147–158. doi: 10.1159/00006619
- Vincent, S. R. (1994). Nitric oxide: a radical neurotransmitter in the central nervous system. *Prog. Neurobiol.* 42, 129–160. doi: 10.1016/0301-0082(94)90023-X
- Vincent, S. R., and Kimura, H. (1992). Histochemical mapping of nitric oxide synthase in the rat brain. *Neuroscience* 46, 755–784. doi: 10.1016/0306-4522(92)90184-4
- Vizzard, M. A., Erdman, S. L., and de Groat, W. C. (1995). Increased expression of neuronal nitric oxide synthase (NOS) in visceral neurons after nerve injury. *Neuroscience* 15, 4033–4045.
- Vizzard, M. A., Erdman, S. L., Förstermann, U., and de Groat, W. C. (1994a). differential distribution of nitric oxide synthase in neural pathways to the urogenital organs (urethra, penis, urinary bladder) of the rat. *Brain Res.* 646, 279–291. doi: 10.1016/0006-8993(94)90090-6
- Vizzard, M. A., Erdman, S. L., Roppolo, J. R., Förstermann, U., and de Groat, W. C. (1994b). differential localization of neuronal nitric oxide synthase immunoreactivity and NADPH-diaphorase activity in the rat spinal cord. *Cell Tissue Res.* 278, 299–309. doi: 10.1007/BF00414174
- Wildemann, B., and Bicker, G. (1999). Developmental expression of nitric oxide/cyclic GMP synthesizing cells in the nervous system of *Drosophila melanogaster*. *J. Neurobiol.* 38, 1–15.

Conflict of Interest Statement: The authors declare that the research was conducted in the absence of any commercial or financial relationships that could be construed as a potential conflict of interest.

Received: 02 January 2014; paper pending published: 17 April 2014; accepted: 05 September 2014; published online: 25 September 2014.

Citation: Mahmoud MA, Fahmy GH, Mofah MZ and Sabry I (2014) Distribution of nitric oxide-producing cells along spinal cord in urodeles. *Front. Cell. Neurosci.* 8:299. doi: 10.3389/fncel.2014.00299

This article was submitted to the journal *Frontiers in Cellular Neuroscience*.

Copyright © 2014 Mahmoud, Fahmy, Mofah and Sabry. This is an open-access article distributed under the terms of the Creative Commons Attribution License (CC BY). The use, distribution or reproduction in other forums is permitted, provided the original author(s) or licensor are credited and that the original publication in this journal is cited, in accordance with accepted academic practice. No use, distribution or reproduction is permitted which does not comply with these terms.

Advantages of publishing in Frontiers



OPEN ACCESS

Articles are free to read,
for greatest visibility



COLLABORATIVE PEER-REVIEW

Designed to be rigorous
– yet also collaborative,
fair and constructive



FAST PUBLICATION

Average 85 days from
submission to publication
(across all journals)



COPYRIGHT TO AUTHORS

No limit to article
distribution and re-use



TRANSPARENT

Editors and reviewers
acknowledged by name
on published articles



SUPPORT

By our Swiss-based
editorial team



IMPACT METRICS

Advanced metrics
track your article's impact



GLOBAL SPREAD

5'100'000+ monthly
article views
and downloads



LOOP RESEARCH NETWORK

Our network
increases readership
for your article

Frontiers

EPFL Innovation Park, Building I • 1015 Lausanne • Switzerland
Tel +41 21 510 17 00 • Fax +41 21 510 17 01 • info@frontiersin.org
www.frontiersin.org

Find us on

